

2010

Structure-activity relationships of PAI-1 inhibitors

Karen Sanders

Follow this and additional works at: <http://commons.emich.edu/theses>



Part of the [Chemistry Commons](#)

Recommended Citation

Sanders, Karen, "Structure-activity relationships of PAI-1 inhibitors" (2010). *Master's Theses and Doctoral Dissertations*. 370.
<http://commons.emich.edu/theses/370>

This Open Access Thesis is brought to you for free and open access by the Master's Theses, and Doctoral Dissertations, and Graduate Capstone Projects at DigitalCommons@EMU. It has been accepted for inclusion in Master's Theses and Doctoral Dissertations by an authorized administrator of DigitalCommons@EMU. For more information, please contact lib-ir@emich.edu.

STRUCTURE-ACTIVITY RELATIONSHIPS OF PAI-1 INHIBITORS

by

Karen Sanders

Thesis

Submitted to the Department of Chemistry

Eastern Michigan University

in partial fulfillment of the requirements

for the degree of

MASTER OF SCIENCE

in

Chemistry

Thesis Committee:

Cory Emal, PhD, Chair

Arthur Howard, PhD

Deborah Heyl-Clegg, PhD

July 12, 2010

Ypsilanti, Michigan

ACKNOWLEDGEMENTS

I would like to take this opportunity to thank my research advisor, Dr. Cory Emal, for his guidance, encouragement, understanding, and contagious positive attitude towards research that motivated me during my time here at Eastern Michigan University.

I would also like to thank the members of my thesis committee for the time they took to give me constructive criticism on numerous rough drafts of this work.

To those who financially maintained me during the course of my education including National Institute of Health, Eastern Michigan University, and my family, I thank you.

I also owe an undying debt of gratitude to Dr. Arthur Howard, Dr. Timothy Brewer, and Dr. Patrick Koehn for their commitment to teaching, their patience, and most importantly for the time they took to help me understand complicated concepts. Without them I would not have been able to achieve this level of education; thank you.

ABSTRACT

The inhibition of plasminogen activator inhibitor-1 (PAI-1) is anticipated to increase our understanding of various human ailments with which high levels of PAI-1 have been associated, including diabetes, stroke, and atherosclerosis. Previous accounts have reported the synthesis of inhibitors that bind to PAI-1 with a low affinity, inhibit the serpin plasma protein antithrombin III, and/or fail to inhibit PAI-1 when vitronectin, a cofactor of PAI-1 is present. The synthesis of small-molecule inhibitors of PAI-1 that improve upon these properties has been the main goal of this research. Research efforts focused on examining changes in inhibitor potency based on the manipulation of the inhibitors' architecture, with particular attention paid to the number and positioning of multiple polyphenolic groups. The refinement of these synthesized moieties into selective and highly active species has been achieved.

TABLE OF CONTENTS

Acknowledgements.....	ii
Abstract	iii
List of Tables	v
List of Figures.....	vi
Introduction and Background.....	1
Chapter 1: Effects of Linker Structure on Inhibitor Potency	33
Background and Objectives.....	33
Results.....	43
Experimental.....	47
Chapter 2: Effects of the Central Sugar and Number of Gallates on Inhibitor Potency.....	66
Background and Objectives.....	66
Results.....	74
Experimental.....	78
Chapter 3: Effects of Gallate Ring Substitution Pattern on Inhibitor Potency.....	90
Background and Objectives.....	90
Results.....	98
Experimental.....	103
Chapter 4: Introduction of Carbamates into PAI-1 Inhibitors	126
Background and Objectives.....	126
Results.....	136
Experimental.....	145
Conclusions and Future Directions.....	183
References	191

LIST OF TABLES

<u>Table</u>		<u>Page</u>
1	Cyclic Linkers.....	39
2	Amide Linkers.....	41
3	Biological Assay Results for Cyclic Linkers.....	44
4	Biological Assay Results for Amide Linkers.....	45
5	Gallotannin Variants.....	68
6	Different Sugar-Centered Molecules.....	72
7	Biological Assay Results: Modifying the Number of Gallates.....	75
8	Biological Assay Results: Modifying the Sugar Center.....	76
9	Ethylene Glycol-Linked Polyphenols.....	96
10	Biological Assay Results: Modifying the Number/Position of Hydroxy Substituents.....	99
11	Carbamate-Based (and Related) Inhibitors.....	131
12	Sulfonamide/Sulfonimide-Based Inhibitors	134
13	Biological Assay Results: Carbamate-Based Inhibitors.....	137
14	Biological Assay Results: Sulfonamide-Based Inhibitors.....	138

LIST OF FIGURES

<u>Figure</u>		<u>Page</u>
1	Processes Composing the Coagulation Cascade and Fibrinolysis.....	1
2	Fibrinolysis.....	3
3	3-D Structure of Human Plasminogen Activator Inhibitor-1 (PDB)	4
4	Position of the PAI-1 gene within a <i>Homo sapiens</i> chromosome 7.....	5
5	Conformational Changes Undergone by PAI-1.....	7
6	Differentiation between the Native and Latent PAI-1 Forms.....	9
7	The Two Domains that Compose PAI-1.....	10
8	PAI-1's Secondary Structure Aligned with its Sequence.....	11
9	Ascofuranone.....	12
10	PAI-749.....	14
11	Schematic Representation of a Heterodimer PAI-1 Inhibitor.....	15
12	Various Published Small Molecule Inhibitors of PAI-1.....	18
13	Arylsulfonimide.....	20
14	Tiplaxtinin.....	21
15	Tannic Acid.....	24
16	Gallic Acid and Bisgallate Molecule.....	25
17	Equation Determining Percent Change in PAI-1 Activity within the Assay System.....	26
18	VAST Alignment of PEDF and PAI-1.....	31
19	Heparin.....	32
20	Tannic Acid, Gallate, and Digallate Groups.....	34
21	General Reaction Scheme for the Amide and Ester-linked Inhibitors.....	35
22	Equation to Determine the Number of Possible Conformational Structures ...	37

23	Tannic Acid.....	70
24	General Reaction Scheme for the Ethylene Glycol-linked Bisgallate Derivatives.....	94
25	Intramolecular Hydrogen Bonding on An Inhibitor.....	100
26	Prontosil.....	127
27	Pymol 3-D Model of PAI-1 with 4 Bound Inhibitory Molecules.....	129
28	General Reaction Scheme for the Carbamates.....	133
29	Possible Silicon-Based Inhibitors.....	188

Introduction

Fibrinolysis is the process that allows for the breakdown of thrombi, or blood clots, within the human body. The coagulation cascade is activated at the site of a tissue injury and results in the formation of thrombi, which are then broken apart by the fibrinolytic process (Figure 1).

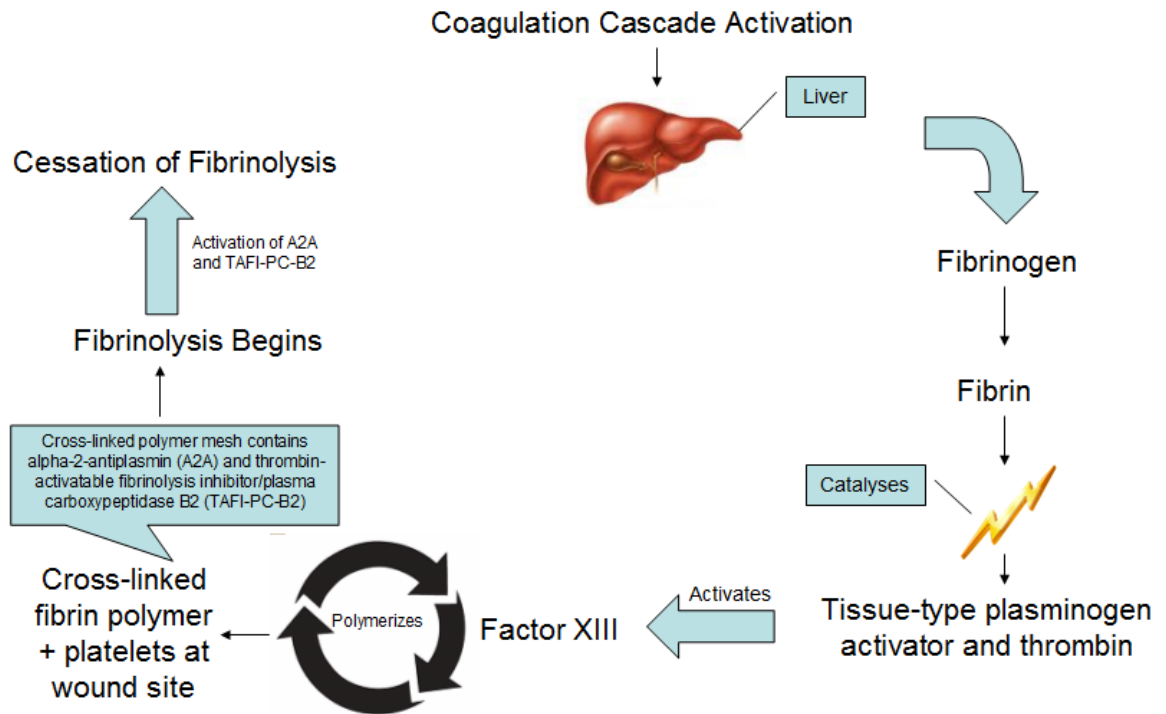


Figure 1: Processes Composing the Coagulation Cascade and Fibrinolysis.

Initially the activation of the coagulation cascade prompts the production of fibrinogen by the liver. Next, fibrin is formed from the liver-produced protein fibrinogen. Fibrin, a fibrous

protein, catalyzes tissue-type plasminogen activator and thrombin, which in turn activates Factor XIII.¹ Then Factor XIII polymerizes fibrin into a cross-linked polymer at a wound and interacts with platelets to form a net-like layer of protein that inhibits bleeding. Two other components are incorporated into the cross-linked structure, alpha-2-antiplasmin and thrombin-activatable fibrinolysis inhibitor/plasma carboxypeptidase B2.² Alpha-2-antiplasmin is a serine protease inhibitor whose main function involves the inhibition of plasmin. The end result of plasmin inhibition is the inhibition of fibrinolysis. Thrombin-activatable fibrinolysis inhibitor is a plasma zymogen that is converted into carboxypeptidase B2 upon interaction with the thrombin-thrombomodulin complex; it is this end product that also acts to inhibit fibrinolysis. The trapping of these active components into the mesh temporarily inhibits their behavior, which allows for them to become activated during fibrinolysis when the mesh is broken down and they are freed.³ Their activation allows for the cessation of the fibrinolytic process.

While the clotting process plays an important physiological role in wound healing, it also can lead to the formation of clots within blood vessels. These clots inhibit blood flow, and hence strokes and heart attacks can result. Therefore, understanding the process of fibrinolysis and developing a means by which to control this process is of interest as a means of preventing heart attacks and strokes by manipulating our ability to break down blood clots. One route available to achieve this goal involves understanding and developing a method for inhibiting either of the two components: alpha-2-antiplasmin and thrombin-activatable fibrinolysis inhibitor/plasma carboxypeptidase B2 (whose active forms both inhibit fibrinolysis) or to understand and develop a method of inhibiting the necessary precursors of these two components. Our research efforts focused on synthesizing an inhibitor for the inhibition of the latter.

Plasminogen is the inactive form of plasmin that is produced in the liver. The serpin plasminogen activator inhibitor-1 (PAI-1) inhibits urokinase plasminogen activator (uPA) and tissue-type plasminogen activator (tPA),⁴ which are the serine proteases that typically activate plasminogen. The activation of plasminogen by conversion into its active form, plasmin, is necessary to fibrinolysis.⁴ Figure 2 is a depiction of the complex interactions of the members of the fibrinolysis pathway. High levels of PAI-1 have been associated with diabetes, stroke, and atherosclerosis. The goal of this research is to develop small molecules that inhibit a natural inhibitor of fibrinolysis and to better understand the structural requirements for potent and selective inhibition of PAI-1.

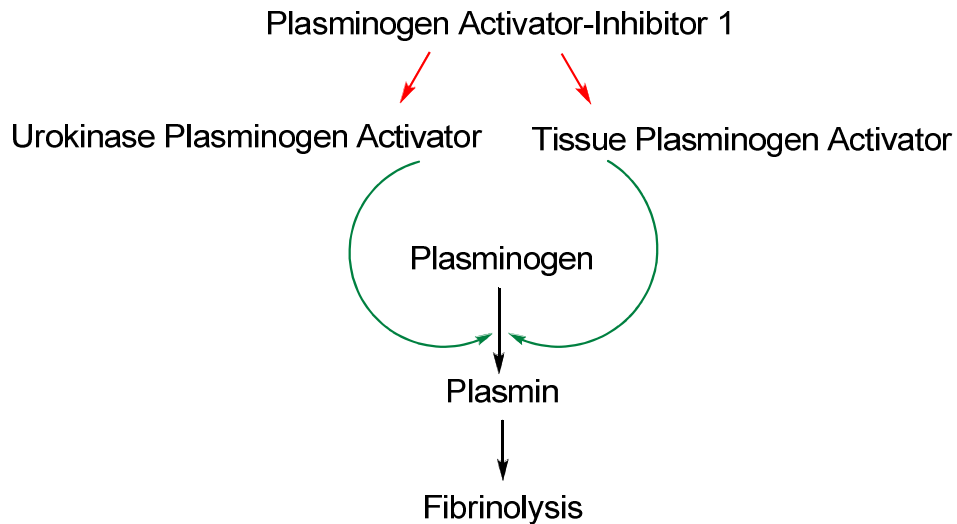


Figure 2: Fibrinolysis.

Green arrows indicate a stimulatory effect, and red arrows indicate an inhibitory effect.

Attempting to inhibit PAI-1 and return high levels of PAI-1 to normalcy has become a point of interest for several researchers.^{4, 19, 34, 35, 39, 40, 41, 29, 39} A thorough understanding of the protein and gene that codes for it is necessary.

Serpins are high molecular weight proteins whose name is derived from SERine Proteinase Inhibitors that belong to the MEROPS inhibitor family I-4 within clade E.^{5,10} Serpins are involved in blood coagulation⁶, diabetes⁷, fibrinolysis⁸, angiogenesis⁹, and inflammation.¹⁰ These serpins exist in both extra- and intra-cellular forms and are found in all taxonomic groups of organisms.¹²

PAI-1 is a member of the serpin super family. Figure 3 illustrates the 3-D structure of the protein.

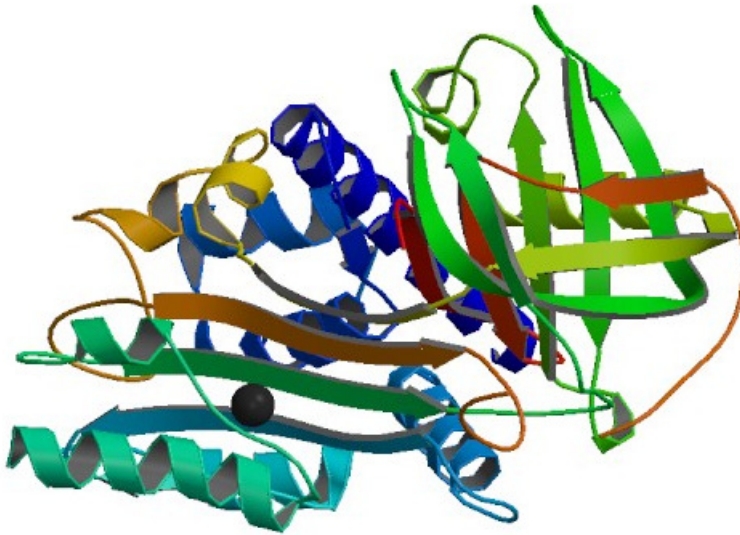


Figure 3: 3-D Structure of Human Plasminogen Activator Inhibitor-1 (PDB). Protein Databank (PDB)¹¹

A pool of information has been gathered concerning the gene and protein, PAI-1. A thorough examination of the information contained within various protein databases concerning the PAI-1 gene and protein has become relevant to this study because of the possibility of finding supporting evidence for the existence of homology between PAI-1 and other proteins. If homology exists between proteins for the active sites of PAI-1 and if other inhibitors have already been found to be successfully synthesized for these homologous active sites, then this

could lead to a breakthrough for the determination of PAI-1 inhibitors. Putative homologs of PAI-1 exist in *pan troglodytes*, *canis lupus familiaris*, *bos Taurus*, *mus musculus*, *rattus norvegicus*, *danio reno*, and *anopheles gambiae*.¹² Alternatively spliced transcript variants encoding different isoforms have been found for this gene.¹³

PAI-1 is a glycoprotein composed of 402 amino acids.²² The gene that encodes for this unique 45 kDa protein is located on chromosome 7 in exon 9 and is composed of 1858 base pairs.¹² The sequencing for the PAI-1 gene [SERPINE1] is considered to be complete.⁵ The gene has been included in the consensus coding sequence (CCDS) project, which consists of an international effort to identify common protein-coding gene sets between human genes and mouse genes. This effort has been undertaken due to the quantity of testing that is commonly done on mice regarding pre-market medicines. The CCDS has resulted in databanks that contain detailed annotated information regarding the gene and protein of PAI-1. Each CCDS gene has been given an identification number of which PAI-1's is CCDS5711.¹⁴ The location of the gene on chromosome 7 is illustrated in Figure 4.

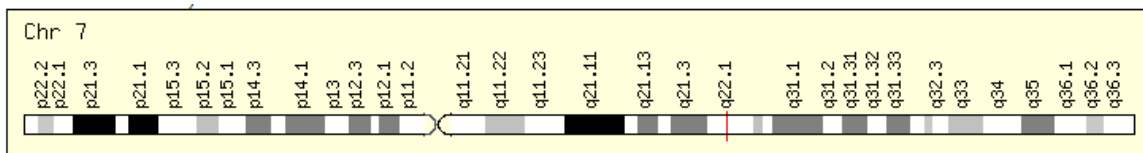


Figure 4: Position of the PAI-1 gene within a *Homo sapiens* chromosome 7.

The red line in the illustration details the position of the PAI-1 gene within the chromosome structure at site q22.1.

The PAI-1 gene has been implicated in two diseases. The first is from a defect in the gene that leads to PAI-1 deficiency and is characterized by abnormal bleeding.¹⁵ Excessive PAI-

1 inhibition, another form of PAI-1 deficiency, could be a cause for a decreased ability of the body to heal wounds.⁶ Serpinopathies, or diseases characterized by the accumulation of serpins, have been noted to result in thrombophilia, which is an autosomal dominant disorder.¹⁶

However, the mechanism by which PAI-1 operates within the body to cause inhibition of tPA and uPA does not occur at the genomic level. It is only the post-translational modification of the gene product that allows for the structure to be inactivated by uPA and tPA; uPA and tPA each utilize a proteolytic attack mechanism that cleaves the 369-Arg-|-Met-370 bond of PAI-1.⁵ To explore this concept further, a look into the shape and nature of the metastable protein should be undertaken.

Serpins are known to be metastable proteins, which indicate that they exist as active-state proteins that interact irreversibly with their appropriate substrate via a conformational change.¹⁷ Figure 5-(d) details this change and illustrates the suicide-like mechanism (irreversibility of the pathway results in inactivation of the serpin) that is characteristic of the serpin family's inhibition of their targets.¹⁸

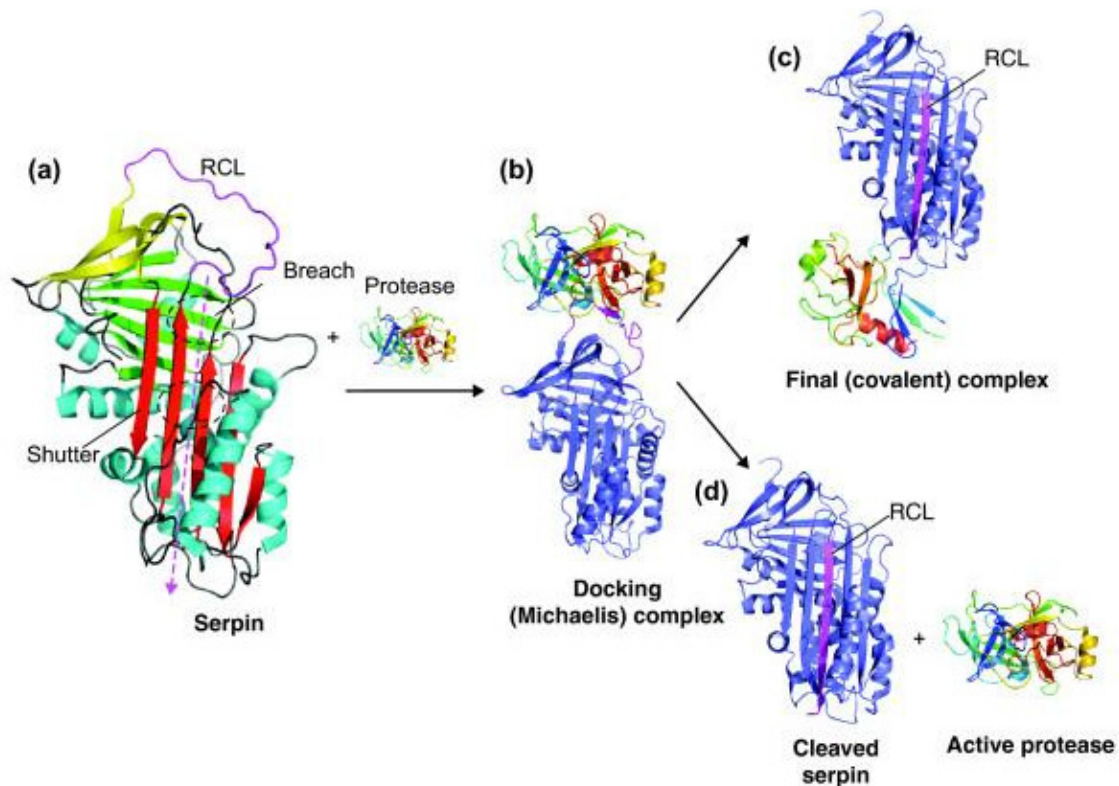


Figure 5: Conformational Changes Undergone by PAI-1.²⁴

(a): Unattached active PAI-1 (b): The RCL of PAI-1 bound to protease (c): Final covalent PAI-1 complex (d): Cleaved inactive PAI-1 form and unattached active protease.

The reactive center loop (RCL) appears in the active configuration of the serpin (Figure 5-a). In this state it appears as a more freely moving strand within the entire protein 3-D structure. The RCL is depicted in Figure 5-c/d inserted into the β -sheet A, and it is this conformation of the RCL that occurs when the serpin is in its inactive state.¹⁹ The catalytic serine residue of the protease attacks the RCL and severs the loop at the C-terminal residue, covalently linking the N-terminal residue via an ester bond to the protease serine. It is at this point that the serpin undergoes a significant conformational change that results in the newly attached protease/N-terminal RCL becoming inserted into the β -sheet A. This binds the

previously freely moving RCL and essentially crushes it within the serpin body, blocking its ability to interact with any other copies of protease.²⁰

Annotations within the database of the pair-wise sequence alignment program BLAST include the information that the inactive form of PAI-1 is more stable than the active form by 9 kcal.²¹ PAI-1's active state is unusually unstable in that it has a half-life of approximately 2 hours, upon which it spontaneously converts to its latent/inactive form (Figure 6).²² Latent state conversions have also been observed due to physiological pH and temperature changes. It was also determined that anionic halide ions may play a role in the active-to-latent structural transition.²² The cleaved form usually is encountered either free or complexed with its target proteinase.¹² The RCL is found in the C-terminal portion of these proteins.¹⁰ Following proteolytic cleavage the RCL is incorporated into the 5 A β -sheet as strand 4 A and acts as a "pseudosubstrate," locking the protein into an inactive state and prohibiting the completion of its catalytic cycle.²³

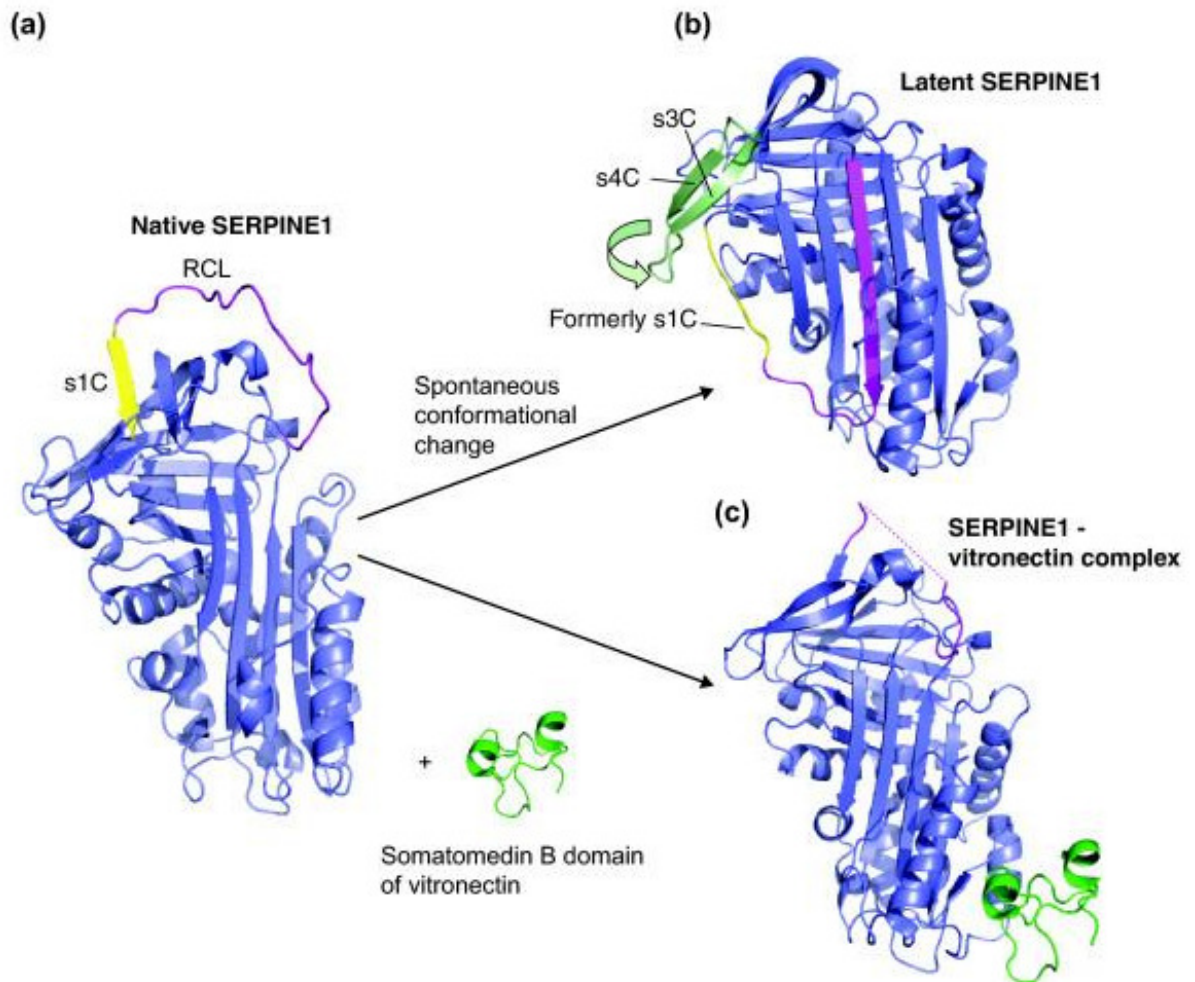


Figure 6: Differentiation between the Native and Latent PAI-1 Forms.

The spontaneous conformational change that occurs in the native PAI-1 serpin allows PAI-1 to change into the latent form. The serpin's interaction with vitronectin locks the protein into its active form.²⁴

Within *Homo sapiens* the PAI-1 protein comprises 2% of the total protein within the organism.¹⁰

Other members of the serpin family within humans include angiotensinogen, corticosteroid-binding globulin, and thyroxin-binding globulin.¹⁰

A more complete grasp of the interactions that PAI-1 is capable of can be achieved by examining the complexity of the protein structure and evaluating how its interactions differ at its

various localizations, as it is found in plasma, blood platelets, endothelial tissue, hepatoma, and fibro-sarcoma cells.²²

In plasma, PAI-1 is commonly observed complexed with vitronectin, a naturally occurring protein.²⁵ Figure 7 illustrates the two main domains that comprise the PAI-1 serpin. Each domain of the serpin is composed of different numbers and types of secondary structures. The domains are architecturally comprised of a roll and a 2-layer sandwich.²⁶

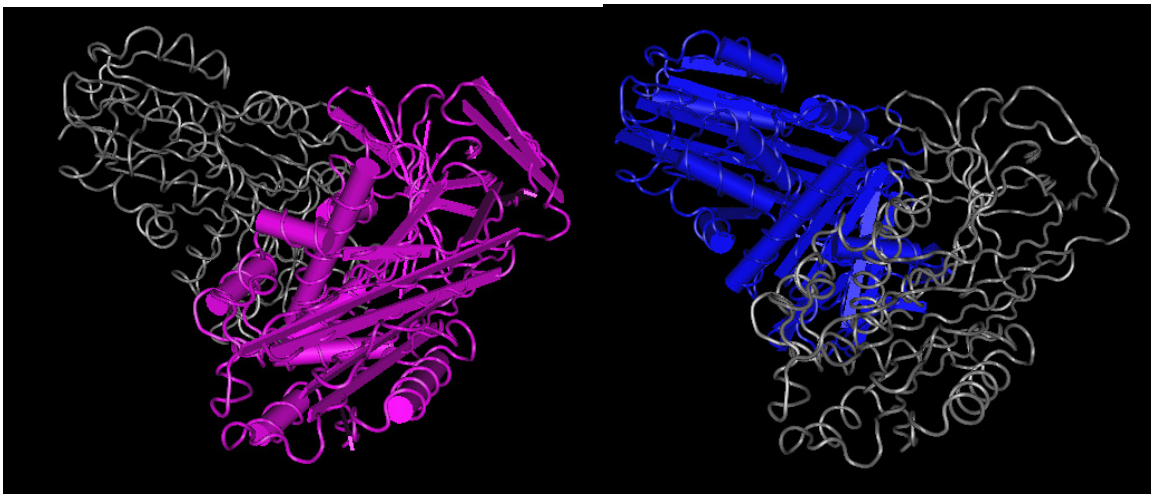


Figure 7: The Two Domains that Compose PAI-1.

Sequence A is the purple part of the 3-D structure on the left; while Sequence B is shown in blue on the right.²⁶

Local inter-residue hydrogen bonding or the lack of this hydrogen bonding is the main feature responsible for the unique secondary structure of proteins. In total the secondary structures that comprise the PAI-1 serpin consist of 3 sheets, 1 beta alpha beta unit, 6 beta hairpins, 1 psi loop, 6 beta bulges, 16 strands, 12 helices, 15 helix-helix units, 30 beta turns, and 30 gamma turns.²⁷ The percent makeup of the secondary structure can be described as 140 residues (37%) composing the strands of PAI-1, 104 residues (27.6%) composing the alpha helices, 9 residues (2.4%) composing 3-10 of the remaining helices, and 124 residues (32.9%)

composing other secondary structural features within the serpin. It is the unique 3-D structure of this serpin which is responsible for its different functional attributes within an organism.

Each of the 402 PAI-1 amino acids have been identified in their role in composing the secondary structure of the serpin. The secondary structure aligned with its sequence is illustrated in Figure 8.²⁷

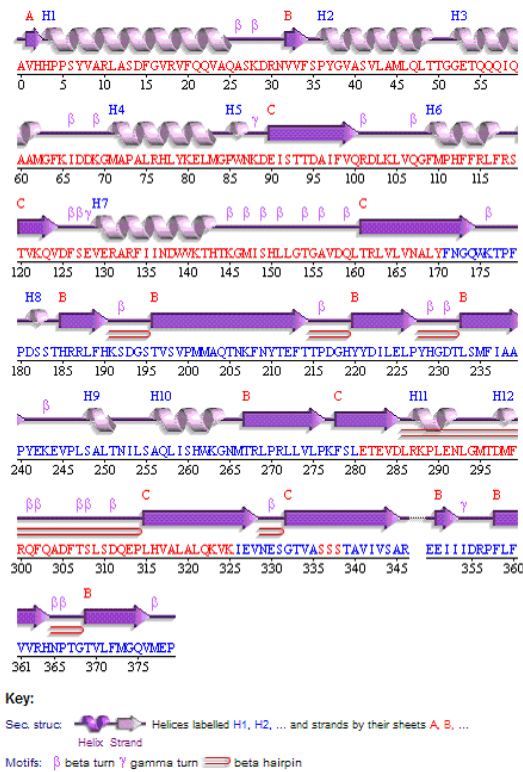


Figure 8: PAI-1's Secondary Structure Aligned with its Sequence.²⁷

Several mechanisms have been implicated in increasing the levels of PAI-1 within *Homo sapiens*. Nox4-produced reactive oxygen species, resulting from the activation of the p38 MAPK/Smads pathway, have been reported to result in the increased expression of PAI-1 by endothelial cells.²⁸ Another route that reportedly results in increased levels of PAI-1 implicates the transforming growth factor (TGF)- β . (TGF)- β is a profibrotic cytokine that up-regulates

PAI-1 by binding to the CAGA box of the PAI-1 promoter region of the PAI-1 gene.²⁹ The corticosteroid aldosterone works in concert with the above pathway by increasing the levels of (TGF)- β , which then consequently leads to increased PAI-1 levels.³⁰ Another style of PAI-1 promotion works via small molecules. The antibiotics 13-deoxytedanolide and anisomycin promote the expression of the PAI-1 gene at nano-molar concentrations via the ribotoxic stress response pathway.³¹

To counteract routes of increased PAI-1 expression, multiple methods of inhibition have been explored. Four noteworthy methods have been utilized to inhibit the PAI-1 protein. These methods focus on the inhibition of the transcription of the gene,²⁹ the synthesis of a protein to substitute for the RLC of PAI-1,¹⁹ the destruction of the tPA/PAI-1 complex via a neutralization method of inhibition,³² and the inhibition of the protein by antibodies.³³

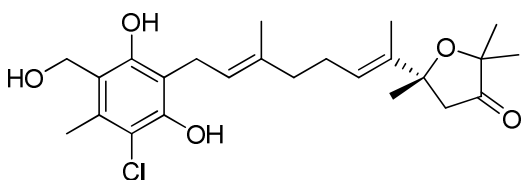


Figure 9: Ascofuranone.

Ascofuranone (Figure 9) inhibits PAI-1 by an inhibitory route that focuses on inhibition of expression of the PAI-1 gene.²⁹ The molecule inhibits the phosphorylation of epidermal growth factor receptor (EGFR) and downstream kinases. PAI-1 gene expression is suppressed along with the suppression of the kinase inhibitors. Also, ascofuranone has been linked to the suppression of metalloproteinase activity, which leads to a suppression of PAI-1 gene

transcription.²⁹ While this method focuses on the expression of the PAI-1 gene and therefore is suppressing the origin of the PAI-1-in-excess problem, its inability to selectively inhibit PAI-1 levels leads to complications if suppression of the other factors involved is concluded to be undesirable and lead to negative health effects in their own right.

The second unique inhibition method focuses on the inhibition of PAI-1 by utilizing a protein with an amino acid sequence that corresponds to that of the RCL of the serpin.¹⁹ The peptide is 14 amino acids in length and specifically corresponds to the RCL amino acid positions 333-346. The hypothesis behind this inhibition method was that a synthetic, free-flowing RCL that could theoretically be made to have an artificially high concentration within the system compared to the serpin/RCL 1:1 ratio would be able to inhibit the serpin more effectively by insertion of the synthetic RCL into the β -sheet A, thus forcing the protein into its inactive form. While the inhibition of PAI-1 was effective in the absence of vitronectin, a marked decrease in its inhibitory potency was noticed in the presence of vitronectin.¹⁹ The inability of a potential inhibitor to inhibit PAI-1 in the presence of vitronectin is a bad omen of the inhibitor's potential effectiveness, because vitronectin is a cell adhesion protein that exists in high effective concentrations within the human body and has a high binding affinity to PAI-1. Thus, the effectiveness of the inhibitor in a whole animal system is limited.

PAI-1 controls the activation of tPA by the initial formation of a sodium dodecyl sulfate-stable complex.³⁴ Gardell and coworkers focused on neutralizing this interaction by designing an inhibitory molecule (PAI-749, Figure 10) whose purpose was to destroy this complex by promoting the polymerization of PAI-1.²⁵

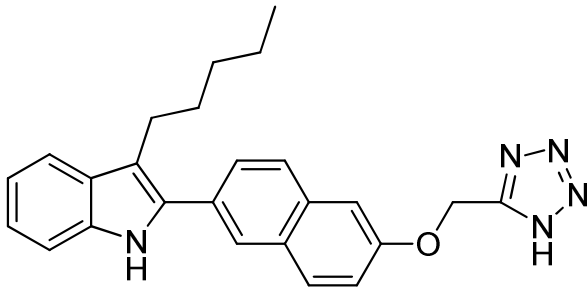


Figure 10: PAI-749.

The largest drawback to this inhibitory method was noticed when researchers pretreated the assay system with vitronectin. In this instance inhibition by PAI-749 was virtually eliminated by the addition of vitronectin.

Develtare and coworkers reported an approach to PAI-1 inhibition by using a synthetic heterodimer body (diabody) that consisted of two connected antibodies composed of the single chain variable fragment (scFv), which is a monovalent antibody fragment (Figure 11).³⁵

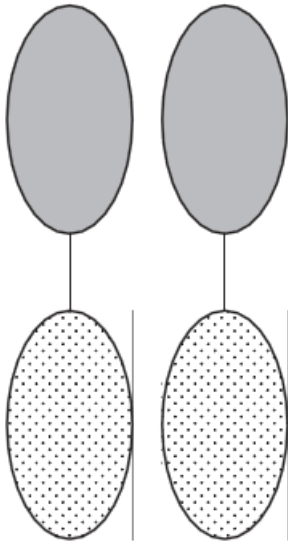


Figure 11: Schematic Representation of a Heterodimer PAI-1 Inhibitor.³⁵

The difference in shading represents the different regions of specificity. The separation of these regions by a linker that disallows interaction is what promotes the formation of the bi-specificity of the antibody.

However, the major drawback with this technique is its lack of inhibitory specificity. The diabody inhibits not only PAI-1, but also a zymogen known as thrombin-activatable fibrinolysis inhibitor (TAFI). TAFI operates to decrease the rate of plasmin generation and therefore the inhibition of it in concurrence with the inhibition of PAI-1 would effectively result in an increase in fibrinolysis. While the overall effect is the desired effect, it is worthwhile to create a specific inhibitor of PAI-1 to eliminate the potential of undesirable and unknown side effects. With this in mind, researchers have developed a series of small-molecule inhibitors of PAI-1 with a drive toward specificity of their inhibitory pathway.

The complex structure that the PAI-1 gene codes for has the potential to possess several binding sites for a wide variety of inhibitory molecules. Several previous research efforts have

reported the synthesis of small-molecule inhibitors of PAI-1.^{4, 40, 41, 29, 40, 39} By examining reported progress concerning the synthesis of effective and ineffective PAI-1 inhibitory molecules, the information gained can be drawn upon to modify and potentially improve our own attempts and the attempts of future synthetic research pathways.

Research focusing on the synthesis of small-molecule inhibitors for PAI-1 was reported by Miyazaki and coworkers.³⁶ A butadiene-imide series of molecules was tested for inhibition against the production of PAI-1; an example of a molecule in this series is illustrated in Figure 12-1.³⁶ This species strongly inhibited anti-thrombin III (ATIII). ATIII is a serpin plasma protein closely related to PAI-1 that inactivates thrombin and plasmin. Therefore, an inhibitor that inhibits ATIII would also lead to an increase in fibrinolysis, but through a separate mechanism than the one we are attempting to follow in this research effort. Therefore, while the overall goal of inhibiting an inhibitor of the fibrinolysis pathway would be achieved, the goal of developing an inhibitor specific for PAI-1 would not be achieved, as this class of inhibitor has an affinity for multiple serpins. This also leads to higher IC₅₀ measurements of the inhibitor due to competitive inhibition effects.³⁶

In an attempt to synthesize a more selective inhibitor, the Miyazaki group reported the synthesis of a set of inhibitors composed of furan-2-one and pyrrolin-2-one derivatives.⁴ The furan-2-one compounds were determined to be biologically unstable due to the α,β -unsaturated lactone ring. Therefore, only the pyrrolin-2-one compounds were evaluated in a rat arterial thrombosis model. The molecule illustrated in Figure 12-2 was highlighted in the paper as having good selectivity for PAI-1 because it showed no inhibition of thrombin, plasmin, trypsin, antithrombin III, antiplasmin, or antitrypsin at 30 μ M. This inhibitor also was reported as having a strong level of inhibition in comparison to their other synthesized inhibitors. The inhibitor activity was reported as an IC₅₀-value of 9.6 μ M.⁴ A molecules' efficacy in *ex vivo*

plasma establishes a measure of inhibition known as the IC₅₀ value. The IC₅₀-value is a measure of the effectiveness of a compound, at a 50% inhibitory concentration, toward the aim of inhibiting a biological or a biochemical function.³⁷ Within this reported series, even their strongest inhibitor did not result in the inhibition of PAI-1 below the micro-molar range.

Miyazaki and coworkers reported in 2010 their results on *in vivo* studies of synthesized inhibitors which were a series of 1,4-diphenylbutadiene derivatives.³⁸ They accomplished the synthesis of an orally active inhibitor of PAI-1 production (Figure 12-3).

The Miyazaki group is continuing its efforts toward more fully evaluating the antithrombic effects of their new class of 1,4-diphenylbutadiene inhibitors. They are also working to develop more efficient synthetic techniques for large scale synthesis of their reported inhibitors.

However, both butadiene series of inhibitors focused on the inhibition of the production of PAI-1 versus the direct inhibition of the serpin.

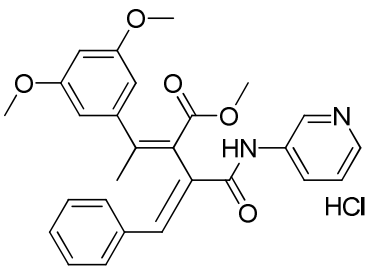
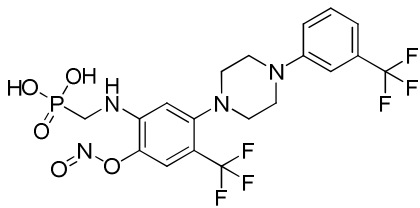
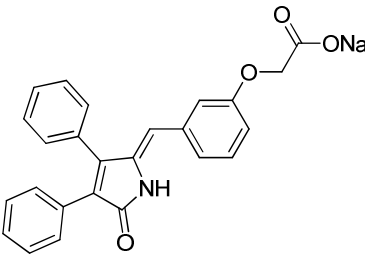
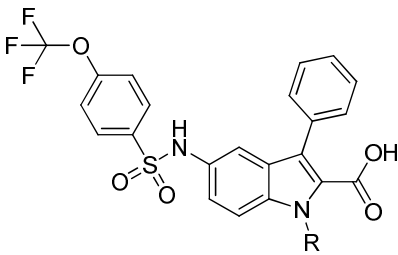
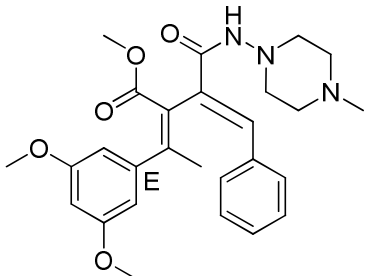
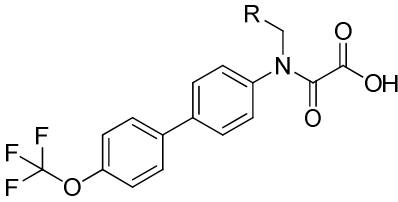
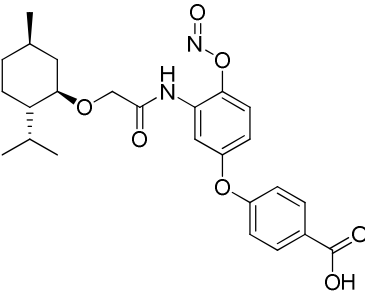
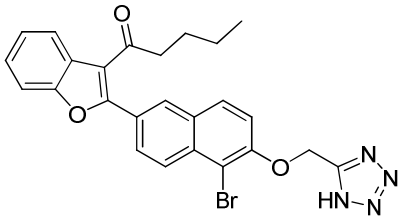
Entry	Inhibitor	Entry	Inhibitor
1		5	
2		6	
3		7	
4		8	

Figure 12: Various Published Small Molecule Inhibitors of PAI-1.

Bin and coworkers focused on synthesizing a series of small molecule inhibitors which would directly inhibit PAI-1 exclusively. They synthesized a series of menthol-based inhibitors that had a strong effect on the activity of PAI-1 ($IC_{50} = 0.38 \mu\text{M}$).³⁹ However, drawbacks associated with this series of molecules include poor solubility and low bioavailability, hence limiting their use as potential drugs.³⁹ One of the molecules in this study is illustrated in Figure 12-4.

The same research group reported a series of piperazine-based derivatives, intending to mitigate this set of drawbacks (poor solubility of the molecules and low bioavailability).³⁹ An example of a molecule from this series is illustrated in Figure 12-5.³⁹ Their efforts resulted in a potent inhibitor ($IC_{50} = 0.01 \mu\text{M}$) and improved bioavailability, solubility, and selectivity over the previous series of inhibitors.

In 2005 researchers working at Wyeth Research Labs in Collegeville, Pennsylvania, had synthesized a series of PAI-1 inhibitors.⁴⁰ They recognized that several effective PAI-1 inhibitors (at the micromolar level) from those past synthetic attempts had a structural commonality. These previous PAI-1 inhibitors included naphthyl benzofuran, 3-indole oxoacetic acid, and oxadiazolidinedione.⁴⁰ The structural feature that they all shared was either a carboxylic acid group or an acid bioisostere attached to a lipophilic aromatic ring scaffold. This group then focused on that structural feature as a lead to the design of a series of 2-indole carboxylic acid-based derivatives (Figure 12-6). This series was tested for inhibition against PAI-1; however, their most potent potential synthetic inhibitor did not reach an IC_{50} -value below the micromolar level.⁴⁰

A series of oxalamide derivatives was tested for inhibition against PAI-1.⁴¹ An example of a molecule in this series is illustrated in Figure 12-7. The oxalamide derivatives resulted in inhibitors with IC_{50} -values no better than a low micromolar inhibition of PAI-1 (IC_{50} range =

non-detectable – 4.5 μM). The authors noted that the addition of electron withdrawing groups (trifluoromethyl) to the oxalamide derivatives resulted in an increase in inhibitor potency. It was also observed that the introduction of a sulfonamide spacer between two phenyl rings did not result in a change in the potency of the inhibitor.⁴¹

A series of 2-aryl-3-acyl-benzofuran derivatives was tested for inhibition against PAI-1.⁴² The molecule in Figure 12-8 is unique in that it was synthesized by utilizing a Suzuki coupling reaction between benzofuran or benzothiophene boronic acids and dibromo substituted naphthalenes.⁴² This series also failed to inhibit PAI-1 below a low micromolar level ($\text{IC}_{50} = 5.0 \mu\text{M}$).

In 2010 El-Ayache, a member of our Eastern Michigan University-based research group, synthesized and reported a novel series of arylsulfonimide and bis-arylsulfonamide PAI-1 inhibitors.⁴³

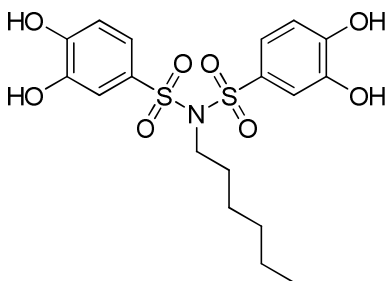


Figure 13: Arylsulfonimide.

These research efforts resulted in the hypothesis that short linking units between the sulfonyl moieties and a 3,4-dihydroxy aryl substitution pattern resulted in the highest degree of PAI-1 inhibition within the series and the lowest degree of ATIII inhibition. The highlighted molecule within this report exhibited an inhibition of PAI-1 at an IC_{50} -level of 0.284 μM and a

reported ATIII inhibition level which exceeded 300 μM (Figure 13).⁴³ Therefore, these research efforts resulted in the first reported non-naturally occurring PAI-1 inhibitor which was highly selective for PAI-1.

Most known natural and synthesized inhibitors of PAI-1 have the negative aspects of either binding with a low affinity to PAI-1 or not inactivating PAI-1 in the presence of its cofactor, vitronectin.⁴⁴ Successful attempts to define the binding sites of these previous inhibitors to PAI-1 via crystal structures have not been reported to date in the literature.

PAI-1 has been hypothesized to play a role in cell movement. Researchers studying this concept noted that tiplaxtinin inhibited PAI-1 with a low micromolar potency.⁹ The structure of the tiplaxtinin molecule is illustrated in Figure 14.

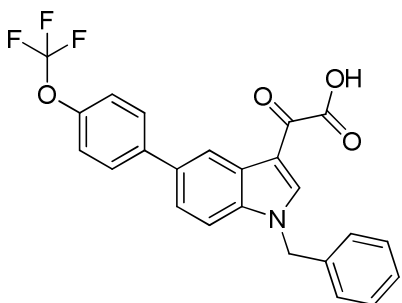


Figure 14: Tiplaxtinin.

However, tiplaxtinin has also been observed to be incapable of inhibiting PAI-1 in the presence of vitronectin and even in the absence of vitronectin, tiplaxtinin shows a low affinity for PAI-1.⁴⁴ At the University of Michigan Medical School, Daniel Lawrence, in conjunction with the Center for Chemical Genomics (CCG), conducted spectral library screens on the MicroSource SPECTRUM compound library, looking for molecules that have a high affinity for PAI-1 and could be modified to be possible PAI-1 inhibitors.⁴⁴ The PAI-1 activity assay was

developed to screen for compounds with anti-PAI-1 activity in the library compound collection. This collection consists of known drugs, compounds approved for agricultural use, natural products, and other bioactive compounds. A chromogenic assay was used with a 2:1 molar ratio of PAI-1 to uPA. uPA was selected because it is considerably more active toward low molecular weight substrates than is tPA, allowing for lower concentrations of uPA and PAI-1 in this screen (5 nM uPA and 10 nM PAI-1). The screen was performed in 384-well microtiter plates in the CCG lab as follows: recombinant active human PAI-1 (final 10 nM) was incubated for 60 minutes at room temperature either with or without 10 μ M of each compound, uPA was added (final 5 nM) to each reaction well, and incubation continued for an additional 30 minutes at room temperature. Residual uPA activity in each reaction mixture was then determined with pGlu-Gly-Arg p-nitroanilide chromogenic substrate (Sigma) (final 0.25 mM) measured spectrophotometrically at 405 nm after 60 minutes.

Compounds that inactivated PAI-1 were identified by the restoration of uPA activity. The extent of uPA activity restoration was determined by comparing each drug-containing sample to wells with untreated PAI-1 (100% PAI-1 activity) and to wells with uPA only (0% PAI-1 activity). The data from this screen were then uploaded to the CCG informatics system, and positive hits were identified as any compound that increased uPA activity by more than 3 standard deviations above control and compound wells on each plate. Using these selection criteria, the primary screen of 32,000 compounds yielded an initial total of 23 compounds deemed positive hits. Each of these hits was then re-assayed (in duplicate by the CCG) by dose response testing using the same chromogenic assay with the compounds at the following concentrations: 0.1, 0.32, 1, 3.2, 10, 32, and 100 μ M.

In this secondary analysis, 19 of the 23 compounds were deemed positive; however, 3 of these compounds were known to have significant toxicity and therefore were not analyzed

further. Samples of the 16 remaining compounds were then obtained from the CCG for further analysis in the Lawrence laboratory. These more detailed analyses first investigated whether each compound had intrinsic absorbance at 405 nm that would give false positive absorbance readings, or was not completely soluble in the assay buffer system used since insolubility and compound precipitation could likewise lead to false positive absorbance readings.

Each compound was also tested for its ability to directly block PAI-1 complex formation with uPA by SDS-PAGE analysis. For this latter analysis, each compound was incubated at 10 μ M with 1 μ g of hPAI-1 for 15 min at 23°C followed by the addition of 1 μ g of uPA for an additional 5 min at 37°C. Approximately half of the 16 compounds either had intrinsic absorbance at 405 nm or insolubility in the buffer system. Of the remaining compounds, 5 directly inhibited PAI-1 activity.

Tannic acid, a natural polyphenolic compound, was one of the molecules identified as a PAI-1 inhibitor. The structure of tannic acid is illustrated in Figure 15.

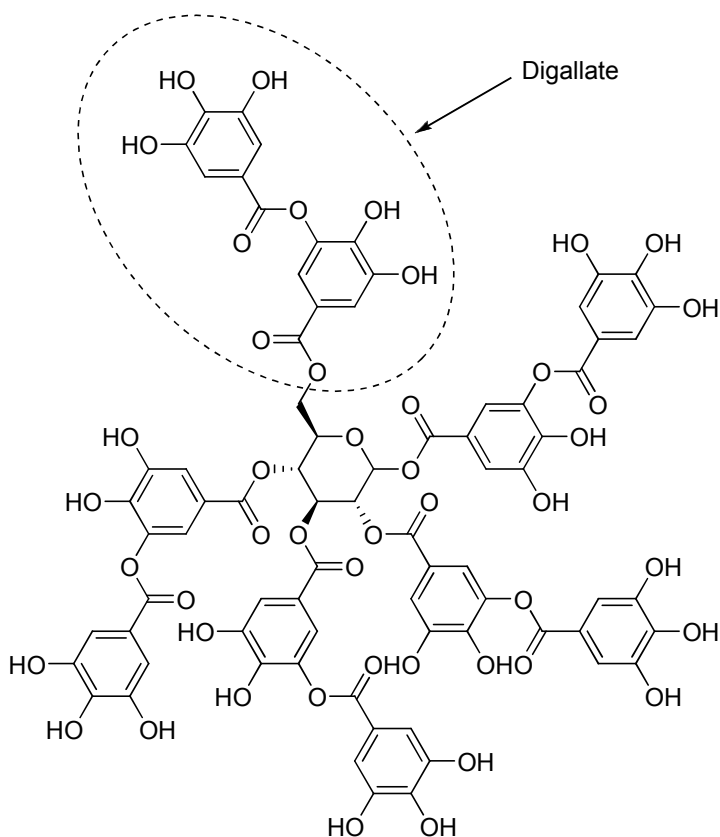


Figure 15: Tannic Acid.

Tannic acid is an effective PAI-1 inhibitor with an IC_{50} -value of 5 μM .

This initial screening process resulted in other molecules besides tannic acid that proved to be inhibitors of PAI-1; several shared a prominent similarity with tannic acid in that they were recognized to contain gallate (Figure 16) or digallate (Figure 15) groups. This recognition allowed for the focus of synthetic efforts on the production of various gallate and bisgallate (Figure 16) analogs.

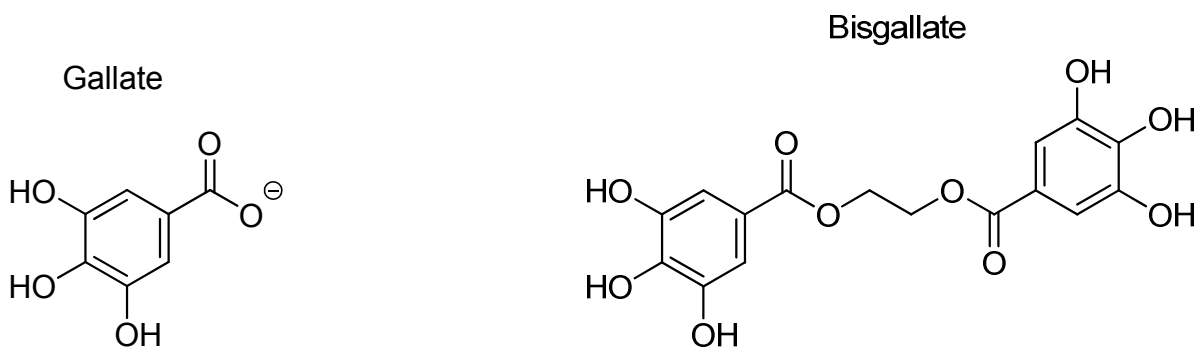


Figure 16: Gallate and Bisgallate Molecule.

The research efforts in the laboratory of Prof. Cory Emal focus on the synthesis of potential small-molecule inhibitors of PAI-1 and evaluation of their ability to inhibit PAI-1. The IC_{50} measurement indicates a measure of the degree of inhibition of the interaction between tPA and PAI-1; thus these values are truly a measure of residual tPA activity. Our efforts also focused on analyzing the IC_{50} s of our inhibitors within biological systems by observing the degree to which PAI-1 activity was blocked *in vivo* in mice.

The enzymatic assay systems utilized in this project, performed in the Lawrence laboratories, consisted of recombinant nonglycosylated or glycosylated active human PAI-1 (PAI-1 and PAI-1glyco, respectively) or recombinant murine PAI-1 (mPAI-1) incubated at 2 nM for 15 min at 23°C with increasing concentrations of each compound in an assay buffer (100 mM NaCl, 40 mM HEPES, pH 7.8, 0.005% Tween-20, 0.1% DMSO), followed by the addition of uPA (Molecular Innovations) or tPA (Genentech) to 3 nM and further incubation for 30 min at 23 °C. At each drug concentration, parallel control reactions without PAI-1 were assembled. Residual enzymatic activity was determined by addition of an equal volume of 100 μ M Z-Gly-Gly-Arg-AMC (Calbiochem) fluorogenic substrate for uPA or Pefafluor tPA (Centerchem) for tPA, and the rate of AMC release monitored at 23°C (Ex 370 nm and Em 440 nm). The percent change in PAI-1 activity was determined according to the equation shown in Figure 17.

$$\text{Percent Change in PAI-1 Activity} = [(E_i - P_i) / E_i] / [(E_0 - P_0) / E_0]$$

Figure 17: Equation Determining Percent Change in PAI-1 Activity within the Assay System.

Equation utilized to determine the percent change in PAI-1 activity within the assay system. Where E_i is the enzyme activity at drug concentration i ; P_i is the enzyme in the presence of PAI-1 at drug concentration i ; E_0 is the enzyme activity in the absence of drug; and P_0 is the enzyme activity in the presence of PAI-1 in the absence of drug.

The effect of the compounds on 2 nM ATIII in the presence of 3 U/ml heparin was also determined using 3 nM α -thrombin. The reactions were assembled as above except that 10% DMSO was included in the assay buffer to ensure compound solubility at the higher concentrations used. Residual α -thrombin activity was measured using an equal volume of 100 μ M benzoyl-Phe-Val-Arg-AMC (Calbiochem).

Surface Plasmon Resonance (SPR) analysis determined the direct binding of PAI-1 protein that had been treated with a vehicle or inhibitor to anhydrotrypsin (Molecular Innovations) and was monitored using a Biacore 2000 optical biosensor. Bovine anhydrotrypsin was immobilized to CM5 SPR chips at the levels of approximately 2000 response units (RU) in 10 mM sodium acetate, pH 5.0. The reference flow cell surface was left blank to serve as a control. Remaining binding sites were blocked by 1 M ethanolamine at pH 8.5. All binding reactions were performed in assay buffer. Then PAI-1 at 2 nM was incubated with the indicated concentrations of inhibitor in running buffer for at least 15 min at 23°C. Binding of PAI-1 to anhydrotrypsin was then monitored at 25°C at a flow rate of 30 μ l/min. for 2.5 min. followed by 2 min. of dissociation. Chip surfaces were regenerated with a 1 min pulse of 10 mM glycine, pH 1.5, followed by a 1 min wash of assay buffer. Injections were performed using Wizard Customized Application program in automated mode. Binding experiments were performed in duplicate and were corrected for background and bulk refractive index by subtraction of the

reference flow cell, and data analyzed with BIAevaluation 3.1 (Biacore) by linear fitting of the initial association phase. Compound-induced alterations in PAI-1 binding to anhydrotrypsin were determined by comparing the initial slopes of the association phases since there is a linear relationship between the slope and the concentration of available active PAI-1. These data were then fit to an exponential association equation to determine the apparent affinity between PAI-1 and compound.

The SDS-PAGE/Western blotting analysis was determined by utilizing human PAI-1 at 2 nM, which was then incubated with the indicated concentration of the compound for 15 min at 23°C in assay buffer, followed by 30 minutes of incubation with 3 nM uPA or tPA. Samples were analyzed via reducing SDS PAGE with 10% Tris-HCl gels (Bio-Rad) and transferred onto PVDF overnight. PAI-1 was then detected using polyclonal high titer sheep anti-human PAI-1 antibody (Molecular Innovations), HRP-conjugated donkey anti-sheep IgG (Jackson ImmunoResearch Laboratories), and Pierce ECL Western Blotting Substrate (Thermo Scientific).

The inhibition of mPAI-1 in *ex vivo* plasma was determined by utilizing murine PAI-1. Murine PAI-1 was added to PAI-1-depleted murine plasma (Molecular Innovations) at 5000 pg/ml. Ten microliters of increasing concentrations of compound in assay buffer containing 10% DMSO and 10 µl of mPAI 1-reconstituted plasma were incubated for 15 min at 23°C in a filter plate (Millipore), followed by the addition of 25 µl of SeroMAP beads (Luminex) coupled to uPA (2500 beads/well), and further incubated in the dark on a microtiter plate shaker for 2 h. The plate was vacuum washed 3X with wash buffer (PBS, 0.05% Tween-20, pH 7.4), 50 µl of PBS, 1% BSA, pH 7.4 and 50 µl of 4 µg/ml biotin-labeled rabbit anti-mPAI-1 (Molecular Innovations) were added to each well and the plate incubated at room temperature in the dark on a microtiter plate shaker for 1 h. After vacuum washing 3X, 50 µl of PBS, 1% BSA, pH 7.4

and 50 μ l of 4 μ g/ml streptavidin-Rphycoerythrin conjugate (Molecular Probes) were added to each well and incubated with shaking at 23°C for 30 min in the dark. After another 3X wash, 100 μ l of sheath fluid (Luminex) was added to each well, shaken for 5 min in dark at 23°C, and read on Luminex100 (Median setting, 50 μ l sample size, 100 events/bead). Mean Fluorescence Intensities (MFI) of unknown samples were converted to pg/ml base on a standard curve of mPAI-1 in mPAI-1-depleted plasma using a five-parameter regression formula (Masterplex QT v4.0, Miraibio).

The plasma enzymatic assay studies were carried out by utilizing citrated blood that was collected from the inferior vena cava (IVC) of C57Bl6J mice that were either PAI-1 null or vitronectin/PAI-1 null and plasma prepared by centrifugation (15 min at 1500 \times g). The plasma was treated with 10 μ g/ml Aprotinin (Roche) for 15 min at 23°C before reconstituting with 20 nM PAI-1. Plasma (10 μ l, with or without PAI-1) was placed in microtiter wells with 80 μ l of CDE-066 or PAI-039,⁴⁵ in assay buffer containing 10% DMSO and incubated for 15 min at 23°C, followed by addition of 10 μ l 25 nM uPA and further incubation for 30 min. Residual enzymatic activity was monitored as above using the fluorogenic uPA substrate, and PAI-1 activity was determined using the equation in Figure 17.

The inhibition of PAI-1 *in vivo* was determined by utilizing transgenic mice that were heterozygous for murine PAI-15 overexpression. These were weighed and then anesthetized with isoflurane for the duration of the experiment. The IVC was isolated, and 50 μ l of citrated blood was collected as pretreatment samples. The syringe was replaced with a syringe containing vehicle or CDE-066 (see Chapter 2) (in lactated Ringers), and 100 μ l was injected for doses of 3, 10, and 30 mg/kg. After 1 h, 300 μ l of citrated blood was collected via IVC, after which the mice were euthanized. Plasma was isolated by centrifugation at 1500 \times g for 15 minutes at 23°C. All animal experiments were approved by the Institutional Animal Care and Use Committee of

Unit for Laboratory Animal Medicine at the University of Michigan. To determine active murine PAI-1 levels in the plasma, 10 μ l of plasma, diluted in PAI-1-depleted murine plasma (Molecular Innovations), 10 μ l buffer (PBS, 1% BSA, pH 7.4) and 25 μ l of uPA-coupled SeroMAP beads were added to a filter plate and incubated with shaking overnight at 4°C in the dark, and the reactions analyzed as above in the *in vivo* plasma assay. Data were analyzed and IC₅₀-values calculated using Grafit 5. Apparent KD values for the binding of compounds to PAI-1 were determined using GraphPad Prism 4. Data from *in vivo* assays were analyzed for significance with a student's t-test using the 0 mg/kg CDE-066 treatment as the control group, with $p < 0.05$ considered significant.

The preceding analytical techniques were all conducted by researchers in the Lawrence laboratory at the University of Michigan Medical School, and while they were essential in determining the effectiveness of our synthetic inhibitors, the main focus of this report concerns the synthesis of the potential inhibitors and the level of inhibition of PAI-1 by these molecules. With that in mind, a focus on the synthetic pathways chosen during this synthetic effort needs to be examined.

There are several key branches to the synthetic directions that our research efforts underwent in an attempt to synthesize the optimal PAI-1 inhibitory molecule. Research efforts focused on examining a change in inhibitor potency based on the linker's properties, the number of gallate substituents, the gallate's substituent pattern, and changes to linker appendages. Our research efforts have led to the refinement of one of these synthesized moieties into a selective and highly active inhibitory species of PAI-1.

While the crystal structures of several other members of the serpin super family have been successfully obtained in their bound active state, no such structure of a PAI-1 inhibitor complex has yet been reported in the literature. The characterization of a crystal structure would

allow for a more logical approach to drug design by revealing to us the exact style in which the synthesized inhibitors are binding to our protein. This approach has been utilized with several other members of the serpin family; one most notably includes the serpin α 1-antitrypsin.²³ However, a crystal structure has been successfully obtained of PAI-1 bound to one of our synthetic inhibitors (CDE-096). This has allowed us to more fully develop our synthetic ideology.

It has previously been reported that PAI-1 deficiency can lead to increased angiogenesis.⁹ Because our main motivation for inhibiting PAI-1 stems from our desire to inhibit the inhibitor of fibrinolysis due to the observation that fibrinolysis inhibition can lead to thrombi development, which in turn leads to strokes and heart attacks, another means of eliminating strokes and heart attacks could involve increasing the rate at which the body develops new circulatory pathways, thus giving the blocked blood a different relief-route.

One way to approach the potential of this idea is through the utilization of various software programs. The VAST software program allows the alignment between two different yet structurally related proteins by their 3-D structure. This allows for new observations between the functional properties of two proteins whose primary structure may not have suggested that any type of similarity between the two was a possibility. The PAI-1 file was examined within VAST for 3-D structural/functional similarities to other proteins.⁴⁶

VAST determined that a high degree of similarity exists between PAI-1 and Pigment Epithelium-Derived Factor (PEDF).⁴⁶ The PEDF protein is widely expressed throughout the human body.⁴⁷ It is known as a potent inhibitor of angiogenesis, the formation of new blood vessels.⁴⁸

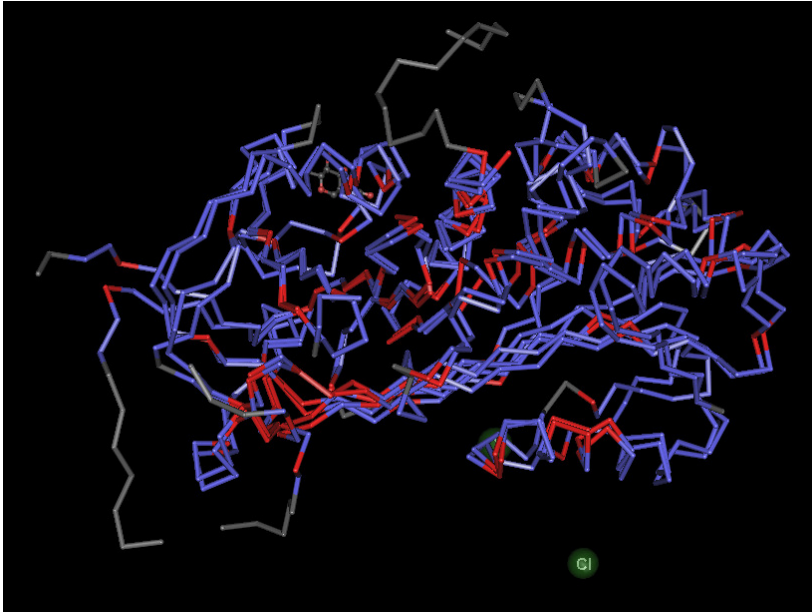


Figure 18: VAST Alignment of PEDF and PAI-1.
Alignment of 1DVM_A with 1IMV; respectively.⁴⁶

PEDF has 349 aligned residues with PAI-1 out of the total existing 402 residues. PAI-1 is another serpin, high levels of which have been associated with heart attack and stroke. The 3-D alignment of the PEDF protein and PAI-1 is illustrated in Figure 18. PEDF has been observed to bind to heparin, a densely negatively charged molecule already well-known for its anti-coagulative properties.⁴⁹ Figure 19 outlines the structure of heparin.

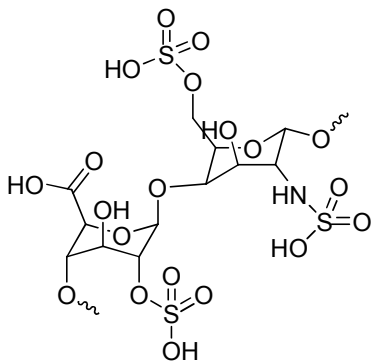


Figure 19: Heparin.

Heparin is already a known activator of anti-thrombin III.²³ The development of a PAI-1 inhibitor which incorporated the PEDF inhibitory properties of heparin and concurrently the PEDF activating properties for ATIII would effectively eliminate any inhibitory competition between ATIII inhibition and PAI-1 inhibition that has previously been one of concern. A new and future direction for the synthetic efforts towards new inhibitors of PAI-1 focuses on synthesizing negatively charged species such as heparin and examining their effect on the inhibition of PAI-1.

Setting aside these future possibilities for enhancing our ability to synthesize a selective and highly active inhibitor of PAI-1, the following chapters will detail the four main branches which our research has already explored in an attempt to achieve this goal. Chapter 1 focuses on the effects that the properties of the linkers have on PAI-1 inhibition and how PAI-1 inhibition is affected by the differing possible geometric isomerism of the inhibitors. Chapter 2 examines the effects of altering the number of gallates and central sugar on PAI-1 inhibition. Chapter 3 focuses on evaluating our research investigating the optimum number and arrangement of substituents on the gallate ring. Chapter 4 highlights our success in obtaining a crystal structure of an active PAI-1 serpin bound to an inhibitor and the carbamates which were synthesized and used in this achievement.

Chapter 1

Effects of Linker Structure on Inhibitor Potency

BACKGROUND AND OBJECTIVES

The inhibition of plasminogen activator-inhibitor-1 (PAI-1) is anticipated to increase our understanding of various human ailments including diabetes, stroke, and atherosclerosis, with which high levels of PAI-1 have been associated. Therefore, the synthesis of small-molecule inhibitors of PAI-1 that improve upon these properties has been the main goal of this research. In an effort to determine potential inhibitors for PAI-1, a high-throughput screen was conducted. The initial MicroSource SPECTRUM compound library screen conducted by our collaborators at the University of Michigan Medical School resulted in the recognition of a wide variety of potential inhibitory molecules for PAI-1.⁴⁴ The primary lead compound tannic acid (Figure 20) shared a prominent similarity with the other potential PAI-1 inhibitors in that they were all recognized to contain gallate or di-gallate groups (Figure 20). This recognition allowed for the focus of our synthetic efforts on the production of inhibitors containing various analogs of gallic acid.

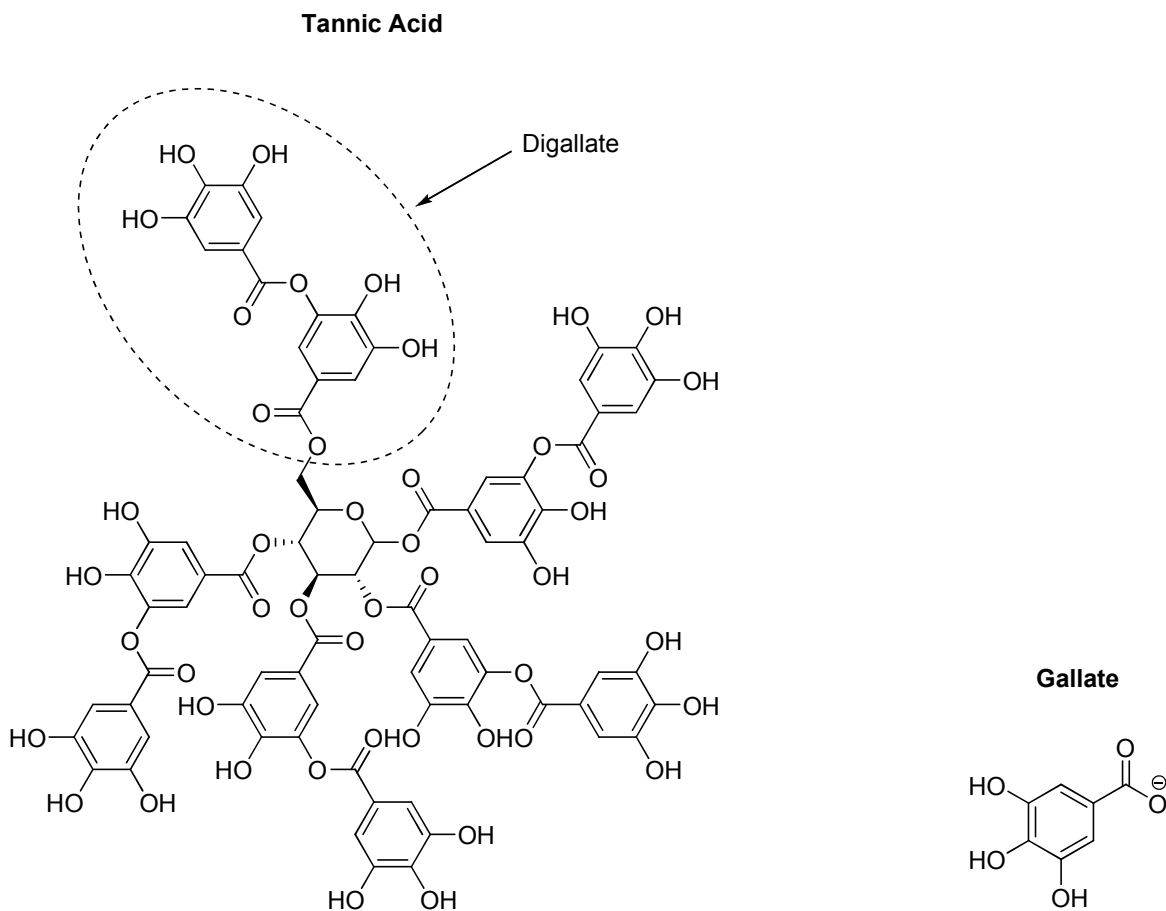
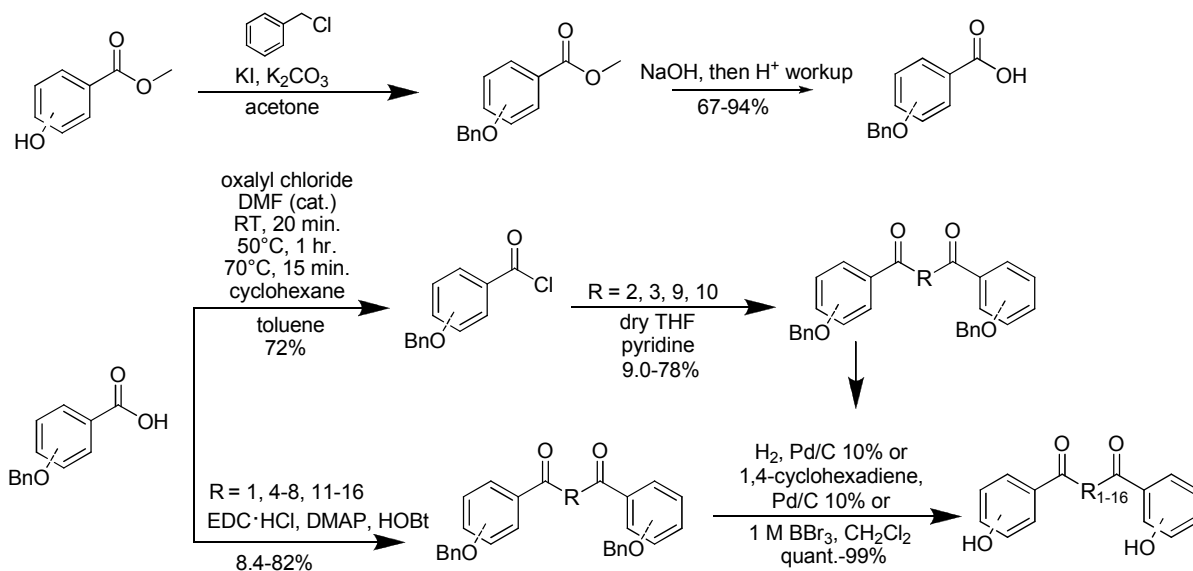


Figure 20: Tannic Acid, Gallate, and Digallate Groups.

Due to the ready commercial availability of gallic acid, inclusion of gallates via esterification reactions became a logical direction for our research efforts.

These esterification efforts involved three main reaction types (Figure 21). The first step involved benzyl protection of the hydroxy groups on the esters of gallic acid or other aromatic acids (gallic acid derivatives). After hydrolysis, two possible synthetic routes were followed: Steiglich acylation or nucleophilic acyl substitution coupled the gallate groups together via differing linker molecules. Last, the removal of the protecting groups was carried out by either a palladium catalyzed hydrogenation reaction or by a boron tribromide assisted mechanism. The

products were purified by either column chromatography or recrystallization. Figure 21 depicts the general reaction scheme for this set of experiments.



R ₁ = CDE-031 (cis) CDE-034 (trans)		R ₂ = CDE-044	<chem>HNCCNH</chem>	R ₃ = CDE-055		R ₄ = CDE-056 CDE-104	
R ₅ = CDE-057 (cis) CDE-058 (trans)		R ₆ = CDE-061 (trans) CDE-062 (cis)		R ₇ = CDE-064	<chem>CNCCN</chem>	R ₈ = CDE-065	
R ₉ = CDE-070	<chem>HNCCCNH</chem>	R ₁₀ = CDE-071	<chem>CNCCN</chem>	R ₁₁ = CDE-111 CDE-124		R ₁₂ = CDE-125 CDE-126	

Figure 21: General Reaction Scheme for the Amide and Ester-linked Inhibitors.

The only protecting groups utilized on the starting gallic acid derivatives were benzyl groups. The benzyl protecting group was used to prevent the hydroxy groups of the starting gallic acid from participating in the Steiglich acylation used in a later step. The benzyl protection

was carried out using a standard procedure⁵⁰ that involved combining methyl-3,4,5-trihydroxybenzoate (or related derivative), KI, anhydrous K₂CO₃, benzyl chloride and acetone.

The Steiglich acylation technique has been used for decades⁵¹ to enhance the yield of acylation reactions. The reaction is catalyzed with 4-(dimethylamino)pyridine (DMAP) and assisted by the carbodiimide 1-ethyl-3-[3-dimethylaminopropyl]carbodiimide hydrochloride (EDC·HCl). These two reagents are combined with the appropriate alcohol/amine and carboxylic acid in a low dielectric solvent under reflux conditions. DMAP's catalytic impact on this reaction stems from its ability to act as a stronger nucleophile than the alcohol. The EDC·HCl reacts with the carbonyl group creating an "active ester" intermediate. DMAP, acting as an acyl transfer agent, reacts with this intermediate and then the product rapidly reacts with the alcohol to give the ester.⁵¹

Last, the removal of the benzyl protecting groups from the coupled gallate entities was conducted. One method involved combining the coupled gallate entities with H₂, low-water THF, and Pd/C 10% as the reagents, while the other involved the replacement of H₂ with 1,4-cyclohexadiene as the hydrogen source, leaving the other reagents unmodified. An alternative procedure for the removal of the benzyl protecting groups involved combining the coupled gallate entities with a 1 M solution of BBr₃ in CH₂Cl₂ under N₂ and stirring the reaction overnight.

Our first generation of ester derivatives attempted to address the effect of varying geometric isomers on the inhibition of PAI-1. The bioactive conformation of our inhibitors is an important characteristic to determine, as it is the most energetically favorable configuration of individual atoms of the inhibitor.⁵² To address this, two gallates were linked together by the diesterification of a linking unit. Compounds were synthesized with differing linking units, and the impact that the different linkers had on the potency of the potential inhibitor was examined.

One of the aspects of a potential inhibitor that was examined during the modifications involved an attempt to determine if a particular dihedral angle between the two gallates had an effect on the inhibitor's strength. An examination of the dihedral angle is relevant since it is well-known that the biological activity of an inhibitor is often dependent on the placement of the functional groups of the inhibitor in a specific 3-D pattern.

Variations in dihedral angle lead to conformational isomers. Conformational isomerism describes molecules that possess identical structural formulas but have different shapes due to their ability to rotate freely about a bond. Due to the high number of conformational structures that a molecule can take (Figure 22) and their ability to constantly and readily interconvert, these conformational structures are rarely isolatable.

$$\text{Number of conformers} = (360^\circ / \text{angle increment})^{(\# \text{ rotatable bonds})}$$

Figure 22: Equation to Determine the Number of Possible Conformational Structures.

Substituents on a ring can be present as either *cis* or *trans* isomers. We chose to study *cis/trans* isomers in order to limit the number of conformers available to each inhibitor in an attempt to identify the optimal dihedral angle.

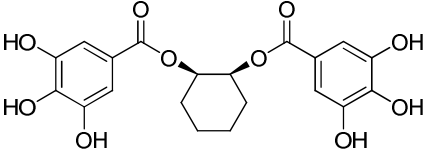
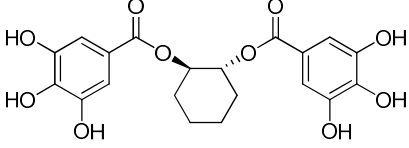
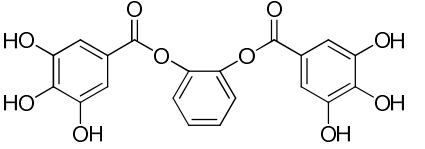
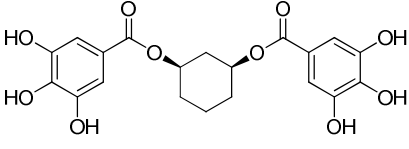
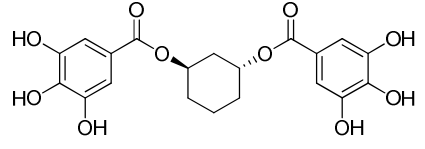
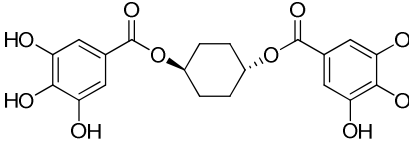
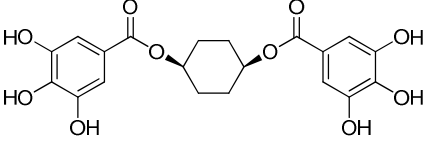
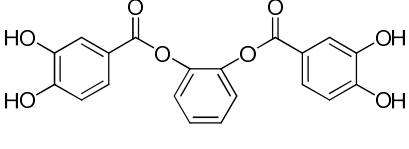
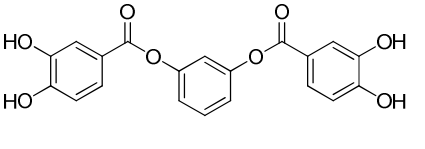
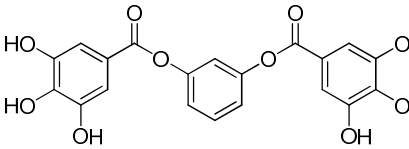
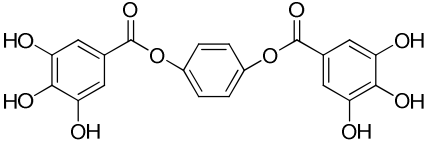
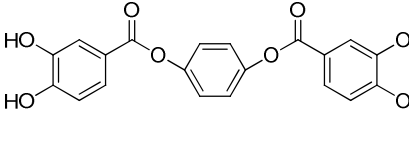
When synthesizing potential drug molecules, it is important to keep in mind that one of the main causes of failure is low bioavailability. The diversity of esterases available within humans elevates the probability that prodrugs containing esters can be synthesized as drugs with a high bioavailability.⁵³ This is the main reason that esters are the most common pro-drug synthesized.⁵² However, this fact is particularly detrimental to our molecules' inhibitory ability

in a whole animal model because our inhibitors must maintain their structure to successfully interact with PAI-1 and cause inhibition. Therefore, although esters have other positive aspects as functional groups, such as their ability to be readily synthesized with a wide range of lipophilic and hydrophilic properties, their potential degradation by the abundant level of esterases within *Homo sapiens* causes concern for their use within the ultimate goals of this research project.⁵² However, we can gain important information in the short-term about interactions between the inhibitors and PAI-1 using ester-containing molecules.

The instability of esters can also be detrimental to a manufacturer's ability to formulate appropriate dosage forms of an ester-containing substance.⁵³ A common manipulation that addresses this issue involves replacing the esters with amide groups, which typically leads to an increase in the metabolic stability of the molecule.⁵⁴ Thus, several gallic acid derivatives that contain amides in place of the ester linkages were synthesized, and the effect on the potency of the inhibitor was measured (Table 1).

Geometric isomerism was studied in an attempt to arrive at a fuller understanding of our inhibitor's bioactive conformations. The synthetic route we followed detailed the linking of two gallic acid molecules (or their analogues) together via different linker groups that would lead to different varieties of conformational isomers.

Table 1: Cyclic Linkers

Entry	Inhibitor	Entry	Inhibitor
CDE-031 ^a cis		CDE-034 ^a trans	
CDE-056 ^a		CDE-057 ^a cis	
CDE-058 ^a trans		CDE-061 ^a trans	
CDE-062 ^a cis		CDE-104 ^b	
CDE-111		CDE-124	
CDE-125 ^c		CDE-126 ^c	

^a Paul North, ^b Jennifer Vogel, ^c Nadine El-Ayache

First we examined the effect of using a cyclohexanediol unit as a linker between the gallates (or their analogues). The compounds using *cis* and *trans* forms of 1,2-cyclohexanediol (CDE-031 and CDE-034) as the linkers were synthesized by Paul North. Next the question was raised regarding the effect of the positioning of the gallates around the ring. Therefore, *cis/trans* forms of the inhibitors containing 1,3 and 1,4-cyclohexanediol linkers (CDE-057/CDE-058 and CDE-061/CDE-062) were synthesized by Paul North, and the effect on PAI-1 inhibition was compared to the 1,2-cyclohexanediol-based inhibitors.

Inhibitors that have an increased number of conformational possibilities provided another source of uncertainty regarding the effect that the *cis/trans* forms of the molecules had on the inhibitor's bioactive conformation. To reduce this uncertainty we synthesized inhibitor molecules containing rigid rings as the linker. These included the 1,2-benzenediol, 1,3-benzenediol, and the 1,4-benzenediol units (CDE-056, CDE-124, CDE-125).

Last, our research efforts indicated that a protocatechuate (a 3,4-dihydroxybenzoate) might have an equal or greater ability to inhibit PAI-1 than the corresponding 3,4,5-trihydroxybenzoate. Therefore, to test for supporting evidence of this hypothesis, a group of molecules was synthesized containing protocatechuates and compared to their gallate analogues. These included the protocatechuates/bisgallates of the following linkers: 1,2-benzenediol, 1,3-benzenediol, and 1,4-benzenediol (CDE-104/CDE-056, CDE-111/CDE-124, and CDE-126/CDE-125, respectively), as illustrated in Table 1.

To address the issue of stability of ester-containing inhibitors, a series of inhibitors was synthesized that contained amide linker units, both cyclic and acyclic, in place of the ester linker units (Table 2).

Table 2: Amide Linkers

Entry	Inhibitor	Entry	Inhibitor
CDE-044		CDE-055	
CDE-064		CDE-065	
CDE-070		CDE-071	

CDE-044 was intended to model the simplest diester (CDE-008) except for the switch from an ester to an amide group. To compare the effect that a more rigid cyclic linker might have on inhibition, CDE-055 and CDE-065 were synthesized. Low solubilities during syntheses of CDE-044 and CDE-055 prompted us to attempt similar syntheses with a slightly modified starting gallate. CDE-044 and CDE-055 utilized benzyl protecting groups on the gallates during the reaction which coupled the linker, while CDE-070 and CDE-071 utilized methyl protecting groups during this same step. The methyl-protected starting material was more soluble than the benzyl-protected one. Improving the solubility of the protected gallates during the synthesis of CDE-070 and CDE-071 allowed for improved yields over previous synthetic attempts.

To simplify the synthesis and to probe the importance of having 3 hydroxy groups on each aromatic ring, an attempt was made to include a syringate (3,5-dimethoxy-4-

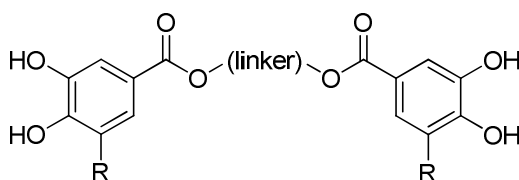
hydroxybenzoate) in place of the gallates. This change allowed for a synthesis that consisted of only the coupling step, reducing the number of steps by half. CDE-064 is the syringate analogue of CDE-071, while CDE-065 is the syringate analogue of CDE-055.

RESULTS

The results of the geometric isomerism study indicated that the inhibitors containing the *trans*-1,4-cyclohexanediol linker (CDE-061) and the *trans*-1,3-cyclohexanediol linker (CDE-058) had the strongest inhibition of PAI-1 ($IC_{50} = 0.051 \mu\text{M}$ and $0.054 \mu\text{M}$, respectively). In comparison, the *cis*-analogues (CDE-062 and CDE-057) had a reduced inhibitor potency ($IC_{50} = 332 \mu\text{M}$ and $448 \mu\text{M}$, respectively). This indicated that a *trans*-position was more desirable for inhibition than a *cis*-position (except in the case of the 1,2-version). An IC_{50} -value comparison also indicated that a more preferential architecture of the inhibitors was one in which an increased number of conformational possibilities was favored, such as the cyclohexanediol linkers, in contrast to their more rigid benzenediol analogues. The *cis*-1,2-cyclohexanediol (CDE-031) and *trans*-1,2-cyclohexanediol (CDE-034) both were more potent ($IC_{50} = 0.293 \mu\text{M}$ and $0.689 \mu\text{M}$, respectively) than the 1,2-benzenediol analogue (CDE-056, $IC_{50} = 2.69 \mu\text{M}$). The *trans*-1,3-cyclohexanediol (CDE-058) was more potent than the 1,3-benzenediol analogue (CDE-124, $IC_{50} = 0.062 \mu\text{M}$). The *trans*-1,4-cyclohexanediol (CDE-061) was more potent than the 1,4-benzenediol analogue (CDE-125, $IC_{50} = 0.061 \mu\text{M}$). Therefore, limiting the number of conformational possibilities by utilizing a benzenediol (a planar linker) molecule (CDE-111, CDE-124, CDE-125, and CDE-126), resulted in a reduction in inhibition as compared to using the *trans*-1,4-cyclohexanediol linker (CDE-061). When the linker moieties were in a 1,2-position (CDE-031 and CDE-034), a reduction in the inhibitor's potency occurred (in comparison to the inhibitory ability of CDE-061, CDE-058, CDE-125, CDE-124, and CDE-126), implying that the bioactive conformer does not occur with this configuration. To reaffirm this, it is noted that the rigid 1,4-benzenediol analogue (CDE-125) showed comparable inhibition to the two top configurations (CDE-058 and CDE-061). This observation provides supporting evidence that

the 1,4-configuration is closer to the ideal bioactive conformation. All of the inhibitors examined within this series only had an inhibition of ATIII up to a 10.54 μM value (CDE-104). A comparison of the IC_{50} of these tested species is outlined in Table 3.

Table 3: Biological Assay Results for Cyclic Linkers.
(R = H or OH)



<u>Compounds</u>	<u>Cyclic Linker</u>	<u>R</u>	<u>IC_{50} vs. PAI-1</u> <u>(μM)</u>
CDE-061	1,4-cyclohexanediol (trans)	-OH	0.051
CDE-058	1,3-cyclohexanediol (trans)	-OH	0.054
CDE-125	1,4-benzenediol	-OH	0.061
CDE-124	1,3-benzenediol	-OH	0.062
CDE-126	1,4-benzenediol	-H	0.151
CDE-031	1,2-cyclohexanediol (cis)	-OH	0.293
CDE-111	1,3-benzenediol	-H	0.37
CDE-034	1,2-cyclohexanediol (trans)	-OH	0.689
CDE-104	1,2-benzenediol	-H	1.17
CDE-056	1,2-benzenediol	-OH	2.69
CDE-062	1,4-cyclohexanediol (cis)	-OH	332
CDE-057	1,3-cyclohexanediol (cis)	-OH	448

The observation was made that, within the series overall, the shorter distances between the gallates tended to cause a decreased inhibition of PAI-1. The 1,2-benzenediols and 1,2-cyclohexanediol-based inhibitors showed (in some cases) a 100-fold decrease in inhibition when compared with their 1,3 or 1,4-diol counterparts.

Replacement of the ester functionality with amides resulted in across the board decreases in potency (Table 4), both as a class of compounds and when compared directly with the analogous esters. For example, the diamide analogous to CDE-008 (CDE-044) resulted in a nearly 2,500-fold decrease in potency, and that analogous to CDE-009 (CDE-070) resulted in a 34-fold decrease in potency. All of the amide-based inhibitors showed non-detectable levels of inhibition against ATIII μM .

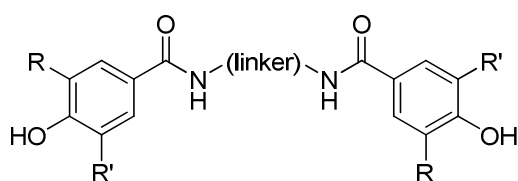


Table 4: Biological Assay Results for Amide Linkers.

<u>Compounds</u>	<u>Linking Unit</u>	<u>R</u>	<u>R'</u>	<u>IC₅₀ vs. PAI-1 (uM)</u>
CDE-055	1,4-piperazine	-OH	-OH	26.83
CDE-065	1,4-piperazine	-O-Me	-O-Me	424
CDE-070	NHCH ₂ CH ₂ CH ₂ NH	-OH	-OH	593
CDE-044	NHCH ₂ CH ₂ NH	-OH	-OH	1757
CDE-064	(Me)NCH ₂ CH ₂ N(Me)	-O-Me	-O-Me	2204
CDE-071	(Me)NCH ₂ CH ₂ N(Me)	-OH	-OH	ND

Last, the protocatechuate-to-bisgallate comparison led to inconclusive results because the change in potency between the two analogues was not substantial. The protocatechuates/bisgallates of the following combinations: 1,2-benzenediol, 1,3-benzenediol, and the 1,4-benzenediol linkers (CDE-104/CDE-056, CDE-111/CDE-124, and CDE-126/CDE-125) had differing relative potencies within a tight range of 0.061-2.69 μM . More

comparisons of these two scaffolds are necessary before a decisive conclusion can be drawn regarding any effect in potency.

EXPERIMENTAL

Unless otherwise noted, all reactions were performed in non-flame dried glassware with magnetic stirring under an atmosphere of dry nitrogen. Tetrahydrofuran (THF) was purified by distillation over sodium benzophenone ketyl or when noted, commercially available low water THF (Aldrich) was utilized. All extraction and chromatography solvents were reagent grade and used without purification.

Analytical thin layer chromatography (TLC) was performed on silica gel-coated glass plates (Sorbent Technologies; 250 μm silica gel with UV254) and visualized with UV light. Flash column chromatography was performed using silica gel (Sorbent Technologies Premium Rf; 60 \AA , 40-75 μm) and utilized the indicated solvent. Infrared spectra (IR) were recorded as thin films on NaCl plates using a Nicolet Impact 410 FTIR.

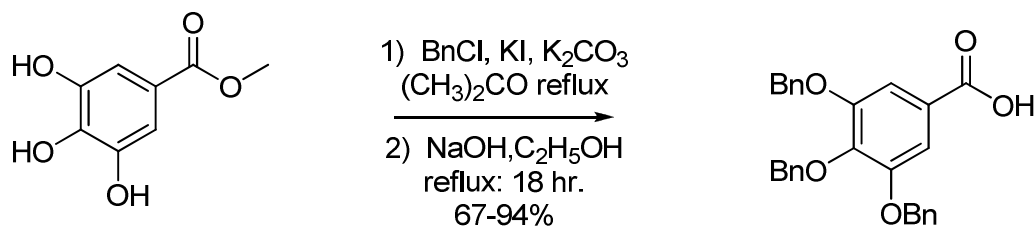
All ^1H (400 MHz), ^{13}C (100 MHz) and ^{19}F spectra (376 MHz) were recorded on a Jeol ECX-400 spectrometer. Chemical shifts are expressed in δ (parts per million, ppm) and are reported relative to the tetramethylsilane (TMS) peak. Coupling constants (J) are expressed in Hertz. Splitting patterns are indicated as follows: s (singlet), d (doublet), t (triplet), q (quartet), quin (quintet), dd (doublet of doublets), td (triplet of doublets), and m (multiplet).

Mass spectra were recorded on a VG 70-250-s2 spectrometer manufactured by Micromass Corp. (Manchester UK) at the University of Michigan Mass Spectrometry Laboratory.

Proof-of-structure analysis is conducted in detail for one of our more structurally interesting compounds, CDE-096 (Chapter 4, Experimental). This molecule is composed of two gallates coupled to an ester-based linking unit which has a handle comprised of a carbamate-linked trifluoromethyl-substituted aromatic ring. The method used in the analysis of the mass

spectra, infrared spectra, and $^1\text{H}/^{19}\text{F}/^{13}\text{C}$ spectra for CDE-096 is similarly used when establishing the identity of all those compounds submitted for testing and allowed for determination of the structure of the compounds.

General procedure for synthesis of 3,4,5-tris(benzyloxy)benzoic acid:



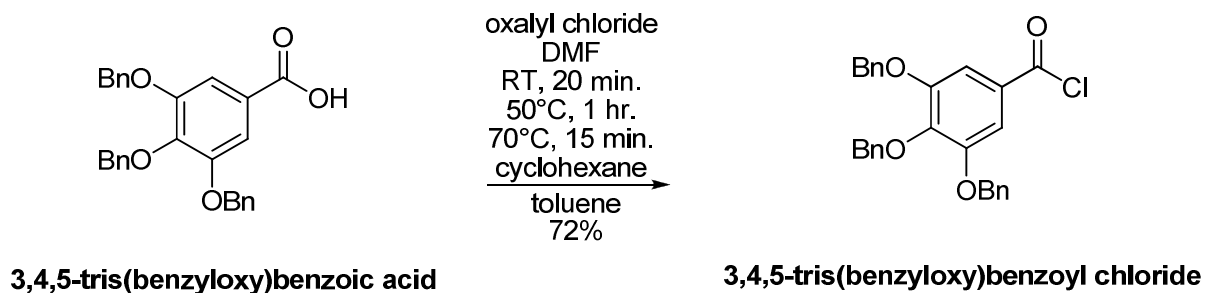
methyl 3,4,5-trihydroxybenzoate

3,4,5-tris(benzyloxy)benzoic acid

Methyl-3,4,5-trihydroxybenzoate (10.0 g, 54.3 mmol), KI (4.00 g, 24.0 mmol), anhydrous K₂CO₃ (44.0 g, 318 mmol) and acetone (500 ml) were combined and stirred for 20 minutes. Benzyl chloride (20.0 ml, 174 mmol) and acetone (100 ml) were combined and then added to the solution. The reaction refluxed for 20 hours under N₂. The solid was filtered off and the filtrate evaporated. The residue was taken up in 400 ml CH₂Cl₂. The suspension was vacuum filtered through Celite, and the filtrate was dried *in vacuo*. Methyl-3, 4, 5-tribenzyloxybenzoate was obtained as a white solid and used without further purification.

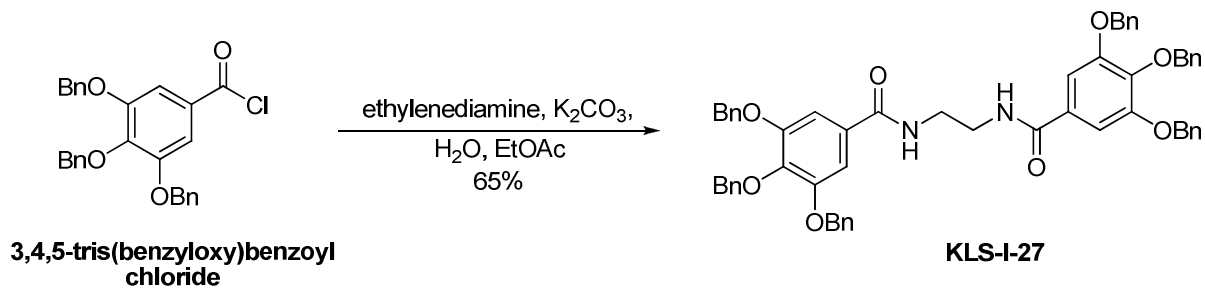
Crude methyl-3, 4, 5-tribenzyloxybenzoate, 95% ethanol (800 mL), and NaOH (3.54 g, 88.5 mmol) were refluxed under N₂ for 2 hours. The hot solution was poured into 525 ml of a 0.6 M HCl solution and stirred for 10 min. The solid was filtered off. The crude product was washed successively with a 1:1 solution of 95% ethanol: H₂O (100 mL), water (100 ml), methanol (100 ml), and tert-butyl methyl ether (100 ml). The solid was dried *in vacuo* to obtain a white solid (21.2 g, 94%). ¹H NMR (CDCl₃, 400 MHz) δ 7.42-7.25 (m, 17H, aromatic), 5.14 (s, 4H, benzylic), 5.13 (s, 2H, benzylic).

General procedure for synthesis of 3,4,5-tris(benzyloxy)benzoyl chloride:

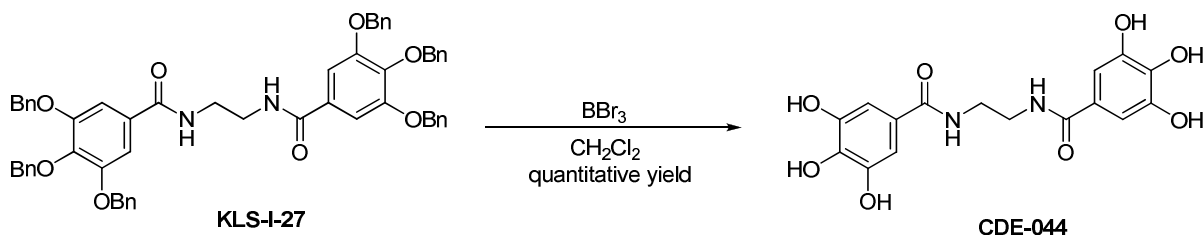


3,4,5-Tris(benzyloxy)benzoic acid (5.79 g, 13.13 mmol) was dissolved in toluene (60 mL, 563 mmol) in a 500 mL flame-dried round-bottomed flask. Anhydrous N,N-dimethylformamide (DMF) (0.10 mL, 94.4 mmol) was syringed into the flask while stirring. A solution of oxalyl chloride (1.72 mL, 19.7 mmol) and toluene (8.5 mL) were added over a period of 10 min under N₂. The mixture was stirred for 20 min. at room temperature and then at 50°C for 1 hour. Solvent was removed *in vacuo*. Residue was taken up in toluene (25 mL) and the solution was stirred at 70°C until dissolution was achieved. Cyclohexane (27.5 mL) was added and stirred. The white powder that formed was filtered, washed with cyclohexane, and dried *in vacuo* to obtain a white solid (4.37 g, 72%). ¹H NMR (DMSO-*d*₆, 400 MHz) δ 7.21-7.44 (m, 17H, aromatic), 5.15 (s, 4H, benzylic), 5.00 (s, 2H, benzylic).

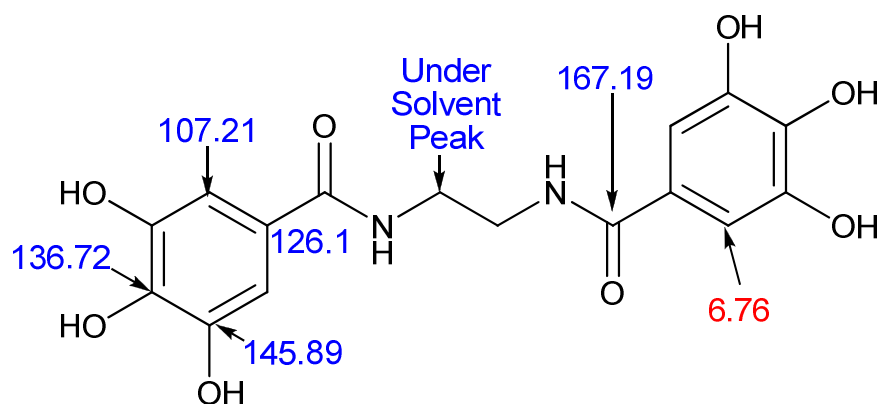
N,N'-(ethane-1,2-diyl)bis(3,4,5-tris(benzyloxy)benzamide)
(905.061 g/mol) C₅₈H₅₂N₂O₈



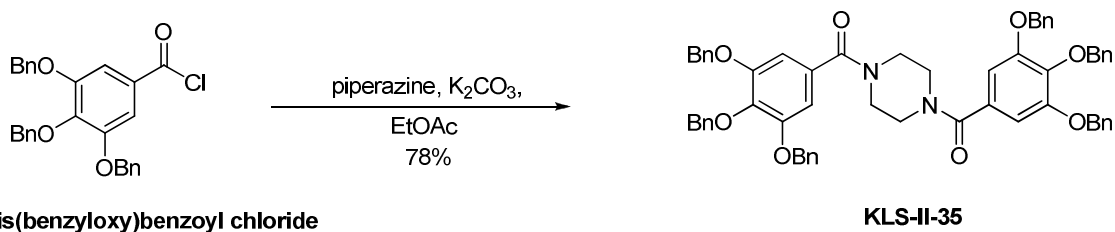
3,4,5-Tris(benzyloxy)benzoyl chloride (0.30 g, 0.65 mmol), ethylenediamine (20.0 μ L, 0.32 mmol), K₂CO₃ (0.11 g, 0.79 mmol), H₂O (5.00 mL), and EtOAc (5.00 mL) were combined and stirred for 24 hours under N₂. The reaction solution was then filtered and washed with EtOAc and H₂O (2x each) to obtain a white solid (192 mg, 65%). ¹H NMR (DMSO-*d*₆, 400 MHz) δ 8.61 (s, 1H, -NH), 7.43-7.19 (m, 17H, aromatic), 5.10 (s, 4H, meta benzylic), 4.93 (s, 2H, para benzylic), 3.40 (s, 2H, -N-CH₂-); ¹³C NMR (DMSO-*d*₆ + D₂O, 100 MHz) δ 166.32, 152.47, 140.01, 137.97, 137.34, 130.24, 128.98, 128.69, 128.59, 128.47, 128.39, 128.20, 106.95, 74.73, 70.85, 40.24.

CDE-044**N,N'-(ethane-1,2-diyl)bis(3,4,5-trihydroxybenzamide)****(364.316 g/mol) C₁₆H₁₆N₂O₈**

CH₂Cl₂ (5.00 mL) and KLS-I-27 (0.17 g, 0.19 mmol) were combined under N₂. A 1 molar solution of BBr₃ in CH₂Cl₂ (4.71 mL, 4.71 mmol) was added over a period of five minutes in a drop-wise fashion using a syringe. The solution was left stirring overnight. The solution changed to a violet color and TLC (95% CH₂Cl₂/CH₃OH) showed the disappearance of starting material. The remaining BBr₃ was quenched by the addition of approximately 5 g of ice over 5 minutes. The solution was then filtered and the solid was washed with H₂O and CH₂Cl₂ (2x each) to obtain a quantitative yield of a violet solid. ¹H NMR (DMSO-*d*₆ and D₂O, 400 MHz) 6.76 (s, 4H, aromatic); ¹³C NMR (DMSO-*d*₆ + D₂O, 100 MHz) δ 167.19, 145.89, 136.72, 125.28, 107.21; HRMS, ES calcd. for C₁₆O₈N₂H₁₆Na [M+Na]⁺ 387.0804, found: 387.0802.



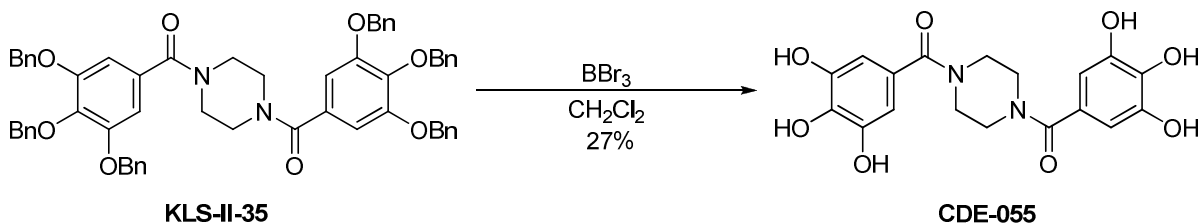
Piperazine-1, 4-diylbis((3,4,5-tris(benzyloxy)phenyl)methanone)
 (931.08 g/mol) $\text{C}_{60}\text{H}_{54}\text{N}_2\text{O}_8$



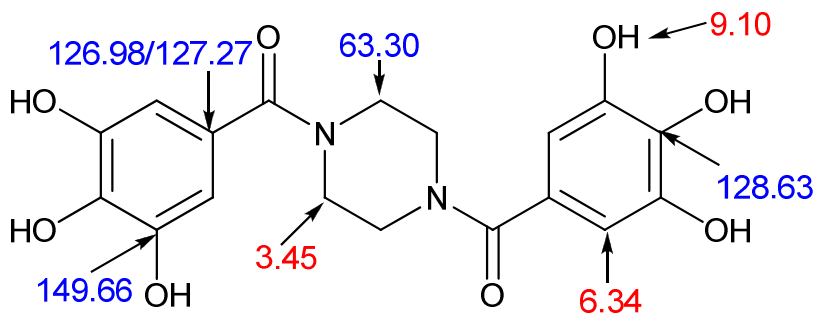
3,4,5-tris(benzyloxy)benzoyl chloride

KLS-II-35

3,4,5-Tris(benzyloxy)benzoyl chloride (0.30 g, 0.65 mmol), piperazine (28.2 mg, 0.32 mmol), K_2CO_3 (54.2 mg, 0.39 mmol), H_2O (5.00 mL), and EtOAc (5.00 mL) were combined and stirred for 48 hours, under N_2 . The solid was filtered off and washed with EtOAc (2x) to obtain a white solid (304 mg, 78%). ^1H NMR ($\text{DMSO}-d_6$, 400 MHz) δ 7.45-7.22 (m, 34H, aromatic), 5.13 (s, 8H, meta benzylic), 4.96 (s, 4H, para benzylic); (CDCl_3 , 400 MHz) δ 3.33 (bs, 8H, $\text{O}=\text{C}-\text{N}-(\text{CH}_2)_2-\text{N}-(\text{CH}_2)_2-$); ^{13}C NMR (CDCl_3 , 100 MHz) δ 170.23, 152.82, 140.05, 137.50, 136.69, 130.08, 128.71, 128.35, 128.17, 127.70, 127.43, 107.41, 75.34, 71.37.

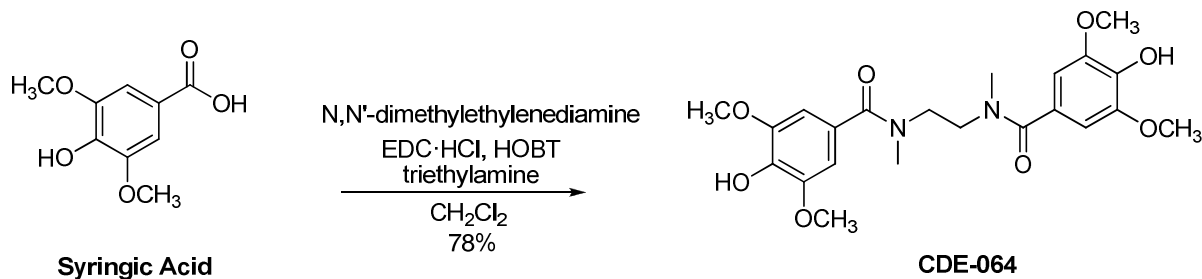
CDE-055**Piperazine-1, 4-diylbis(3,4,5-trihydroxyphenyl)methanone****(390.33 g/mol) C₁₈H₁₈N₂O₈**

KLS-II-35 (0.20 g, 0.22 mmol), CH₂Cl₂ (6.85 mL) were combined under N₂. A 1 molar solution of BBr₃ in CH₂Cl₂ (6.45 mL, 6.45 mmol) was added over a period of five minutes in a drop-wise fashion using a syringe. The reaction was left stirring overnight. Approximately, 5.00 g of ice was added to the reaction to quench the BBr₃. The organic layer was extracted from the filtrant with EtOAc (2x), dried with MgSO₄, filtered, and the solvent was evaporated *in vacuo* to obtain a solid (83.9 mg, 27%). ¹H NMR (DMSO-*d*₆, 400 MHz) δ 9.10 (bs, 6H, -OH), 6.34 (s, 4H, aromatic), 3.45 (s, 8H, -N-(CH₂-CH₂)₂-N-); ¹³C NMR (DMSO- *d*₆, 100 MHz) δ 149.66, 128.63, 127.27, 126.98, 63.30; HRMS, ES calcd. for C₁₈H₁₈N₂O₈Na [M+Na]⁺ 413.0961, found: 413.0946.

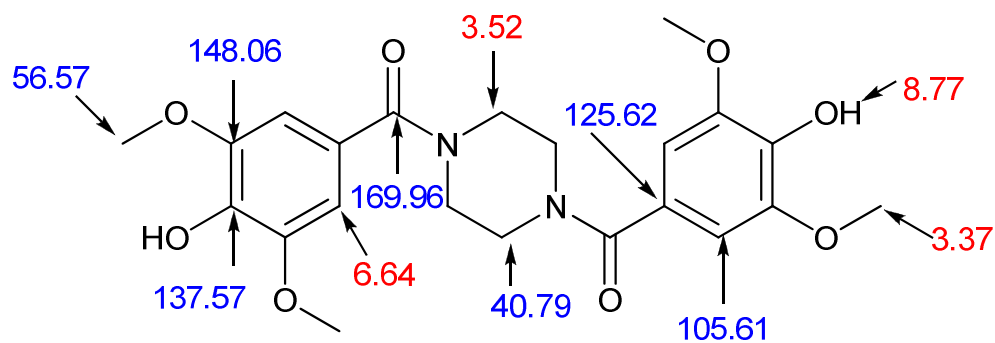


CDE-064

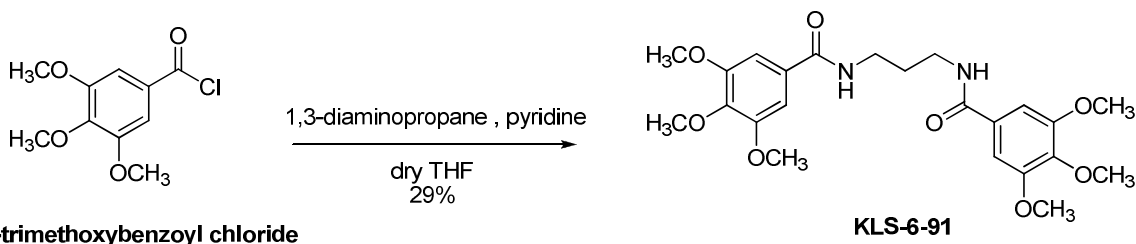
N,N'-(ethane-1, 2-diyl)bis(4-hydroxy-3, 5-dimethoxy-N-methylbenzamide. (448.457 g/mol) C₂₂H₂₈N₂O₈



Syringic acid (0.50 g, 2.52 mmol), N,N'-dimethylethylenediamine (108 μ L, 1.01 mmol), EDC·HCl (0.48 g, 2.52 mmol), HOBT (0.34 g, 2.52 mmol), triethylamine (0.35 mL, 2.52 mmol), and CH₂Cl₂ (2.00 mL) were combined and stirred under N₂ overnight. A TLC (100% EtOAc) indicated complete disappearance of the starting material. The reaction solution was washed with 1 N HCl, 1 N NaHCO₃, and a brine solution. It was dried with MgSO₄, filtered, and evaporated *in vacuo* to obtain a solid (78%). ¹H NMR (CDCl₃, 400 MHz) δ 6.64 (s, 4H, aromatic), 5.59 (s, 2H, -OH), 3.96 (s, 12H, -OCH₃), 3.93 (s, 4H, -N-CH₂-), 3.11 (s, 6H, -N-CH₃); ¹³C NMR (CDCl₃, 400 MHz) δ 171.81, 146.65, 135.87, 127.06, 104.51, 56.34, 44.61, 38.28; HRMS, ES calcd. for C₂₂H₂₈O₈N₂Na [M+Na]⁺ 471.1743, found: 471.1749.



N,N'-(propane-1, 3-diyl)bis(3, 4,5-trimethoxybenzamide)
 (462.48 g/mol) $C_{23}H_{30}N_2O_8$



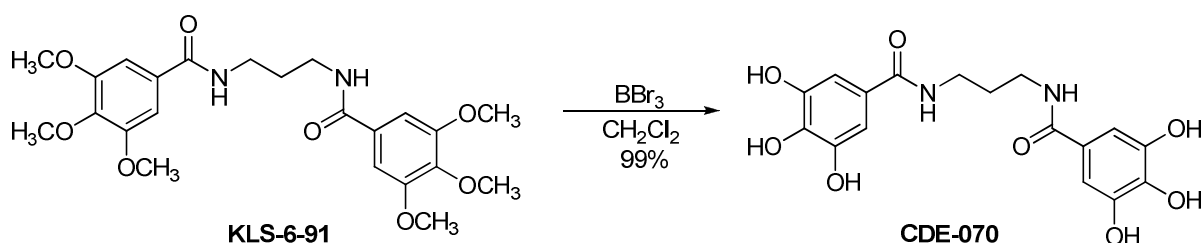
3,4,5-Trimethoxybenzoyl chloride (1.50 g, 6.52 mmol), 1,3-diaminopropane (0.27 mL, 3.25 mmol) and dry THF (9.91 mL) were combined and stirred under N_2 . Pyridine (0.53 mL, 6.50 mmol) was syringed into the flask. It was stirred overnight at room temperature. The solid that formed was filtered, washed with low water THF, HCl 1 N, and then triturated 2x with EtOAc to obtain a solid (883 mg, 29%). 1H NMR (DMSO- d_6 , 400 MHz) δ 8.50 (t, $J = 5.50$ Hz, 1H, -NH), 7.16 (s, 2H, aromatic), 3.78 (s, 6H, -OCH₃), 3.66 (s, 3H, -OCH₃), 3.28 (q, $J = 6.41$ Hz, 2H, -N-CH₂-CH₂-CH₂-N-), 2.83 (q, $J = 6.41$ Hz, 2H, -N-CH₂-CH₂-CH₂-N-), 1.85-1.71 (m, 2H, -N-

CH₂-CH₂-CH₂-N-); ¹³C NMR (DMSO-*d*₆, 100 MHz) δ 166.10, 153.06, 140.29, 130.25, 105.17, 60.58, 56.48, 39.61, 29.94.

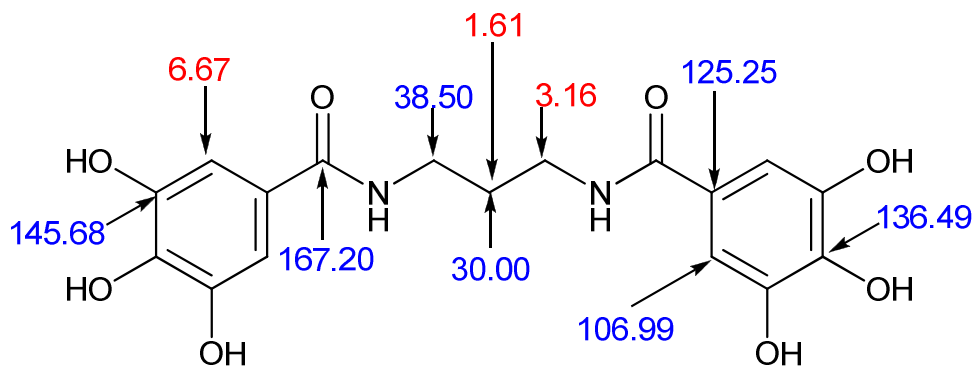
CDE-070

N, N'-(propane-1,3-diyl) bis (3,4,5-trihydroxybenzamide)

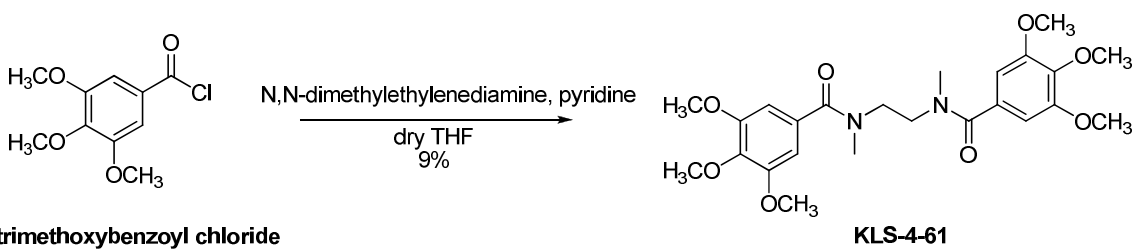
(378.33 g/mol) C₁₇H₁₈N₂O₈



KLS-6-91 (0.75 g, 0.86 mmol) and CH₂Cl₂ (25.7 mL) were combined under N₂. A 1 molar solution of BBr₃ in CH₂Cl₂ (27.2 mL, 1 molar solution) was added over a period of five minutes in a drop-wise fashion using a syringe. The reaction was left stirring overnight. TLC (70% CH₂Cl₂/MeOH) showed the disappearance of starting material. A white solid was filtered off and washed with H₂O and CH₂Cl₂. The solid was then triturated with EtOAc and a yellow liquid separated from the solid. This was filtered off from the solid to obtain a yellow solid (317 mg, 99%). ¹H NMR (DMSO-*d*₆ + D₂O, 400 MHz) δ 6.76 (s, 4H, aromatic), 3.16 (t, *J* = 6.87 Hz, 4H, -N-CH₂-CH₂-CH₂-N-), and 1.61 (quin, *J* = 6.87 Hz, 2H, -N-CH₂-CH₂-CH₂-N-); ¹³C NMR (DMSO-*d*₆ + D₂O, 100 MHz) δ 167.20, 145.68, 136.49, 125.25, 106.99, 38.50, 30.00; HRMS, ES calcd. for C₁₇H₁₈O₈N₂Na [M+Na]⁺ 401.0961, found: 401.0958.



N,N'-(ethane-1,2-diyl)bis(3,4,5-trimethoxy-N-methylbenzamide)
 (476.511 g/mol) $C_{24}H_{32}N_2O_8$



3,4,5-Trimethoxybenzoyl chloride (1.50 g, 6.52 mmol) and dry THF (10.0 mL) were combined under N_2 . Pyridine (0.52 mL, 6.50 mmol) and N,N-dimethylethylenediamine were syringed into the flask. Immediately after the amine was added, the solution changed to a bright yellow color. It was stirred for 24 hours under N_2 . The pale yellow powder which formed was filtered, washed with low water THF, and triturated with EtOAc to obtain a yellow solid (286 mg, 9%).

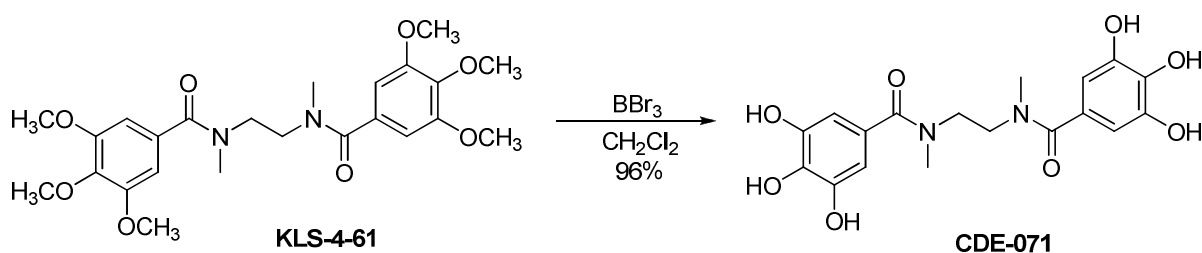
1H NMR (DMSO- d_6 , 400 MHz) δ 6.59 (s, 2H, aromatic), 3.74 (s, 3H, -OCH₃), 3.62 (s, 3H, -

OCH₃), 3.61 (s, 3H, -OCH₃), 3.58 (s, 3H, -NCH₃), 2.95 (s, 2H, -N-CH₂-); ¹³C NMR (DMSO-*d*₆, 100 MHz) δ 170.55, 153.21, 153.01, 138.52, 132.36, 104.97, 104.22, 60.57, 56.24, 40.44, 38.00.

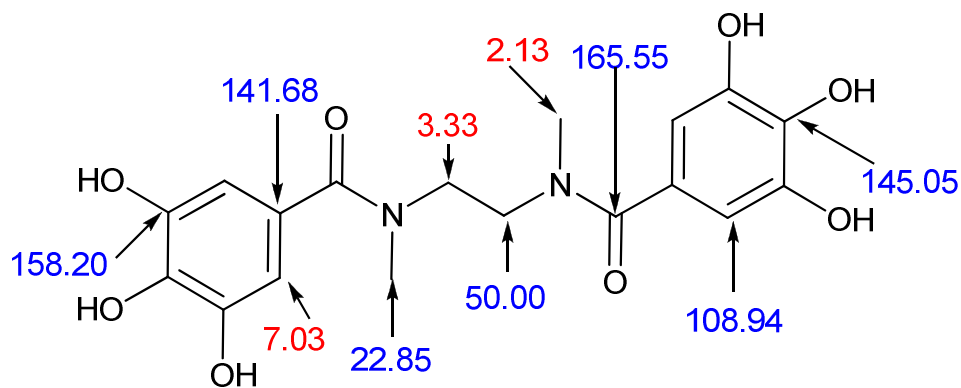
CDE-071

N, N'-(ethane-1,2-diyl) bis (3,4,5-trihydroxy-N-methylbenzamide)

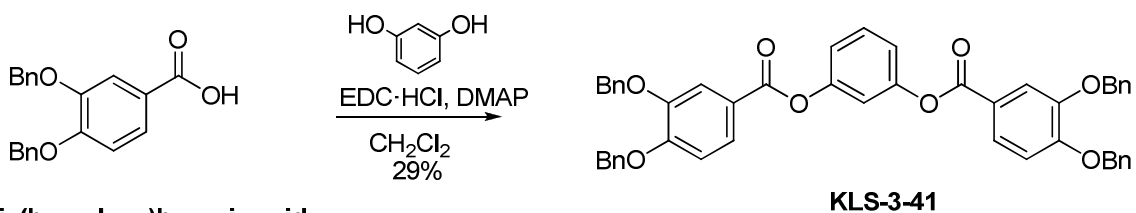
(392.35 g/mol) C₁₈H₂₀N₂O₈



KLS-4-61 (0.20 g, 0.42 mmol) and a 1 molar solution of BBr₃ in CH₂Cl₂ (12.6 mL) were combined under N₂ and stirred overnight. TLC (100% EtOAc) showed disappearance of starting material. The remaining BBr₃ was quenched by the addition of approximately 5 g of ice over 5 minutes. The grayish powder that formed was filtered off, triturated with acetone, and discarded. The pink filtrant was evaporated *in vacuo* to obtain a solid (159 mg, 96%). ¹H NMR (CD₃OH, 400 MHz) δ 7.03 (s, 2H, aromatic), 3.33 (s, 2H, -N-CH₂-), and 2.13 (s, 3H, -NCH₃); ¹³C NMR (CD₃OH, 100 MHz) δ 165.55, 158.20, 145.05, 141.68, 108.94, 50.00, 22.85; HRMS, ES calcd. for C₁₈H₂₀O₈N₂Na [M+Na]⁺ 415.1117, found: 415.1113.



1,3-Phenylene bis(3,4-bis(benzyloxy)benzoate)
(742.81 g/mol) C₄₈H₃₈O₈



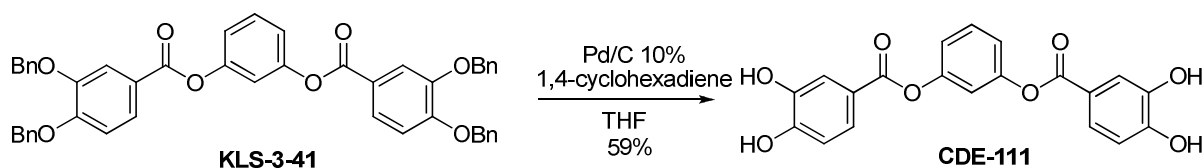
Resorcinol (0.30 g, 2.72 mmol), 3,4-bis(benzyloxy)benzoic acid (2.73 g, 8.18 mmol), EDC·HCl (4.77 g, 24.9 mmol), DMAP (2.80 g, 22.9 mmol), and CH₂Cl₂ (172 mL); were combined and refluxed over the weekend, while stirring, under N₂. TLC (80% hexanes/EtOAc), indicated that the majority of the starting material had been consumed. The solvent volume was reduced *in vacuo* and the residue was purified by column chromatography (65% hexanes/EtOAc), to produce a white solid (296 mg, 29%). ¹H NMR (CDCl₃, 400 MHz) δ 7.78 (td, *J* = 1.83, 8.24 Hz, 4H, ortho aromatic and meta aromatic), 7.51-7.28 (m, 21H, aromatic and -O-C-CH-CH-CH-C-

O-), 7.12-7.08 (m, 3H, $-\text{O}-\text{C}-\underline{\text{CH}}-\text{CH}-\underline{\text{CH}}-\text{C}-\text{O}-$ and $-\text{O}-\text{C}-\text{CH}-\text{C}-\text{O}-$), 6.99 (d, $J = 8.24$ Hz, 2H, ortho aromatic), and 5.26 (s, 4H, benzylic) 5.19 (s, 4H, benzylic); ^{13}C NMR (CDCl_3 , 100 MHz) δ 164.55, 153.65, 151.61, 148.52, 136.78, 136.47, 130.00, 128.73, 128.66, 128.16, 128.09, 127.52, 127.21, 124.93, 122.03, 119.25, 116.00, 115.93, 113.32, 71.33, 70.92.

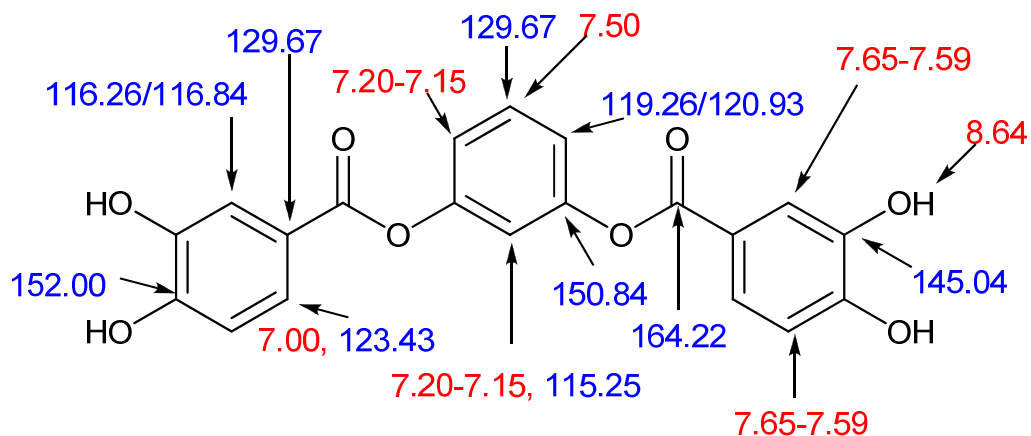
CDE-111

1,3-Phenylene bis(3,4-dihydroxybenzoate)

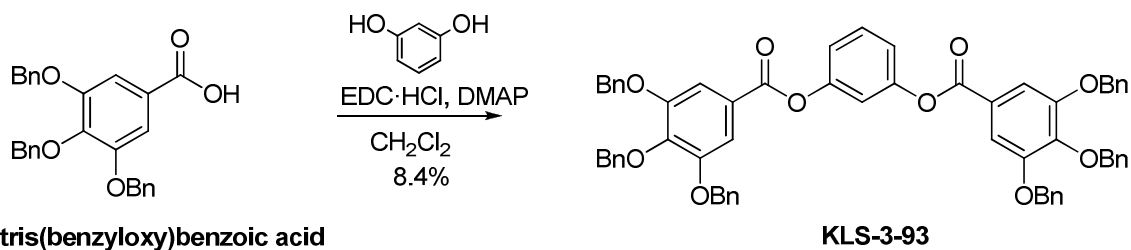
(382.32 g/mol) $\text{C}_{20}\text{H}_{14}\text{O}_8$



1,3-Phenylene bis(3,4-bis(benzyloxy)benzoate) (0.30 g, 0.40 mmol) was dissolved in low-water THF (3.70 mL). Then Pd/C 10% (0.02 g, 0.20 mmol) and 1,4-cyclohexadiene (0.36 mL, 3.98 mmol) were added. The reaction was stirred for 24 hours, under N_2 , at 40°C . A TLC (95% $\text{CH}_2\text{Cl}_2/\text{MeOH}$) indicated the starting material had been consumed. The reaction solution was syringed through a PTFE 0.2 μM syringe prepared with MeOH to remove the Pd/C catalyst. The solvent was then removed *in vacuo* to obtain a solid (90 mg, 59%). ^1H NMR (acetone- d_6 , 400 MHz) δ 8.64 (bs, 4H, -OH), 7.64-7.59 (m, 4H, two ortho and two meta aromatic), 7.50 (t, $J = 8.24$ Hz, 1H, $-\text{O}-\text{C}-\text{CH}-\underline{\text{CH}}-\text{CH}-\text{C}-\text{O}-$), 7.20-7.14 (m, 3H, $-\text{O}-\text{C}-\underline{\text{CH}}-\text{CH}-\underline{\text{CH}}-\text{C}-\text{O}-$ and $\text{O}-\text{C}-\text{CH}-\text{C}-\text{O}-$), and 7.00 (d, $J = 8.24$ Hz, 2H, ortho aromatic); ^{13}C NMR (CDCl_3 , 100 MHz) δ 164.22, 152.00, 150.84, 145.04, 129.67, 123.43, 120.93, 119.26, 116.84, 116.26, 115.25; HRMS, ES calcd. for $\text{C}_{20}\text{H}_{14}\text{O}_8\text{Na}$ $[\text{M}+\text{Na}]^+$ 405.0586, found: 405.0585.



1,3-Phenylene bis(3,4,5-tris(benzyloxy)benzoate)
(742.81 g/mol) C₄₈H₃₈O₈



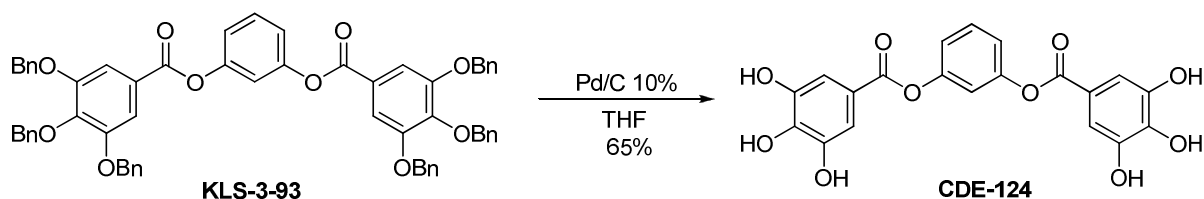
Resorcinol (0.30 g, 2.72), 3,4,5-tris(benzyloxy)benzoic acid (3.60 g, 8.18 mmol), EDC·HCl (4.77 g, 24.9 mmol), DMAP (2.80 g, 22.9 mmol), and CH₂Cl₂ (228 mL); were combined and refluxed over the weekend, while stirring, under N₂. TLC (65% hexanes/EtOAc), indicated that the majority of the starting material had been consumed. The solvent was reduced *in vacuo* and the residue was purified by column chromatography (65% hexanes/EtOAc), to produce a white powder (190 mg, 8.4%). ¹H NMR (CDCl₃, 400 MHz) δ 7.52 (s, 4H, aromatic), 7.49-7.30 (m,

30H, aromatic), 7.33 (s, 1H, -O-CH-O-), 7.27-7.28 (m, 2H, -O-C-CH-CH-CH-C-O-), 7.13-7.11 (m, 1H, -O-C-CH-CH-CH-C-O-), 5.16 (s, 4H, benzylic) and 5.15 (s, 8H, benzylic).

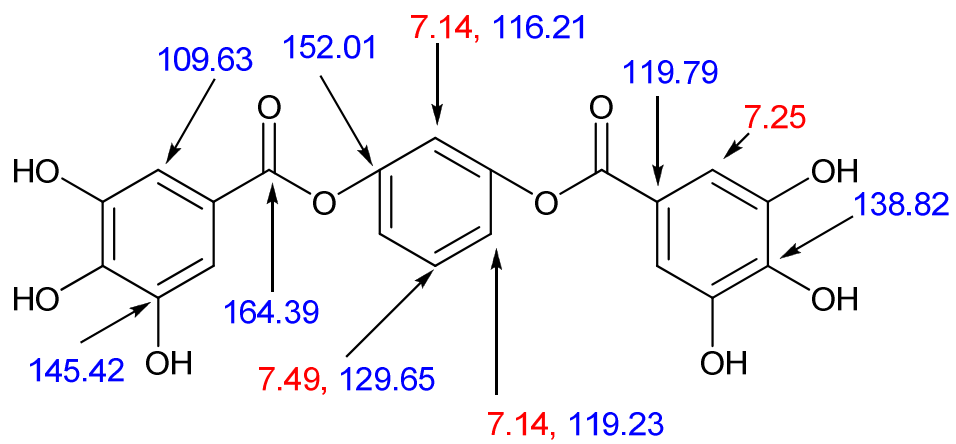
CDE-124

1,3-Phenylene bis(3,4,5-trihydroxybenzoate)

(414.32 g/mol) $C_{20}H_{14}O_{10}$



1,3-Phenylene bis(3,4,5-tris(benzyloxy)benzoate) (0.20 g, 0.21 mmol) was dissolved in low-water THF (2.00 mL). Then Pd/C 10% (0.01 g, 0.10 mmol) was added. The reaction was stirred for 24 hours, under H_2 , at 40°C. TLC (95% $CH_2Cl_2/MeOH$) indicated the starting material had been consumed. The reaction was syringed through a PTFE 0.2 μ M syringe prepared with MeOH to remove the Pd/C catalyst. The solvent was then removed *in vacuo* to obtain thick orange-brown product (560 mg, 65%). 1H NMR (acetone- d_6 , 400 MHz) δ 7.49 (t, $J = 8.24$ Hz, 1H, -O-C-CH-CH-CH-C-O-), 7.25 (s, 4H, aromatic), 7.14-7.19 (m, 3H, -O-C-CH-CH-CH-C-O- and -O-C-CH-C-O-); ^{13}C NMR (acetone- d_6 , 100 MHz) δ 164.39, 152.01, 145.42, 138.82, 129.68, 119.79, 119.23, 116.21, and 109.63; HRMS, ES calcd. for $C_{20}H_{14}O_{10}Na$ $[M+Na]^+$ 437.0485, found: 437.0482.



Chapter 2

Effects of the Central Sugar and Number of Gallates on Inhibitor Potency

BACKGROUND AND OBJECTIVES

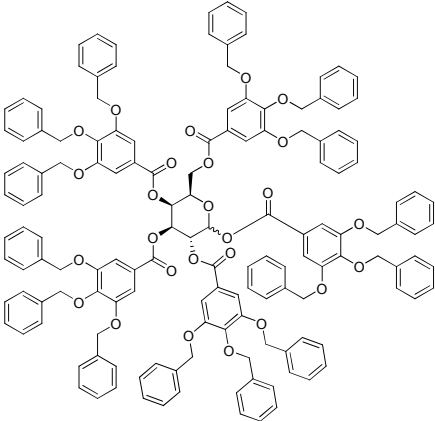
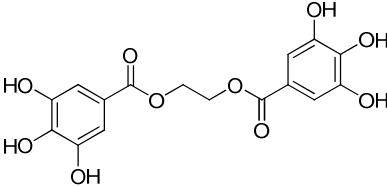
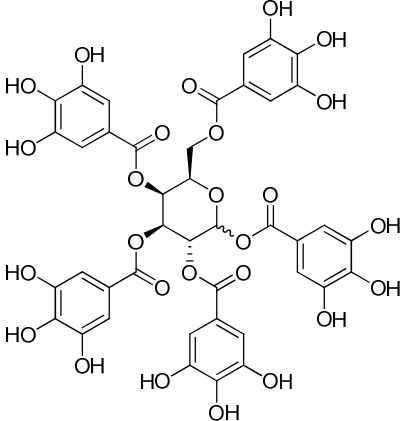
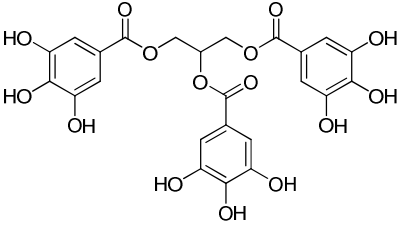
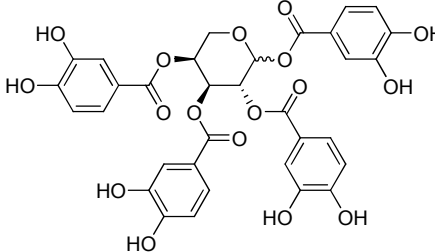
In 2001 Christopher Lipinski published a set of guidelines for synthesizing drug-like molecules known as Lipinski's Rule of Five.⁵⁵ These rules stand as a tentative guide for drug-development by the medicinal chemist. He proposed that if the rules composing his hypothesis were followed, then the molecules synthesized would have an increased likelihood of having acceptable bioavailability, thus increasing the oral absorption and distribution properties of the synthetic species.⁵⁵ These rules focused on the optimization of certain key characteristics of the molecules, including a molecular weight of less than 500 g/mol, a log P-value of less than 5, fewer than 5 hydrogen-bond donor capable species (including hydroxy and amine groups) and fewer than 10 hydrogen bond acceptor species (including nitrogen and oxygen atoms).⁵⁵

It should be noted, however, that these rules are not absolute, and several important exceptions to the rules exist. These include drugs that are substrates for absorptive transporters such as cephalosporins (a class of β -lactam antibiotics) and several natural plant compounds that have been isolated and utilized as drugs without significant modification to their high molecular weight.⁵⁶ Also, while pharmaceutical companies tend to synthesize lead compounds according to the Lipinski guidelines, it is common that their final compounds do not adhere to all four of the rules. Most often it is the rule involving the log P-value of less than 5 (lipophilicity of the compound) that falls outside the recommended range.⁵⁶

Our collaborator's initial screens of the MicroSource SPECTRUM compound library looked for molecules that might be high affinity PAI-1 inhibitors.⁴⁴ One of the molecules identified was a natural polyphenolic compound, tannic acid. Our analysis of the high-throughput screen resulted in the hypothesis that tannic acid would act as a strong inhibitor of PAI-1. An attempt was then made to modify this species to comply with Lipinski's Rule of Five.

One of the first attempts that was made was to reduce the molecular weight of our lead compound, tannic acid (approximately 1700 g/mol). We approached this problem by synthesizing a series of inhibitors that resembled tannic acid but had fewer gallate groups. This series included an α/β -galactose-centered molecule with five gallate groups attached in which all hydroxy positions were benzyl-protected (CDE-006), an α/β -galactose-centered molecule with five gallate groups (unprotected) (CDE-066), an α/β -arabinose-centered molecule with four protocatechuate groups (CDE-112), a gallate-coupled glycerol (CDE-082), and a gallate-coupled ethylene glycol (CDE-008) (Table 5).

Table 5: Gallotannin Variants

Entry (central sugar/linker) and Molecular Weight	Inhibitor	Entry (central sugar/linker) and Molecular Weight	Inhibitor
<p>CDE-006^a (α/β-galactose) MW = 2292 g/mol</p>		<p>CDE-008^a (ethylene glycol) MW = 366 g/mol</p>	
<p>CDE-066 (α/β-galactose) MW = 940 g/mol</p>		<p>CDE-082 (glycerol) MW = 548 g/mol</p>	
<p>CDE-112 (α/β-arabinose) MW = 694 g/mol</p>			

^a = Originally synthesized by Maria Pascua

We then compared the inhibitors' potency and selectivity against PAI-1 with the aim of determining the inhibitor that would have the fewest number of gallates and yet would still give acceptable activity.

The next point of comparison studied the optimization of the central sugar. This work was based on the previously discussed concept that the biological activity of a potential inhibitor is often dependent on the placement of the functional groups of the inhibitor in a specific three-dimensional pattern. Each sugar center arranges the gallates in a unique 3-D arrangement with the ability to readily interconvert amongst their large variety of conformational isomers (Equation 2, Chapter 1). Several similar species were synthesized with differing sugar centers, including β -mannose, α/β -galactose, α/β -glucose, α/β -2-deoxy-D-galactose, and α/β -arabinose. It was hypothesized that one particular arrangement might have an optimal effect upon the inhibitory ability of the molecule.

The synthetic sequences contained within Chapter 2 involved the same reaction steps described in detail in Chapter 1: the benzyl protection of the hydroxy groups, the Steiglich esterification, and the removal of the benzyl protecting groups. Last, the products were purified by either column chromatography or recrystallization. The main difference between the reactions described below and the ones described in Chapter 1 is that the removal of the protecting groups solely utilized the H_2 source and palladium-catalyzed method.

The first step in this process involved an attempt to more fully understand exactly how many gallate attachments were necessary to ensure that the molecule still possessed sufficient inhibitory properties while reducing the overall size of the lead molecule, tannic acid. This led to the synthesis of the molecules in Table 5.

Tannic acid is composed of a glucose center coupled to five gallate derivatives that are in turn coupled to one gallate each, for a total of ten (Figure 23). CDE-006 was synthesized by

coupling α/β -galactose via the Steiglich esterification to benzyl-protected gallic acid. Galactose was chosen because it tends to form the pyranose form allowing for a straightforward synthesis.⁵⁰

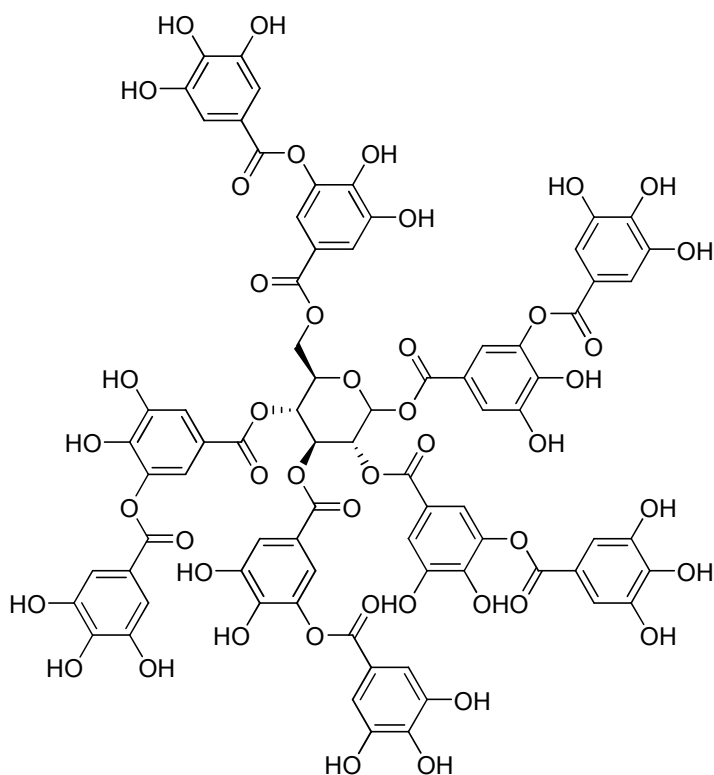


Figure 23: Tannic Acid.

While this molecule was larger than tannic acid, it was also our desire to determine if the elimination of the free hydroxys from the inhibitor would have an effect on its ability to inhibit PAI-1. CDE-066 was synthesized from the precursor CDE-006 to determine the importance of the hydroxy substituents. CDE-112, which contained an α/β -arabinose-center and therefore only had four available esterification sites, CDE-082, which utilized a glycerol molecule and therefore contained only three attachment sites for the gallates, and CDE-008 contained an

ethylene glycol linker, limiting the number of gallate attachments to two were all synthesized.

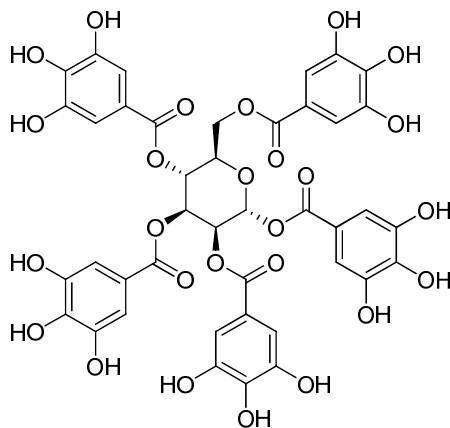
The synthetic inhibitors in this series are illustrated in Table 6.

Table 6: Different Sugar-Centered Molecules.

Entry
(central
sugar/linker)

Inhibitor

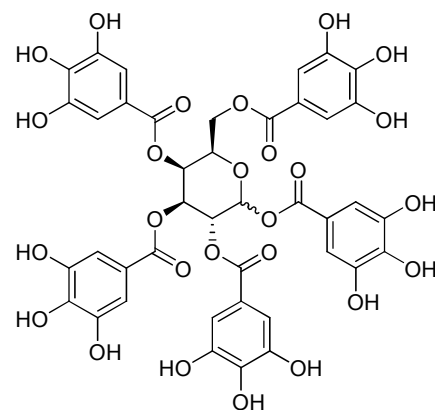
CDE-002^a
(β -mannose)



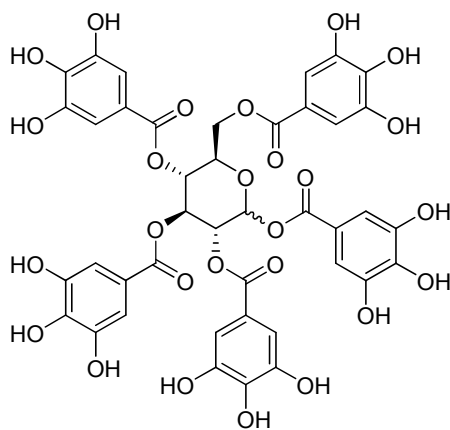
Entry
(central
sugar/linker)

Inhibitor

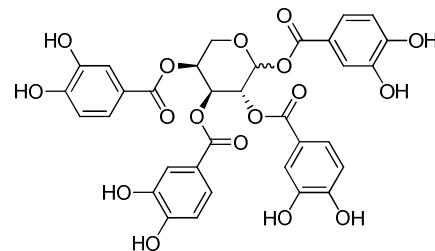
CDE-066
(α/β -galactose)



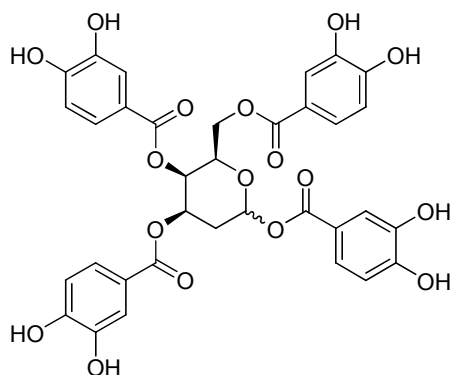
CDE-073
(α/β -glucose)



CDE-112
(α/β -arabinose)



CDE-114
(α/β -2-deoxy-
D-galactose)



Inhibitors containing different sugar centers coupled to either four or five esterified gallates were synthesized and their respective inhibitory potencies against PAI-1 were compared. These inhibitors included molecules containing the following sugar centers: β -mannose (CDE-002), α/β -galactose (CDE-066), α/β -glucose (CDE-073), 2-deoxy-D-galactose (CDE-114), and arabinose (CDE-112). Altering the identity of the sugar centers allows for the gallate attachments to arrange in either *cis* or *trans* geometry. The potency of the inhibitors was examined to determine if a particular sugar-centered inhibitor allowed for an optimum bioactive form.

RESULTS

One of our early objectives was to simplify the structure of the inhibitors significantly from the expansive structure of tannic acid (molecular weight ~1700 g/mol) to determine the minimum number of gallate moieties required for significant inhibitory activity. We synthesized a series of inhibitors containing from one to five gallate esters (Table 4). The sugar-centered penta-gallyl compounds were the most potent inhibitors, but the differences between the inhibitors that contained three, four, and five gallates were small. When attempting to use these data as a guide for further modifying our lead molecule, we noted the relationship between two important factors: our desire to inhibit PAI-1 was countered by our desire not to inhibit PAI-1's closely related analogue, ATIII. Consequently, while the structure containing five gallates led to the strongest inhibitory effect against PAI-1, it also had a strong inhibitory effect against PAI-1's target, tissue-type plasminogen activator (tPA), although it showed only a low level of inhibition for ATIII.

Inhibition of tPA results in the inhibition of fibrinolysis; therefore, a potential PAI-1 inhibitor that also inhibits tPA should be modified to eliminate this extra activity. This is because tPA acts in a stimulatory manner for the production of plasminogen, which stimulates plasmin production, which in turn is the direct stimulatory precursor for the process of fibrinolysis. In contrast, ATIII is a serpin plasma protein that inactivates thrombin and plasmin. Therefore, an inhibitor that inhibits ATIII would also lead to an increase in fibrinolysis but through a separate mechanism than the one we are attempting to follow in this research effort. This leads to the potential inhibitor being deemed a non-specific inhibitor in regards to our target of inhibition, PAI-1. Therefore, an inhibitor having only a small level of inhibition of ATIII compared to that of PAI-1 designates it as a specific inhibitor of PAI-1.

CDE-112, which contains four gallates, resulted in strong nonspecific inhibition of PAI-1 (0.012 μM) and ATIII (0.804 μM). CDE-006, which contains zero unprotected gallates, showed non-detectable inhibition levels of PAI-1 and ATIII. Gallic acid showed PAI-1 inhibition at the relatively low level of only 6.60 μM (Table 7).

Table 7: Biological Assay Results: Modifying the Number of Gallates.

<u>Entry</u>	<u># of Gallates</u>	<u>IC₅₀ vs. PAI-1 (uM)</u>	<u>ATIII (uM)</u>
CDE-066	5	0.013	2435
CDE-112	4	0.012	0.804
CDE-082	3	0.025	14.2
CDE-008	2	0.558	ND
Gallic Acid	1	6.60	n/a
CDE-006	0	ND	ND

Examining the remaining possibilities reveals that the inhibitors containing either two (CDE-008) or three gallates (CDE-082) have conflicting advantages/disadvantages. The tri-gallate molecule (CDE-082) has a similar inhibition of PAI-1 as compared to the tetra or penta-gallate (CDE-112 and CDE-066)) and a similar level of ATIII inhibition (Table 6). The bisgallate (CDE-008) has a non-detectable level of ATIII inhibition while still displaying a decent level of PAI-1 inhibition. Therefore, the bisgallate (CDE-008) among this set of inhibitors contained the optimum number of gallates for specific inhibition of PAI-1.

Our observation that the sugar-centered compounds all displayed strong inhibition of PAI-1 led us to examine the possibility that optimizing the central sugar could lead to increased inhibition of PAI-1 and reduced inhibition of ATIII. The data are displayed in Table 8.

Table 8: Biological Assay Results: Modifying the Sugar Center.

<u>Entry</u>	<u>Sugar Identity</u>	<u>IC₅₀ vs. PAI-1</u> <u>(uM)</u>	<u>ATIII (uM)</u>
CDE-002	β -Mannose	0.012	ND
CDE-112	α/β -Arabinose	0.012	0.804
CDE-066	α/β -Galactose	0.013	2435
CDE-073	α/β -Glucose	0.014	ND
CDE-114	α/β -2-deoxy-D-galactose	0.028	ND

By changing the central sugar, the arrangements of the esterified gallate attachments will differ in their 3-D arrangements. To examine the effect that these different 3-D arrangements of the inhibitors may have on the IC₅₀-values, several species with differing central sugars were synthesized. These inhibitors contain the following sugars: β -mannose (CDE-002), α/β -galactose (CDE-066), α/β -glucose (CDE-073), α/β -2-deoxy-D-galactose (CDE-114), and α/β -arabinose (CDE-112). All IC₅₀-values were within a narrow range (0.012-0.028 uM), displaying a pattern of strong PAI-1 inhibition (Table 7) while displaying low or non-detectable levels of ATIII inhibition, with the exception of CDE-112. Therefore, the conclusion was drawn that the particular sugar used as the core does not affect the potency of the inhibitor by a large degree, suggesting that the precise location of each of the gallates is not important when a large number of gallates are present. This discovery also encouraged us to drastically reduce the molecular weight of our inhibitor scaffold, bringing it more in-line with the weight of oral drugs while still leaving us room to add additional structures to hone the selectivity and potency of our molecule further.

The synthetic efforts to determine the optimum number of gallate substituents indicated that a molecule containing two gallate moieties was ideal, as it provided for inhibition of PAI-1

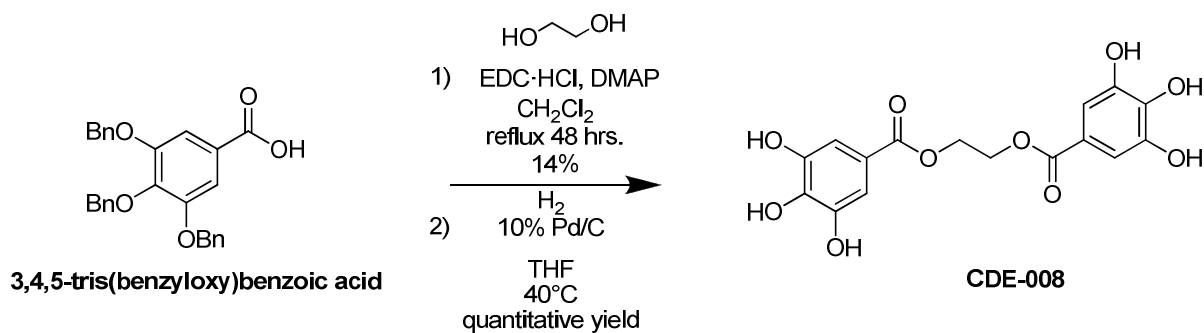
with limited inhibition of ATIII. The second most desirable alternative was a molecule containing three gallates as it provided for increased inhibition of PAI-1; however, this gain was offset by increased inhibition of ATIII.

EXPERIMENTAL

CDE-008

Ethane-1,2-diyl bis(3,4,5-trihydroxybenzoate)

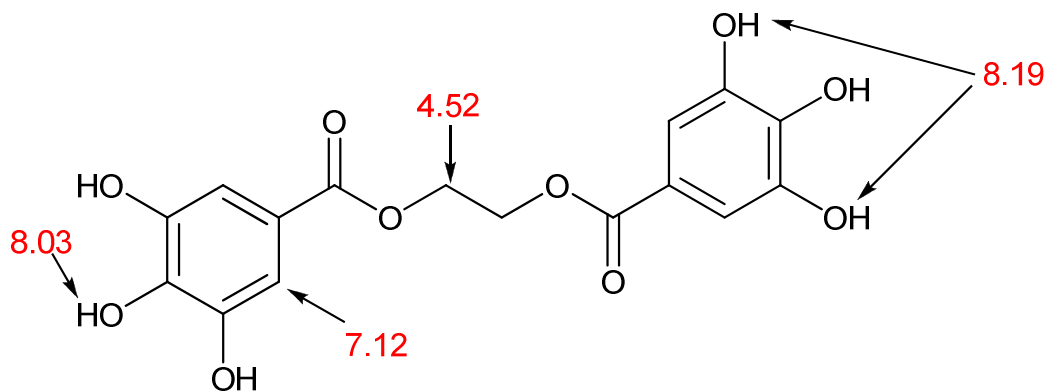
(366.06 g/mol) $C_{16}H_{14}O_{10}$



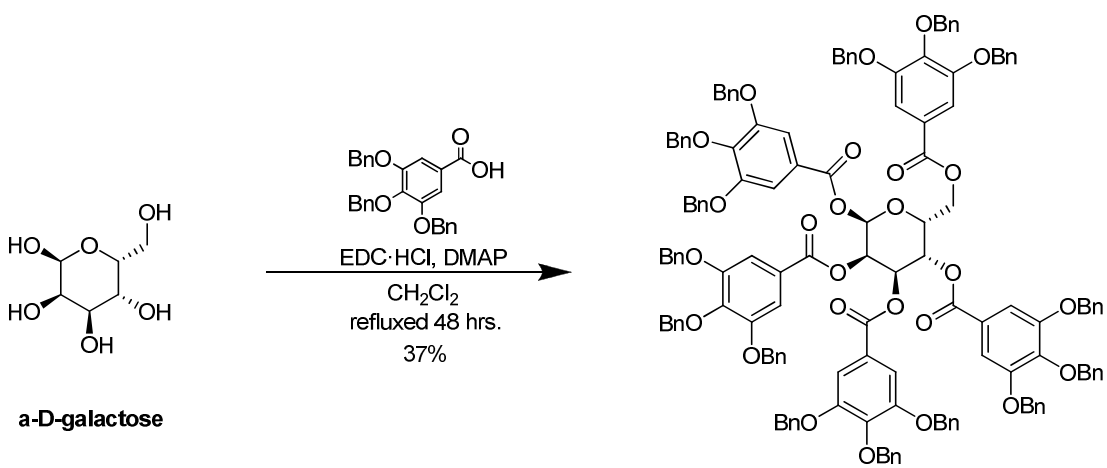
Ethylene glycol (124 mg, 2.00 mmol), 3,4,5-tris(benzyloxy)benzoic acid (2.60 g, 6.00 mmol), EDC·HCl (1.43 g, 10.7 mmol), DMAP (0.84 g, 6.90 mmol), and CH_2Cl_2 (120 ml) were combined and refluxed for 48 hours under N_2 . The organic layer was washed with 10% citric acid (3 X 50 ml), saturated NaHCO_3 (2 X 50 ml), and brine (2 X 30 ml). The organic phase was dried over anhydrous Na_2SO_4 , filtered, and evaporated *in vacuo*. The crude compound was purified by flash column chromatography (90% ethyl acetate/hexane), to obtain a white solid. (258 mg, 14%).

di-O-(3,4,5-Tribenzyloxybenzoyl)ethane glycol (0.26 g, 0.28 mmol) was dissolved in 25 ml THF. A catalytic amount (0.025 g, 0.23 mmol) of 10 wt% palladium on carbon was suspended in the mixture and stirred for 18 hrs. at room temperature under H_2 and then filtered through Celite, and the filtrate was dried *in vacuo* to obtain a white solid (quantitative yield). ^1H NMR (acetone- d_6 , 400 MHz) \square 8.19 (s, 4H, meta -OH), 8.03 (s, 2H, para -OH), 7.12 (s, 4H,

aromatic), 4.52 (s, 4H, -O-CH₂-). HRMS, ES calcd. for C₁₆H₁₄O₁₀Na [M+Na]⁺ 389.0485, found: 389.0476.



D-Galactopyranose pentakis[3,4,5-tris(benzyloxy)-benzoate]
(2290.96 g/mol) C₁₄₆H₁₂₂O₂₆



α/β -D-galactopyranose pentakis[3,4,5-tris(benzyloxy)-benzoate]

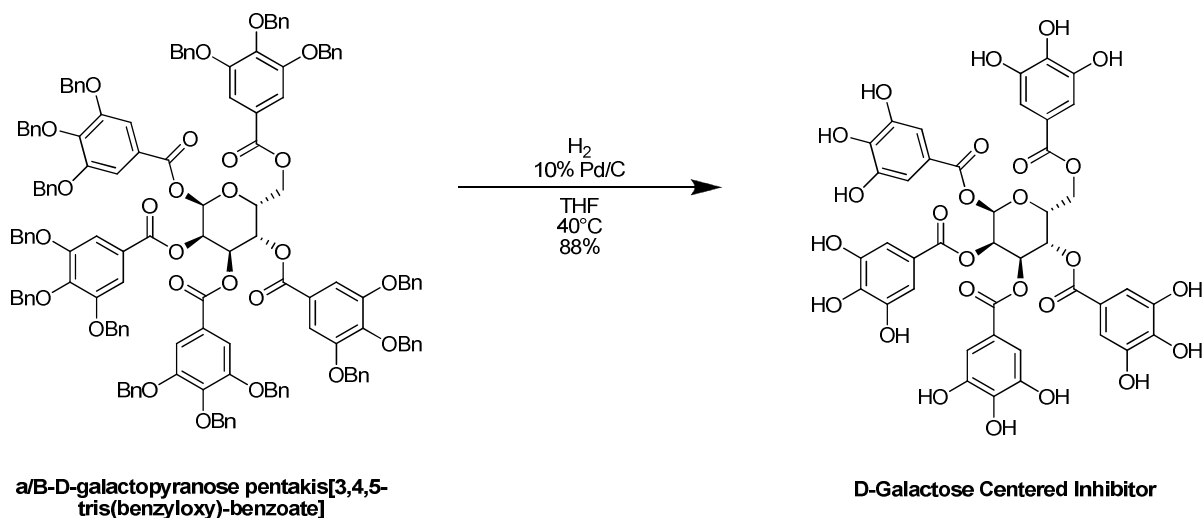
3,4,5-Tris(benzyloxy)benzoic acid (18.8 g, 42.6 mmol), α -D-galactose (1.05 g, 5.82 mmol), EDC·HCl (10.2 g, 53.1 mmol), DMAP (5.98 g, 49.0 mmol), and CH₂Cl₂ (500mL) were combined and refluxed for 48 hours while stirring under N₂. The reaction mixture changed to a dark brown color. The reaction was allowed to cool while stirring. A TLC (65% hexane/EtOAc) indicated complete conversion of the starting material. The CH₂Cl₂ was evaporated *in vacuo*. It was taken up in EtOAc and washed in 1 N HCl (2 x), 1 N saturated aqueous sodium bicarbonate (2 x), and a brine solution (2 x), dried with MgSO₄, filtered, and evaporated *in vacuo*. The residue was purified by column chromatography (65% hexane/EtOAc) to obtain a brown solid (4.84 g, 37%).

Literature values agree with the experimentally determined ¹H NMR spectral data.⁵⁰

CDE-066

(2R,3R,4R,5S,6R)-6-((3,4,5-Trihydroxybenzoyloxy)methyl)tetrahydro-2H-pyran-2,3,4,5-tetraoltetrakis(3,4,5-trihydroxybenzoate).

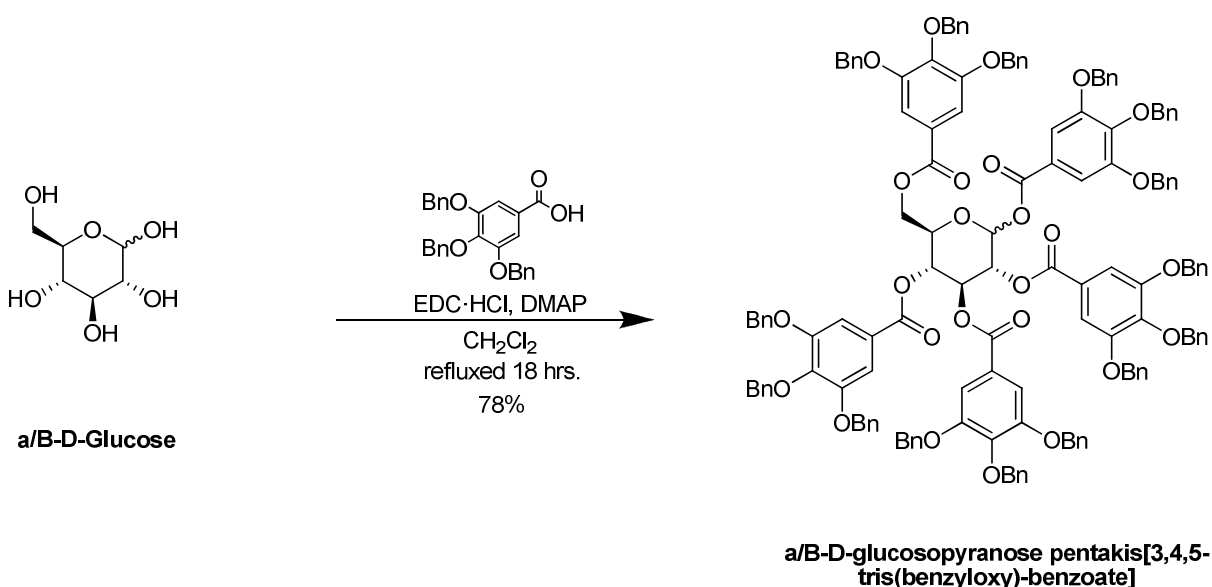
(940.68 g/mol) C₄₁H₃₂O₂₆



D-Galactopyranose pentakis[3,4,5-tris(benzyloxy)-benzoate] (2.40 g, 1.06 mmol) was dissolved in dry THF (150 mL). 10% Pd/C (1.60 g, 15.0 mmol) was added. The reaction was left stirring overnight at 40°C under H₂. A TLC (70% hexane/EtOAc) indicated complete conversion of the starting material. The reaction solution was filtered through Celite to remove the Pd/C. The residue was purified by column chromatography (100% acetone) to obtain a solid (0.89 g, 88%). HRMS, ES calcd. for C₄₁H₃₂O₂₆Na [M+Na]⁺ 963.1080, found: 963.1082.

Literature values agree with the experimentally determined ¹H NMR spectral data.⁵⁰

α/β-D-glucosopyranose pentakis[3,4,5-tris(benzyloxy)-benzoate]
(2292.31 g/mol) C₁₄₆H₁₂₂O₂₆



D-Glucose (1.05 g, 5.82 mmol), 3,4,5-tris(benzyloxy)benzoic acid (18.8 g, 42.9 mmol), EDC·HCl (10.2 g, 53.1 mmol), and CH₂Cl₂ (500 mL) were combined in a flame-dried flask and refluxed

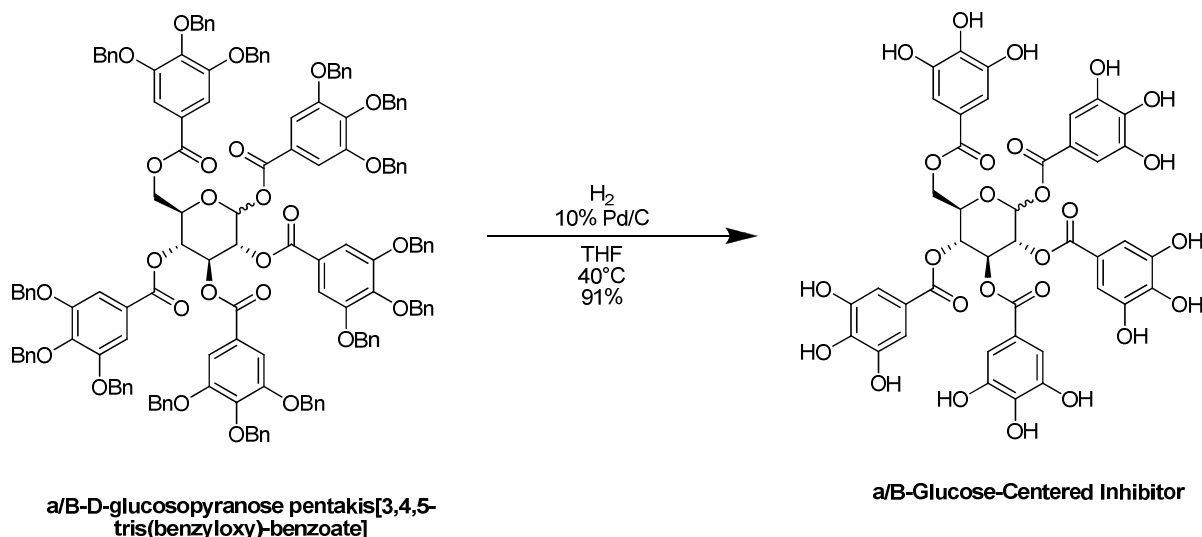
overnight. A TLC (65% hexanes/EtOAc) indicated the reaction had reached completion. The reaction was washed with 1 N HCl (2 x), saturated aqueous NaHCO₃ (2 x), and a brine solution (2 x). The residue was purified by column chromatography (35% EtOAc/hexanes) to obtain a solid (10.34 g, 78%).

Literature values agree with the experimentally determined ¹H NMR spectral data.⁵⁰

CDE-073

(2R, 3R, 4S, 5R, 6R)-6-((3,4,5-Trihydroxybenzoyloxy)methyl)tetrahydro-2H-pyran-2,3,4,5-tetrayl tetrakis (3,4,5-trihydroxybenzoate).

(940.68 g/mol) C₄₁H₃₂O₂₆



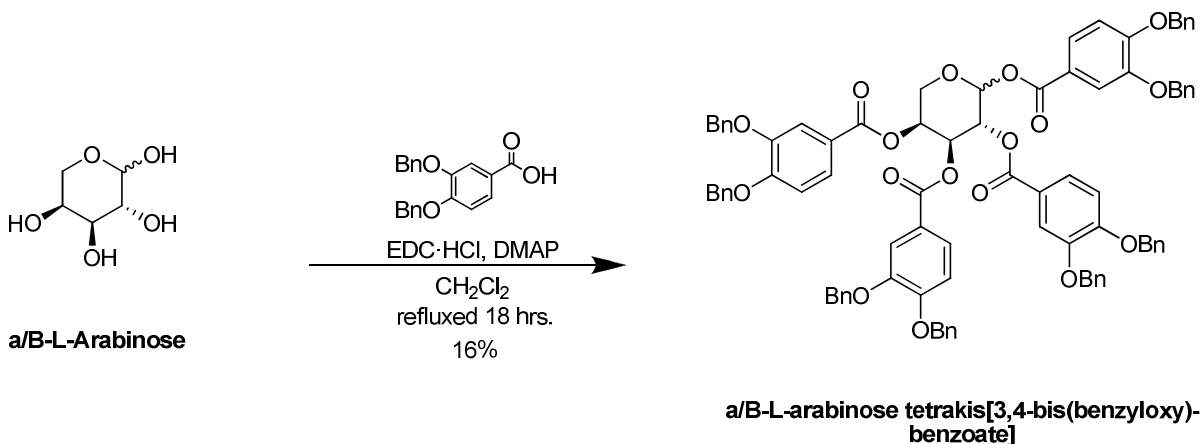
α/β -D-Glucosopyranose pentakis[3,4,5-tris(benzyloxy)-benzoate] (6.50 g, 2.87 mmol) and Pd/C 10% (4.27 g, 40.7 mmol) were combined. Dry THF (40.6 mL) was syringed into the flask. This was stirred at 40°C under H₂ overnight. The reaction was filtered through Celite and rinsed with

acetone. The residue was recrystallized from EtOAc to obtain a white crystalline solid (2.49 g, 91.3%).

HRMS, ES calcd. for $C_{41}H_{32}O_{26}Na$ $[M+Na]^+$ 963.1080, found: 963.1082.

Literature values agree with the experimentally determined 1H NMR spectral data.⁵⁰

α/β -L-Arabinose tetrakis[3,4-bis(benzyloxy)-benzoate]
(1415.53 g/mol) $C_{89}H_{74}O_{17}$

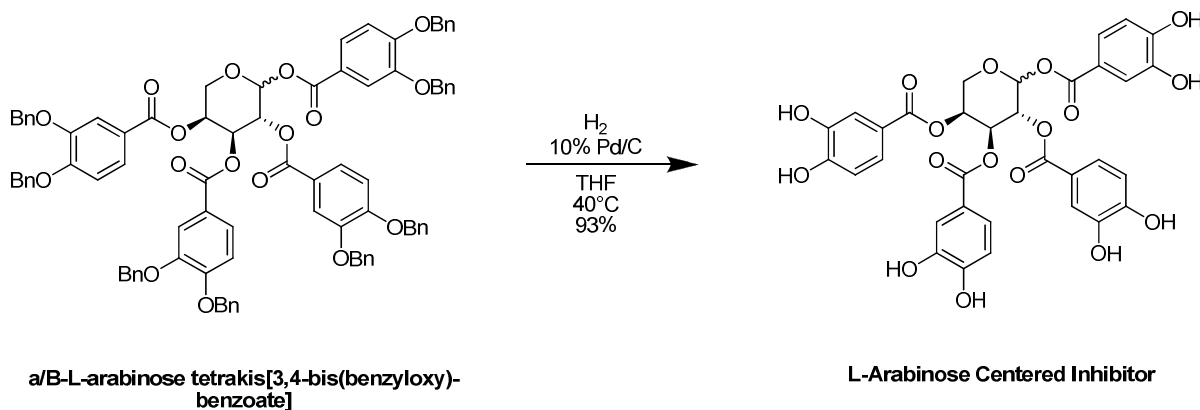


α/β -L-Arabinose (0.28 g, 2.18 mmol), 3,4-bis(benzyloxy)benzoic acid (5.33 g, 15.9 mmol), EDC·HCl (3.81 g, 19.9 mmol), DMAP (2.24 g, 18.3 mmol), and CH_2Cl_2 (140 mL); were combined and refluxed overnight, while stirring, under N_2 . A TLC (65% hexanes/EtOAc), indicated that the majority of the starting material was still present. Therefore, another equivalency of DMAP was added, and the reaction was left stirring over the weekend. A second TLC indicated that the majority of the starting material had been consumed. The solvent was evaporated *in vacuo*. The residue was purified by column chromatography (75%

hexanes/EtOAc, 65% hexanes/EtOAc, 55% hexanes/EtOAc), to obtain a white solid (623 mg, 16%).

CDE-112

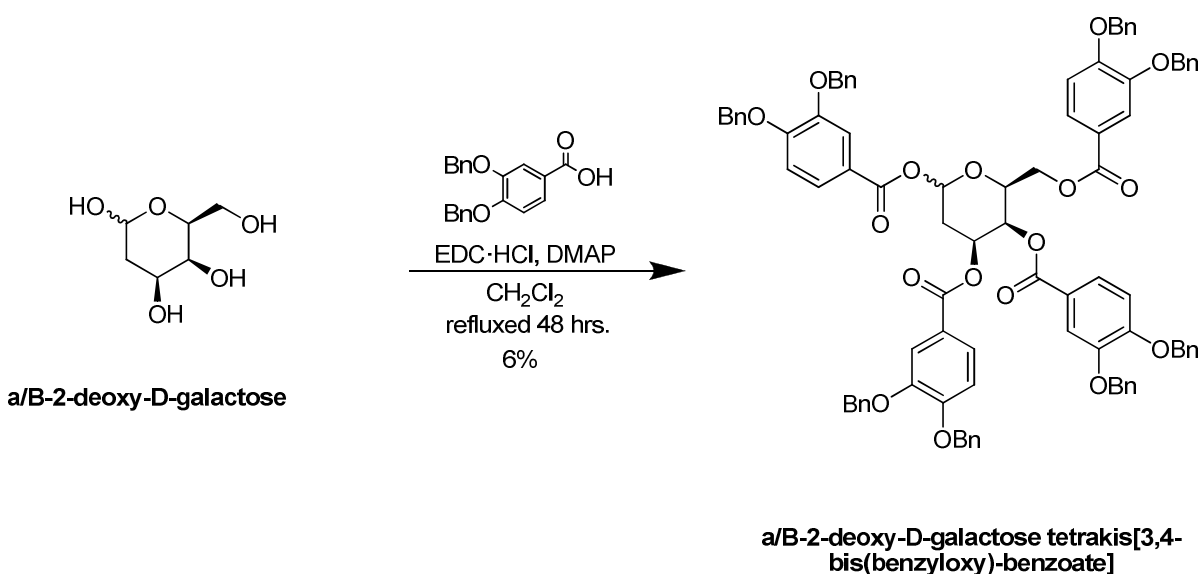
(3R,4S,5S)-Tetrahydro-2H-pyran-2,3,4,5-tetrayl tetrakis(3,4-dihydroxybenzoate)
(694.12 g/mol) $C_{33}H_{26}O_{17}$



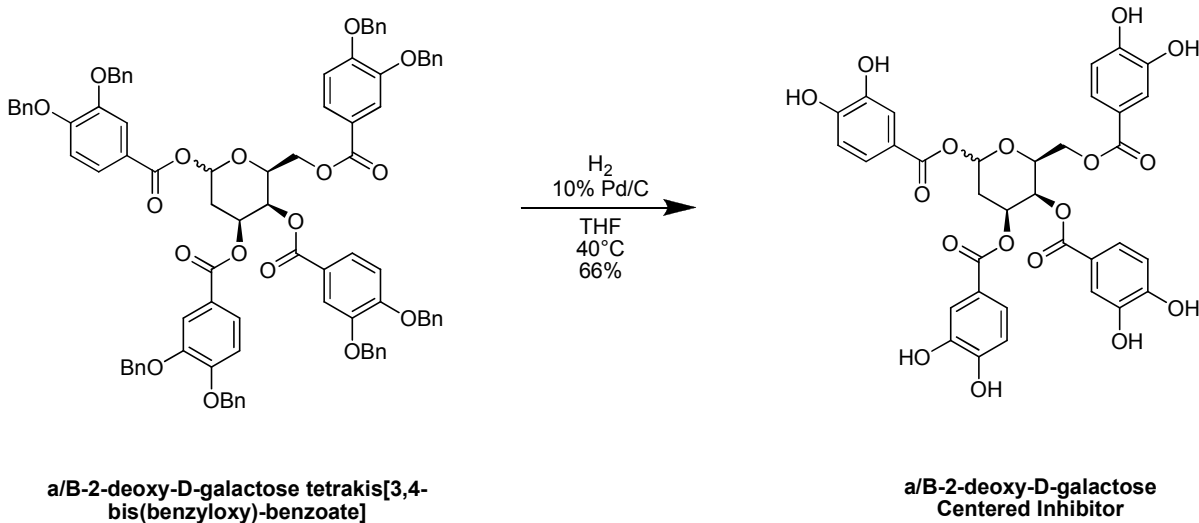
α/β -L-Arabinose tetrakis[3,4-bis(benzyloxy)-benzoate] (550 mg, 0.31 mmol) was dissolved in Ethanol (2.10 mL). Pd/C 10% (0.02 g, 0.2 mmol) and 1,4-cyclohexadiene (0.6 mL, 6.24 mmol) were added. Hexanes (1.00 mL) was added as a cosolvent. The reaction was stirred under N_2 , at 40°C overnight. A TLC (95% $CH_2Cl_2/MeOH$) indicated the starting material had been consumed. The reaction was syringed through a PTFE 0.2 μ M syringe prepared with MeOH to remove the Pd/C catalyst. The solvent was then removed *in vacuo*. The material was then recrystallized from H_2O . The material was then dried in a vacuum oven for 48 hours to remove the excess water, obtaining a solid (202 mg, 93%).

HRMS, ES calcd. for $C_{33}H_{26}O_{17}Na$ $[M+Na]^+$ 717.1068, found: 717.1068.

α/β -2-Deoxy-D-galactose tetrakis[3,4-bis(benzyloxy)-benzoate]
(1429.56 g/mol) $C_{90}H_{76}O_{17}$

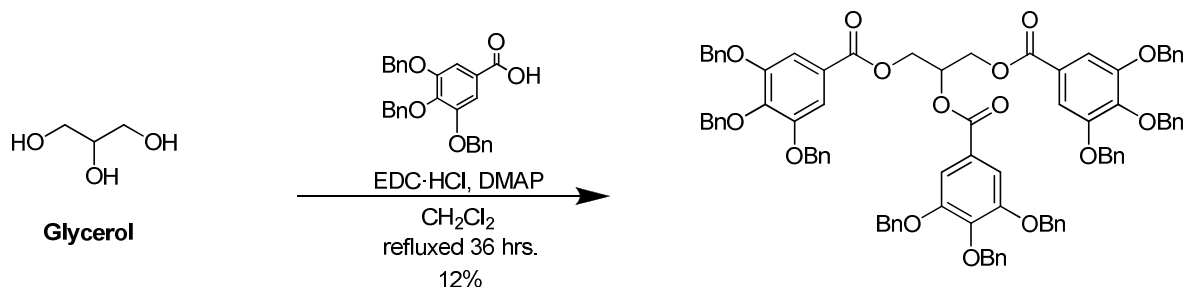


α/β -2-Deoxy-D-galactose (0.3 g, 1.82 mmol), 3,4-bis(benzyloxy)benzoic acid (4.47 g, 13.3 mmol), EDC·HCl (3.20 g, 16.7 mmol), DMAP (1.88 g, 15.4 mmol), and CH₂Cl₂ (116 mL); were combined and refluxed overnight, while stirring, under N₂. A TLC (65% hexanes/EtOAc) indicated that the majority of the starting material had been consumed. The majority of the solvent was removed *in vacuo*. The residue was purified by column chromatography (75% hexanes/EtOAc, 65% hexanes /EtOAc, and 55% hexanes/EtOAc) to obtain a white solid (147 mg, 6.0%).

CDE-114**(4R,5R,6R)-6-((3,4-Dihydroxybenzoyloxy)methyl)tetrahydro-2H-pyran-2,4,5-triyl tris(3,4-dihydroxybenzoate)****(708.58 g/mol) C₃₄H₂₈O₁₇**

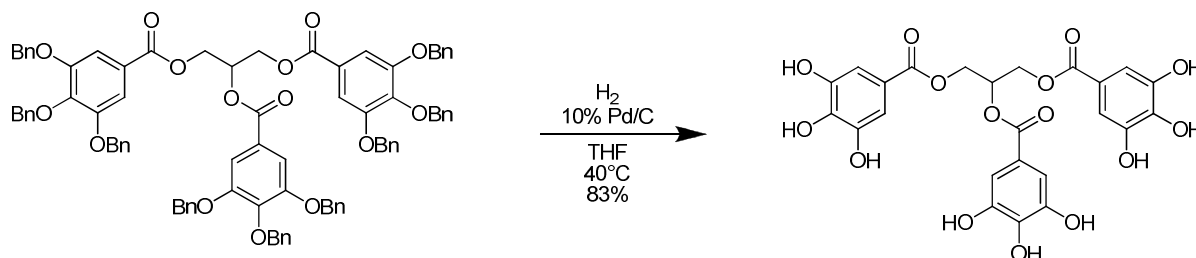
α/β -2-Deoxy-D-galactose tetrakis[3,4-bis(benzyloxy)-benzoate] (140 mg, 0.10 mmol) was dissolved in Ethanol (0.66 mL). Low-water THF (0.5 mL) was added as a co-solvent. Pd/C 10% (0.01 g, 0.05 mmol) and 1,4-cyclohexadiene (0.10 mL, 0.99 mmol) were added. The reaction was stirred for 24 hours, under N₂, at room temperature. A TLC (95% CH₂Cl₂/MeOH) indicated the starting material had been consumed. The reaction was syringed through a PTFE 0.2 μ M syringe prepared with MeOH to remove the Pd/C catalyst. The solvent was then removed *in vacuo*. The material was then dried in a vacuum oven for 48 hours, triturated with acetone, filtered, and the filtrant was evaporated *in vacuo* to obtain a brown solid (45.0 mg, 66%).

Propane-1,2,3-triyl tris(3,4,5-tris(benzyloxy)benzoate)
(1359.52 g/mol) C₈₇H₇₄O₁₅

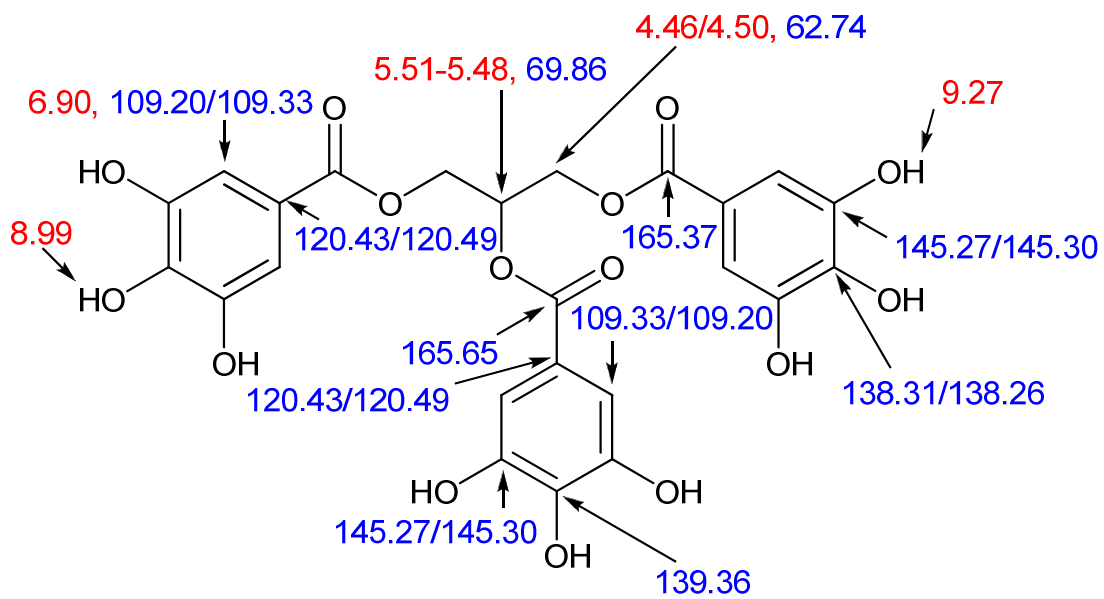


Benzyl-protected-gallate coupled glycerol

3,4,5-Tris(benzyloxy)benzoic acid (2.58 g, 5.85 mmol), DMAP (61 mg, 0.50 mmol), glycerol (0.15 g, 1.67 mmol), and CH₂Cl₂ (6.35 mL, 100.20 mmol) were combined and stirred under N₂. In a separate flask the EDC·HCl (1.21 g, 5.85 mmol) and CH₂Cl₂ (3.17 mL) were mixed and then this solution was syringed drop-wise into the reaction. This reaction was left refluxing for 36 hours. A TLC (70% hexanes/EtOAc) indicated the conversion of the majority of the starting material. The organic layer was washed with 1 N HCl (2 x), saturated aqueous sodium bicarbonate (2 x), and brine (1 x), dried over MgSO₄, filtered, and concentrated *in vacuo*. The residue was purified by column chromatography (70% hexanes/EtOAc) to obtain a solid (266 mg, 12%). ¹H NMR (CDCl₃, 400 MHz) δ 7.36-7.25 (m, 51H, aromatic), 5.73 (quin, *J* = 4.58 Hz, 1H, -CH₂-CH-CH₂-), 5.12-4.96 (m, 18H, benzylic), 4.73-4.69 (m, 2H, -OCH₂-), and 4.53-4.49 (m, 2H, -O-CH₂-); ¹³C NMR (DMSO-*d*₆, 100 MHz) δ 165.65, 165.34, 152.68, 142.09, 142.91, 137.47, 136.59, 136.48, 128.62, 128.14, 127.64, 124.48, 109.44, 109.29, 75.20, 71.27, 70.03, 62.96.

CDE-082**Propane-1,2,3-triyl tris(3,4,5-trihydroxybenzoate)****(548.407 g/mol) C₂₄H₂₀O₁₅****Benzyl-protected-gallate coupled glycerol****Gallate coupled glycerol**

Propane-1,2,3-triyl tris(3,4,5-tris(benzyloxy)benzoate) (200 mg, 0.15 mmol), dry THF (2.09 mL), and Pd/C 10% (0.22 g, 2.08 mmol) were combined and stirred for 6 hours at 40°C under H₂. A TLC (95% CH₂Cl₂/MeOH) confirmed the consumption of the starting material. The reaction was gravity filtered through filter paper, Celite, and a PTFE 0.2 μM syringe to remove the Pd/C catalyst. The solvent was then removed *in vacuo* to obtain a solid (67.1 mg, 83%). ¹H NMR (DMSO-*d*₆, 400 MHz) δ 9.27 (s, 6H, -OH), 8.99 (s, 3H, -OH), 6.90 (s, 6H, aromatic), 5.51-5.48 (m, 1H, -O-CH-), 4.50 (dd, *J* = 3.66, 11.45 Hz, 2H, -O-CH₂-), 4.46 (dd, *J* = 6.41, 11.91 Hz, 2H, -O-CH₂-); ¹³C NMR (acetone-*d*₆, 100 MHz) δ 165.65, 165.37, 145.30, 145.27, 138.31, 138.26, 120.49, 120.43, 109.33, 109.20, 69.86, 62.74; HRMS, ES calcd. for C₂₄H₂₀O₁₅Na [M+Na]⁺ 571.0700, found: 571.0701.



Chapter 3

Effects of Gallate Ring Substitution Pattern on Inhibitor Potency

BACKGROUND AND OBJECTIVES

The following facts regarding PAI-1 inhibitor potency have thus far been established: 1) inhibitors containing ester-linker groups were more effective at inhibiting PAI-1 than those containing amides; 2) the geometric isomerism study indicated that in most cases the cyclic linkers that allowed for a *trans*-positioning of the gallates led to higher inhibition as compared to those with a *cis*-positioning; 3) a molecule containing a cyclic linker molecule that allowed for an increased number of conformations and consequently greater motion of the gallates such as the cyclohexanediol linker (in contrast to the benzenediol linker) was a stronger inhibitor of PAI-1; 4) the negligible activity of the α/β -galactose-centered-molecule with five gallate groups attached in which all hydroxy positions were benzyl-protected (CDE-006) suggests that the hydroxy functional groups on the gallates were a necessary aspect for the success of the inhibitor or that other electronically similar species were necessary; 5) the identity of the sugar at the center of the penta-gallate inhibitors was an unimportant factor regarding PAI-1 inhibitor potency; and 6) an inhibitor containing as few as two gallate attachments (CDE-088, 366 g/mol) was established to be a potent inhibitor while adhering to the Lipinski molecular weight guideline.

Even with all of the above determinations, it was still desirable to hone the inhibitor scaffold further because an inhibitor had not yet been synthesized which inhibited PAI-1 at the nanomolar range and did not also inhibit ATIII. The next aspect that we examined as a means

of improving our potential inhibitor was examining the importance of the number and placement of the hydroxy attachments on the aromatic ring of the gallate or gallate derivatives. With that aim, a series of similar compounds was synthesized with the central structural features unchanged. Instead the number and positioning of the hydroxy attachments on the aromatic ring of the gallate or gallate derivatives were manipulated. The positioning of the hydroxys was manipulated in order to determine if the electronic properties of the aromatic rings would have a significant effect on inhibitor potency.

The number of hydroxy substituents on the aromatic ring was manipulated with the aim of synthesizing an inhibitor that more closely follows one of the Lipinski guidelines. The particular guideline states: “Effective drugs are consistent with molecules that contain fewer than 5 hydrogen-bond donor capable species (including hydroxy and amine groups) and less than 10 hydrogen bond acceptor species (including nitrogen and oxygen atoms).”⁵⁵ Therefore, a series of inhibitors was synthesized in an attempt to ascertain how many hydroxys could be eliminated without a significant decrease in the potency and selectivity of the inhibitor. Due to the unique properties of a benzene ring and the effects that substituents can have on the electronic properties of the ring, a brief overview of these seems necessary.

The effect that newly attached species can have on the electron density of a benzene ring is divided into two main categories: species that either donate to or withdraw electron density from the ring. Both of these can occur through two different pathways, either inductive effects or resonance effects.

Substituents that are electronegative (commonly species that are more electronegative than carbon⁵⁷) cause an inductive effect on the aromatic ring that results in an overall reduction in the ring’s electron density. Substituents that contain lone pairs or π -bonds require extra resonance structures of the aromatic ring; when this new resonance structure is composed of a

benzene species with a positive charge on one of its carbons, then the overall resonance effect is an electron-withdrawing effect.⁵⁷ This occurs when the resonance structure's substituent is composed of an atom possessing a partial positive charge resulting in the transfer of the positive charge onto an aromatic carbon.

The net effect of both the inductive and resonance effects that substituents can induce on an aromatic ring must be considered when determining the overall effect that a substituent has on a benzene ring's electron density. This is easily accomplished when examining groups that only contribute one effect, such as alkyl groups. Alkyl groups display no resonance effect and are more electron rich than a benzene ring and thus always donate electron density.⁵⁷ If a neutral species containing oxygen or nitrogen is directly attached to benzene, then the substituent has an overall electron donating effect via the resonance structure it forms.⁵⁷ If a halogen is directly bonded to benzene, then the net effect is one of electron withdrawal as the inductive effect predominates.⁵⁷ Carbonyl groups withdraw electron density from benzene through both resonance and inductive effects.⁵⁷

The substituents examined in this chapter include only hydroxy groups and carbonyl groups. Hydroxys donate electron density to the benzene ring, and carbonyl groups withdraw electron density from the benzene ring. However, our inhibitors focused only on the modification of the hydroxy substituents, leaving the carbonyls unaltered. Our modification of the number of hydroxy substituents resulted in a manipulation of the electronic character of the bisgallate analogues.

The positioning of substituents on the aromatic ring can also have an effect on how the inhibitor will interact with the functional groups within the binding site on the protein target. Different arrangements may provide for a 3-D structure that could allow the inhibitor to more strongly interact with PAI-1's binding site.

Hydrogen-bonding is the interaction of hydrogen with a more electronegative atom such as sulfur,⁵⁸ fluorine,⁵⁹ oxygen,⁶⁰ or nitrogen.⁶⁰ Experimental and theoretical studies have been conducted to ascertain the characteristics of hydrogen bonding, yet the physical nature of hydrogen bonding remains a topic of much debate within the scientific community.⁶¹ Even so, hydrogen-bonding is an important quality for a drug molecule to possess as it increases the solubility of the drug in a biological system and quite often allows for them to form the necessary interactions with their targets.⁶⁰ The various molecular conformations which intramolecular hydrogen-bonding allows have been investigated utilizing computational software programs and experimental methods.⁶² Intramolecular hydrogen-bonding can often occur between hydroxy substituents on the ortho-position of benzoic acids and the carbonyl's oxygen atom. This intramolecular hydrogen-bonding possibility is hypothesized to play a unique role in the potency of our inhibitors.

The examination of the optimal number and positioning of the hydroxy substituents on the bisgallate analogues will allow us to further our research efforts by analyzing the effects (change in IC₅₀-values) the modifications have on the inhibitors' potency and selectivity.

There were two different starting points followed regarding the synthesis of these inhibitors. Illustrations of the reaction steps of each are outlined in Figure 24.

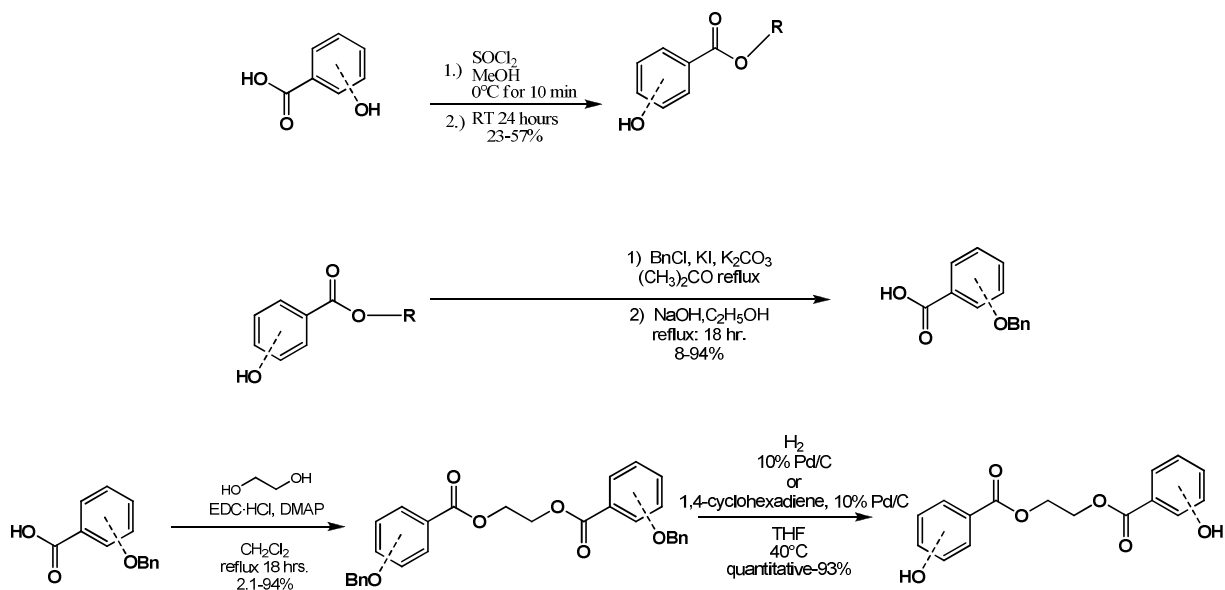


Figure 24: General Reaction Scheme for the Ethylene Glycol-linked Bisgallate Derivatives.

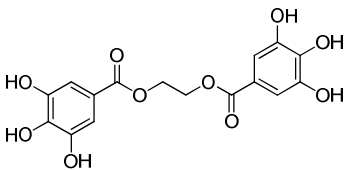
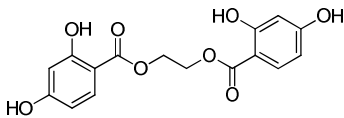
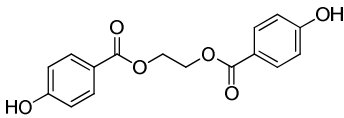
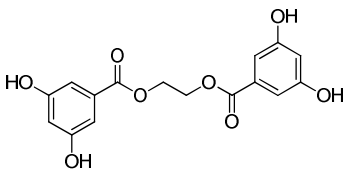
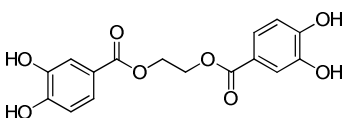
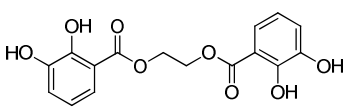
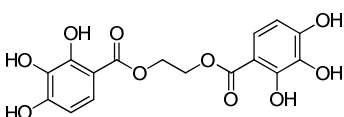
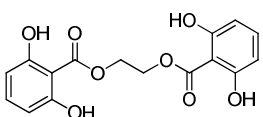
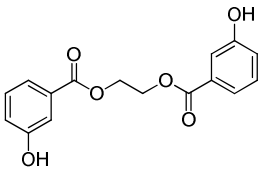
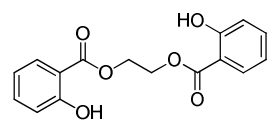
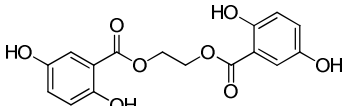
The main point of differentiation is in regard to the first step. When the starting gallate derivative could be purchased as the methyl/ethyl ester, then benzyl-protection and formation of the acid was the first step. When it could only be purchased as the carboxylic acid, then it was necessary to first protect the carboxylic acid (utilizing thionyl chloride and methanol) as the ester prior to benzyl protection of the remaining hydroxy substituents on the aromatic ring. Steiglich esterification formed the ethylene glycol-linked bisgallates, and the protecting groups were removed in THF with a catalytic amount of 10 wt% palladium on carbon and H_2 or 1,4-cyclohexadiene as the hydrogen source.

When determining the optimal substitution pattern on the aromatic rings, it was imperative to obtain results that could be used to indicate that a single modification on the inhibitor resulted in a change in potency. Therefore a series of compounds containing the same

linker but differing in the number and positioning of the hydroxy attachments on the aromatic rings was synthesized.

The series of molecules was synthesized (Table 9) with the aim of determining the number of hydrogen-bond donor capable species (hydroxys) that could be removed from the aromatic ring of the inhibitor without significantly impacting the potency and selectivity of the inhibitor.

Table 9: Ethylene Glycol-Linked Polyphenols

Entry	Inhibitor	Entry	Inhibitor
CDE-008 ^c		CDE-051 ^b	
CDE-081 ^a		CDE-084 ^b	
CDE-090		CDE-094	
CDE-098		CDE-101	
CDE-106 ^d		CDE-123	
CDE-151			

Synthesized by:
a = Melinda Myers
b = Kristi Henricks
c = Maria Puscau
d = Nadine El-Ayache

The same series of inhibitors (Table 9) was examined, focusing on the positioning of the hydroxys and whether differing positions affected the inhibitor's potency. The electron-donating character of the hydroxy substituents allows for us to determine if a higher degree of electron density of the aromatic ring leads to increased potency of the inhibitor or vice versa. This was accomplished by modifying the number of hydroxy substituents and thus the electronic character of the bisgallate analogues.

The positioning of attachments on the aromatic ring can also have an effect on how the inhibitor will interact with the functional groups within the binding site on the protein target. It is our hypothesis that a preferential 3-D arrangement of the substituents on the aromatic ring will allow for an increased potency of the inhibitor as it will enable it to interact with the serpin more readily.

RESULTS

The Lipinski guideline detailing the optimal number of hydrogen-bond donor capable species led us to examine how many hydroxys we could effectively remove from the aromatic ring and still maintain inhibitor potency. The inhibitors that contain only one hydroxy per aromatic ring (CDE-81, CDE-106, CDE-123), ranged in potency from a non-detectable IC_{50} -value to a value of 565 μM (Table 10). The inhibitors that contain only two hydroxys per aromatic ring (CDE-051, CDE-084, CDE-090, CDE-094, CDE-101, CDE-151) ranged in potency from a non-detectable IC_{50} -value to a value of 0.33 μM . The inhibitors that contain three hydroxys per aromatic ring (CDE-008, CDE-098) ranged in potency from IC_{50} -values of 680.6-0.558 μM . It is apparent from the IC_{50} -values that more than one hydroxy group is necessary for any significant level of inhibition. All three single hydroxy molecules, including the 2-hydroxy, 3-hydroxy, and 4-hydroxy moieties showed correspondingly poor or non-existent levels of PAI-1 inhibition (Table 10).

Table 10: Biological Assay Results: Modifying the Number/Position of Hydroxy Substituents

<u>Compounds</u>	<u>Aromatic Substitution</u>	<u>IC₅₀ vs. PAI-1 (uM)</u>
CDE-090	3,4-OH	0.33
CDE-008	3,4,5-OH	0.558
CDE-101	2,6-OH	7.86
CDE-051	2,4-OH	33.37
CDE-151	2,5-OH	136
CDE-084	3,5-OH	175
CDE-106	3-OH	565
CDE-098	2,3,4-OH	680.6
CDE-123	2-OH	ND
CDE-081	4-OH	1400
CDE-094	2,3-OH	ND

Comparable low IC₅₀-values were found between an analogue containing two hydroxy substituents per aromatic ring (CDE-090) and an analogue containing three hydroxy substituents per aromatic ring (CDE-008) (0.33 μM and 0.558 μM, respectively). Therefore, it was determined that optimal potency could still be maintained with two fewer hydroxy groups than our original bisgallate (CDE-008). This determination successfully brought our inhibitor in line with Lipinski's guidelines which recommended fewer than 5 hydrogen-bond donor capable species.

The 3,4-dihydroxy molecule (CDE-090) showed the highest inhibition, 0.33 μM and a non-detectable level of ATIII inhibition. The second highest inhibition was displayed by the 3,4,5-trihydroxy substituted gallate (CDE-008) with an IC₅₀-value of 0.558 μM and a non-detectable level of ATIII inhibition.

Inhibitors lacking the hydroxy group at either the 3- or 4-position suffered a significant decrease in potency. However, it is not apparent if one of these positions is more important

than the other. The compound with a single hydroxy group present at the 3-position (CDE-106) with an IC_{50} -value of 565 μ M proves more potent than the one with a single hydroxy at the 4-position (CDE-081) with an IC_{50} -value of 1400 μ M, while the compound with a 2,4-dihydroxylated ring (CDE-051) with an IC_{50} -value of 33.37 μ M is more potent than a 2,3-dihydroxyated version (CDE-094) with a non-detectable level of inhibition.

There is an interesting aspect to the inhibitors that contain ortho-substituted hydroxy groups. The reversible intramolecular hydrogen bonding between the hydroxy groups and the carbonyl oxygen encourages the inhibitor to take on a different conformation (Figure 25). This conformation differs in stability when comparing inhibitors with only one ortho-hydroxy or with two ortho-hydroxy substituents. The inhibitor containing only one ortho-hydroxy substituent (CDE-123) has non-detectable levels of PAI-1 inhibition, while the 2,6-dihydroxy-substituted inhibitor (CDE-101) shows a substantial increase in potency with an IC_{50} -value of 7.86 μ M.

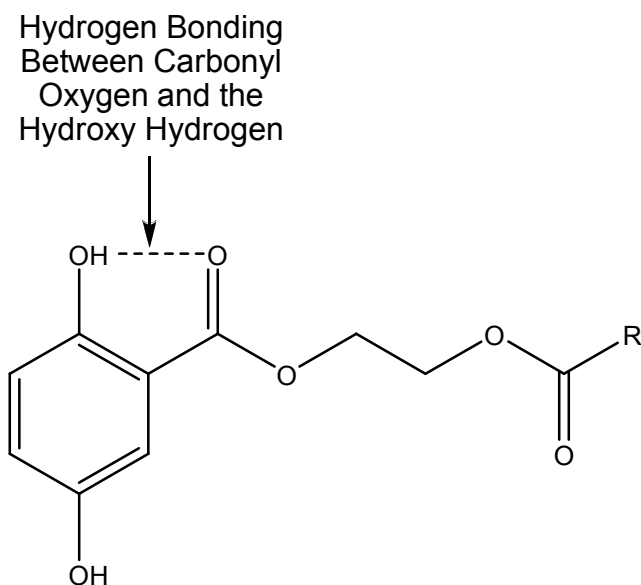


Figure 25: Intramolecular Hydrogen Bonding on An Inhibitor.

The lower IC_{50} -value for the 2,6-disubstituted molecule (CDE-101) could be accounted for by examining this interaction. Due to the reversibility of the intramolecular hydrogen-bond, the inhibitor contains both a hydrogen-bonded substituent and a free hydroxy functional group (Figure 25). It has previously been proposed that small-molecule inhibitors of PAI-1 bind in pocket sites on the serpin.⁶³ It is hypothesized that the hydrogen-bonded inhibitor's 3-D shape allows it to position itself more tightly within the binding site of PAI-1. Then due to its ability to exist correspondingly as the free hydroxy, it could conform and bind to PAI-1, inhibiting it.⁶⁴ This accounts for the 2,6-dihydroxy substituted inhibitor's (CDE-101) low IC_{50} -value (7.86 μ M) in comparison to the mono-ortho-hydroxy substituted, inhibitor (CDE-123) which has non-detectable levels of PAI-1 inhibition.

The remaining moieties, including the 2,4-dihydroxy (CDE-051, $IC_{50} = 33.37 \mu$ M), 2,5-dihydroxy (CDE-151, $IC_{50} = 136 \mu$ M), and the 2,3-dihydroxy (CDE-094, non-detectable inhibition), have poorer inhibition effects than the 2,6-dihydroxy substituted analogue (CDE-101, $IC_{50} = 7.86 \mu$ M). Again this can be understood by the intramolecular hydrogen bonding of the hydroxy group on the ortho-position. The 2,4-dihydroxy (CDE-051, $IC_{50} = 33.37 \mu$ M) and the 2,5-dihydroxy (CDE-151, $IC_{50} = 136 \mu$ M) have free hydroxys (at the 4th and 5th position) available to interact with the inhibitory site of PAI-1 before the molecule has reached its optimum inhibitory conformation within the pocket of the serpin's binding site. This interaction hinders it from reaching this position regardless of the 2-hydroxy intramolecular hydrogen bonding configuration. Also, because the ortho-hydroxy substituent is hydrogen bonded to the carbonyl, it is not free to interact at this optimal position, therefore only allowing for the interaction of one hydroxy group which has already been established to result in poor inhibition of the protein (CDE-106 with $IC_{50} = 565 \mu$ M, CDE-123 with non-detectable inhibition levels, CDE-081 with $IC_{50} = 1400 \mu$ M).

A counter to this argument is the inhibition level of the 2,3,4-trihydroxy inhibitor (CDE-098 with $IC_{50} = 680.6 \mu\text{M}$). The 3,4-dihydroxy inhibitor (CDE-090) showed the highest inhibition, $0.33 \mu\text{M}$ and therefore, with the 2-hydroxy position being hydrogen bonded to the carbonyl and the 3,4-dihydroxys being free to act on the inhibitory site of the molecule, it would seem that the inhibition levels would be comparable between CDE-090 and CDE-098. However, the new conformation of the intramolecularly hydrogen bonded 2,3,4-trihydroxy inhibitor results in the meta-hydroxy being shifted from its usual position, thus making it less able to interact than it was in its previous non-hydrogen bonded conformation.⁶⁴ It is a note of interest that the 2,3,4-trihydroxy moiety is the only one of this series that inhibits ATIII ($IC_{50} = 502 \mu\text{M}$).

The remaining two inhibitors CDE-151 and CDE-106 showed PAI-1 inhibition levels of 136 and $565 \mu\text{M}$, respectively, and both showed non-detectable levels of ATIII inhibition. This indicates that these species were selective in their PAI-1 inhibition and that further modifications will be necessary to increase their affinity for PAI-1.

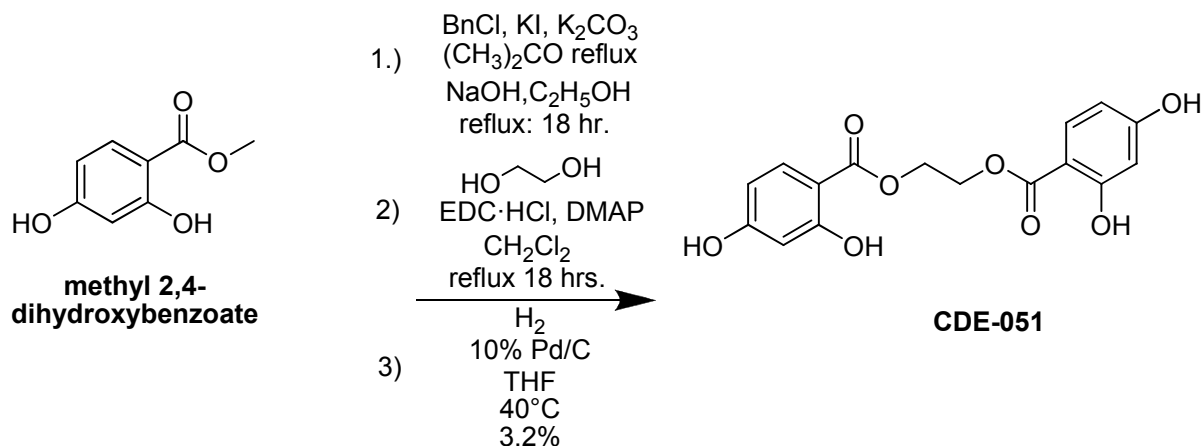
While the results from Chapter 1 regarding the potency change between inhibitors that were 3,4-dihydroxy substituted in comparison to their bisgallate analogues were inconclusive, our attempt to bring our inhibitors in line with the Lipinski guideline regarding the suggested limitation on hydrogen-bond donor capable species supports the use of the 3,4-dihydroxy substitution, as it allows for the synthesis of an inhibitor which has fewer than five hydroxyl groups.

EXPERIMENTAL

CDE-051

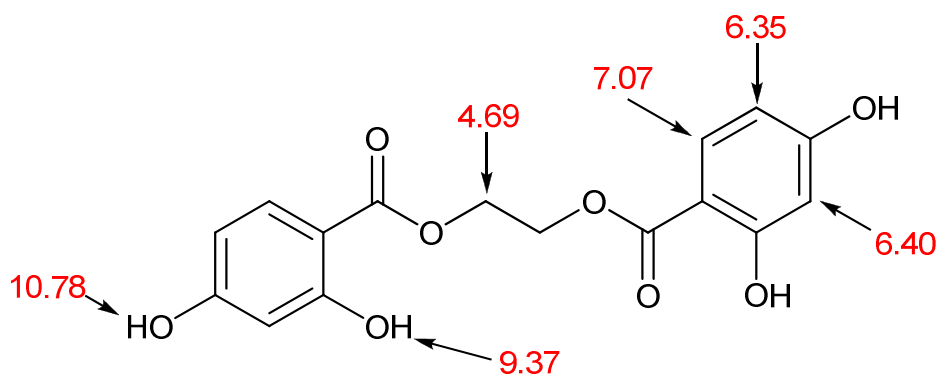
Ethane-1,2-diyl bis(2,4-dihydroxybenzoate)

(334.28 g/mol) $C_{16}H_{14}O_8$



Step #3 Step #2's product (111 mg, 0.16 mmol) was dissolved in CH_2Cl_2 (0.80 mL). 1,4-cyclohexadiene (0.30 mL, 3.20 mmol) and a catalytic amount of Pd/C 10% (1.70 mg, 3.2%) was added. The reaction was stirred at room temperature for 48 hours. A TLC (95%: $CH_2Cl_2/MeOH$) indicated the consumption of the starting material. The reaction was purified by prep-TLC (95%: $CH_2Cl_2/MeOH$).

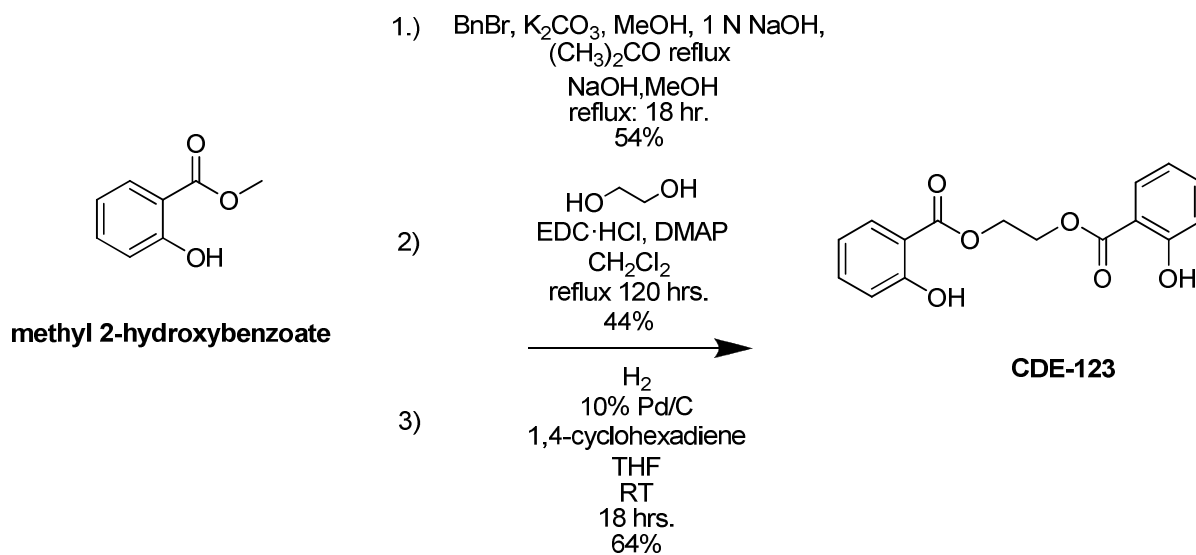
1H NMR (acetone- d_6 , 400 MHz) δ 10.78 (s, 2H, para -OH), 9.37 (s, 2H, ortho -OH), 7.07 (d, $J = 9.16$ Hz, 2H, ortho aromatic), 6.40 (dd, $J = 2.29, 8.70$ Hz, 2 H, meta aromatic between hydroxy-substituted carbons), 6.35 (d, $J = 2.29$ Hz, 2H, meta aromatic), 4.69 (s, 4H, -O- CH_2); HRMS, EI calcd. for $C_{16}H_{14}O_8$ $[M+]^+$ 334.0688, found: 334.0690.



CDE-123

Ethane-1,2-diyl bis(2-hydroxybenzoate)

(302.08 g/mol) C₁₆H₁₄O₆



Step #1: Benzyl bromide (4.70 mL, 39.4 mmol) and acetone (200 ml) were combined. Methyl 2-hydroxybenzoate (4.26 mL, 32.9 mmol) and anhydrous K₂CO₃ (18.0 g, 130 mmol) were added.

Solution was refluxed under N₂ overnight. K₂CO₃ was filtered off and the filtrant was evaporated. The solid was taken up in MeOH (180 mL) and 1 N NaOH (1.43 g, 35.8 mmol) was added. Solution was stirred overnight at room temperature under N₂. A TLC (100% hexanes) indicated that the starting material was consumed. Then 1 N HCl (350 mL) was added. A bright yellow oily liquid formed and settled to the bottom of the flask and was pipetted away from the solution. The bright yellow oily liquid was dried *in vacuo* to obtain a yellow solid (4.03 g, 54%).

Literature values agree with the experimentally determined NMR spectral data.⁶⁵

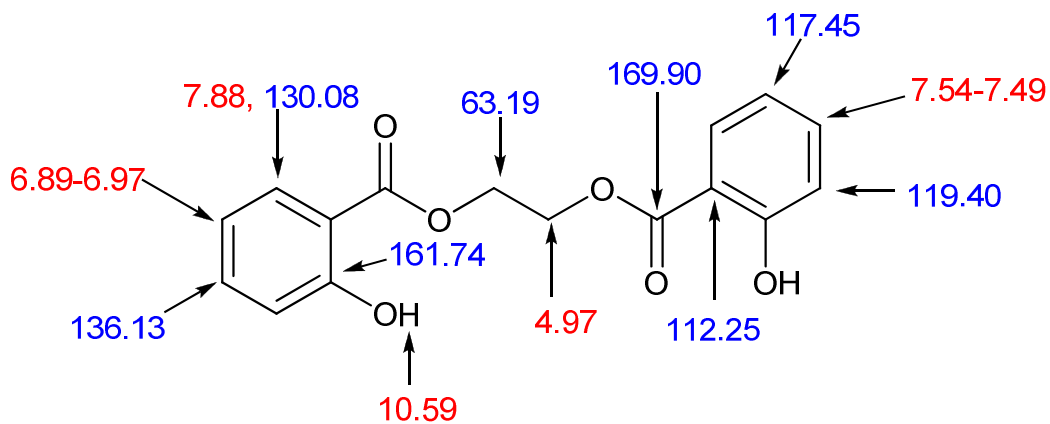
Step #2: Ethylene glycol (390 μ L, 7.00 mmol), 2-(benzyloxy)benzoic acid (4.00 g, 17.5 mmol), EDC·HCl (3.61 g, 17.5 mmol), DMAP (0.214 g, 1.75 mmol), and CH₂Cl₂ (222 ml) were combined and refluxed for 120 hours under N₂. A TLC (85% hexanes/EtOAc) indicated that the starting material was consumed. The crude compound was purified by flash column chromatography (85% hexanes/EtOAc), to obtain a yellow oil.

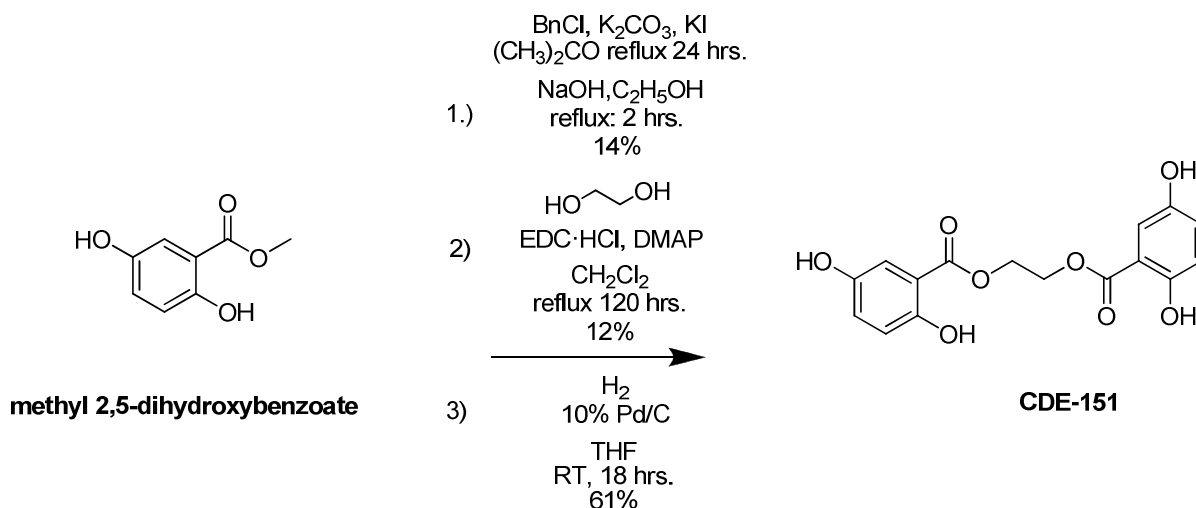
¹H NMR (CDCl₃-d₆, 400 MHz) δ 7.83 (dd, J = 1.84, 7.76 Hz, 2H, ortho aromatic), 7.22-7.50 (m, 12H, para aromatic), 6.92-6.98 (m, 4H, meta aromatic), 5.14 (s, 4H, benzylic), 4.60 (s, 4H, -O-CH₂).

Step #3: The benzyl-protected ethylene glycol linked bisgallate derivative (1.40 g, 2.90 mmol) was dissolved in 35 ml THF. 10 wt% Pd/C (3.08 g, 29.0 mmol) and 1,4-cyclohexadiene (2.70 mL, 29.0 mmol) were added and the reaction was stirred under H₂ for 18 h at room temperature. A TLC (95% CH₂Cl₂/MeOH) indicated that the starting material was consumed. The reaction mixture was filtered through Celite and the filtrate was evaporated. Solid that formed was recrystallized from hexanes and the white solid crystals which formed were dried *in vacuo* (0.56 g,

64%).

^1H NMR (acetone- d_6 , 400 MHz) δ 10.59 (s, 2H, -OH), 7.88 (dd, $J = 1.84, 7.80$ Hz, 2H, ortho aromatic), 7.54-7.49 (m, 2H, para aromatic), 6.97-6.89 (m, 4H, meta aromatic), 4.79 (s, 4H, -O-CH $_2$ -); ^{13}C NMR (acetone- d_6 , 100 MHz) δ 169.90, 161.74, 136.13, 130.08, 119.40, 117.45, 112.25, 63.19; HRMS, EI calcd. for $\text{C}_{16}\text{H}_{14}\text{O}_6$ $[\text{M}]^+$ 302.0790, found: 302.0792.



CDE-151**Ethane-1,2-diyl bis(2,5-dihydroxybenzoate)****(334.28 g/mol) C₁₆H₁₄O₈**

Step #1: Benzyl chloride (3.65 mL, 31.7 mmol) and acetone (126 mL) were combined. Methyl 2,5-dihydroxybenzoate (2.50 mL, 14.9 mmol), anhydrous K_2CO_3 (8.22 g, 59.5 mmol), and KI (0.74 g, 4.46 mmol) were added. Solution was refluxed under N_2 overnight. A TLC (80% hexanes/EtOAc) indicated that the starting material was consumed. Solution was filtered and the filtrant was evaporated. The solid was taken up in CH_2Cl_2 (22 mL), filtered through Celite, and the filtrate was dried *in vacuo*.

The methyl-protected gallate derivative, 95% ethanol (133 mL), and NaOH (0.96 g, 24.2 mmol) were refluxed under N_2 for 2 hours. The hot solution was poured into 8.75 mL of a 0.6 M HCl solution and stirred for 10 min. The yellow solid was filtered off. The crude product was washed successively with a 1:1 solution of 95% Ethanol: H_2O (100 mL), water (100 mL),

methanol (100 ml) and tert-butyl methyl ether (100 ml). The solid was dried *in vacuo* to obtain a yellow solid (0.67 g, 14%).

^1H NMR (CDCl_3-d_6 , 400 MHz) δ 11.06 (bs, 1H, -OH), 7.80 (d, $J = 3.20$ Hz, 1H, ortho aromatic), 7.45-7.30 (m, 10H, aromatic), 7.17-7.14 (m, 1H, meta aromatic), 7.08-7.04 (m, 1H, para aromatic), 5.23 (s, 2H, benzylic), 5.06 (s, 2H, benzylic); ^{13}C NMR (CDCl_3-d_6 , 100 MHz) δ 165.21, 153.79, 151.82, 136.49, 134.55, 129.27, 129.23, 128.74, 128.26, 128.08, 127.68, 122.84, 118.83, 117.72, 115.01, 73.05, 70.76.

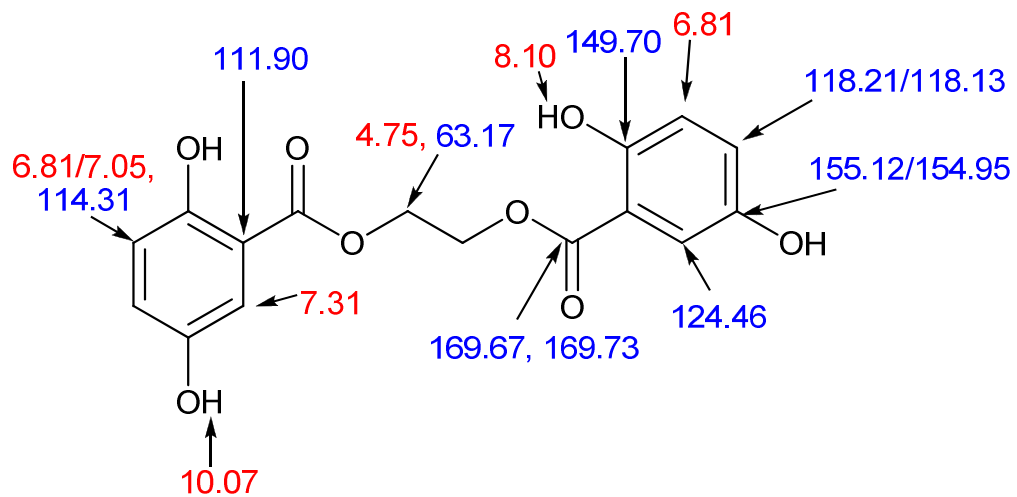
Step #2: Ethylene glycol (44.8 μL , 803 μmol), 2,5-bis(benzyloxy)benzoic acid (672 mg, 2.00 mmol), EDC \cdot HCl (415 mg, 2.00 mmol), DMAP (24.5 mg, 0.20 mmol), and CH_2Cl_2 (25.0 ml) were combined and refluxed for 120 hours under N_2 . A TLC (80% hexanes/EtOAc) indicated that the starting material was consumed. The crude compound was purified by flash column chromatography (80% hexanes/EtOAc), to obtain a white powder (12%).

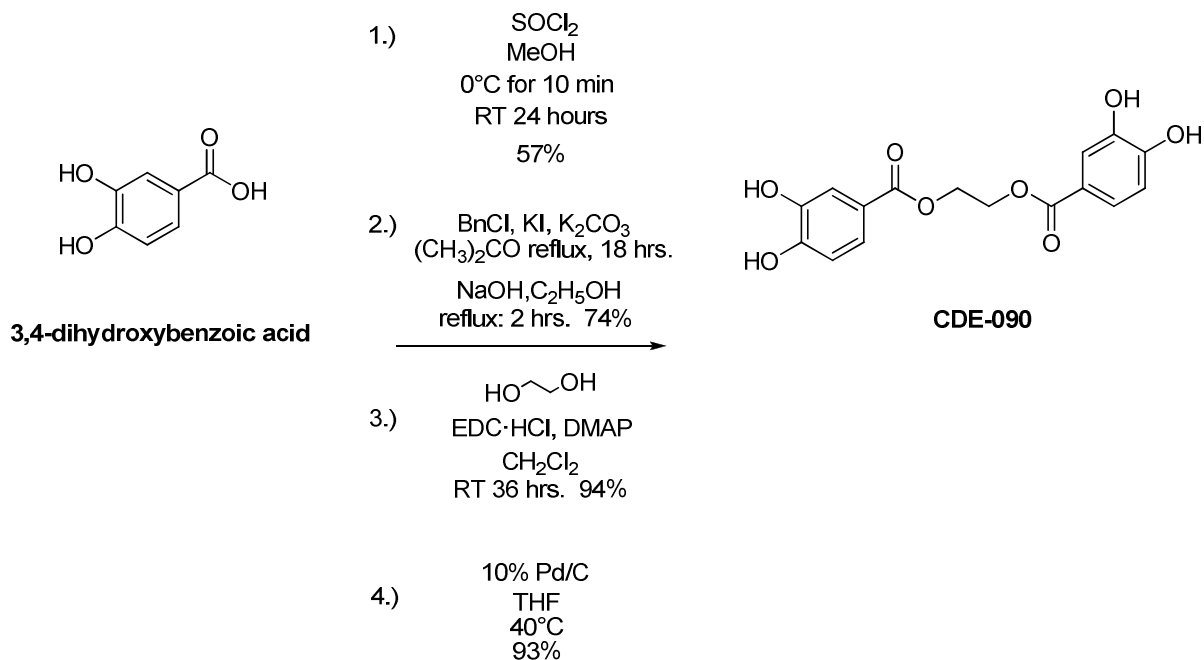
^1H NMR (CDCl_3-d_6 , 400 MHz) δ 7.80 (d, $J = 3.21$ Hz, 1 H, ortho aromatic), 7.46 (d, $J = 2.75$ Hz, 1H, ortho aromatic), 7.44-7.20 (m, 20H, aromatic), 7.15 (dd, $J = 3.21, 9.16$ Hz, 1H, para aromatic), 7.06 (d, $J = 9.16$ Hz, 1H, meta aromatic), 7.01 (dd, $J = 3.21, 9.16$ Hz, 1H, para aromatic), 6.88 (d, $J = 9.16$ Hz, 1H, meta aromatic), 5.24 (s, 2H, meta benzylic), 5.07 (s, 2H, ortho benzylic), 5.05 (s, 2H, meta benzylic), 4.92 (s, 2H, ortho benzylic), 4.59 (s, 4H, -O- CH_2 -).

Step #3: The glycol-linked benzyl-protected bisgallate (64.9 mg, 0.09 mmol) was dissolved in 1.14 ml THF. 10 wt% palladium on carbon (99 mg, 0.93 mmol) was added and the reaction was stirred under H_2 for 18 h at room temperature. A TLC (95% $\text{CH}_2\text{Cl}_2/\text{MeOH}$) indicated that the starting material was consumed. The reaction mixture was filtered through a MeOH-prepped PTFE syringe. The filtrate was evaporated, triturated with diethyl ether, and dried *in vacuo* (18.9

mg, 61%).

^1H NMR (acetone- d_6 , 400 MHz) δ 10.07 (bs, 2H, meta -OH), 8.10 (bs, 2H, ortho -OH), 7.31 (d, $J = 2.72$, Hz, 2H, ortho aromatic), 7.05 (dd, $J = 2.76$, 8.68 Hz, 2H, para aromatic), 6.81 (d, $J = 8.70$ Hz, 2H, meta aromatic), 4.75 (s, 4H, -O-CH $_2$ -); ^{13}C NMR (acetone- d_6 , 100 MHz) δ 169.73, 169.67, 155.12, 154.95, 149.70, 124.46, 118.21, 118.13, 114.31, 111.90, 63.17.



CDE-090**Ethane-1,2-diyl bis(3,4-dihydroxybenzoate)****(334.28 g/mol) C₁₆H₁₄O₈**

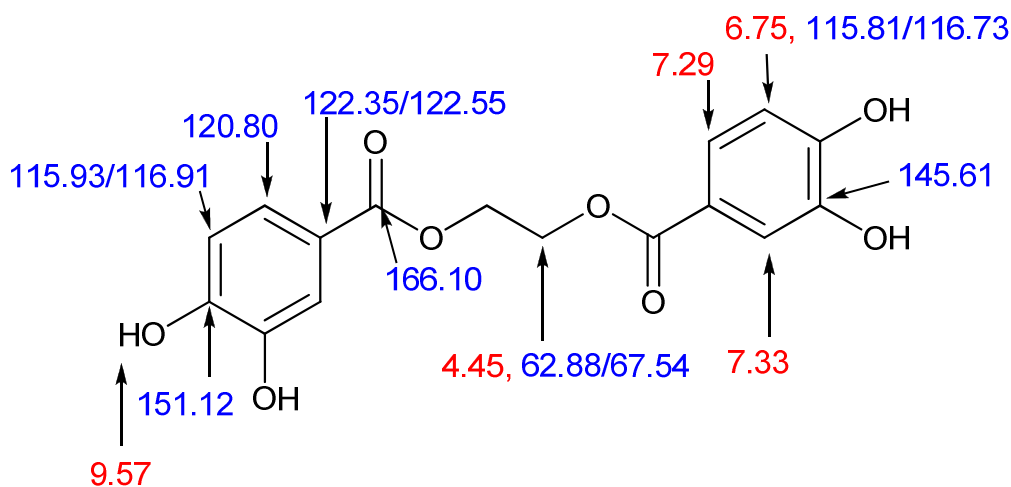
Step #1: Thionyl chloride (3.93 mL, 53.9 mmol) was added drop-wise to MeOH (40 mL) while held at 0°C and while stirring under N₂. This solution was stirred for an additional 10 minutes, and 3,4-dihydroxybenzoic acid (5.00 g, 32.4 mmol) was added to the flask. This mixture was then stirred at room temperature 24 hrs. A TLC (45% EtOAc/hexanes) indicated that the majority of the starting material had been consumed. The SOCl₂ was evaporated *in vacuo*. CH₂Cl₂ (10 mL) was added and filtered to obtain a white solid (3.10 g, 57%). ¹H NMR (DMSO-*d*₆, 400 MHz) δ 9.76 (bs, 1H, para -OH), 9.34 (bs, 1H, meta -OH), 7.31 (d, *J* = 1.83 Hz, 1H, ortho aromatic), 7.27 (dd, *J* = 2.29, 8.24 Hz, meta aromatic), 6.76 (d, *J* = 8.24 Hz, 1H, ortho aromatic), 3.71 (s, 3H, -OCH₃); ¹³C NMR (DMSO -*d*₆, 100 MHz) δ 166.68, 150.93, 145.59, 122.28, 120.99, 116.76, 115.84, and 51.00.

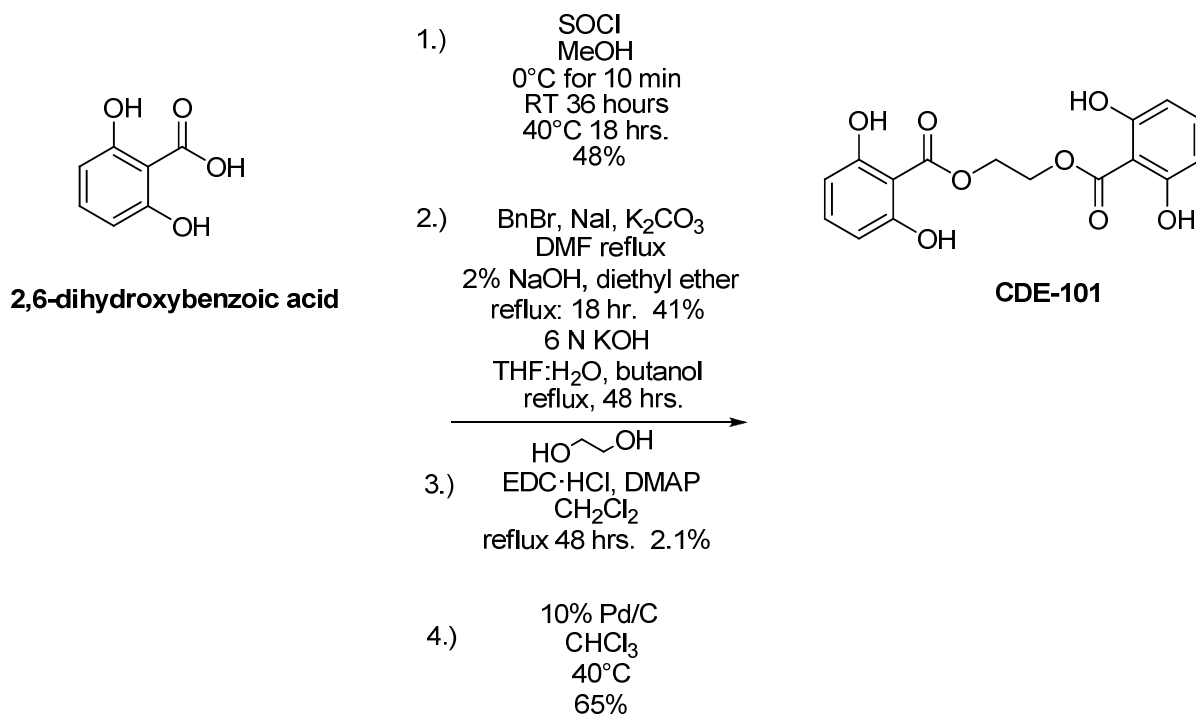
Step #2: Methyl 3,4-dihydroxybenzoate (2.80 g, 16.7 mmol), KI (0.83 g, 5.0 mmol), K₂CO₃ (9.20 g, 66.6 mmol), and acetone (142 mL) were combined and stirred under N₂ for 20 minutes. In a 50 mL Erlenmeyer flask benzyl chloride (4.09 mL, 35.5 mmol) and acetone (28.4 mL) were mixed and then syringed into the first reaction. The reaction was refluxed overnight. A TLC (80% hexanes/EtOAc) indicated that the starting material was consumed. The reaction was filtered and dried *in vacuo* to obtain a solid. CH₂Cl₂ (81.73 mL) was added and then this mixture was filtered through Celite. The CH₂Cl₂ was evaporated *in vacuo*, and then the remaining solid material was dried for 1 hour *in vacuo*. 95% Ethanol (333 mL) and NaOH (0.73 g, 18.2 mmol) were added and the solution refluxed for 2 hours. The hot reaction was then poured into an Erlenmeyer flask containing a 0.6 M HCl solution (350 mL). A white voluminous solid formed. The reaction was filtered and the solid was washed with a 1:1 mix of 95% ethanol:H₂O, 100% H₂O, 95% ethanol, MeOH, and tert-butyl methyl ether (100 mL each), then dried *in vacuo* in a desiccator to obtain a white solid (4.11 g, 74%). ¹H NMR (DMSO-*d*₆, 400 MHz) δ 7.52 (s, 1H, ortho aromatic), 7.50 (d, *J* = 1.83 Hz, 1H, ortho aromatic), 7.45-7.25 (m, 10H, aromatic), 7.12 (d, *J* = 9.16 Hz, 1H, meta aromatic), and 5.18 (s, 2H, para benzylic), 5.14 (s, 2H, meta benzylic); ¹³C (DMSO-*d*₆, 100 MHz) δ 167.50, 152.58, 148.13, 128.99, 128.95, 128.10, 127.98, 123.99, 123.77, 115.02, 113.60, 70.47, 70.36.

Step #3: Ethylene glycol (0.15 g, 2.39 mmol), 3,4-bis(benzyloxy)benzoic acid (2.00 g, 5.98 mmol), DMAP (0.07 g, 0.60 mmol), and CH₂Cl₂ (5.00 mL) were combined and stirred under N₂. In a separate flask, EDC·HCl (1.23 g, 5.98 mmol) and CH₂Cl₂ (10.0 mL) were combined and held at 0°C. Then this mixture was syringed into the first reaction in a drop-wise fashion. This was stirred at room temperature for 36 hrs. A TLC (50% hexanes/EtOAc) indicated that the majority of the starting material had been converted to product. The reaction was purified by

column chromatography (50% hexanes/EtOAc) to obtain a solid (1.56 g, 94%). ^1H NMR (DMSO- d_6 , 400 MHz) δ 7.85-7.10 (m, 26H, aromatic), 5.11 (s, 4H, para benzylic), 5.03 (s, 4H, meta benzylic), and 4.51 (s, 4H, -O-CH $_2$ -); ^{13}C NMR (DMSO- d_6 , 100 MHz) δ 165.78, 153.09, 148.25, 137.31, 137.08, 128.99, 127.96, 124.14, 124.03, 122.47, 115.01, 114.89, 113.77, 113.58, 70.86, 70.19, 63.04.

Step #4: Ethane-1,2-diyl bis(3,4-bis(benzyloxy)benzoate) (1.50 g, 2.16 mmol) dry THF (30.5 mL), and Pd/C 10% (3.26 g, 30.6 mmol) were combined and stirred overnight at 40°C under H $_2$. A TLC (90% CH $_2$ Cl $_2$ /MeOH) confirmed the consumption of the starting material. The reaction was syringed through a PTFE 0.2 μM syringe to remove the Pd/C catalyst. The solvent was then removed *in vacuo* to obtain a solid which was triturated with toluene (0.67 g, 93%). ^1H NMR (DMSO- d_6 , 400 MHz) δ 9.57 (bs, 4H, -OH), 7.33 (d, $J = 2.29$ Hz, 2H, ortho aromatic), 7.29 (dd, $J = 2.29, 8.24$ Hz, 2H, meta aromatic), 6.75 (d, $J = 8.24$ Hz, 2H, ortho aromatic), and 4.45 (s, 4H, -O-CH $_2$ -); ^{13}C NMR (DMSO- d_6 , 100 MHz) δ 166.10, 151.12, 145.61, 120.80, 122.55, 122.35, 116.91, 116.73, 115.93, 115.81, 67.54, 62.88, 25.65; HRMS, ES calcd. for C $_{16}$ H $_{14}$ O $_8$ Na [M+Na] $^+$ 357.0586, found: 357.0593.



CDE-101**Ethane-1,2-diyl bis(2,6-dihydroxybenzoate)****(334.28 g/mol) C₁₆H₁₄O₈**

Step #1: Thionyl chloride (3.93 mL, 53.9 mmol) was added drop-wise to MeOH (40.0 mL) while held at 0°C and while stirring under N₂. This solution was stirred for an additional 10 minutes. 2,6-Dihydroxybenzoic acid (5.00 g, 32.4 mmol) was added to the flask and this mixture stirred at room temperature for 36 hours. A TLC (50% EtOAc/hexanes) provided supporting evidence that the majority of the starting material was still present. The reaction was, therefore, gently heated at 40°C overnight. Another TLC (50% EtOAc/hexanes) indicated the disappearance of the majority of the starting material. The organic layer was washed with 1 N HCl (2 x), saturated aqueous sodium bicarbonate (2 x), and brine (1 x), dried over MgSO₄,

filtered, and concentrated *in vacuo* to obtain a solid (2.60 g, 48%). ¹H NMR (CDCl₃, 400 MHz) δ 9.65 (bs, 2H, -OH), 7.30 (t, *J* = 8.24 Hz, 1H, para aromatic), 6.48 (d, *J* = 8.24 Hz, 2H, meta aromatic), and 4.07 (s, 3H, -OCH₃); ¹³C NMR (CDCl₃, 100 MHz) δ 170.07, 160.91, 136.84, 136.72, 108.38, 108.31, 100.05, 53.05, 52.91.

-Note: Intramolecular hydrogen-bonding is proposed to play a significant role here, in that it causes a deformation to the shape of the molecule. This allowed the carbonyl carbon and methyl group to exist in two different electronic environments, allowing for 2 peaks of each to appear in the ¹³C spectra and allowing for five of the aromatic carbons to have their own unique peaks (the para-aromatic carbon remains unaffected).

Step #2: Methyl 2,6-dihydroxybenzoate (2.54 g, 15.1 mmol), K₂CO₃ (8.34 g, 60.4 mmol), NaI (158 mg, 1.06 mmol), and DMF (130 mL) were combined and mixed under N₂. In a separate flask, benzyl bromide (3.82 mL, 32.1 mmol) and DMF (24.0 mL) were mixed together, and then this mixture was syringed into the first reaction. It was refluxed overnight. A TLC (80% hexanes/EtOAc) revealed that the majority of the starting material had been consumed. The reaction was filtered and the filtrant was diluted with diethyl ether and then washed with 2% NaOH. The organic layer was dried with MgSO₄ and filtered, and then the solvent was evaporated *in vacuo* to obtain a powder. The powder was dissolved into 50 mL of a 1:1 mixture of THF:H₂O. To this, butanol (25.0 mL) and 6 N KOH (1.68 g, 5.00 mL) were added. Then the reaction was refluxed for 48 hours under N₂. 1 N HCl was added drop-wise to the reaction until it was acidified. A white solid formed and was filtered off. The filtrate was then evaporated *in vacuo*. The residue was purified by column chromatography (80% EtOAc/hexanes) to obtain a solid (2.08 g, 41%). ¹H NMR (CDCl₃, 400 MHz) δ 10.80 (bs, 1 H, -OH), 7.41 (d, *J* = 7.33 Hz, 4H, para aromatic on main ring and three ortho aromatic on

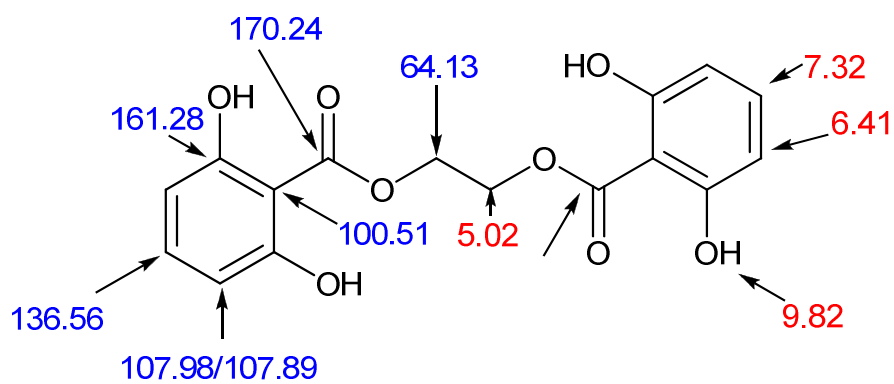
protecting groups' rings), 7.33 (t, $J = 7.33$ Hz, 4H, meta aromatic on protecting groups' rings), 7.25 (m, 3H, 1 ortho aromatic and two para aromatic hydrogen on protecting groups' ring), 6.61 (d, $J = 8.24$ Hz, 2H, meta aromatic), and 5.15 (s, 4H, benzylic);

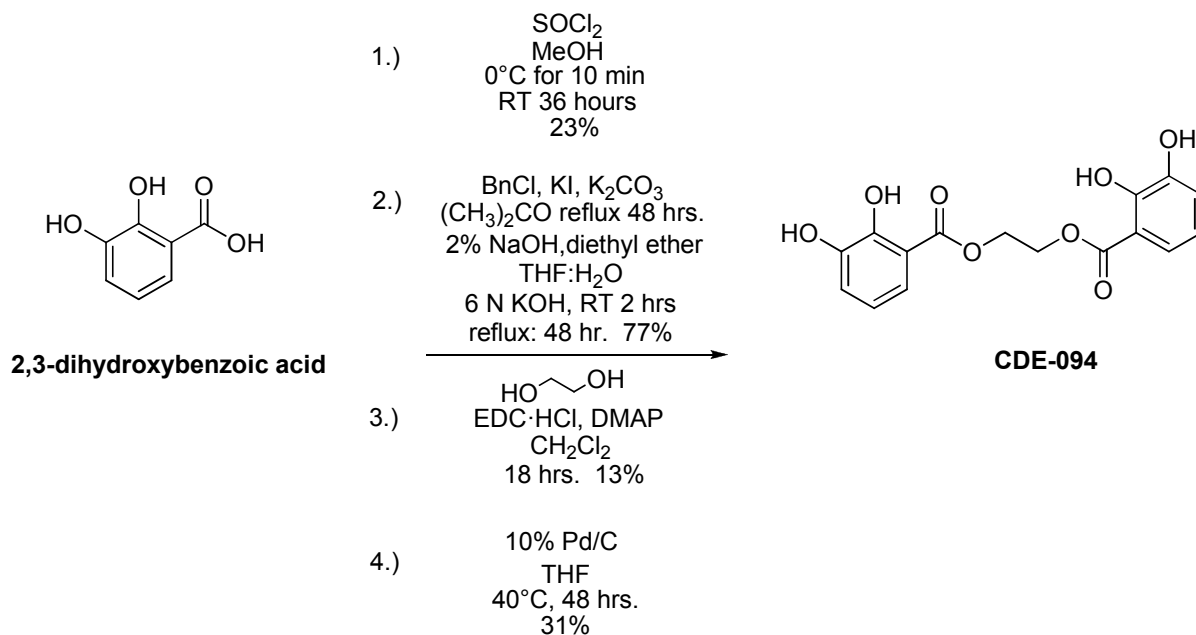
Step #3: Ethylene glycol (148 mg, 2.39 mmol), 2,6-bis(benzyloxy)benzoic acid (2.00 g, 5.98 mmol), DMAP (73.0 mg, 0.60 mmol), and CH_2Cl_2 (2.29 mL, 36.1 mmol) were combined and stirred under N_2 . In a separate flask EDC·HCl (1.24 g, 5.98 mmol) and CH_2Cl_2 (2.00 mL) were combined. Then this mixture was syringed into the first reaction in a drop-wise fashion. This was refluxed for 48 hours. A TLC (70% hexanes/EtOAc) showed that the majority of the starting material had been consumed. The solvent was reduced *in vacuo*, and the residue was then purified by column chromatography (70% hexanes/EtOAc) to obtain a solid (35.1 mg, 2.1%). ^1H NMR (CDCl_3 , 400 MHz) δ 7.33 (s, 2H, meta aromatic), 7.31 (s, 2H, meta aromatic), 7.26-7.12 (m, 10H, aromatic), 6.51 (s, 1H, para aromatic), 6.49 (s, 1H, para aromatic), 5.00 (s, 4H, benzylic), and 4.53 (s, 4H, -O- CH_2 -); ^{13}C NMR (CDCl_3 , 100 MHz) δ 166.27, 156.64, 136.75, 131.09, 128.57, 127.84, 126.96, 114.09, 105.80, 70.47, 63.03.

Step #4: Ethane-1,2-diyl bis(2,6-bis(benzyloxy)benzoate) (35.0 mg, 0.05 mmol), CHCl_3 (0.61 mL), and Pd/C 10% (0.05 g, 0.5 mmol) were combined and stirred for 48 hours at 40°C under H_2 . A TLC (95% $\text{CH}_2\text{Cl}_2/\text{MeOH}$) confirmed the consumption of the starting material. The reaction was syringed through a PTFE 0.2 μM syringe (prepped with MeOH) to remove the Pd/C catalyst. The solvent was then removed *in vacuo* and triturated with hexanes to obtain a green solid (10.9 mg, 65%). ^1H NMR (acetone- d_6 , 400 MHz) δ 9.82 (s, 4H, -OH), 7.32 (t, $J = 8.24$ Hz, 2H, para aromatic), 6.41 (d, $J = 8.24$ Hz, 4H, meta aromatic), and 5.02 (s, 4H, -O- CH_2 -

); ^{13}C NMR (acetone- d_6 , 100 MHz) δ 170.24, 161.28, 136.56, 107.98, 107.89, 100.51, 64.13;

HRMS, EI calcd. for $\text{C}_{16}\text{H}_{14}\text{O}_8$ $[\text{M}]^+$ 334.0689, found: 334.0692.



CDE-094**Ethane-1,2-diyl bis(2,3-dihydroxybenzoate)****(334.07 g/mol) C₁₆H₁₄O₈**

Step #1: Thionyl chloride (3.93 mL, 53.9 mmol) was added drop-wise to MeOH (40.0 mL) while held at 0°C and while stirring under N₂. This solution was stirred for an additional 10 minutes. 2,3-Dihydroxybenzoic acid (5.00 g, 32.4 mmol) was added to the flask and stirred at room temperature for 36 hours. A TLC (50% EtOAc/hexanes) indicated that the majority of the starting material had been consumed. The SOCl₂ was evaporated *in vacuo*. Then CH₂Cl₂ (10 mL) was added and evaporated *in vacuo* (3x) in an attempt to remove any remaining traces of thionyl chloride. The mixture was then dissolved in EtOAc. The organic layer was washed with saturated aqueous sodium bicarbonate (6 x), dried over MgSO₄, filtered, and concentrated *in vacuo* to obtain a solid (1.25 g, 23%). ¹H NMR (CDCl₃, 400 MHz) δ 10.89 (s, 1H, ortho -OH),

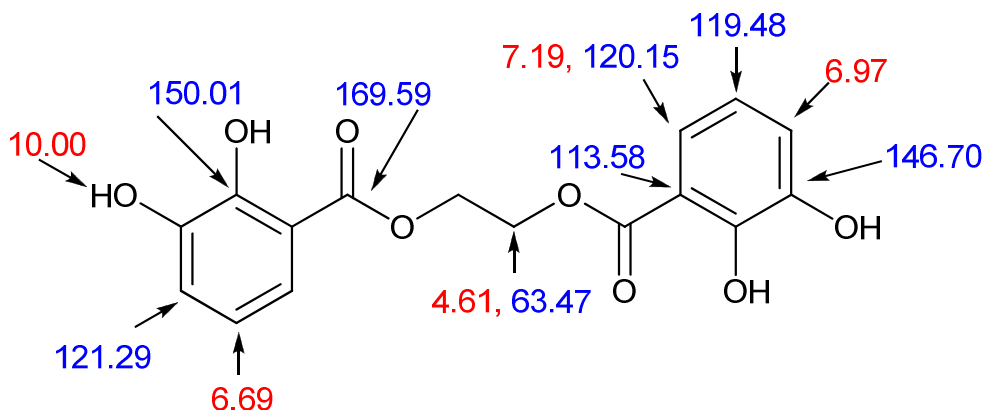
7.35 (dd, $J = 1.37, 8.24$ Hz, 1H, ortho aromatic), 7.11 (dd, $J = 1.37, 8.24$ Hz, 1H, para aromatic), 6.79 (t, $J = 7.79$ Hz, 1H, meta aromatic), 5.70 (s, 1H, meta -OH), and 3.94 (s, 3H, -OCH₃); ¹³C NMR (CDCl₃, 100 MHz) δ 170.85, 148.91, 145.11, 120.70, 120.59, 119.98, 119.85, 119.35, 119.28, 112.47, 52.60, 52.45.

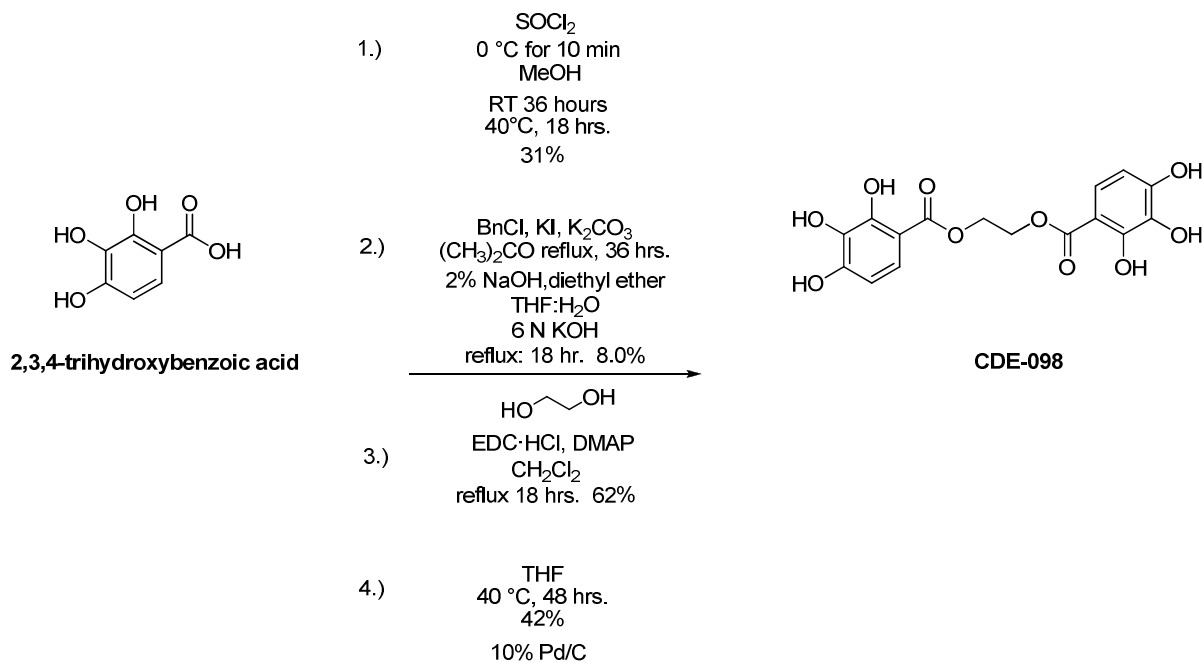
Step #2: Methyl 2,3-dihydroxybenzoate (0.82 g, 4.88 mmol), K₂CO₃ (2.70 g, 19.5 mmol), KI (0.24 g, 1.46 mmol), and acetone (41.0 mL) were combined and mixed under N₂. In a separate flask; benzyl chloride (1.19 mL, 10.4 mmol) and acetone (8.31 mL) were mixed together and then this mixture was syringed into the first reaction flask. It was refluxed for 48 hours. A TLC (80% hexanes/EtOAc) revealed that the majority of the starting material had been consumed. The reaction was filtered and the filtrant was diluted with diethyl ether and then washed with 2% NaOH. The organic layer was then dried with MgSO₄, filtered, and the solvent was evaporated *in vacuo* to obtain a powder which was taken up in 50 mL of a 1:1 mixture of THF:H₂O. To this 6 N KOH (1.68 g, 5.00 mL) was added and the reaction was stirred for 2 hours at room temperature under N₂. 1 N HCl was added drop-wise to the reaction until it was acidified. The organic layer was washed with 1 N HCl (2 x) and brine (1 x), dried over MgSO₄, filtered, and concentrated *in vacuo* to obtain a solid (1.26 g, 77%). ¹H NMR (CDCl₃, 400 MHz) δ 7.71 (dd, $J = 1.83, 7.79$ Hz, 1H, ortho aromatic), 7.48 (dd, $J = 1.83, 7.79$ Hz, 2H, para aromatic), 7.46-7.24 (m, 10H, aromatic), 7.17 (t, $J = 8.24$ Hz, 1H, meta aromatic), 6.25 (bs, 1H, -OH), 5.25 (s, 2H, benzylic), and 5.19 (s, 2H, benzylic); ¹³C NMR (CDCl₃, 100 MHz) δ 165.91, 151.55, 147.33, 129.40, 129.32, 136.01, 134.96, 128.92, 128.63, 127.91, 125.10, 124.41, 123.28, 119.08, 71.59.

Step #3: Ethylene glycol (0.07 g, 0.07 mmol), 2,3-bis(benzyloxy)benzoic acid (1.00 g, 2.99 mmol), DMAP (37.0 mg, 0.03 mmol), and CH₂Cl₂ (15.0 mL, 18.1 mmol) were combined and

stirred under N₂. In a separate flask EDC·HCl (1.14 g, 3.00 mmol) and CH₂Cl₂ (12.5 mL, 36.1) were combined. Then this mixture was syringed into the first reaction in a drop-wise fashion. This was stirred at room temperature overnight. A TLC (50% hexanes/EtOAc) showed that the majority of the starting material had been converted to product. The solvent was reduced *in vacuo* and the residue was purified by column chromatography (50% hexanes/EtOAc) to obtain a solid (109 mg, 13%). ¹H NMR (CDCl₃, 400 MHz) δ 7.42-7.33 (m, 6H, aromatic), 7.27-7.23 (m, 20H, aromatic), 5.11 (s, 2H, benzylic), 5.05 (s, 2H, benzylic), and 4.50 (s, 4H, -O-CH₂-).

Step #4: Ethane-1,2-diyl bis(2,3-bis(benzyloxy)benzoate) (0.11 g, 0.16 mmol), THF (2.00 mL), and Pd/C 10% (0.17 g, 1.57 mmol) were combined and stirred for 48 hours at 40°C under H₂. A TLC (95% CH₂Cl₂/MeOH) confirmed the consumption of the starting material. The reaction was syringed through a PTFE 0.2 μM syringe to remove the Pd/C catalyst. The solvent was then removed *in vacuo* and triturated with hexanes to obtain a solid (15.9 mg, 31%). ¹H NMR (DMSO-*d*₆, 400 MHz) δ 10.00 (bs, 4H, -OH), 7.19 (dd, *J* = 1.37, 7.79 Hz, 2H, ortho aromatic), 6.97 (dd, *J* = 1.37, 7.33 Hz, 2H, para aromatic), 6.69 (t, *J* = 8.24 Hz, 2H, meta aromatic), and 4.61 (s, 4H, -O-CH₂-); ¹³C NMR (DMSO-*d*₆, 100 MHz) δ 169.59, 150.01, 146.70, 121.29, 120.15, 119.48, 113.58, 63.47; HRMS, EI calcd. for C₁₆H₁₄O₈ [M⁺] 334.0689, found: 334.0685.



CDE-098**Ethane-1,2-diyl bis(2,3,4-trihydroxybenzoate)****(366.28 g/mol) C₁₆H₁₄O₁₀**

Step #1: Thionyl chloride (3.56 mL, 48.8 mmol) was added drop-wise to MeOH (36.0 mL) while held at 0°C and while stirring under N₂. This solution was stirred for an additional 10 minutes. 2,3,4-Trihydroxybenzoic acid (5.00 g, 29.39 mmol) was added to the flask and this mixture stirred at room temperature for 36 hours. A TLC (50% EtOAc/hexanes) showed that the majority of the starting material was still present. The reaction was, therefore, gently heated at 40°C overnight. Another TLC (50% EtOAc/hexanes) indicated the disappearance of the majority of the starting material. The organic layer was washed with 1 N HCl (2 x), saturated aqueous sodium bicarbonate (6 x), and brine (1 x), dried over MgSO₄, filtered, and concentrated *in vacuo* to obtain a solid (1.68 g, 31%). ¹H NMR (CDCl₃, 400 MHz) δ 10.97 (s, 1H, ortho -OH), 7.36 (d, *J* = 8.70 Hz, 1H, ortho aromatic), 6.51 (d, *J* = 8.70 Hz, 1H, meta aromatic), 5.75 (s, 1H,

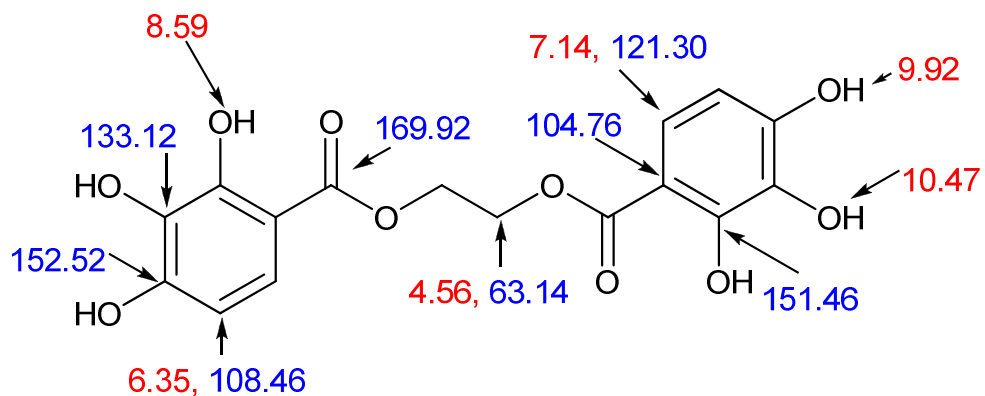
meta -OH), 5.41 (s, 1H, para -OH), and 3.91 (s, 3H, -OCH₃). ¹³C NMR (CDCl₃, 100 MHz) δ 170.65, 149.50, 149.19, 131.03, 122.12, 122.00, 107.48, 107.44, 105.72, 52.32.

Step #2: Methyl 2,3,4-trihydroxybenzoate (1.55 g, 8.42 mmol), KI (0.42 g, 2.53 mmol), K₂CO₃ (4.65 g, 33.7 mmol), and acetone (70.5 mL) were combined and mixed under N₂ for 20 minutes. In a separate flask, benzyl chloride (2.06 mL, 17.9 mmol) and acetone (14.3 mL) were mixed together, and then this mixture was syringed into the first reaction flask. It was refluxed for 36 hours. A TLC (80% hexanes/EtOAc) revealed that the majority of the starting material had been consumed. The reaction was filtered and the filtrate was diluted with diethyl ether and then washed with 2% NaOH. The organic layer was dried with MgSO₄ and filtered, and then the solvent was evaporated *in vacuo* to obtain a powder. The powder was dissolved into 50 mL of a 1:1 mixture of THF:H₂O. 6 N KOH (1.68 g, 5.00 mL) was added. Then the reaction was refluxed overnight under N₂. 1 N HCl was added drop-wise to the reaction until it was acidified. A white solid formed and was filtered off. The solid was triturated with ethanol; however, this didn't purify the product. The residue was purified by column chromatography (80% EtOAc/hexanes) to obtain a solid (282 mg, 8.0%). ¹H NMR (CDCl₃, 400 MHz) δ 10.94 (s, 1H, -OH), 7.89 (d, *J* = 9.16 Hz, 1H, ortho aromatic), 7.34-7.25 (m, 15H, aromatic), 6.90 (d, *J* = 8.70 Hz, 1H, meta aromatic), 5.29 (s, 2H, benzylic), 5.19 (s, 2H, benzylic), and 5.07 (s, 2H, benzylic); ¹³C NMR (CDCl₃, 100 MHz) δ 165.43, 157.56, 152.08, 140.83, 136.71, 135.79, 134.77, 129.43, 129.00, 128.89, 128.85, 128.64, 128.58, 128.43, 128.34, 127.70, 127.57, 115.47, 109.68, 77.91, 75.98, 71.16.

Step #3: Ethylene glycol (0.07 g, 1.18 mmol), 2,3,4-tris(benzyloxy)benzoic acid (1.30 g, 2.95 mmol), DMAP (36.0 mg, 0.30 mmol), and CH₂Cl₂ (2.24 mL) were combined and stirred under

N₂. In a separate flask EDC·HCl (0.61 g, 2.95 mmol) and CH₂Cl₂ (5.00 mL) were combined. Then this mixture was syringed into the first reaction in a drop-wise fashion. This was stirred at room temperature for 48 hours. A TLC (70% hexanes:EtOAc) showed that the majority of the starting material had been converted to product. The residue was purified by column chromatography (70% hexanes:EtOAc) and dried in vacuo to obtain a yellow oil (0.66 g, 62%). ¹H NMR (CDCl₃, 400 MHz) δ 7.62 (dd, *J* = 2.75, 8.70 Hz, 1H, aromatic), 7.46-7.20 (m, 30H, aromatic), 6.71 (dd, *J* = 2.29, 8.70 Hz, 1H, aromatic), 5.10 (s, 4H, benzylic), 4.99 (s, 2H, benzylic), and 4.53 (s, 2H, -O-CH₂-); ¹³C NMR (CDCl₃, 100 MHz) δ 165.08, 156.78, 154.08, 142.67, 137.37, 137.29, 136.24, 128.84, 128.76, 128.72, 128.41, 128.37, 128.29, 128.15, 128.07, 127.55, 127.39, 118.40, 108.76, 76.34, 75.67, 70.91, 62.66.

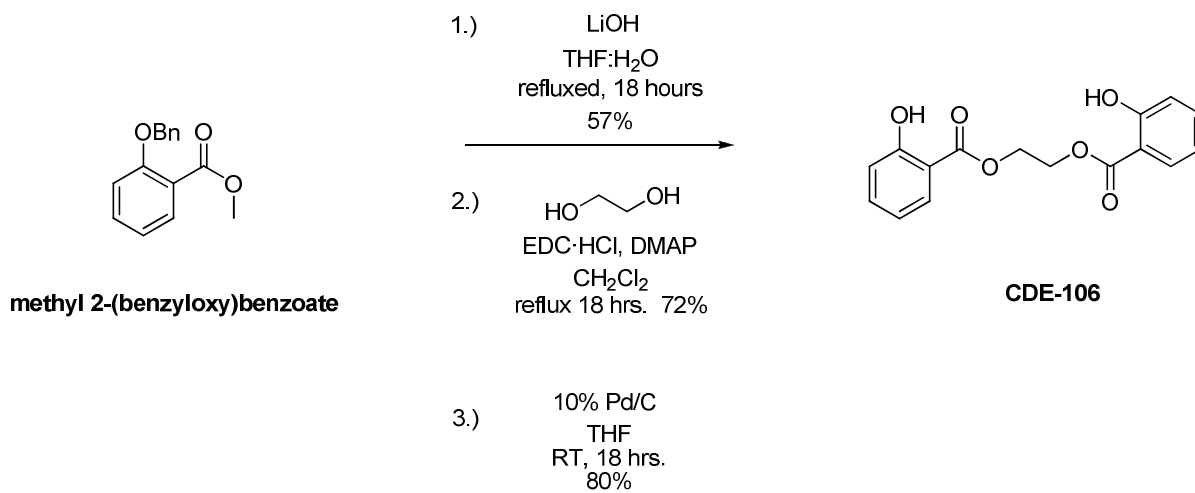
Step #4: Ethane-1,2-diyl bis(2,3,4-tris(benzyloxy)benzoate) (0.66 g, 1.51 mmol), THF (18.00 mL), and Pd/C 10% (1.61 g, 15.1 mmol) were combined and stirred for 48 hours at 40°C under H₂. A TLC (95% CH₂Cl₂/MeOH) confirmed the consumption of the starting material. The reaction was syringed through a PTFE 0.2 μM syringe to remove the Pd/C catalyst. The solvent was then removed *in vacuo* and triturated with hexanes to obtain a solid (233 mg, 42%). ¹H NMR (DMSO-*d*₆, 400 MHz) δ 10.47 (s, 2H, -OH), 9.92 (s, 2H, -OH), 8.59 (s, 2H, -OH), 7.14 (d, *J* = 8.70 Hz, 2H, ortho aromatic), 6.35 (d, *J* = 8.70 Hz, 2H, meta aromatic), and 4.56 (s, 4H, -O-CH₂-); ¹³C NMR (DMSO-*d*₆, 100 MHz) δ 169.92, 152.52, 151.46, 133.12, 121.30, 108.46, 104.76, 63.14; HRMS, EI calcd. for C₁₆H₁₄O₁₀ [M⁺] 366.0587, found: 366.0577.



CDE-106

Ethane-1,2-diyl bis(3-hydroxybenzoate)

(302.28 g/mol) $C_{16}H_{14}O_6$

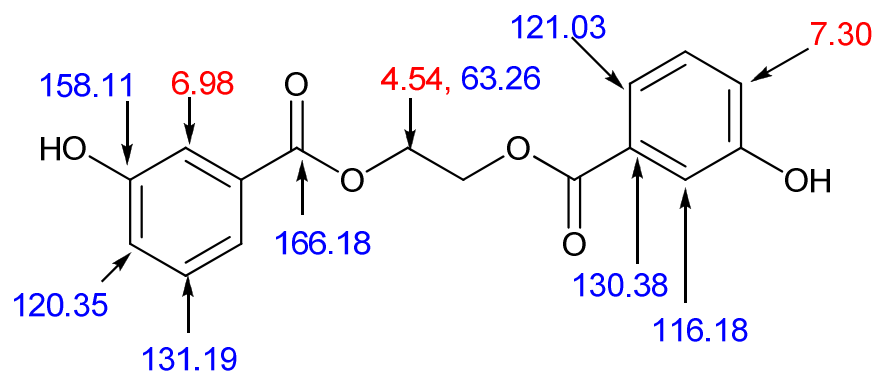


Step #1: Methyl 3-(benzyloxy)benzoate (0.25 g, 1.03 mmol) was dissolved in 1.5 mL THF and 1.5 mL H₂O. LiOH (0.05 g, 1.14 mmol) was added and the reaction was refluxed overnight. TLC (50% hexanes:EtOAc) indicated the consumption of the starting material. The organic phase was extracted with a mixture of EtOAc:3 N HCl, washed over brine, dried with MgSO₄, and dried *in vacuo* yielding a solid (0.24 g, 57%).

Step #2: The product from Step #1 (0.13 g, 0.569 mmol), ethylene glycol (0.0128 mL, 0.228 mmol), EDC·HCl (0.164 g, 0.798 mmol), and DMAP (8.30 mg, 68.4 μmol) were dissolved in CH₂Cl₂ (5 mL) and refluxed overnight. A TLC (65% EtOAc:hexanes) indicated the consumption of the starting material. The organic layer was washed with 1 N HCl, saturated NaHCO₃, brine (2x each), dried with MgSO₄, and dried *in vacuo* to produce a solid (0.12 g, 72%).

Step #3: The product from Step #2 (86.2 mg, 179 μmol) was dissolved in THF (2.6 mL). Pd/C 10% (114 mg, 1.07 mmol) was added and the reaction was stirred at room temperature, overnight, under H₂. A TLC (50% hexanes:EtOAc) revealed the consumption of starting material. The residue was purified by column chromatography (50% hexanes:EtOAc) and dried *in vacuo* to obtain a solid (67.0 mg, 80%).

¹H NMR (DMSO-*d*₆, 400 MHz) δ 7.30-7.26 (m, 6H, aromatic), 6.98-6.77 (m, 2H, ortho aromatic), 4.54 (s, 4H, -O-CH₂-); ¹³C NMR (DMSO-*d*₆, 100 MHz) δ 166.18, 158.11, 131.19, 130.38, 121.03, 120.35, 116.18, 63.26; HRMS, EI calcd. for C₁₆H₁₄O₆ [M+]⁺ 302.0790, found: 302.0802.



Chapter 4

Introduction of Carbamates into PAI-1 Inhibitors

BACKGROUND AND OBJECTIVES

A variation of the Schotten-Baumann reaction provides one method for the formation of carbamates.⁶⁶ Carbamates are readily synthesized through the reaction of chloroformates with either 1° or 2° amines and a base required to absorb the formed acidic proton. Carbamates have been utilized in anticancer,⁶⁷ antimicrobial,⁶⁸ and antimalarial⁶⁹ agents and to aid in the treatment of central nervous system and cardiovascular system disorders.⁷⁰ However, carbamate-containing insecticides have also been linked to numerous health hazards.⁷¹ Carbamate insecticides reversibly inhibit acetylcholinesterase by carbamylation.⁷¹ In a unique drug trial in 1966, urethane (a carbamate ester) was used in a controlled trial in human patients to treat multiple myeloma yet was deemed more toxic than the placebo and dropped from further trials.⁷² Due to these toxic effects, research was conducted in order to determine the level of urethane found in fermented foods; consequently, legislation was passed in the U.S. and the European Union to limit the levels of urethane in these products.⁷³

However, the simplicity of the synthesis of carbamates and the non-toxic by-products formed encourages their use in early-stage drug discovery. A wide variety of substituents incorporated in potential inhibitors increases the odds that a particular chemical property can be shown to be favored over another; therefore, it is to our advantage to utilize a synthetic technique that is simple, relatively quick, and produces nontoxic by-products.

Sulfonamides are commonly synthesized by the reaction of a sulfonyl chloride with an amine, producing HCl as the by-product. Prontosil, the first marketed antibiotic, contains a single sulfonamide group and was discovered (1927) by Gerhard Domagk while working for Bayer Pharmaceuticals (Figure 26).⁷⁴

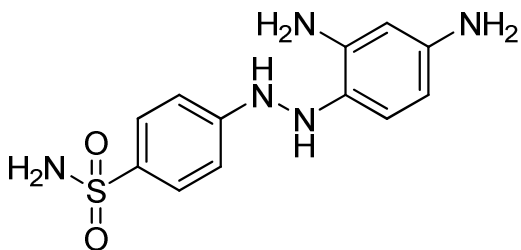


Figure 26: Prontosil.

Since then, hundreds of drugs serving a variety of functions containing the sulfonamide functional group,⁷⁵ such as non-steroidal anti-inflammatory drugs (NSAIDs), have been synthesized.⁷⁶ However, some sulfonamide containing antibiotics have been linked to Stevens-Johnson syndrome (SJS) and toxic epidermal necrolysis (TEN), also known as Lyell Syndrome: these are different forms of a life-threatening skin disease caused by an allergic reaction to some sulfonamide-containing antibiotics.⁷⁷

In spite of these known negative aspects, sulfonamide-containing antibiotics, are still widely marketed. While a link has been established between some sulfonamide-containing antibiotics and SJS, the pathogenesis of the syndrome is still unclear⁷⁸ and the incident rate of the syndrome is very low ranging from 0.4-1.2 (SJS) and 1.2-6 (TEN) per million persons per year.⁷⁹ Approximately 120 sulfonamide-containing drugs were being marketed as recently as

2008. Due to the ease with which esters are broken down in the body, sulfonamides (a biostere for the ester functional group) were suggested as new linker unit for our inhibitory molecules.

An important aspect to consider when designing an inhibitor involves the study of how a drug binds to its receptor. One of the methods employed to determine this binding involves the examination of a crystal structure of an inhibitor bound to its target. Materials studied using X-ray crystallography that do not occur in a natural crystal form are grown into crystals in a solution utilizing vapor diffusion over a period of several weeks to months. Diffraction patterns of the grown crystals are then captured using X-ray radiation. Mathematical software programs then analyze the patterns and propose 3-D structures of the atoms. Crystals are defined as having a regular repeating internal unit of structure in a 3-D space; therefore, when examining the results one can determine the degree to which the inhibitor's different atoms bind to different contact points on the protein by analyzing the degree of symmetry throughout the crystal unit.

In our pursuit of a selective and potent inhibitor of PAI-1, understanding how our inhibitor forms contacts with PAI-1 would enhance our ability to modify the inhibitor effectively. Currently there are no published reports of a crystal structure in which active PAI-1 is bound to an inhibitor. In 2008 a study published by the American Heart Association focused on determining effective inhibitors for PAI-1 by using the Pymol software program (DeLano Scientific LLC) to model a 3-D structure of the serpin bound to these inhibitors (Figure 27).⁸⁰ Pymol software allows for the 3-D visualization of several biological units, including serpins.

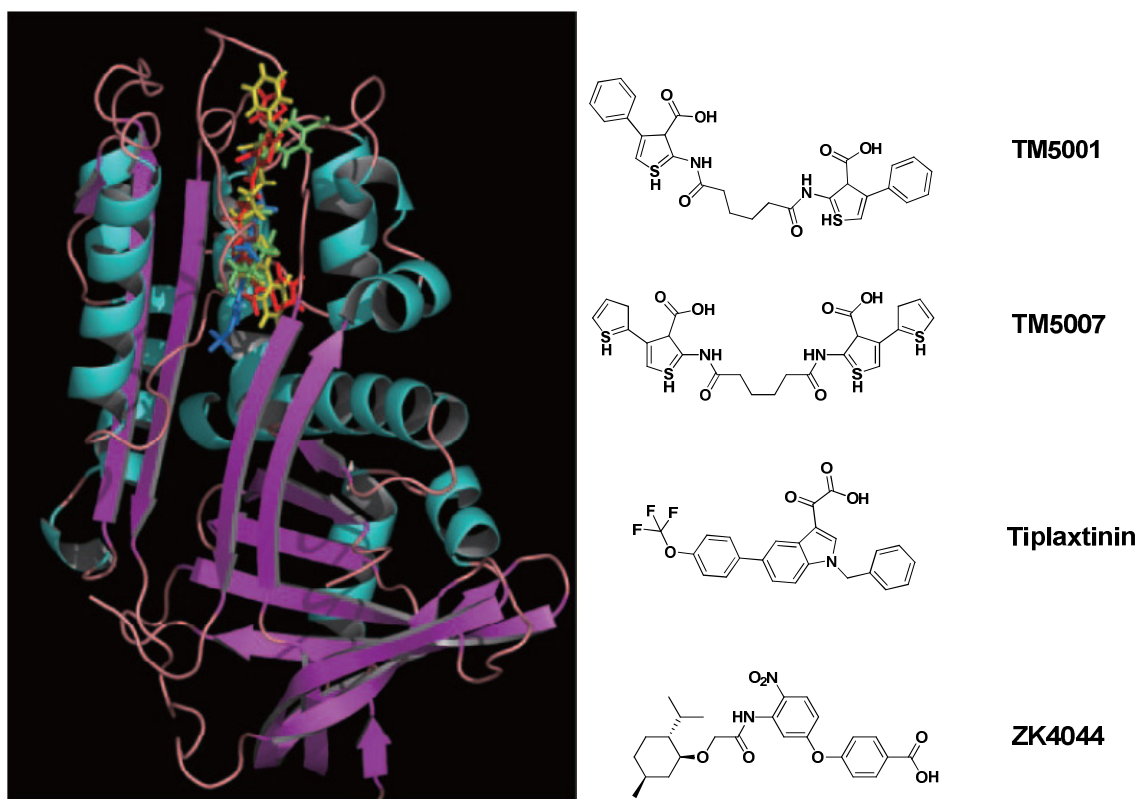


Figure 27: Pymol 3-D Model of PAI-1 with 4 Bound Inhibitory Molecules. TM5001 in yellow. TM5007 in blue. Tiplaxtinin in red. ZK4044 in green.⁸⁰

The first serpin crystal structure obtained was the cleaved form of α_1 -antitrypsin⁸¹. Since that time several other intact serpin crystal structures have also been obtained including α_1 -antichymotrypsin,⁸² antithrombin,⁸³ and α_1 -antitrypsin.⁸⁴ The crystal structure of an active mutant form of PAI-1 was reported in 1999; however, no structures of wild-type active forms of PAI-1 have been reported.⁸⁵ It has previously been proposed that small-molecule inhibitors of PAI-1 bind in pockets on the serpin.⁸⁶ Mutagenesis studies have been conducted to show the binding between PAI-1 and uPA,⁸⁷ the monoclonal antibody 33B8,⁸⁸ the monoclonal antibodies MA-8H9D4 and MA-56A7C10 and their single-chain variable fragments,⁸⁹ vitronectin,⁹⁰ and a low-molecular-weight inhibitor AR-H029953XX.⁸⁶

The various detrimental effects that elevated PAI-1 levels have been associated with have been the driving force behind our research efforts to synthesize and determine effective inhibitors of PAI-1. Effective PAI-1 inhibition would be an aid to more fully understanding these detrimental conditions on human health and a pathway to the design of a drug that would function to counteract elevated PAI-1 levels. Our research efforts have allowed us to establish several new experimentally supported hypotheses regarding the optimum scaffold for an inhibitor.

The results from Chapter 2 indicated that the bisgallate CDE-008 contains the optimum number of gallates for specific inhibition of PAI-1 ($IC_{50} = 0.558 \mu\text{M}$ and $ATIII = \text{ND}$). The tri-gallate molecule (CDE-082) was a more potent PAI-1 inhibitor ($IC_{50} = 0.025 \mu\text{M}$), yet acted less specifically ($ATIII = 14.2 \mu\text{M}$). Therefore, our research efforts turned to optimization of the tri-gallate inhibitor in an effort to retain the 20-fold increased inhibition of PAI-1 that this molecule displayed, while reducing its inhibition of ATIII.

Considering that the only difference between the bisgallate and tri-gallate inhibitor involved a single extra gallate unit, it was hypothesized that the manipulation of this extra unit might enhance the potency of the inhibitor while decreasing the inhibitor's potency against ATIII. A series of inhibitors were synthesized that shared a similar scaffold except the third gallate unit was replaced with various moieties (Table 11). The third gallate position will be referred to henceforth as "the handle" of the inhibitor. The attachments chosen were highly varied in the hopes that the chemical properties of one of the handles would prove to be an ideal match for inhibitor/serpin binding and consequently for inhibitor potency.

Table 11: Carbamate-Based Inhibitors.

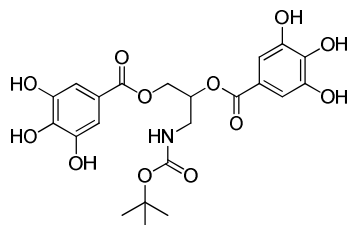
Entry

Inhibitor

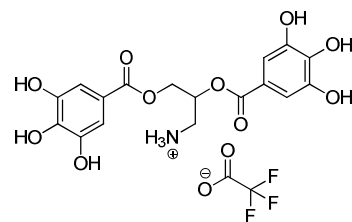
Entry

Inhibitor

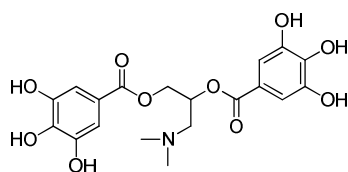
CDE-075



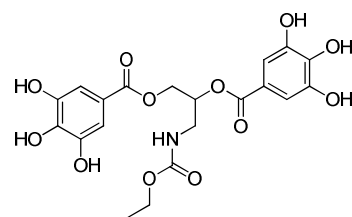
CDE-077



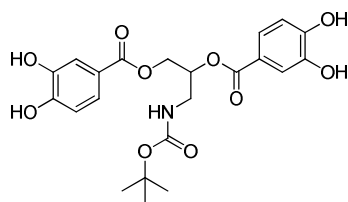
CDE-083



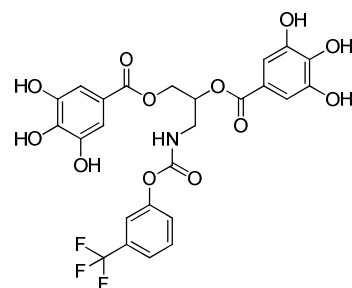
CDE-089



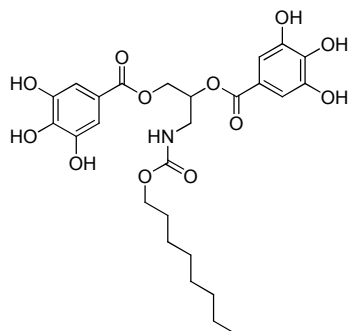
CDE-095



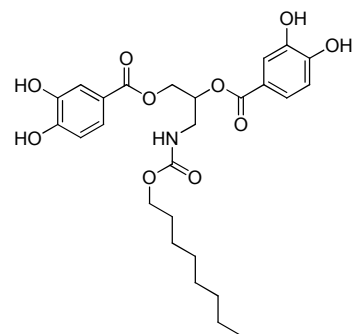
CDE-096



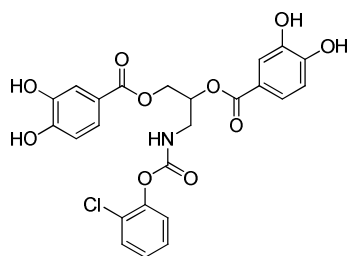
CDE-107



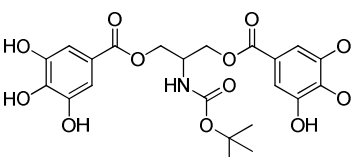
CDE-108

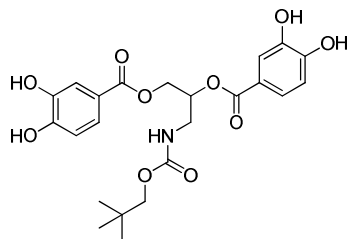
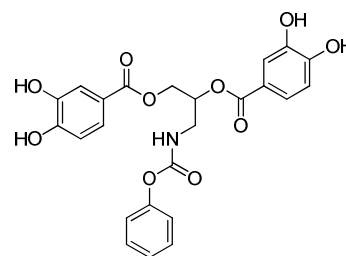


CDE-110



CDE-115



CDE-116**CDE-117**

A general synthetic scheme for these carbamates is illustrated in Figure 28. The first and second steps closely matched the procedures detailed in Chapter 1. The linker contained a Boc-protecting group and the removal of this group to produce the amine, composed the third step of the synthesis. This step was easily accomplished by the addition of trifluoroacetic acid (TFA) in CH_2Cl_2 for 10 minutes at room temperature, producing the corresponding trifluoroacetate salt. The fourth synthetic step installed the carbamate functionality. Finally, removal of the benzyl-protecting groups followed the same procedure outlined in Chapter 1.

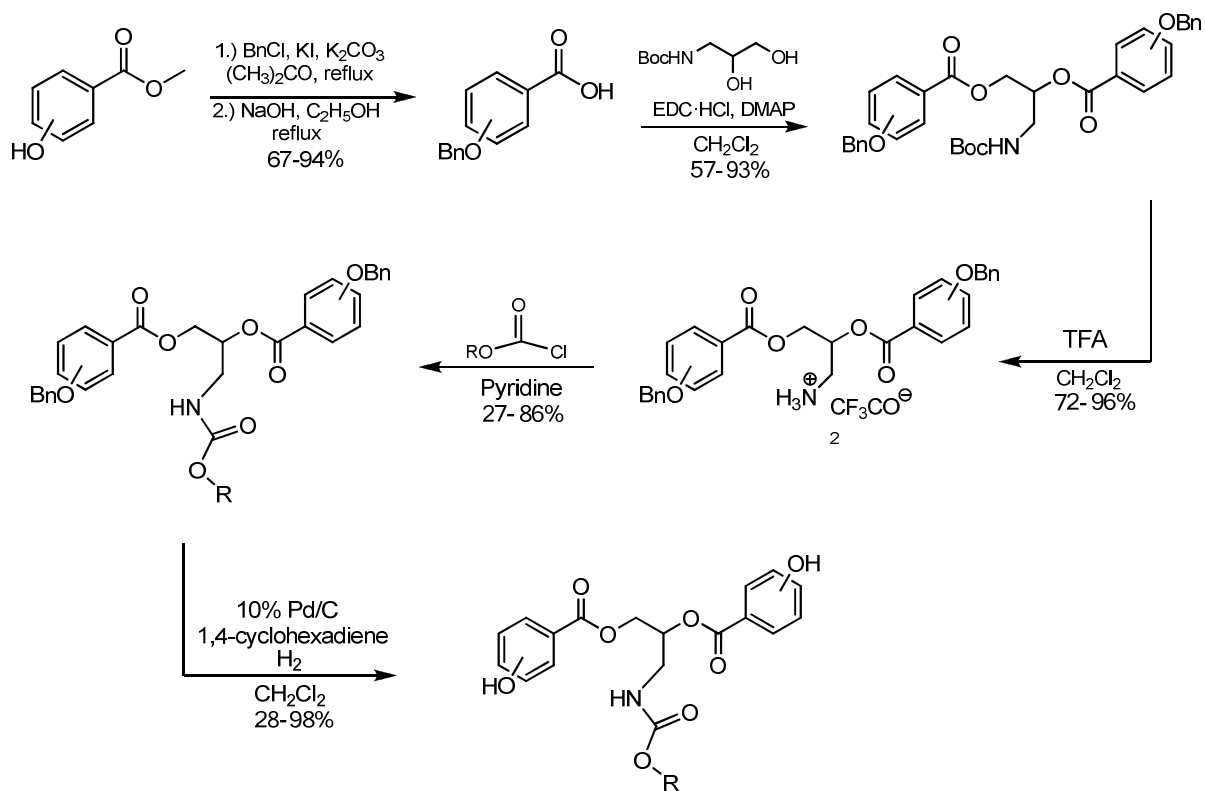
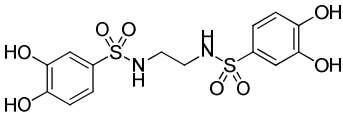
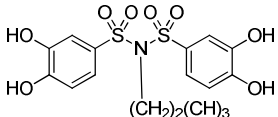
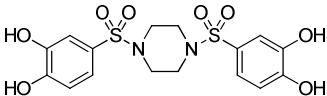
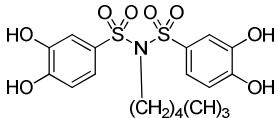
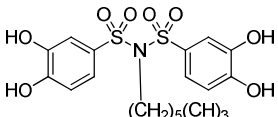
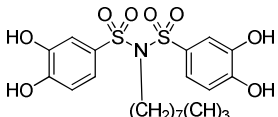
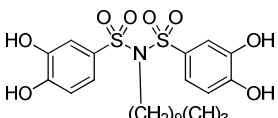
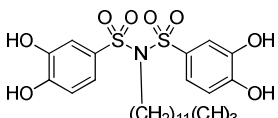


Figure 28: General Reaction Scheme for the Carbamates.

Our research efforts thus far had suggested that the ester linker units were highly favored over amide linker units (Chapter 1). However, due to the ease with which esterases break down ester-based pharmaceuticals, it was still desirable to replace this functional group with a more stable one. The sulfonamide group was utilized in this capacity. A series of inhibitors that contain sulfonamide and sulfonimide functional groups in place of the ester linkers were synthesized by Nadine El-Ayache and tested for their PAI-1 inhibition capacity (Table 12).^{43, 91}

Table 12: Sulfonamide/Sulfonimide-Based Inhibitors.

<u>Entry</u>	<u>Inhibitor</u>	<u>Entry</u>	<u>Inhibitor</u>
CDE-021		CDE-102	
CDE-119		CDE-143	
CDE-133		CDE-146	
CDE-157		CDE-158	

In concert with our attempt to determine if the sulfonimide linker could replace our ester linker unit, the variability in the synthesized sulfonimide series was also chosen with the aim of attempting to discern an optimum length for the handle on sulfonimides. Therefore the scaffold remained constant except in regard to the length of the handle unit.

The sulfonimide inhibitors were tested in the same biological assay system as was used for the previous inhibitors, and the IC_{50} -values obtained were graphed against the number of methylene units on the handle in an attempt to ascertain if an optimal handle length existed.⁹¹

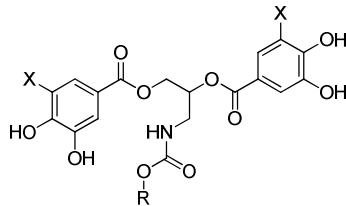
Ester and sulfonamide analogues were then compared in an attempt to ascertain the effect of the sulfonamide linker substitution.

In an effort to more fully understand the variability in the IC_{50} -values of our inhibitors and to postulate future inhibitory species, our focus turned to that of determining the inhibitor's binding site on PAI-1. Collaborators at the University of Michigan successfully obtained a crystal structure of active PAI-1 bound to the 3-(trifluoromethyl)phenyl-carbamate derivative (CDE-096). The Pymol software package was utilized to model a 3-D structure of the captured species which was then examined to establish the contact points being made between the inhibitor and the serpin. The chemical properties of these contact points were also examined, and new inhibitors were proposed based on these findings.

RESULTS

The biological assay results for the carbamate inhibitors are illustrated in Table 13. Eight of the carbamate inhibitors displayed IC_{50} -values in the range of 11-62 nM (CDE-075, CDE-095, CDE-096, CDE-107, CDE-108, CDE-110, CDE-116, CDE-117) with non-detectable levels of ATIII inhibition (no data were available for CDE-095 ATIII inhibition potency). In comparison CDE-082 (tri-gallate) was a comparable inhibitor ($IC_{50} = 0.025 \mu\text{M}$) and yet inhibited ATIII ($14.2 \mu\text{M}$). Two of the inhibitors showed inhibition of PAI-1 in a range of 100-160 nM (CDE-077, CDE-089). For these two no data were available for their inhibition of ATIII. The remaining two inhibitors (CDE-083, CDE-115) showed inhibition of PAI-1 in the range of 4-5 μM with CDE-115 showing inhibition of ATIII = 470 μM .

Table 13: Biological Assay Results: Carbamate-Based (and Related) Inhibitors.
(ND = not detected)



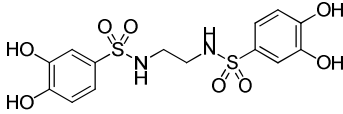
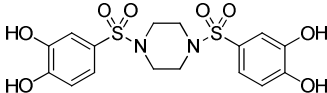
<u>Entry</u>	<u>R</u>	<u>X</u>	<u>IC₅₀ vs. PAI-1 (uM)</u>	<u>ATI_{III} (uM)</u>
CDE-075	<i>tert</i> -butyl	OH	0.062	ND
CDE-077	trifluoroacetate salt	OH	0.104	---
CDE-089	ethyl	OH	0.159	---
CDE-095	<i>tert</i> -butyl	H	0.048	---
CDE-096	3-(trifluoromethyl)phenyl	OH	0.059	ND
CDE-107	octyl	OH	0.0108	ND
CDE-108	octyl	H	0.02	100
CDE-110	2-chlorophenyl	H	0.027	ND
CDE-116	neopentyl	H	0.029	ND
CDE-117	phenyl	H	0.022	ND

<u>Entry</u>	<u>Inhibitor</u>	<u>X</u>	<u>IC₅₀ vs. PAI-1 (uM)</u>	<u>ATI_{III} (uM)</u>
CDE-082		OH	0.025	14.2
CDE-083		OH	4.75	---
CDE-115		OH	4.69	470

Three of the four inhibitors showing the lowest degree of inhibition (CDE-077, CDE-083, CDE-089) all share the common characteristic of possessing a handle that is much smaller than any of the other inhibitors in this series. This suggests that the handle size is indeed important to inhibitor potency. The low inhibition of PAI-1 by CDE-115 may possibly be explained by the observation that it is the only inhibitor in the series containing three methylene linker units, in contrast to the other inhibitors which utilize a two-methylene linker unit. Earlier results suggest that linker length impacts inhibitor potency substantially.

The carbamate inhibitors' range in inhibitor potency (illustrated by the IC_{50} -values) indicated that the handle length was an important factor in inhibitor potency. The biological assay results for the published sulfonamide-based inhibitors are illustrated in Table 13. The sulfonimide series of inhibitors included handle lengths ranging from two methylene units through eleven methylene units. This series of inhibitors showed a range in IC_{50} -values from 0.086-2.67 μM .⁹¹

Table 14: Biological Assay Results: Sulfonamide-Based Inhibitors.
(ND = not detected)

<u>Entry</u>	<u>Inhibitor</u>	<u>IC_{50} vs. PAI-1 (μM)</u>	<u>ATIII (μM)</u>
CDE-021		547	7500
CDE-119		ND	ND

Based on these results, it appears that sulfonimide inhibitors with a handle approximately a length of 6.5 methylene units would yield the largest degree of PAI-1 inhibition. This number of methylene units correlates to a chain length of approximately 780-1000 pm. These results support the idea that inhibitor potency is highly dependent on the length of the handle, presuming that both classes of inhibitors interact with PAI-1 in the same fashion.

In order to examine the IC_{50} -values from the perspective of their ability to influence inhibitor potency based on the linker's composition, the sulfonimide inhibitor with eleven methylene units (CDE-158) can be compared with its ester-linked analogue (CDE-108, Table 13). These two were chosen for comparison because they both contain hydroxy substituents in the 3,4-positions of the aromatic rings and they share a similar total length in their handle attachments: approximately 1420-1928 pm for CDE-108 and approximately 1440-1848 pm for CDE-158. One important point to note regarding this comparison is the nature of the linker of the sulfonimide inhibitor. Previous results have found supporting evidence that the optimum linker length is two methylene units; therefore, this is one factor (among others) that affects potency that is not identical between the sulfonimide-linked inhibitor and the ester-linked inhibitor and therefore influences the validity of the comparison. However, without a better comparison available within the series of ester-carbamates, these two were chosen in an attempt to determine the effect that the sulfonimide linker alone has on inhibitor potency. CDE-108 was found to be a more potent ($IC_{50} = 0.02 \mu M$) and specific (non-detectable levels of ATIII inhibition) PAI-1 inhibitor than CDE-158 ($IC_{50} = 2.60 \mu M$, $ATIII = 547 \mu M$).

Another valid comparison can be made between the ethylene glycol-linked protococatechuate (CDE-090, Table 9) and ethane-1,2-diamine-linked sulfonamide (CDE-021). In this instance the linker length is approximately the same, and the number of hydroxys on each ring is also consistent. Both of these lack a handle unit and, therefore, a more direct comparison

can be made regarding the impact of changing the linker unit from an ester linker to a sulfonamide linker. When comparing the ethylene glycol-linked protocatechuate (CDE-090, Table 9) and ethane-1,2-diamine-linked sulfonamide (CDE-021, Table 14), CDE-090 has a higher potency ($IC_{50} = 0.33 \mu\text{M}$) than the sulfonamide analogue ($IC_{50} = 547 \mu\text{M}$). CDE-090 also has a non-detectable level of ATIII inhibition as compared to the sulfonamide analogue's 7500 μM inhibition of ATIII.

Last, a comparison between the piperazine-linked inhibitors can be examined to determine the impact of modifying the linker unit from an amide (CDE-055) to a sulfonamide (CDE-119). It is important to point out that for this comparison to be valid, the unproven assumption is made that the sulfonamide/sulfonimide inhibitors are binding to PAI-1 in the same orientation. However, since a crystal structure detailing the binding between an inhibitor and PAI-1 has only been successfully accomplished for the CDE-096 inhibitor, this comparison may be shown to be invalid in the future.

The piperazine-linked inhibitor (CDE-055 (Table 4)) from the amide series has a heightened PAI-1 potency ($IC_{50} = 26.83 \mu\text{M}$) and non-detectible ATIII potency, when compared with its piperazine-sulfonamide analogue (CDE-119) that reported non-detectable levels of PAI-1 and ATIII inhibition.

A 100-fold drop in PAI-1 potency (CDE-108 vs. CDE-158) and a 1650-fold drop in PAI-1 potency (CDE-090 vs. CDE-021) occur when a switch is made from an ester-linked inhibitor to a sulfonamide-linked inhibitor. Also a drop in PAI-1 potency occurs from micromolar inhibition levels to non-detectable inhibition levels (CDE-055 vs. CDE-119) when a switch is made from an amide-linked inhibitor to a sulfonamide-linked inhibitor. Therefore, the results show higher PAI-1 inhibition and lower ATIII inhibition for the ester and amide-linked inhibitors than for the sulfonamide-linked inhibitors.

The crystal structure introduced a new source of supporting evidence for several of our previous hypotheses concerning modification of our inhibitors. Pymol software effectively produced 3-D images of the crystal structure of active PAI-1 contacting one of our inhibitors, the 3-(trifluoromethyl)phenyl-carbamate derivative (CDE-096). The information gathered from the crystal structure does support the earlier hypothesis that small-molecule inhibitors of PAI-1 bind in pockets on the serpin.⁸⁶

The geometric isomerism study results from Chapter 1 and the inhibitor potency results in Chapter 4 (comparison of sulfonamide/sulfonimide, ester, and amide linker potencies) can be understood now in terms of the shape of the serpin's binding site as indicated by the crystal structure. The barrier to rotation of the carbon-nitrogen bond in amides ($E_a = 65-92 \text{ kJ/mol}$)⁹² and the sulfur-nitrogen bond in sulfonamide/sulfonimides ($E_a = 62-71 \text{ kJ/mol}$)⁹³ is greater than the barrier to rotation of the oxygen-carbon bond ($E_a = 50 \pm 3 \text{ kJ/mol}$)⁹² in the esters. This discrepancy between the ease of rotation of these bonds may account for the ester-linked molecules' improved inhibition of PAI-1 when compared to their amide and sulfonamide/sulfonimide analogues, because the higher activation energy may be preventing these inhibitors from adopting the most biologically active conformation that would allow the inhibitor to enter the pocket site on the serpin.

The results from the geometric isomerism study (Chapter 1) detailing our comparison of cyclic linkers can also now be rationalized through our new knowledge obtained from the crystal structure. The improved inhibition of the *trans*-positioning of the gallates as compared to a *cis*-positioning of the gallates and the improved inhibition of the cyclic linker molecule that allows for an increased number of conformational possibilities for the gallates such as the cyclohexanediol linker (in contrast to the benzenediol linker) can now be accounted for more fully through our observation that the binding site on the serpin is a pocket. The *trans*-position

would more easily allow for part of the molecule to conform to the bent shape necessary to interact with the pocket, as would inhibitors that have an increased number of conformational possibilities, such as the cyclohexanediol linkers, in contrast to their more rigid benzenediol analogues.

Our results from Chapter 2 that examined the effects on PAI-1 inhibition of the alteration of the number of gallates and the central sugar can also be understood more fully from our newly acquired knowledge that the serpin's binding site is a pocket. The specific central sugar was unimportant to the inhibitor's potency because all of the sugars allowed for at least two of the gallates to be arranged in a *trans*-position and it would be those two that interacted with the serpin's binding site (one entering the pocket site and the other binding outside the pocket). The bisgallate (CDE-008) contained the optimum number of gallates for specific inhibition of PAI-1 ($IC_{50} = 0.558 \mu\text{M}$) because it had non-detectable levels of ATIII inhibition versus the tri-gallate molecule (CDE-082) that was a more potent PAI-1 inhibitor ($IC_{50} = 0.025 \mu\text{M}$) yet inhibited less specifically (ATIII $IC_{50} = 14.2 \mu\text{M}$). These findings are also supported by the observation that the binding site on PAI-1 interacts with the inhibitor by the binding of one gallate in the pocket and one gallate outside the pocket. The additional gallates have an unknown advantageous role in binding and might inhibit binding via steric hindrances.

Other potentially important points of contact between the serpin and the inhibitor (CDE-096) include a carbonyl oxygen interacting with an electropositive region on the serpin, the 3,4-dihydroxy oxygens on one of the gallates interacting with an electropositive region on the serpin, and the handle unit buried deep within a largely hydrophobic pocket.

Our finding that only one of the gallates' hydroxys binds strongly to the serpin in the crystal structure and that only two of the hydroxys (3,4-dihydroxy arrangement) are strongly involved in the binding also provides supporting evidence for our conclusions drawn in Chapter

3 that determined the optimum number of gallates (two/three) and arrangement of substituents (3,4-dihydroxy arrangement) on the aromatic ring.

The crystal structure's confirmation of the binding site on the serpin as a pocket also provides for supporting evidence regarding our observation in Chapter 4 that improved potency of the inhibitors occurred in molecules that had a handle unit capable of interacting with a pocket on the serpin. The two gallate moieties of the inhibitor are located outside of the pocket, while the handle of the inhibitor is buried within the pocket of the serpin.

An electropositive region within a larger electroneutral region on the serpin's binding site indicates that handles composed of electroneutral and electronegative atoms could produce stronger binding to PAI-1 in this region. This observation would account for the enhanced potency of the inhibitors whose handles were composed of phenyl rings or variously lengthed and arranged methylene handles (CDE-075, CDE-082, CDE-096, CDE-107, CDE-108, CDE-110, CDE-116, CDE-117). This observation also supports our results from Chapter 2 that displayed a lack of inhibitor potency of the galactose-centered molecule with five gallate groups attached in which all hydroxy positions were benzyl-protected (CDE-006). This observation led us to propose the hypothesis that the hydroxy functional groups on the gallates were a necessary aspect for inhibitor potency or that other electronically similar species were necessary.

The above findings account for observed changes in inhibitor specificity in the carbamate derivatives. The electrostatic repulsion between the positive nitrogen atom of the ammonium group in CDE-077 and the electropositive region can now be seen as a possible reason for this molecule's lowered inhibitor potency. Similarly, the shortened length of the dimethyl and ethyl handle species (CDE-083, CDE-089) result in a decrease in inhibitor potency because the handle region is not long enough to interact with the pocket on the serpin.

The consistently improved inhibitor potencies of our carbamate derivatives indicated that a handle unit was an essential piece to our scaffold. The sulfonimide inhibitor series allowed for us to hypothesize that a handle unit composed of 6.5 methylene units (approx. 780-1000 pm) in chain length would allow for the optimum interaction of the handle unit with the serpin's pocket.

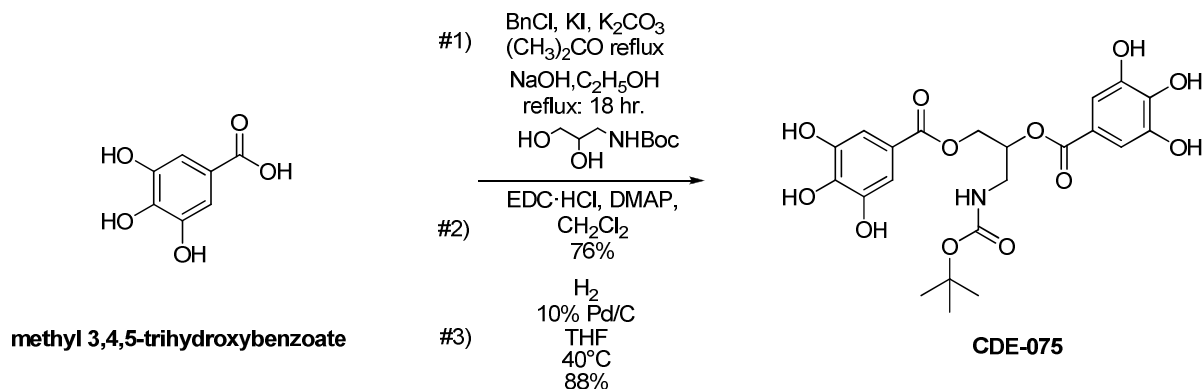
In summary, this chapter highlights our success at obtaining a crystal structure of an active PAI-1 serpin bound to an inhibitor and the carbamates that were synthesized and used in this achievement. The main focus of our research efforts turned to the optimization of the tri-gallate inhibitor in an effort to retain the 20-fold increased inhibition of PAI-1 that this molecule displayed, while reducing its inhibition of ATIII. This goal was achieved and is illustrated by the high potency against PAI-1 and non-detectable inhibition of ATIII shown by a number of the carbamate inhibitors, including CDE-075 (tert-butyl handle, $IC_{50} = 0.062 \mu\text{M}$), CDE-096 (3-(trifluoromethyl)phenyl, $IC_{50} = 0.059 \mu\text{M}$), CDE-107 (octyl handle, $IC_{50} = 0.01 \mu\text{M}$), CDE-110 (2-chlorophenyl handle, $IC_{50} = 0.027 \mu\text{M}$), CDE-116 (neopentyl handle, $IC_{50} = 0.029 \mu\text{M}$), and CDE-117 (phenyl handle, $IC_{50} = 0.022 \mu\text{M}$); these molecules are highly active and specific inhibitors of PAI-1. The selectivity of the inhibitors was further optimized by CDE-096 (3-(trifluoromethyl)phenyl handle), which inhibited PAI-1 at nanomolar IC_{50} level even in the presence of vitronectin, while showing non-detectable levels of ATIII inhibition.

EXPERIMENTAL

CDE-075

3-(Tert-butoxycarbonylamino)propane-1,2-diyl bis(3,4,5-trihydroxybenzoate)

(495.43 g/mol) $C_{22}H_{25}NO_{12}$

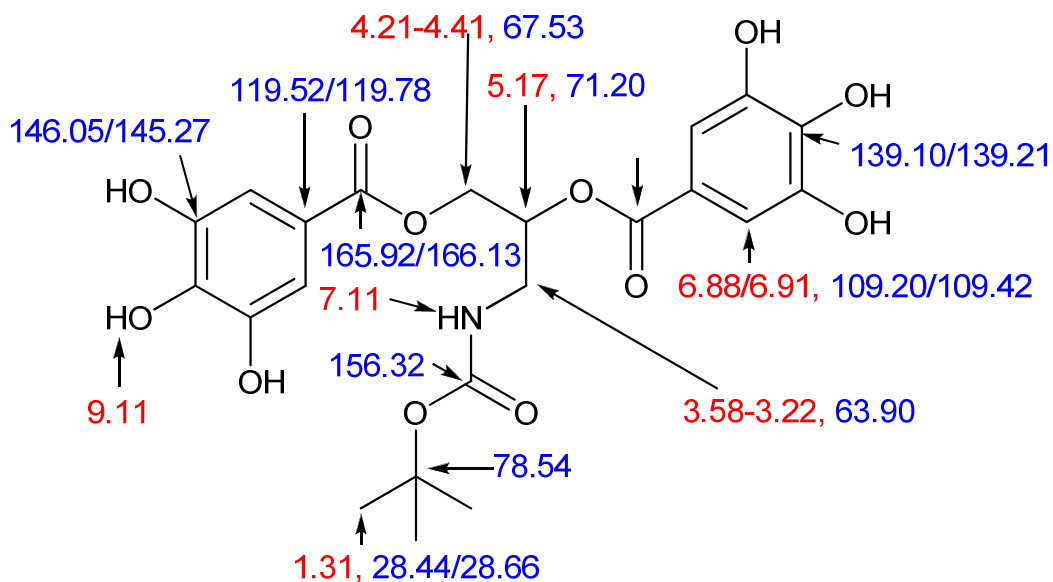


Step #1: Was conducted without modification of the “General procedure for synthesis of 3, 4,5-tribenzyloxybenzoate” (Chapter 1, Experimental).

Step #2: Tert-butyl N-(2,3-dihydroxypropyl) carbamate (1.00 g, 5.23 mmol), 3,4,5-tribenzyloxybenzoate (5.77 g, 13.1 mmol), DMAP (0.16 g, 1.31 mmol), and CH₂Cl₂ (5.00 mL) were combined and stirred under N₂. In a separate flask, EDC·HCl (2.70 g, 13.1 mmol) and CH₂Cl₂ (10 mL, 157 mmol) were mixed at 0°C. This mixture was then syringed into the reaction in a drop-wise manner. The reaction stirred at room temperature overnight under N₂. The organic layer was washed with 1 N HCl (2 x), saturated aqueous sodium bicarbonate (2 x), and brine (1 x), dried over MgSO₄, filtered, and concentrated *in vacuo*. A TLC (60% hexanes/EtOAc) indicated impurities. The residue was purified by column chromatography (60%

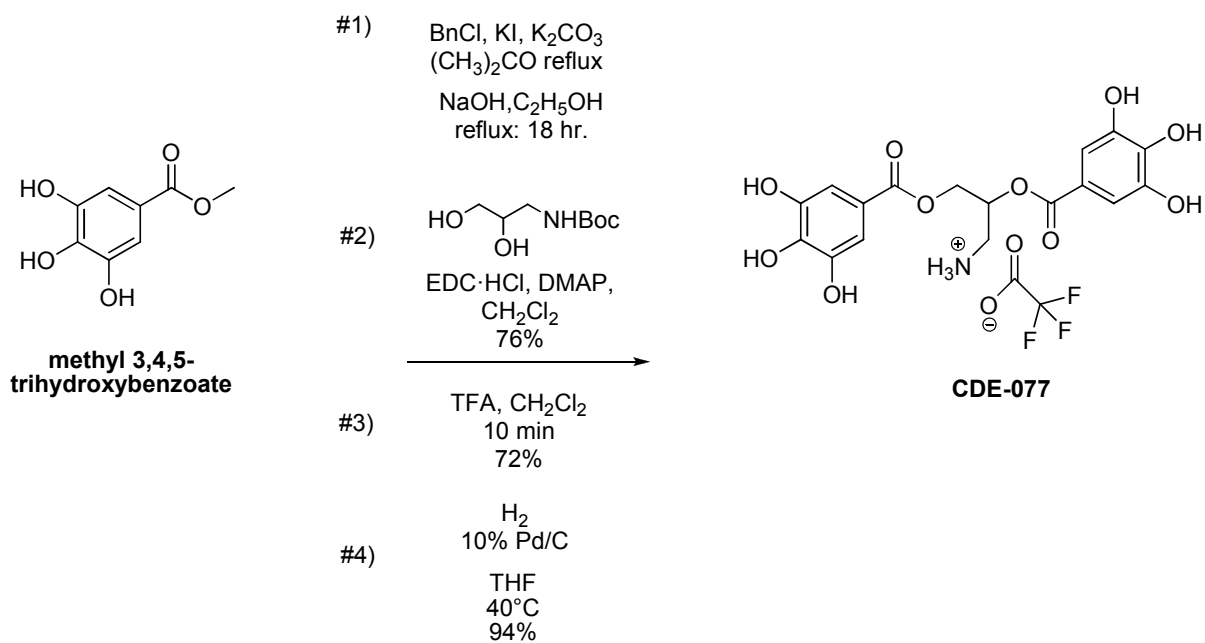
hexanes/EtOAc) to obtain a solid (4.12 g, 76%). ^1H NMR (CDCl_3 , 400 MHz) δ 7.41-7.20 (m, 34H, aromatic), 5.42 (quin, $J = 4.58$ Hz, 1H, -O-CH₂-CH-O-), 5.07 (s, 4H, benzylic), 5.05 (s, 8H, benzylic), 4.81 (t, $J = 5.95$ Hz, 1H, -HN-), 4.58 (dd, $J = 4.12, 11.91$ Hz, 2H, -O-CH₂-CH-O-), 3.57-3.48 (m, 2H, -N-CH₂-), and 1.43 (s, 9H, (CH₃)₃); ^{13}C NMR (CDCl_3 , 100 MHz) δ 165.82, 165.63, 155.91, 152.64, 142.89, 142.70, 137.48, 137.43, 136.62, 128.62, 128.58, 128.30, 128.28, 128.17, 128.13, 128.08, 128.04, 127.67, 124.65, 109.44, 109.19, 79.99, 75.19, 71.93, 71.33, 71.21, 63.53, 60.52, 41.12, 28.45.

Step #3: 3-(Tert-butoxycarbonylamino) propane-1,2-diyl bis (3,4,5-tris(benzyloxy)benzoate) (0.50 g, 0.48 mmol), dry THF (6.83 mL), and Pd/C 10% (0.73 g, 6.84 mmol) were combined and stirred overnight at 40°C under H₂. A TLC (70% hexanes/EtOAc) confirmed the consumption of the starting material. The reaction was filtered through Celite to remove the Pd/C catalyst. The solvent was then removed *in vacuo* to obtain a solid (210 mg, 88%). ^1H NMR ($\text{DMSO-}d_6$, 400 MHz) δ 9.11 (bs, 4H, -OH), 6.91 (s, 2H, aromatic), 6.88 (s, 2H, aromatic), 7.11 (t, $J = 5.95$ Hz, 1H, -HN-), 5.17 (quin, $J = 3.66$ Hz, 1H, -O-CH₂-CH-O-), 4.39-4.35 (m, 1H, -O-CH₂-CH-O-), 4.21-4.26 (m, 1 H, -O-CH₂-CH-O-), 3.58-3.22 (m, 2H, -N-CH₂-), and 1.31 (s, 9H, (CH₃)₃); ^{13}C NMR ($\text{DMSO-}d_6$, 100 MHz) δ 166.13, 165.92, 156.32, 146.05, 145.97, 139.21, 139.10, 119.78, 119.52, 109.42, 109.20, 78.54, 71.20, 67.53, 63.90, 28.66, 28.44; HRMS, ES calcd. for C₂₂H₂₅NO₁₂Na [M+Na]⁺ 518.1274, found: 518.1268.



CDE-077

2,3-Bis(3,4,5-trihydroxybenzoyloxy)propan-1-aminium 2,2,2-trifluoroacetate
 (509.34 g/mol) $C_{19}H_{18}NF_3O_{12}$



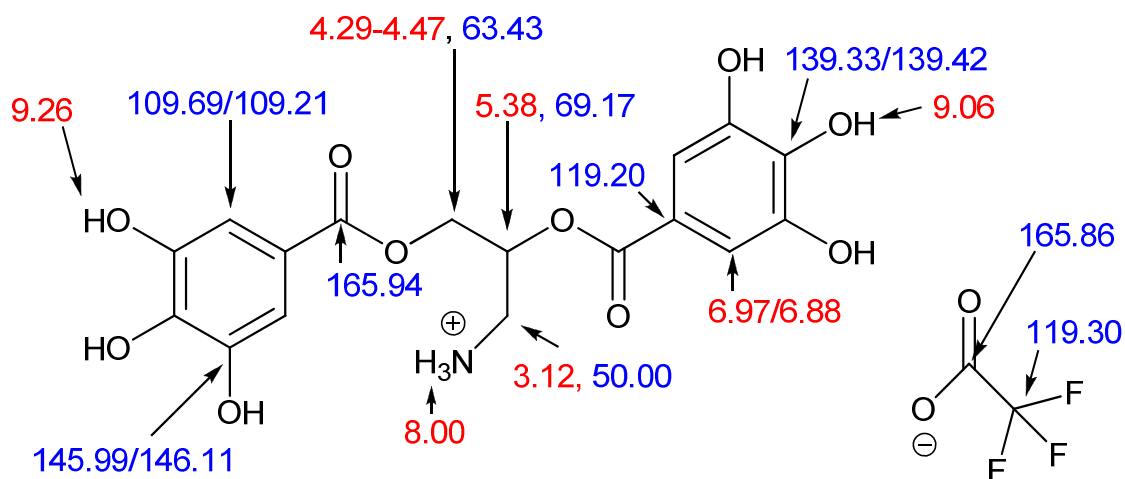
Step #1: Was conducted without modification of the “General procedure for synthesis of 3,4,5-tribenzyloxybenzoate” (Chapter 1, Experimental).

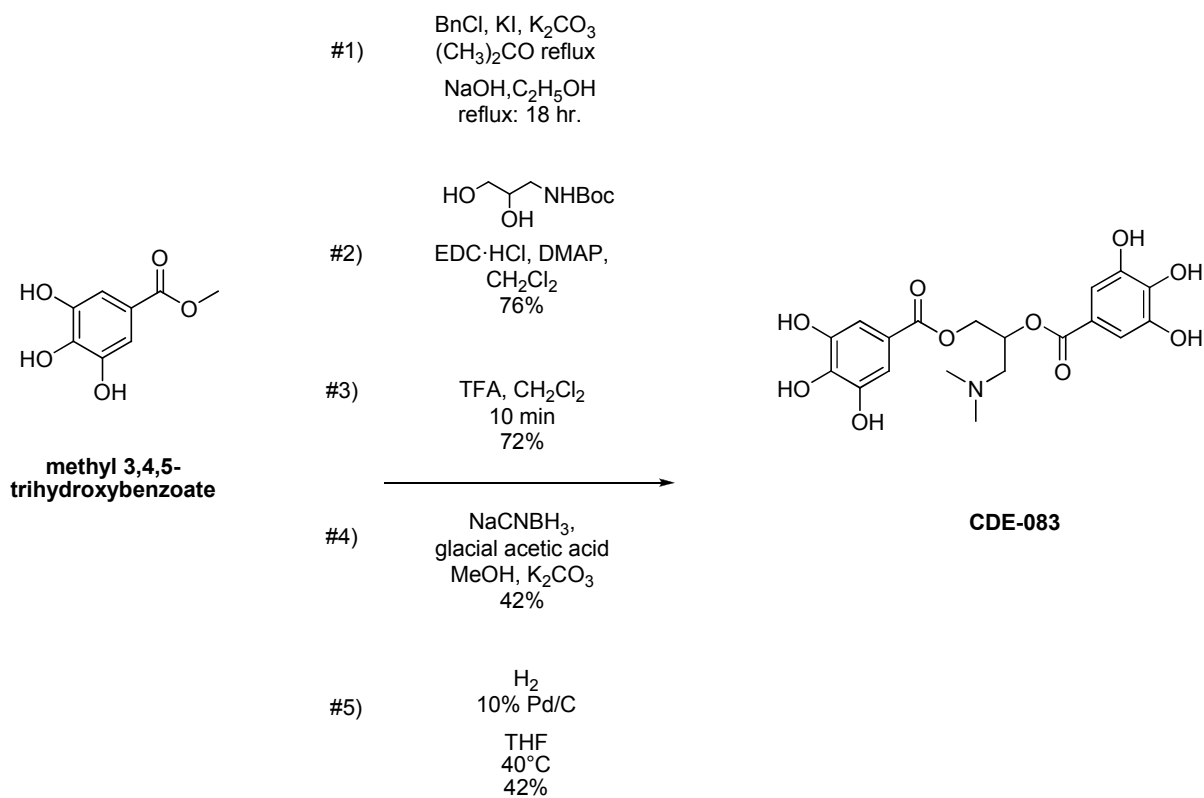
Step #2: Followed the same procedure as Step #2 for CDE-075 synthesis.

Step #3: 3-(Tert-butoxycarbonylamino) propane-1,2-diyl bis (3,4,5-tris(benzyloxy)benzoate) (150 mg, 0.15 mmol) and CH_2Cl_2 (0.50 mL) were combined and held at 0°C under N_2 . TFA (0.50 mL, 6.73 mmol) was syringed into the flask in a drop-wise fashion. The reaction was stirred for 10 minutes. A TLC (50% hexanes/EtOAc) indicated the consumption of starting material. The solvent was then evaporated *in vacuo*. EtOAc (5.00 mL) was added and evaporated three times successively to obtain a white solid (97.9 mg, 72%). ^1H NMR (CDCl_3 , 400 MHz) δ 8.31 (bs, 1H, -HN-), 7.30-7.25 (m, 34H, aromatic), 5.48 (s, 1H, -O-CH-), 5.06-4.90 (m, 12H, benzylic), 4.70-4.58 (m, 1H, -O- CH_2 -), 4.52-4.41 (m, 1H, -O- CH_2 -), and 3.46-3.20 (m, 2H, - CH_2 -N-); ^{13}C NMR (CDCl_3 , 100 MHz) δ 166.25, 165.88, 152.64, 143.33, 143.02, 137.39, 136.47, 128.76, 128.37, 128.10, 127.87, 127.80, 127.55, 127.47, 123.84, 123.31, 109.50, 109.15, 75.16, 71.53, 71.12, 69.76, 63.36, 40.78.

Step #4: 2,3-Bis(3,4,5-tris(benzyloxy)benzoyloxy)propan-1-aminium 2,2,2-trifluoroacetate (200 mg, 0.19 mmol), dry THF (2.69 mL, 33.1 mmol), and Pd/C 10% (0.29 g, 2.69 mmol) were combined and stirred overnight at 40°C under H_2 . A TLC (95% CH_2Cl_2 /MeOH) confirmed the consumption of the starting material. The reaction was filtered through Celite to remove the Pd/C catalyst. Then gravity filtered through filter paper. The solvent was then removed *in vacuo* to obtain a solid (70.6 mg, 94%). ^1H NMR ($\text{DMSO}-d_6$, 400 MHz) δ 9.26 (s, 4H, -OH), 9.06 (s, 2H, -OH), 8.00 (s, 3H, - NH_3), 6.97 (s, 2H, aromatic), 6.88 (s, 2H, aromatic), 5.38 (s, 1H, -O-CH-

), 4.47-4.44 (m, 1H, -O-CH₂-), 4.33-4.29 (m, 1H, -O-CH₂-), and 3.12 (s, 2H, -N-CH₂-); ¹³C NMR (DMSO-d₆, 100 MHz) δ 165.94, 165.86, 146.11, 145.99, 139.42, 139.33, 119.30, 119.20, 109.69, 109.21, 69.17, 63.43, 50.00; HRMS, ES calcd. for C₁₇H₁₈NO₁₀ [M+]⁺ 396.0931, found: 396.0920.



CDE-083**3-(Dimethylamino)propane-1,2-diyl bis(3,4,5-trihydroxybenzoate) (423.37 g/mol)** **$C_{19}H_{21}NO_{10}$** 

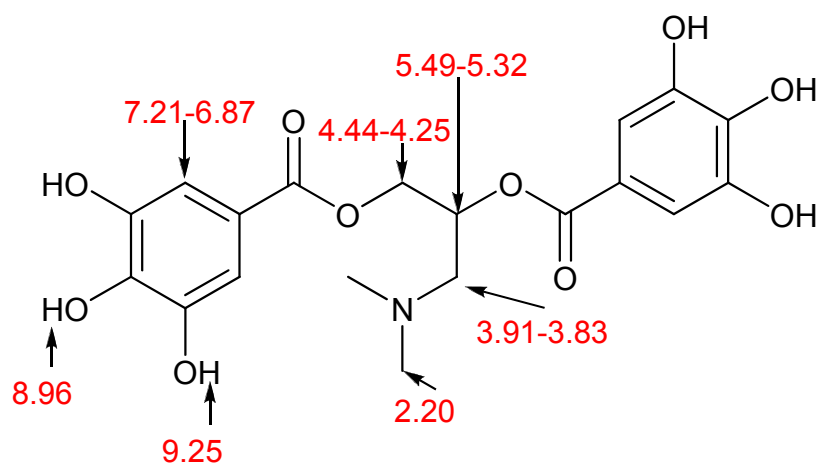
Step #1: Was conducted without modification of the “General procedure for synthesis of 3,4,5-tribenzyloxybenzoate” (Chapter 1, Experimental).

Step #2: Followed the same procedure as Step #2 for CDE-075 synthesis.

Step #3: Followed the same procedure as Step #2 for CDE-077 synthesis.

Step #4: 2,3-Bis(3,4,5-tris(benzyloxy)benzoyloxy)propan-1-aminium 2,2,2-trifluoroacetate (200 mg, 0.19 mmol), glacial acetic acid (29.0 μ L, 0.51 mmol), MeOH (1.00 mL) and NaCNBH₃ (22 mg, 0.34 mmol) were combined and stirred under N₂ for 3 hours upon which a solid formed. A TLC (95% CH₂Cl₂/MeOH) indicated that the starting material had been consumed. A saturated aqueous solution of K₂CO₃ was pipetted into the reaction mixture until pH paper indicated that the reaction was basic, upon which the solution turned cloudy. The solvent was evaporated *in vacuo*. The residue was extracted with EtOAc, dried with MgSO₄, filtered, and evaporated *in vacuo*. The residue was purified by column chromatography (95% CH₂Cl₂/MeOH) to obtain a solid (78.4 mg, 42%). ¹H NMR (CDCl₃, 400 MHz) δ 7.35-7.25 (m, 34H, aromatic), 5.88 (m, 1H, -O-CH-), 5.10-4.93 (m, 12H, benzylic), 4.63-4.70 (m, 1H, -O-CH₂-), 4.37-4.47 (m, 1H, -O-CH₂-), 3.90-4.05 (m, 2H, -N-CH₂-), and 2.31 (s, 6H, N(CH₃)₂); ¹³C NMR (DMSO-*d*₆, 100 MHz) δ 165.89, 165.67, 152.64, 152.60, 146.05, 137.51, 136.63, 136.23, 128.84, 128.65, 128.49, 128.00, 127.78, 127.57, 125.15, 124.95, 120.84, 120.72, 109.46, 108.97, 71.56, 70.61, 60.50, 46.33.

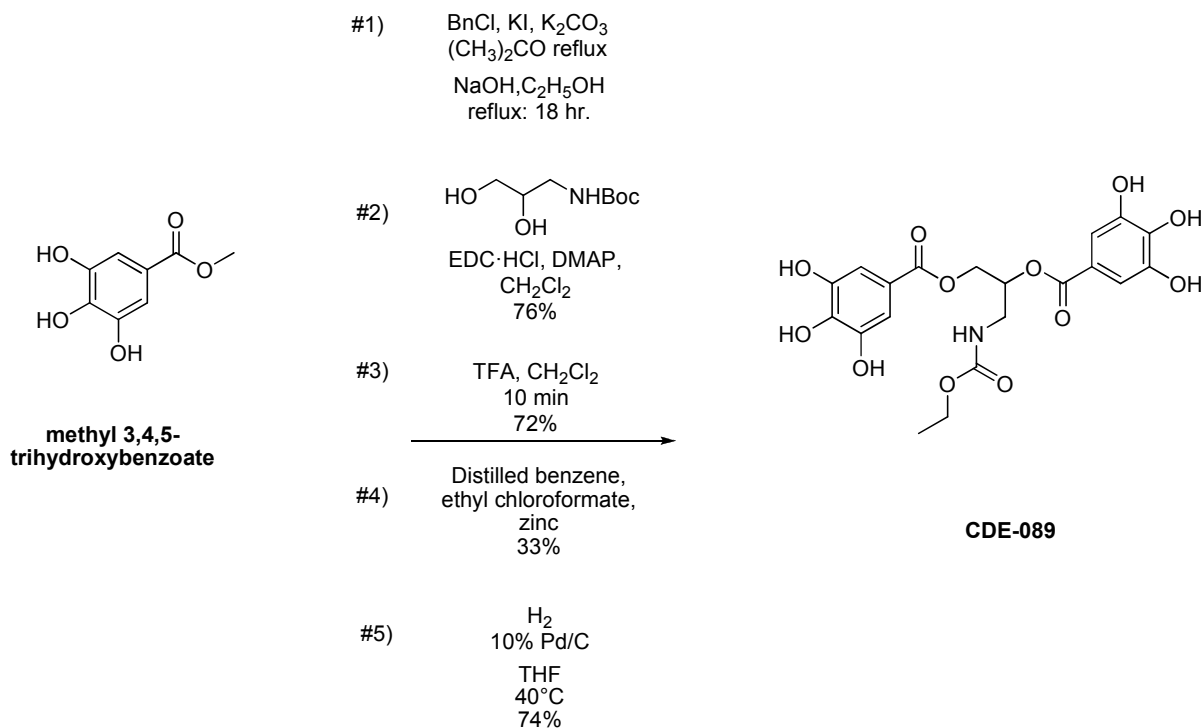
Step #5: 3-(Dimethylamino)propane-1,2-diyl bis(3,4,5-tris(benzyloxy)benzoate) (70.0 mg, 0.07 mmol), dry THF (1.04 mL), and Pd/C 10% (0.11 g, 1.03 mmol) were combined and stirred for 3 hours at 40°C under H₂. A TLC (95% CH₂Cl₂/MeOH) confirmed the consumption of the starting material. The reaction was syringed through a PTFE 0.2 μ M syringe to remove the Pd/C catalyst. The solvent was then removed *in vacuo* to obtain a solid (13.1 mg, 42%). ¹H NMR (DMSO-*d*₆, 400 MHz) δ 9.25 (s, 4H, meta -OH), 8.96 (s, 2H, para -OH), 7.21-6.87 (m, 4H, aromatic), 5.49-5.32 (m, 1H, -O-CH-), 4.44-4.25 (m, 2H, -O-CH₂-), 3.91-3.83 (m, 2H, -N-CH₂-), 2.20 (s, 6H, -N(CH₃)₂); HRMS, ES calcd. for C₁₉H₂₁NO₁₀ [M+]⁺ 424.1244, found: 424.1242.



CDE-089

3-(Ethoxycarbonylamino)propane-1,2-diyl bis(3,4,5-trihydroxybenzoate)

(467.38 g/mol) $C_{20}H_{21}NO_{12}$



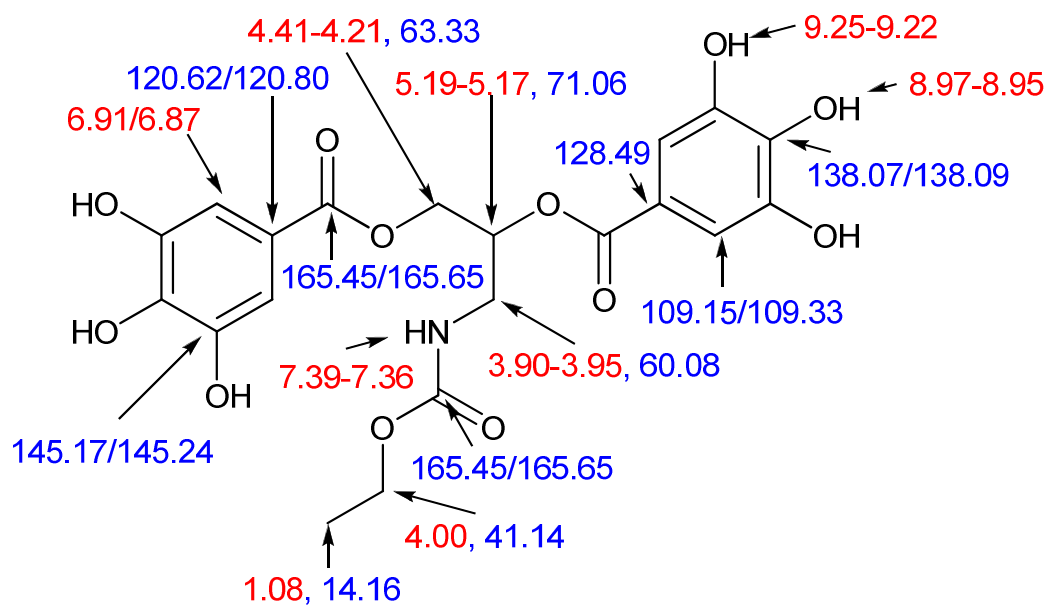
Step #1: Was conducted without modification of the “General procedure for synthesis of 3,4,5-tribenzyloxybenzoate” (Chapter 1, Experimental).

Step #2: Followed the same procedure as Step #2 for CDE-075 synthesis.

Step #3: Followed the same procedure as Step #2 for CDE-077 synthesis.

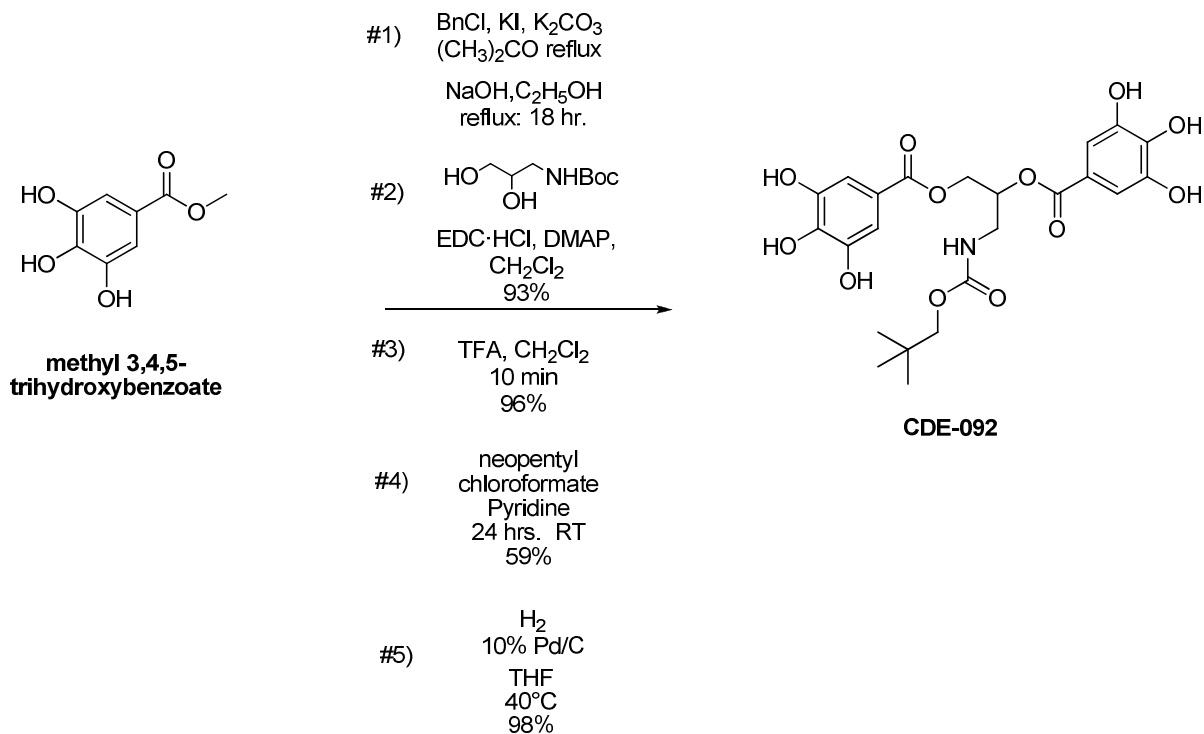
Step #4: 2,3-Bis(3,4,5-tris(benzyloxy)benzoyloxy)propan-1-aminium 2,2,2-trifluoroacetate (200 mg, 0.19 mmol) was dissolved in distilled benzene (0.50 mL, 5.32 mmol). Ethyl chloroformate (18.2 μ L, 0.19 mmol) and zinc (12.4 mg, 0.19 mmol) was stirred separately for 10 min. Then the first solution was slowly syringed into the second solution and the reaction was stirred overnight at room temperature under N_2 . A TLC (60% hexanes/EtOAc) confirmed the consumption of the starting material. The residue was purified by column chromatography (60% hexanes/EtOAc) to obtain a solid (63.4 mg, 33%).⁹⁴

Step #5: 3-(Ethoxycarbonylamino)propane-1,2-diyl bis(3,4,5-tris(benzyloxy)benzoate) (50.0 mg, 0.05 mmol), distilled THF (1.00 mL), and Pd/C 10% (75.0 mg, 0.71 mmol) were combined and stirred for 24 hours at 40°C under H_2 . A TLC (95% CH_2Cl_2 /MeOH) confirmed the consumption of the starting material. The reaction was syringed through a PTFE 0.2 μ M syringe to remove the Pd/C catalyst. The solvent was then removed *in vacuo* to obtain a solid, which was then triturated with hexanes (17.4 mg, 74%). 1H NMR (DMSO- d_6 , 400 MHz) δ 9.22-9.25 (m, 4H, meta -OH), 8.95-8.97 (m, 2H, para -OH), 7.36-7.39 (m, 1H, NH), 6.91 (s, 2H, aromatic), 6.87 (s, 2H, aromatic), 5.19-5.17 (m, 1H, -O-CH), 4.21-4.41 (m, 2H, -O-CH₂), [in acetone 4.00 (q, J = 6.87 Hz, 2H, CH₂-O), 3.95-3.90 (m, 2H, -N-CH₂), and 1.08 (t, J = 6.87 Hz, 3H, CH₃); ^{13}C NMR (DMSO- d_6 , 100 MHz) δ 165.65, 165.45, 145.24, 145.17, 138.09, 138.07, 128.49, 120.80, 120.62, 109.33, 109.15, 71.06, 63.33, 60.08, 41.14, 14.16.



CDE-092

3-(Neopentylloxycarbonylamino)propane-1,2-diyl bis(3,4,5-trihydroxybenzoate)
(509.46 g/mol) $C_{23}H_{27}NO_{12}$



Step #1: Was conducted without modification of the “General procedure for synthesis of 3,4,5-tribenzyloxybenzoate” (Chapter 1, Experimental).

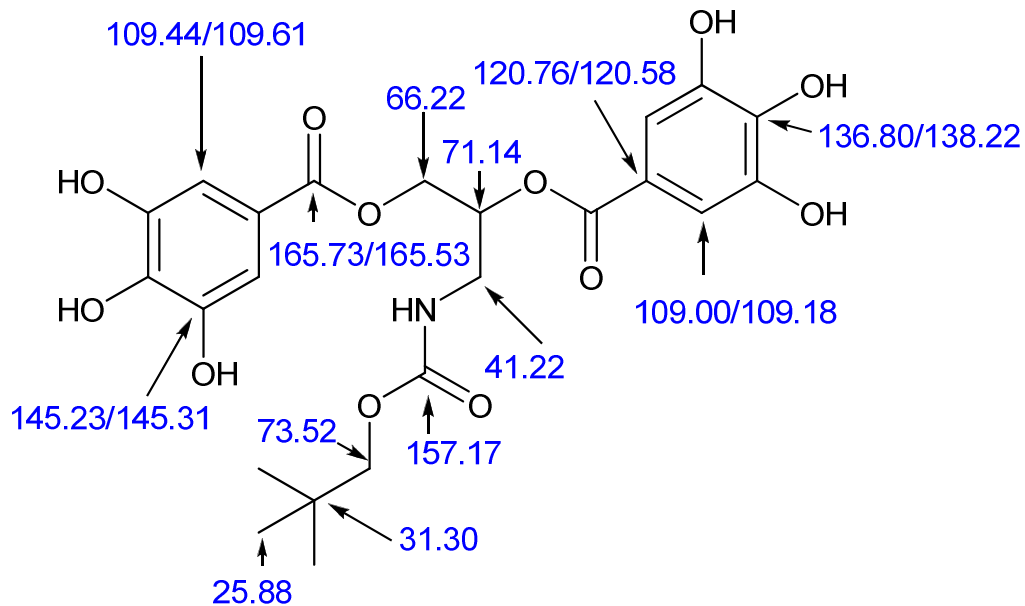
Step #2: Followed the same procedure as Step #2 for CDE-075 synthesis.

Step #3: Followed the same procedure as Step #2 for CDE-077 synthesis.

Step #4: Step #4: 2,3-Bis(3,4,5-tris(benzyloxy)benzoyloxy)propan-1-aminium 2,2,2-trifluoroacetate (0.85 g, 0.81 mmol), pyridine (2.00 mL), and neopentyl chloroformate (0.15 mL, 0.97 mmol) were combined and stirred at room temperature for 24 hours. Then a TLC (50% hexanes/EtOAc) revealed the consumption of the majority of the starting material. The reaction was diluted with EtOAc and the organic layer was washed with 1 N HCl (2 x), saturated aqueous sodium bicarbonate (2 x), and brine (1 x), dried over MgSO₄, filtered, and concentrated *in vacuo*. The residue was purified by column chromatography (50% hexanes/EtOAc) to obtain a brown crystalline solid (501 mg, 59%).

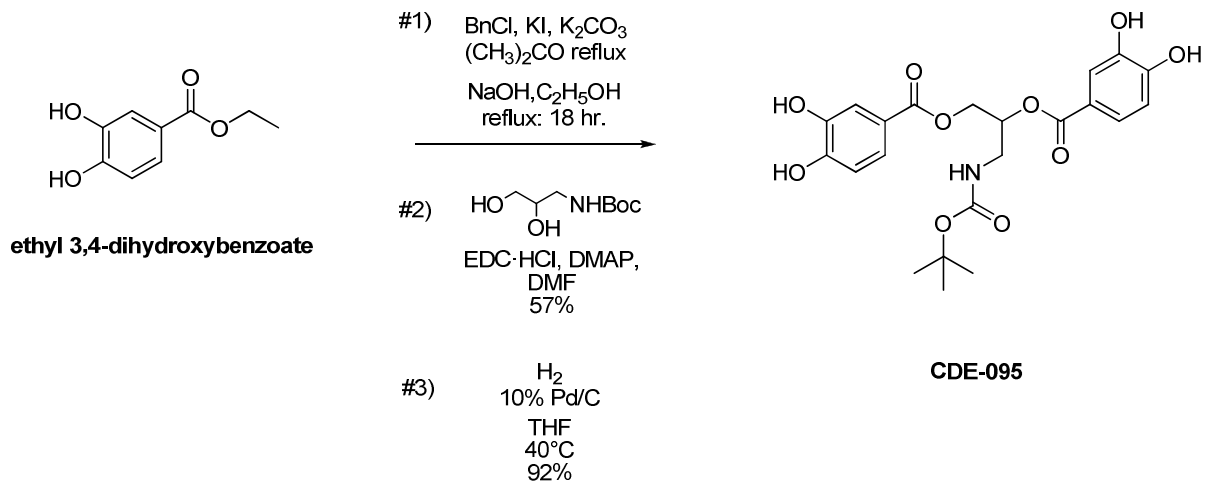
Step #5: 3-(Neopentylloxycarbonylamino)propane-1,2-diyl bis(3,4,5-tris(benzyloxy)benzoate) THF (5.80 mL), and Pd/C 10% (0.10 g, 4.76 mmol) were combined and stirred for 24 hours at 40°C under H₂. A TLC (90% CH₂Cl₂/MeOH) confirmed the consumption of the starting material. The reaction was syringed through a PTFE 0.2 μM syringe prepared with MeOH to remove the Pd/C catalyst. The solvent was then removed *in vacuo* and triturated with hexanes to obtain a solid (239 mg, 98%).

¹³C NMR (acetone-*d*₆, 100 MHz) δ 165.73, 165.53, 157.17, 145.31, 145.23, 138.22, 136.80, 120.76, 120.58, 109.61, 109.44, 109.18, 109.00, 73.52, 71.14, 66.22, 41.22, 31.30, 25.88.



CDE-095

3-(Tert-Butoxycarbonylamino)propane-1,2-diyl bis(3,4-dihydroxybenzoate)
 (463.43 g/mol) $C_{22}H_{25}NO_{10}$

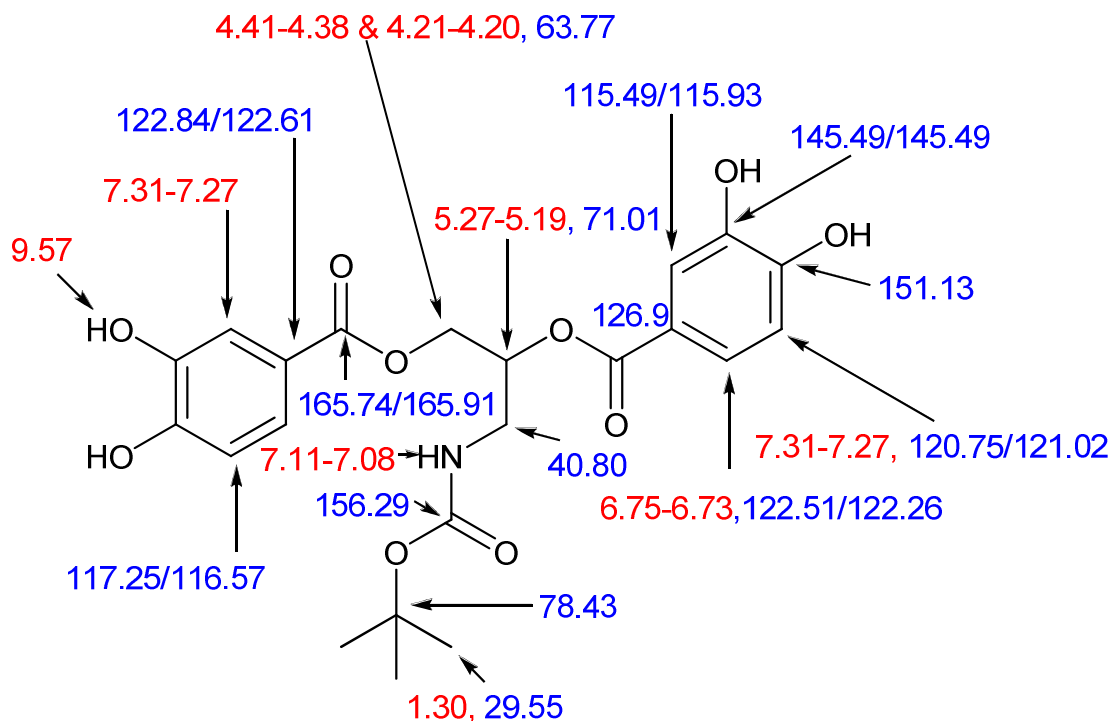


Step #1: Was conducted without modification of the “General procedure for synthesis of 3,4-dibenzyloxybenzoate” (Chapter 1, Experimental).

Step #2: 3,4-Bis(benzyloxy)benzoic acid (1.00 g, 2.99 mmol), DMAP (0.05 g, 0.36 mmol), tert-Butyl N-(2,3-dihydroxypropyl) carbamate (0.23 g, 1.20 mmol), and DMF (4.55 mL) were combined and stirred under N₂. In a separate flask EDC·HCl (0.86 g, 4.19 mmol) and DMF (9.10 mL) were mixed together and then syringed into the first reaction mixture. The reaction was stirred overnight at room temperature under N₂. It was then heated to 40°C and stirred under N₂ overnight. A TLC (65% hexanes/EtOAc) determined that the majority of the starting material had been consumed. The solvent was reduced *in vacuo* and the residue was taken up in a 4:1 mixture of EtOAc:hexanes and filtered. The filtrate was washed with 1 N HCl (2 x), saturated aqueous sodium bicarbonate (2 x), and brine (1 x), dried over MgSO₄, filtered, and concentrated *in vacuo* and triturated with hexanes. The residue was purified by column chromatography (65% hexanes/EtOAc) to obtain a solid (464 mg, 57%). ¹H NMR (CDCl₃, 400 MHz) δ 7.62-7.56 (m, 4H, ortho and meta aromatic), 7.41-7.25 (m, 20H, aromatic), 6.89 (d, *J* = 9.16 Hz, 2H, meta aromatic), 5.38 (quin, *J* = 5.04 Hz, 1H, -O-CH-), 5.18 (s, 4H, meta benzylic), 5.13 (s, 2H, para benzylic), 5.11 (s, 2H, para benzylic), 4.83-4.81 (m, 1H, -NH-), 4.55-4.51 (m, 1H, -OCH₂-), 4.47-4.45 (m, 1H, -OCH₂-), 3.53-3.47 (m, 2H, -NCH₂-), and 1.40 (s, 9H, -(CH₃)₃); ¹³C NMR (CDCl₃, 100 MHz) δ 165.90, 165.66, 153.29, 153.18, 148.43, 136.85, 136.53, 128.68, 128.60, 128.08, 128.02, 127.51, 127.16, 124.39, 124.25, 122.53, 115.77, 115.50, 113.28, 79.84, 70.87, 63.38, 41.20, 28.41.

Step #3: 3-(Tert-butoxycarbonylamino)propane-1,2-diyl bis(3,4-bis(benzyloxy)benzoate) (0.4 g, 0.58 mmol), THF (8.00 mL), and Pd/C 10% (0.63 g, 5.88 mmol) were combined and stirred for

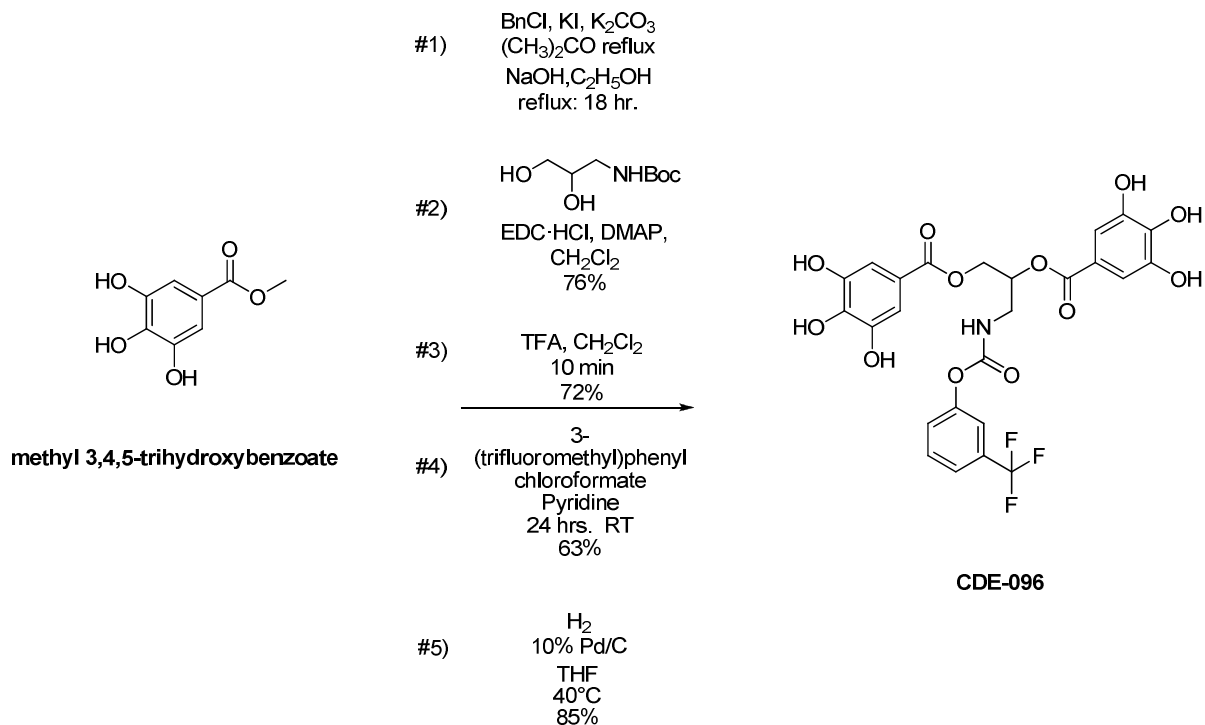
36 hours at 40°C under H₂. A TLC (95% CH₂Cl₂/MeOH) confirmed the consumption of the starting material. The reaction was syringed through a PTFE 0.2 μM syringe prepared with MeOH to remove the Pd/C catalyst. The solvent was then removed *in vacuo* and triturated with hexanes to obtain a yellow solid (250 mg, 92%). ¹H NMR (DMSO-*d*₆, 400 MHz) δ 9.57 (bs, 4H, -OH), 7.31-7.27 (m, 4H, aromatic), 6.75-6.73 (m, 2H, aromatic), 7.10 (t, *J* = 5.95 Hz, 1H, -NH), 5.27-5.19 (m, 1H, -OCH-), 4.40 (m, 1H, -OCH₂), 4.21-4.38 (m, 1H, -OCH₂-), and 1.30 (s, 9H, -OC(CH₃)₃); ¹³C NMR (DMSO-*d*₆, 100 MHz) δ 178.34, 175.10, 165.91, 165.74, 156.29, 151.13, 145.59, 145.49, 122.84, 122.61, 122.51, 122.26, 121.02, 120.75, 117.25, 116.57, 115.93, 115.49, 78.43, 71.01, 63.77, 40.80, 29.55; HRMS, ES calcd. for C₂₂H₂₅NO₁₀Na [M+Na]⁺ 486.1376, found: 486.1378.



CDE-096

3-((3-(Trifluoromethyl)phenoxy)carbonylamino)propane-1,2-diyl bis(3,4,5-trihydroxybenzoate)

(583.09 g/mol) C₂₅H₂₀F₃NO₁₂



Step #1: Was conducted without modification of the “General procedure for synthesis of 3,4,5-tribenzyloxybenzoate” (Chapter 1, Experimental).

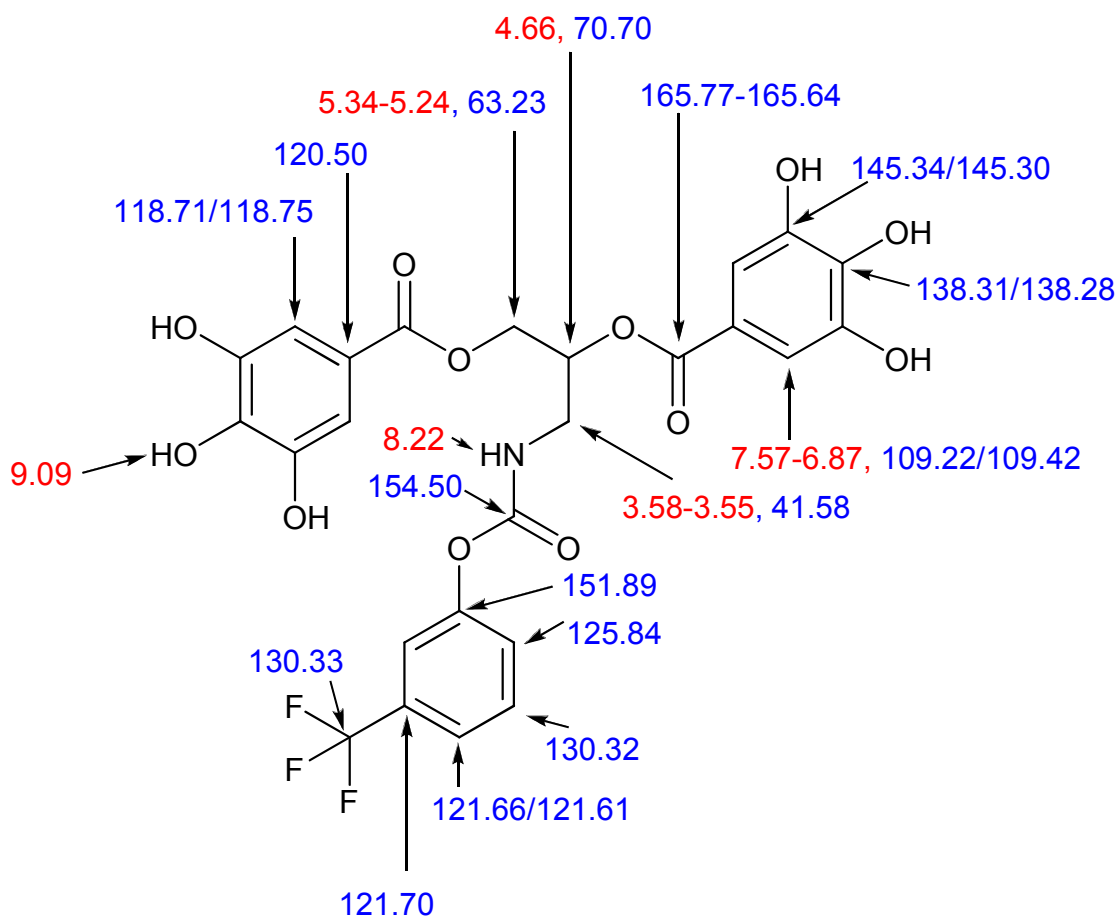
Step #2: Followed the same procedure as Step #2 for CDE-075 synthesis.

Step #3: Followed the same procedure as Step #2 for CDE-077 synthesis.

Step #4: 2,3-Bis(3,4,5-tris(benzyloxy)benzoyloxy)propan-1-aminium 2,2,2-trifluoroacetate (0.20 g, 0.19 mmol), pyridine (0.50 mL), and 3-(trifluoromethyl)phenyl chloroformate (0.36 μ L, 0.23 mmol) were combined and stirred at room temperature for 24 hours. Then a TLC (50% hexanes/EtOAc) revealed the consumption of the majority of the starting material. The reaction was diluted with EtOAc and the organic layer was washed with 1 N HCl (2 x), saturated aqueous sodium bicarbonate (2 x), and brine (1 x), dried over MgSO₄, filtered, and concentrated *in vacuo*. The residue was purified by column chromatography (50% hexanes/EtOAc) to obtain a brown crystalline solid (135 mg, 63%). ¹H NMR (CDCl₃, 400 MHz) δ 7.36-7.25 (m, 38H, aromatic), 5.47 (t, *J* = 5.95 Hz, 1H, -NH), 5.07-5.02 (m, 12H, meta or para benzylic), 4.66-4.63 (m, 1H, -OCH-), 4.52-4.50 (m, 1H, -OCH₂-), 3.94 (m, 1H, -O-CH₂-), 3.73 (m, 1H, -NCH₂-), 3.65 (m, 1H, -NCH₂-); ¹³C NMR (CDCl₃, 100 MHz) δ 165.85, 152.70, 146.12, 136.57, 128.74, 128.59, 128.26, 128.12, 127.90, 127.62, 118.85, 109.53, 71.34, 29.77.

Step #5: 3-((3-(Trifluoromethyl)phenoxy)carbonylamino)propane-1,2-diyl bis(3,4,5-tris(benzyloxy)benzoate) (134 mg, 0.12 mmol), THF (2.00 mL), and Pd/C 10% (0.13 g, 1.19 mmol) were combined and stirred for 36 hours at 40°C under H₂. A TLC (95% CH₂Cl₂/MeOH) confirmed the consumption of the starting material. The reaction was syringed through a PTFE 0.2 μ M syringe prepared with MeOH to remove the Pd/C catalyst. The solvent was then removed *in vacuo* and triturated with hexanes to obtain a solid (59.1 mg, 85%). ¹H NMR (DMSO-*d*₆, 400 MHz) δ 9.09 (bs, 6H, -OH), 8.22 (t, *J* = 5.95 Hz, 1H, -NH), 7.57-7.32 (m, 3H, aromatic), 7.70-6.97 (m, 2H, aromatic), 6.95 (s, 1H, aromatic), 6.87-6.90 (m, 2H, aromatic), 5.34-5.24 (m, 2H, -OCH₂), 4.46-4.43 (m, 1H, -OCH-), 3.58-3.55 (m, 2H, -NCH₂); ¹³C NMR (acetone-*d*₆, 100 MHz) δ 165.77, 165.64, 154.50, 151.89, 145.34, 145.30, 138.31, 138.28, 130.33, 125.84, 121.70, 121.66, 121.61, 120.50, 118.75, 118.71, 109.42, 109.22, 70.70, 63.23, 41.58. ¹⁹F

NMR (DMSO-*d*₆, 376 MHz) δ -60.9681(singlet representing the three fluorines on the molecule), -61.1524(singlet representing the fluorine signal from the rotamer of the molecule), -74.2434 (singlet confirmed to be the TFA anion by taking an ¹⁹F NMR of TFA + pyridine in DMSO-*d*₆); HRMS, ES calcd. for C₂₅H₂₀F₃NO₁₂Na[M+Na]⁺ 606.0835, found: 606.0821.



Proof-of-Structure Analysis

¹H NMR: The broad singlet at δ 9.09 integrated for 6H and is representative of the expected 6H for the hydroxyls on the rings. The triplet at δ 8.22 correlates to the amide hydrogen that is coupled with an adjacent -CH₂ group. A complex spectra worth a total of 8H is expected in the aromatic region, and this is found from δ 7.56-6.89. A peak integrating to 2H was expected for the -O-CH₂- group and found as a multiplet at δ 5.34-5.24. A peak integrating to 1H was expected for the -OCH- group and was found as a multiplet at δ 4.46-4.43. A peak integrating for 2H was expected for the -N-CH₂- group and was found as a multiplet at δ 3.58-3.55.

¹³C NMR: Two peaks were expected for the ester carbonyl carbons (δ 160-180), and two were found at δ 165.77 and 165.64. The third carbonyl carbon was found farther upfield δ 154.50 and represents the more shielded carbamate carbonyl carbon on the handle. Fourteen signals were expected for the aromatic ring hydrogens within the aromatic region (δ 160-100), and these were found. The CF₃ signal should also appear in the aromatic region, and this was found at δ 130.33. Two peaks were expected in the δ 60-80 region for the linker carbons, and two peaks were found at δ 70.70 and 63.23. The slow rotation of the carbamate C-N bond is known to affect chemical shifts of nearby carbons by anisotropic shielding by the carbamate carbonyl group shielding these atoms and producing signals further upfield.⁹⁵ Therefore, the -NCH₂- shift was expected upfield, and a signal was found in this region at δ 41.58.

¹⁹F NMR: The CF₃ group has previously been reported⁹⁶ to give a single peak at approximately -62.08 ppm. A verification of our compound containing this group was a singlet at δ -60.9681 and the singlet at δ -61.1524 (rotamer). A third unexpected singlet peak was observed in the spectra at δ -74.2434, and to verify its identity, a control ¹⁹F NMR was conducted consisting of

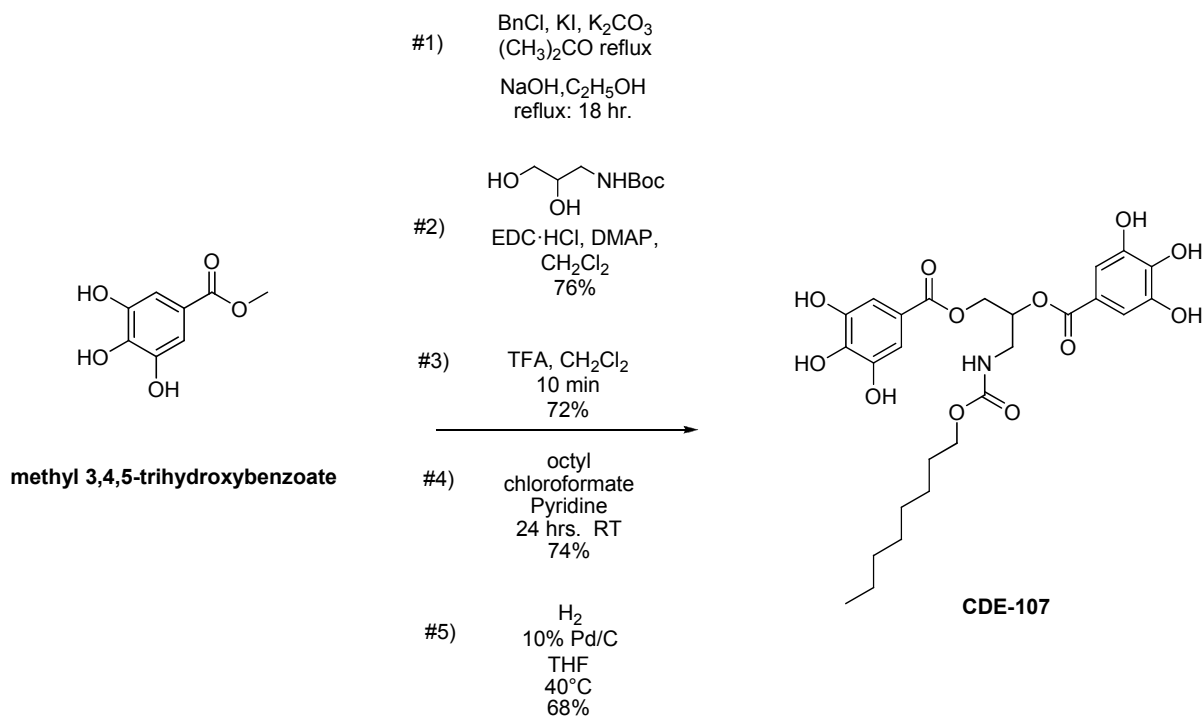
TFA + pyridine in DMSO- d_6 . This experiment confirmed the identity of the third peak as that of trifluoroacetic acid anion.

The composition of the molecule was verified by obtaining the exact mass using a VG 70-250-s2 spectrometer manufactured by Micromass Corp. (Manchester UK) at the University of Michigan Mass Spectrometry Laboratory. The measured mass of 606.0821 g/mol was in agreement with the calculated value of 606.0835 g/mol.

CDE-107

3-(((Octyloxy)carbonyl)amino)propane-1,2-diyl bis(3,4,5-trihydroxybenzoate)

(551.54 g/mol) C₂₆H₃₃N₁O₁₂



Step #1: Was conducted without modification of the “General procedure for synthesis of 3,4,5-tribenzyloxybenzoate” (Chapter 1, Experimental).

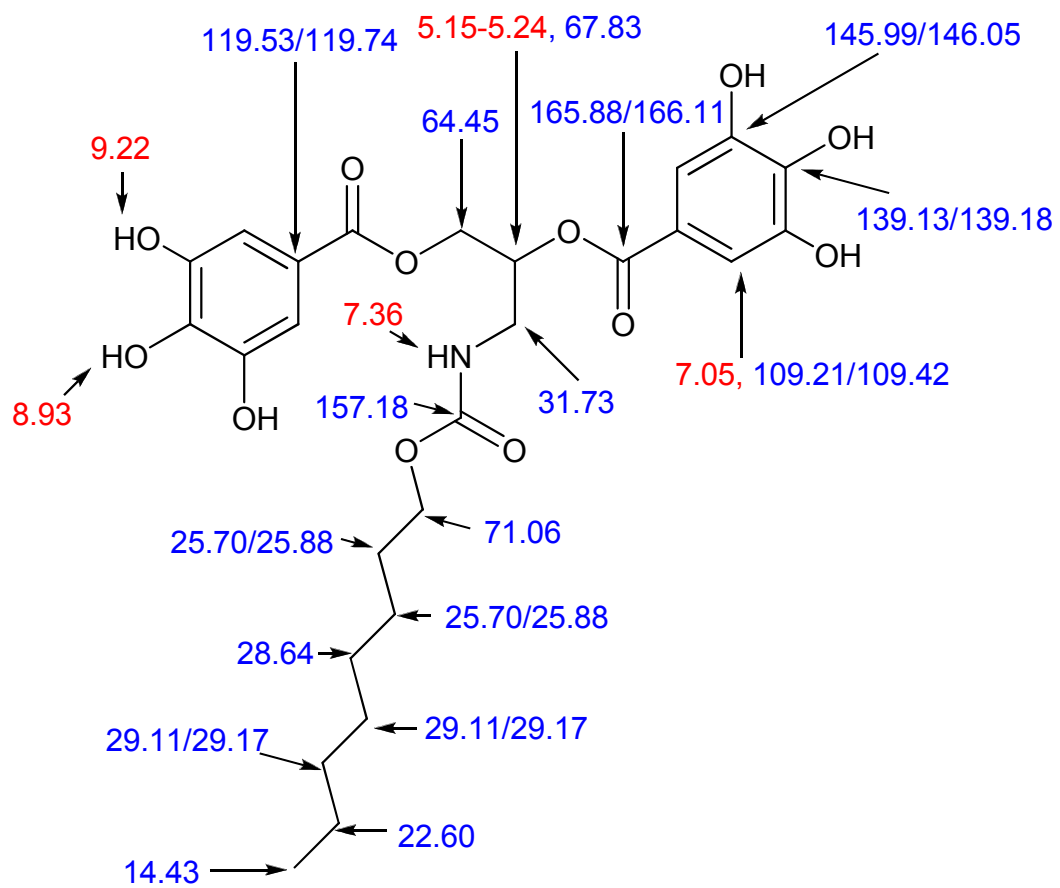
Step #2: Followed the same procedure as Step #2 for CDE-075 synthesis.

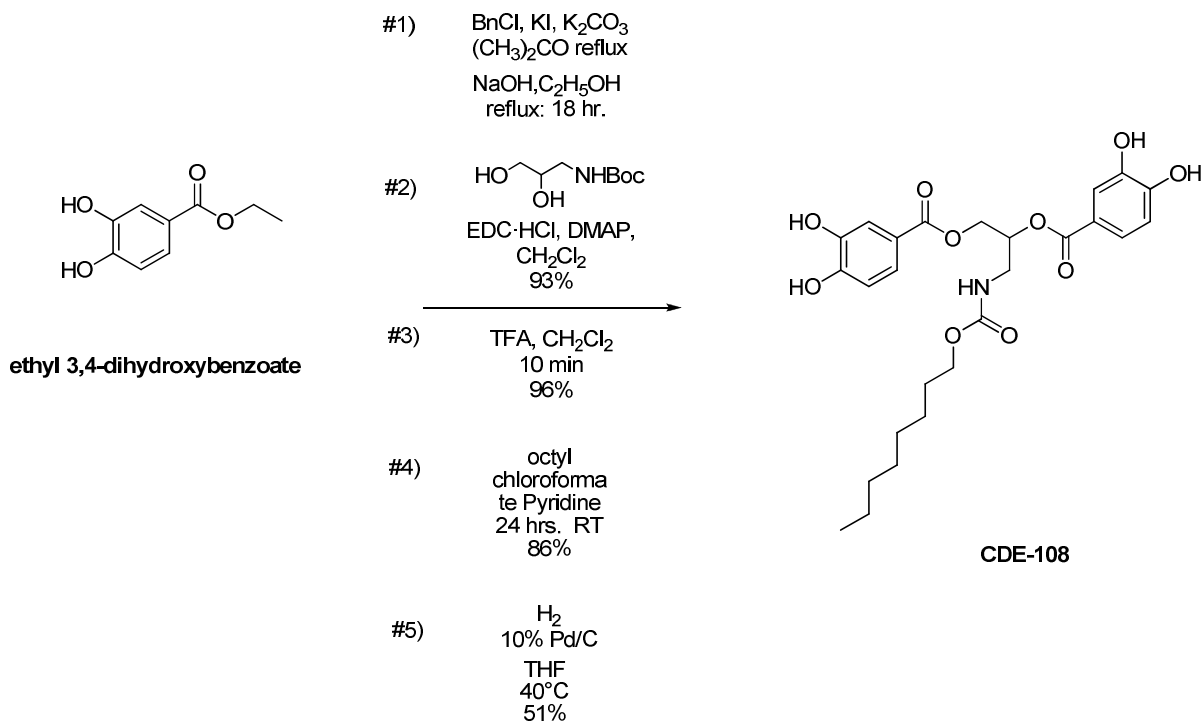
Step #3: Followed the same procedure as Step #2 for CDE-077 synthesis.

Step #4: 2,3-Bis(3,4,5-tris(benzyloxy)benzoyloxy)propan-1-aminium 2,2,2-trifluoroacetate (1.0 g, 0.95 mmol), pyridine (2.33 mL), and octyl chloroformate (0.22 mL, 1.13 mmol) were

combined and stirred at room temperature for 24 hours. A TLC (50% hexanes/EtOAc) revealed the consumption of the majority of the starting material. The solvent was evaporated *in vacuo*. The residue was purified by column chromatography (50% hexanes/EtOAc) to obtain a solid (759 mg, 74%). ¹H NMR (CDCl₃, 400 MHz) δ 7.39-7.25 (m, 34H, aromatic), 5.98-5.93 (m, 1H, -NH), 5.42-5.41 (m, 1H, -OCH), 5.06 (s, 4H, benzylic), 5.08 (s, 8H, benzylic), 4.61-4.59 (m, 1H, -OCH₂), 4.50-4.40 (m, 1H, -OCH₂), 4.08-4.04 (t, *J* = 6.41 Hz, 2H, -O-CH₂-CH₂-), 3.67-3.47 (bm, 2H, -OCH₂-NH), 1.70-1.50 (m, 2H, -O-CH₂-CH₂-), 1.27-1.26 (m, 10H, tail), and 0.95-0.85 (t, *J* = 5.95 Hz, 3H, -CH₃); ¹³C NMR (CDCl₃, 100 MHz) δ 165.81, 165.65, 156.91, 152.67, 146.07, 136.64, 136.23, 128.62, 127.66, 124.60, 109.47, 109.01, 75.21, 71.63, 71.06, 69.42, 68.15, 65.59, 63.43, 41.54, 31.89, 29.34, 29.10, 25.93, 25.65, 22.74, 14.20.

Step #5: 3-(((Octyloxy)carbonyl)amino)propane-1,2-diyl bis(3,4,5-tris(benzyloxy)benzoate) (0.5 g, 0.46 mmol) was dissolved in low water THF (65.5 mL). Pd/C 10% (0.68 g, 6.40 mmol) was added and stirred overnight at 40°C under N₂. A TLC (95% CH₂Cl₂/MeOH) confirmed the consumption of the starting material. The reaction was syringed through a PTFE 0.2 μM syringe prepared with MeOH to remove the Pd/C catalyst. The solvent was then removed *in vacuo* and triturated with hexanes to obtain a solid (252 mg, 68%). ¹H NMR (DMSO-*d*₆, 400 MHz) δ 9.22 (m, 4H, meta -OH), 8.93 (s, 2H, para -OH), 7.36 (t, *J* = 5.95 Hz, 1H, -HN-), 7.05 (m, 4H, aromatic), 5.15-5.24 (m, 1H, -O-CH-), 4.42-4.05 (m, 4H, -O-CH₂-CH-O- and -O-CH₂-(CH₂)₆-CH₃), 4.02-3.81 (m, 4H, -NCH₂- and -O-CH₂-(CH₂)₂-(CH₂)₄-CH₃), 1.20 (s, 8H, -(CH₂)₄-), and 0.82 (s, 3H, -CH₃); ¹³C NMR (DMSO-*d*₆, 400 MHz) δ 166.11, 165.88, 157.18, 146.05, 145.99, 139.18, 139.13, 119.74, 119.53, 109.42, 109.21, 71.06, 67.83, 64.45, 31.73, 29.17, 29.11, 28.64, 25.88, 25.70, 22.60, 14.43.



CDE-108**3-(Heptyloxycarbonylamino)propane-1,2-diyl bis(3,4-dihydroxybenzoate)****(519.54 g/mol) C₂₆H₃₃N₁O₁₀**

Step #1: Was conducted without modification of the “General procedure for synthesis of 3,4-dibenzoyloxybenzoate” (Chapter 1, Experimental).

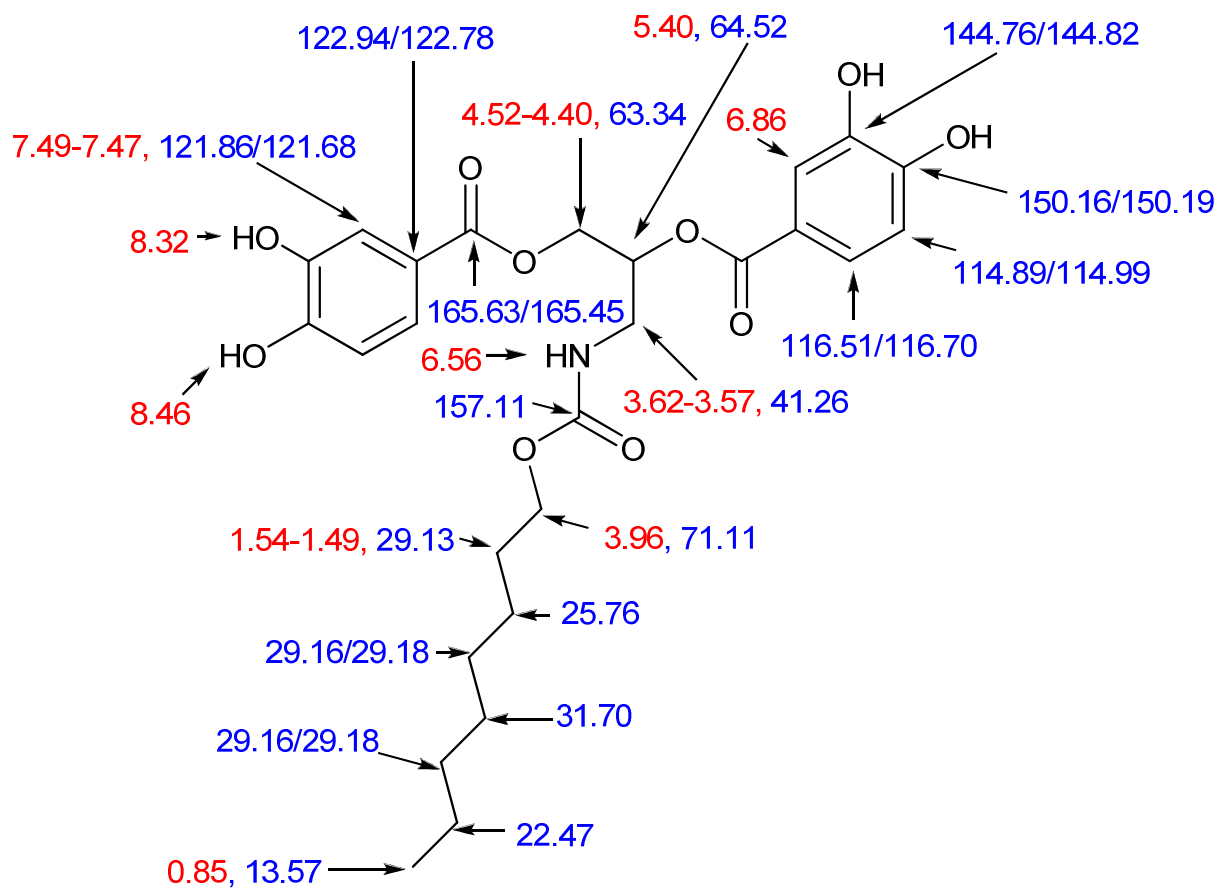
Step #2: Followed the same procedure as Step #2 for CDE-075 synthesis, except 3,4-dibenzoyloxybenzoic acid was used in place of 3,4,5-tribenzoyloxybenzoic acid.

Step #3: Followed the same procedure as Step #2 for CDE-077 synthesis.

Step #4: 2,3-Bis((3,4-bis(benzyloxy)benzoyl)oxy)propan-1-aminium 2,2,2-trifluoroacetate (1.0 g, 1.19 mmol), pyridine (3.0 mL), and octyl chloroformate (0.28 mL, 1.43 mmol) were combined and stirred at room temperature overnight. Then a TLC (50% hexanes/EtOAc) revealed the consumption of the majority of the starting material. The majority of the solvent was removed *in vacuo*. The residue was purified by column chromatography (65% hexanes/EtOAc) to obtain a solid (0.91 g, 86%). ¹H NMR (CDCl₃, 400 MHz) δ 7.62-7.59 (m, 4H, ortho and meta aromatic), 7.44-7.27 (m, 20H, benzylic), 6.90 (dd, *J* = 1.37, 9.16 Hz, 2H, ortho aromatic), 5.40 (quin, *J* = 4.58 Hz, 1H, -O-CH-), 5.18 (s, 4H, meta benzylic), 5.13 (s, 2H, para benzylic), 5.11 (s, 2H, para benzylic), 4.56-4.47 (m, 2H, -O-CH₂-), 4.01 (t, *J* = 6.89 Hz, 2H, -O-CH₂-CH₂-), 3.63-3.53 (m, 2H, -N-CH₂-), 1.58-1.53 (m, 2H, -O-CH₂-CH₂-), 1.26-1.25 (bm, 10H, -O-CH₂-CH₂-(CH₂)₅-CH₃) and 0.87 (t, *J* = 7.33 Hz, 3H, -CH₃); ¹³C NMR (CDCl₃, 100 MHz) δ 165.89, 153.33, 157.00, 148.43, 136.84, 136.56, 136.84, 136.56, 128.69, 128.60, 128.09, 127.52, 127.16, 124.36, 124.26, 122.43, 115.71, 115.49, 113.26, 71.28, 71.17, 70.87, 63.25, 63.18, 32.90, 31.90, 29.49, 29.07, 25.91, 25.84, 22.73, 14.19.

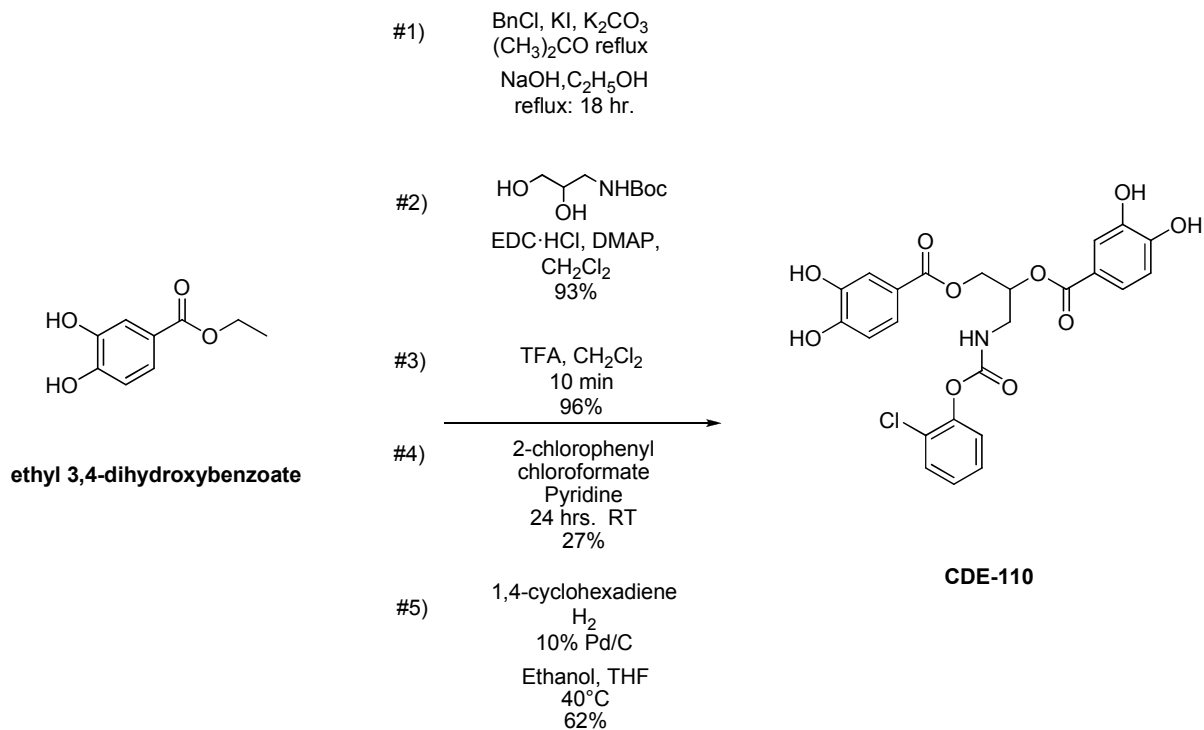
Step #5: 3-(Heptyloxycarbonylamino)propane-1,2-diyl bis(3,4-bis(benzyloxy)benzoate) (0.91 g, 1.03 mmol) was dissolved in low water THF (9.62 mL). Pd/C 10% (0.06 g, 0.52 mmol) and 1,4-cyclohexadiene (1.00 mL, 10.3 mmol) were added and stirred overnight at 40°C under N₂. A TLC (95% CH₂Cl₂/MeOH) confirmed the consumption of the starting material. The reaction was syringed through a PTFE 0.2 μM syringe prepared with MeOH to remove the Pd/C catalyst. The solvent was then removed *in vacuo* and triturated with hexanes to obtain a solid (272 mg, 51%). ¹H NMR (acetone-*d*₆, 400 MHz) δ 8.46 (bs, 2H, -OH), 8.32 (bs, 2H, -OH), 7.49-7.47 (m, 4H, ortho and meta aromatic), 6.86 (dd, *J* = 1.37, 8.24 Hz, 2H, meta aromatic), 6.56 (t, *J* = 5.95 Hz, 1H, -NH), 5.40 (q, *J* = 5.95 Hz, 1H, -OCH), 4.52-4.50 (m, 1H, -OCH₂-), 4.45-4.40 (m,

1H, -OCH₂-), 3.96 (t, *J* = 6.87 Hz, 2H, -O-CH₂-), 3.62-3.57 (m, 2H, -N-CH₂-), 1.54-1.49 (m, 2H, -O-CH₂-CH₂-), 1.24 (bs, 10H, -O-CH₂-CH₂-(CH₂)₅-CH₃), and 0.85 (t, *J* = 7.17 Hz, 3H, -CH₃);
¹³C NMR (acetone-*d*₆, 400 MHz) δ 165.63, 165.45, 157.11, 150.19, 150.16, 144.82, 144.76, 122.94, 122.78, 121.86, 121.68, 116.70, 116.51, 114.99, 114.89, 71.11, 64.52, 63.34, 41.26, 31.70, 29.18, 29.16, 29.13, 25.76, 22.47, 13.57; HRMS, ES calcd. for C₂₆H₃₃NO₁₀Na [M+ Na]⁺ 542.2002, found: 542.2017.



CDE-110

3-((2-Chlorophenoxy)carbonylamino)propane-1,2-diyl bis(3,4-dihydroxybenzoate)
(517.87 g/mol) C₂₄H₂₀ClNO₁₀



Step #1: Was conducted without modification of the “General procedure for synthesis of 3,4-dibenzoyloxybenzoate” (Chapter 1, Experimental).

Step #2: Followed the same procedure as Step #2 for CDE-075 synthesis, except 3,4-dibenzoyloxybenzoate was used in place of 3,4,5-tribenzoyloxybenzoate

Step #3: Followed the same procedure as Step #2 for CDE-077 synthesis.

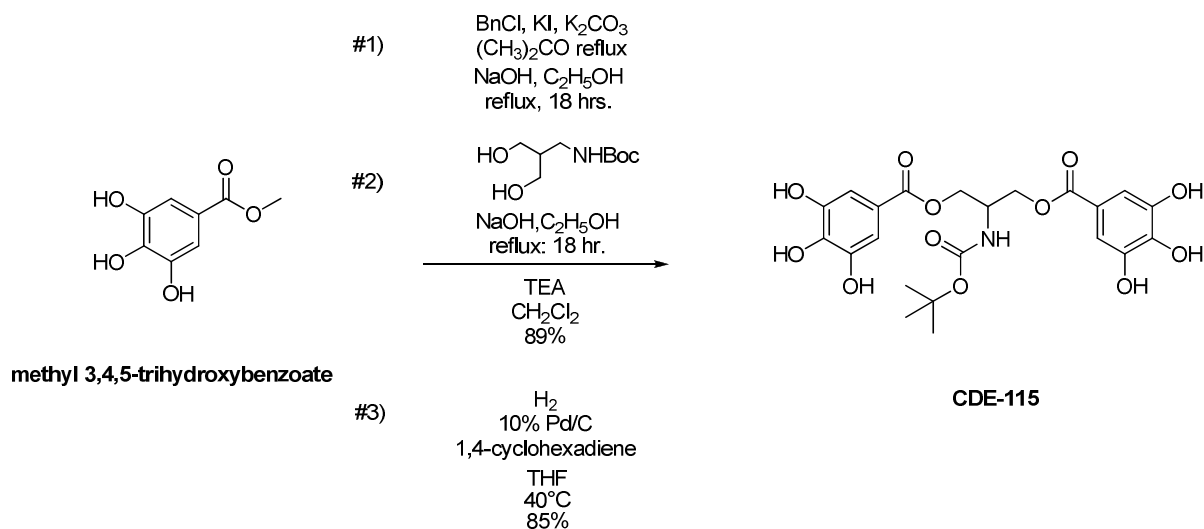
Step #4: 2,3-Bis((3,4-bis(benzyloxy)benzoyl)oxy)propan-1-aminium 2,2,2-trifluoroacetate (1.00 g, 1.19 mmol) was dissolved in pyridine (3 mL). Then 2-chlorophenyl chloroformate (0.20 mL, 1.43 mmol) was added. The reaction was stirred under N₂ overnight. A TLC (65% hexanes/EtOAc) confirmed the consumption of starting material. The residue was purified by column chromatography (65% hexanes/EtOAc) to obtain a solid (333 mg, 27%). ¹H NMR (CDCl₃, 400 MHz) δ 7.65-7.60 (m, 4H, ortho and meta aromatic), 7.44-7.29 (m, 20H, benzylic), 7.23-7.12 (m, 4H, Cl-containing ring), 6.92-6.88 (m, 2H, ortho aromatic), 5.57 (t, *J* = 5.95 Hz, 1H, -NH), 5.46 (t, *J* = 5.04 Hz, 1H, -O-CH-), 5.19 (s, 2H, benzylic), 5.18 (s, 2H, benzylic), 5.14 (s, 2H, benzylic), 5.07 (s, 2H, benzylic), 4.63-4.50 (m, 2H, -O-CH₂), and 3.85-3.64 (m, 2H, -N-CH₂); ¹³C NMR (CDCl₃, 100 MHz) δ 165.93, 165.76, 153.90, 153.39, 153.29, 148.47, 147.10, 136.86, 136.56, 130.29, 128.70, 128.59, 128.11, 128.05, 127.74, 127.55, 127.52, 127.19, 126.86, 124.48, 124.32, 124.13, 122.39, 122.33, 115.76, 115.52, 113.33, 71.25, 70.89, 63.08, 42.02, 29.80.

Step #5: 3-((2-Chlorophenoxy)carbonylamino)propane-1,2-diyl bis(3,4-bis(benzyloxy)benzoate) (0.30 g, 0.342 mmol) was dissolved in ethanol (2.30 mL). Low-water THF (1.00 mL) was added as a co-solvent. Pd/C 10% (0.02 g, 0.17 mmol) and 1,4-cyclohexadiene (0.64 mL, 6.84 mmol) were added. The reaction was stirred for 48 hours, under N₂, at 40°C.

A TLC (95% CH₂Cl₂/MeOH) indicated the starting material had been consumed. The reaction was syringed through a PTFE 0.2 μM syringe prepared with MeOH to remove the Pd/C catalyst. The solvent was removed *in vacuo* to obtain a solid (110 mg, 62%). ¹H NMR (acetone-*d*₆, 400 MHz) δ 8.80-8.30 (bs, 4H, -OH), 7.61-7.41 (m, 5H, ortho-H + H adjacent to the Cl), 7.32-7.25 (m, 1H, para-H to Cl), 7.22-7.10 (m, 2H, meta-H to Cl), 6.88 (dd, *J* = 2.29, 8.24 Hz, 2H, meta aromatic), 5.52 (q, *J* = 5.50 Hz, 1H, -O-CH), 4.45-4.63 (m, 2H, -O-CH₂) and 3.81-3.89 (m, 2H, -N-CH₂); ¹³C NMR (CDCl₃, 100 MHz) δ 165.94, 165.77, 155.30, 154.26, 147.47, 145.65,

CDE-115

2-((Tert-butoxycarbonyl)amino)propane-1,3-diyl bis(3,4,5-trihydroxybenzoate)
(495.43 g/mol) $C_{22}H_{25}NO_{12}$



Step #1: Was conducted without modification of the “General procedure for synthesis of 3,4,5-tribenzyloxybenzoate” (Chapter 1, Experimental).

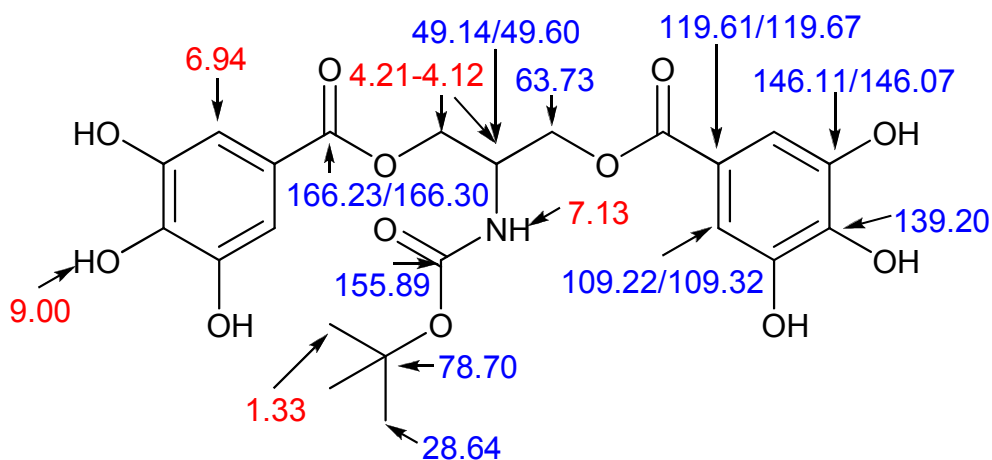
Step #2: Tert-butyl (1,3-dihydroxypropan-2-yl)carbamate (0.36 g, 1.88 mmol) and 3,4,5-tribenzyloxybenzoate (2.16 g, 4.70 mmol) were dissolved in a flame-dried flask and stirred under N_2 . Next the triethylamine (1.00 mL, 5.63 mmol) and dry CH_2Cl_2 (10.0 mL) were syringed into the flask. The reaction was stirred for 96 hours. A TLC (65% hexanes/EtOAc) provided supporting evidence that product had formed. The organic layer was washed with 1 N HCl (2 x), saturated aqueous sodium bicarbonate (2 x), and brine (1 x), dried over $MgSO_4$, filtered, and concentrated *in vacuo* to obtain a solid (1.70 g, 89%). 1H NMR (benzene- d_6 , 400 MHz) δ 7.50-6.90 (m, 34H, aromatic), 5.14 (s, 4H, para benzylic), 4.75 (s, 8H, meta benzylic), 4.61 (s, 1H, -NH), 4.36 (bs, 1H, -N-CH), 4.21-4.13 (m, 4H, $-O(CH_2)_2$), and 1.34 (s, 9H, $-OC(CH_3)_3$); ^{13}C

NMR (benzene-*d*₆, 100 MHz) δ 165.65, 155.14, 152.85, 143.18, 138.03, 136.98, 124.88, 109.52, 79.29, 75.01, 70.91, 64.05, 49.24, 28.13.

Step #3: 2-(Tert-butoxycarbonylamine)propane-1,3-diyl bis (3,4,5-tris(benzyloxy)benzoate)

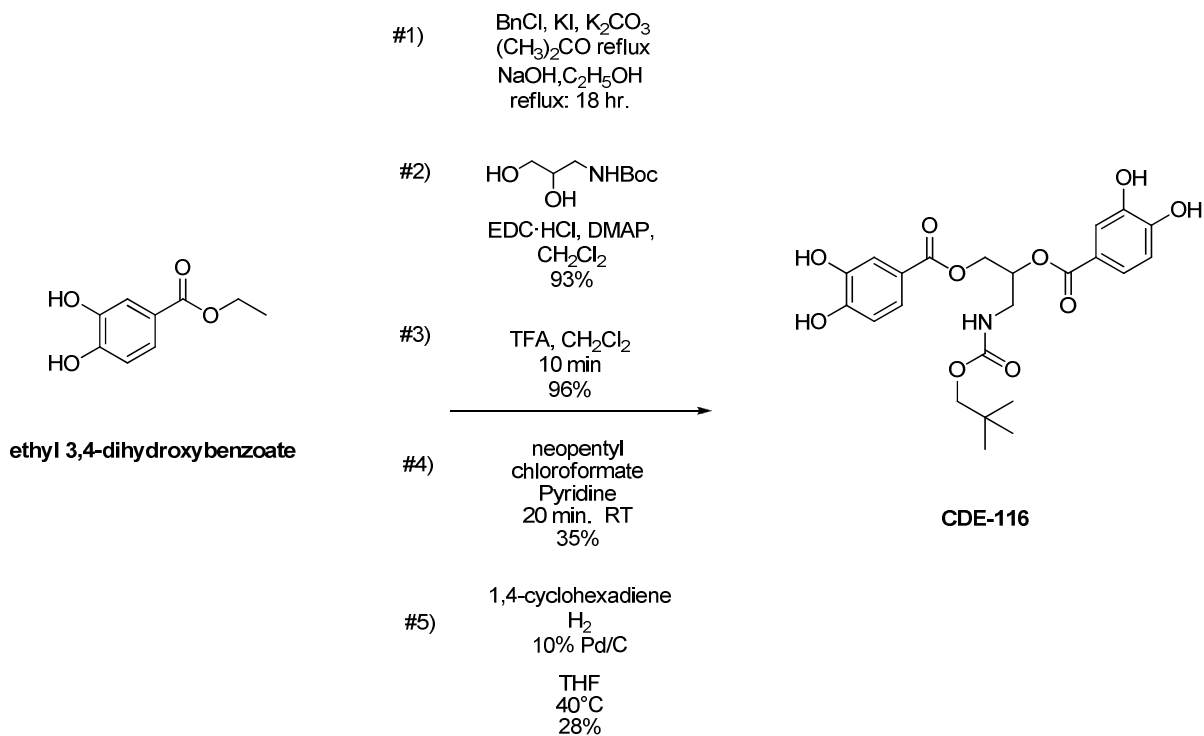
(0.30 g, 0.30 mmol) was dissolved in low water THF (2.70 mL). Then Pd/C 10% (0.2 g, 0.14 mmol) and 1,4-cyclohexadiene (0.26 mL, 2.90 mmol) were added and stirred overnight at 40°C under N₂. A TLC (95% CH₂Cl₂/MeOH) confirmed the consumption of the starting material.

The reaction was syringed through a PTFE 0.2 μM syringe prepared with MeOH to remove the Pd/C catalyst. The solvent was then removed *in vacuo* and triturated with hexanes to obtain a solid (121 mg, 85%). ¹H NMR (DMSO-*d*₆, 400 MHz) δ 9.00 (bs, 6H, -OH), 7.13 (d, 1H, -NH), 6.94 (s, 4H, aromatic), 4.21-4.12 (m, 5H, -OCH₂-CH-CH₂), and 1.33 (s, 9H, ((CH₃)₃)); ¹³C NMR (DMSO-*d*₆, 100 MHz) δ 166.30, 166.23, 155.89, 146.11, 146.07, 139.20, 119.67, 119.61, 109.32, 109.22, 78.70, 63.73, 49.60, 49.14, 28.64; HRMS, ESI calcd. for C₂₂H₂₅NO₁₂Na [M+Na]⁺ 518.1274, found: 518.1284.



CDE-116

3-(Neopentyloxycarbonylamino)propane-1,2-diyl bis(3,4-dihydroxybenzoate)
(477.46 g/mol) $C_{23}H_{27}NO_{10}$



Step #1: Was conducted without modification of the “General procedure for synthesis of 3,4-dibenzyloxybenzoate” (Chapter 1, Experimental).

Step #2: Followed the same procedure as Step #2 for CDE-075 synthesis, except 3,4-dibenzyloxybenzoate was used in place of 3,4,5-tribenzyloxybenzoate

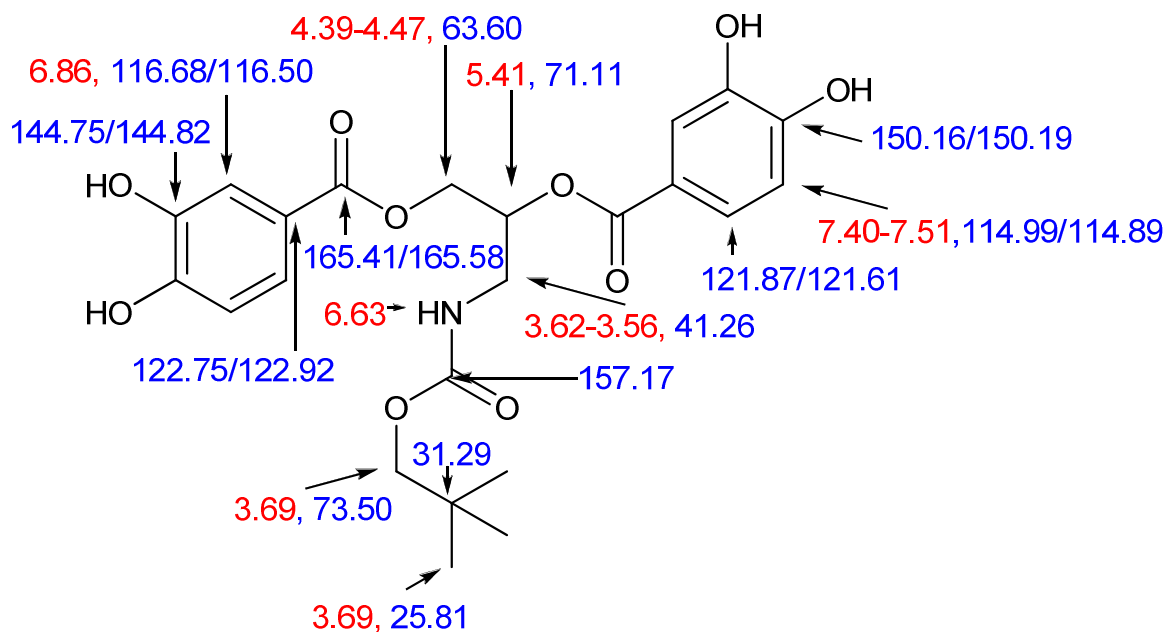
Step #3: Followed the same procedure as Step #2 for CDE-077 synthesis.

Step #4: 2,3-Bis(3,4-bis(benzyloxy)benzoyloxy)propan-1-aminium 2,2,2-trifluoroacetate (1.00 g, 1.19 mmol) was dissolved in pyridine (2.88 mL). Neopentyl chloroformate (0.21 mL, 1.43 mmol) was added. The reaction was stirred for 20 minutes, at room temperature, under N₂. A TLC (50% hexanes/EtOAc) provided supporting evidence that the majority of the starting material had been consumed. The residue was purified by column chromatography (75% hexanes/EtOAc) to obtain a white solid (348 mg, 35%). ¹H NMR (CDCl₃, 400 MHz) δ 7.63-7.59 (m, 4H, ortho aromatic), 7.44-7.26 (m, 20H, aromatic), 6.90 (dd, *J* = 1.83, 9.16 Hz, 2H, meta aromatic), 5.41 (q, *J* = 4.58 Hz, 1H, -O-CH), 5.18 (s, 4H, meta benzylic), 5.13 (s, 2H, para benzylic), 5.11 (s, 2H, para benzylic), 4.57-4.47 (m, 2H, -O-CH₂), 3.76 (s, 2H, -CH₂-((CH₃)₃)), 3.62-3.53 (m, 2H, -N-CH₂), 0.89 (s, 9H, -((CH₃)₃)); ¹³C NMR (CDCl₃, 100 MHz) δ 165.91, 165.70, 157.05, 153.33, 153.23, 148.45, 136.86, 136.57, 136.54, 128.70, 128.62, 128.10, 128.04, 127.54, 127.18, 124.38, 124.27, 122.48, 115.76, 115.52, 113.30, 74.60, 71.41, 71.18, 70.88, 63.30, 41.67, 31.58, 26.48.

Step #5: 3-(Neopentylloxycarbonylamino)propane-1,2-diyl bis(3,4-bis(benzyloxy)benzoate) (0.30 g, 0.358 mmol) was dissolved in low water THF (3.31 mL). Pd/C 10% (0.02 g, 0.18 mmol) and 1,4-cyclohexadiene (0.335 mL, 3.58 mmol) were added. The reaction was stirred for 48 hours, under N₂, at 40°C.

A TLC (95% CH₂Cl₂/MeOH) indicated the starting material had been consumed. The reaction was syringed through a PTFE 0.2 μM syringe prepared with MeOH to remove the Pd/C catalyst. The solvent was removed *in vacuo* to obtain a solid (48.6 mg, 28%). ¹H NMR (acetone-*d*₆, 400 MHz) δ 7.40-7.51 (m, 4H, ortho and meta aromatic), 6.86 (dd, *J* = 1.37, 8.24, Hz, 2H, ortho aromatic), 6.63 (bs, 1H, NH), 5.41 (quin, *J* = 4.12 Hz, 1H, -O-CH-), 4.55 (dd, *J* = 4.12, 11.91 Hz, 1H, -OCH₂), 4.39-4.47 (m, 1H, -O-CH₂), 3.69 (s, 1H, CH₂(CH₃)₃) 3.62-3.56 (m, 2H, -

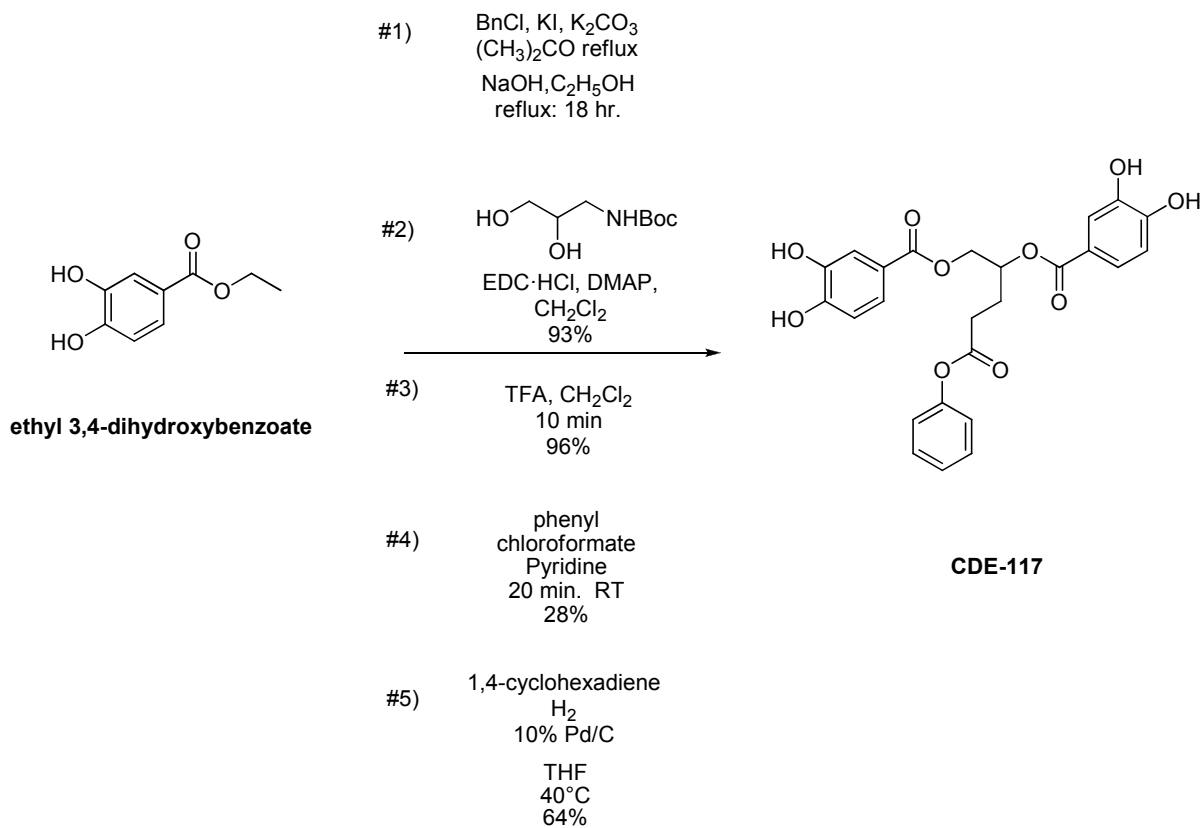
NCH₂) and 0.85 (s, 9H, (CH₃)₃); ¹³C NMR (acetone-*d*₆, 100 MHz) δ 165.58, 165.41, 157.17, 150.19, 150.16, 144.82, 144.75, 122.92, 122.75, 121.87, 121.68, 116.68, 116.50, 114.99, 114.89, 73.50, 71.11, 63.60, 41.26, 31.29, 25.81; HRMS, ESI calcd. for C₂₃H₂₇NO₁₀Na [M+Na]⁺ 500.1533, found: 500.1519.



CDE-117

3-(Phenoxycarbonylamino)propane-1,2-diyl bis(3,4-dihydroxybenzoate)

(483.42 g/mol) $C_{24}H_{21}NO_{10}$



Step #1: Was conducted without modification of the “General procedure for synthesis of 3,4-dibenzyloxybenzoate” (Chapter 1, Experimental).

Step #2: Followed the same procedure as Step #2 for CDE-075 synthesis, except 3,4-dibenzyloxybenzoate was used in place of 3,4,5-tribenzyloxybenzoate

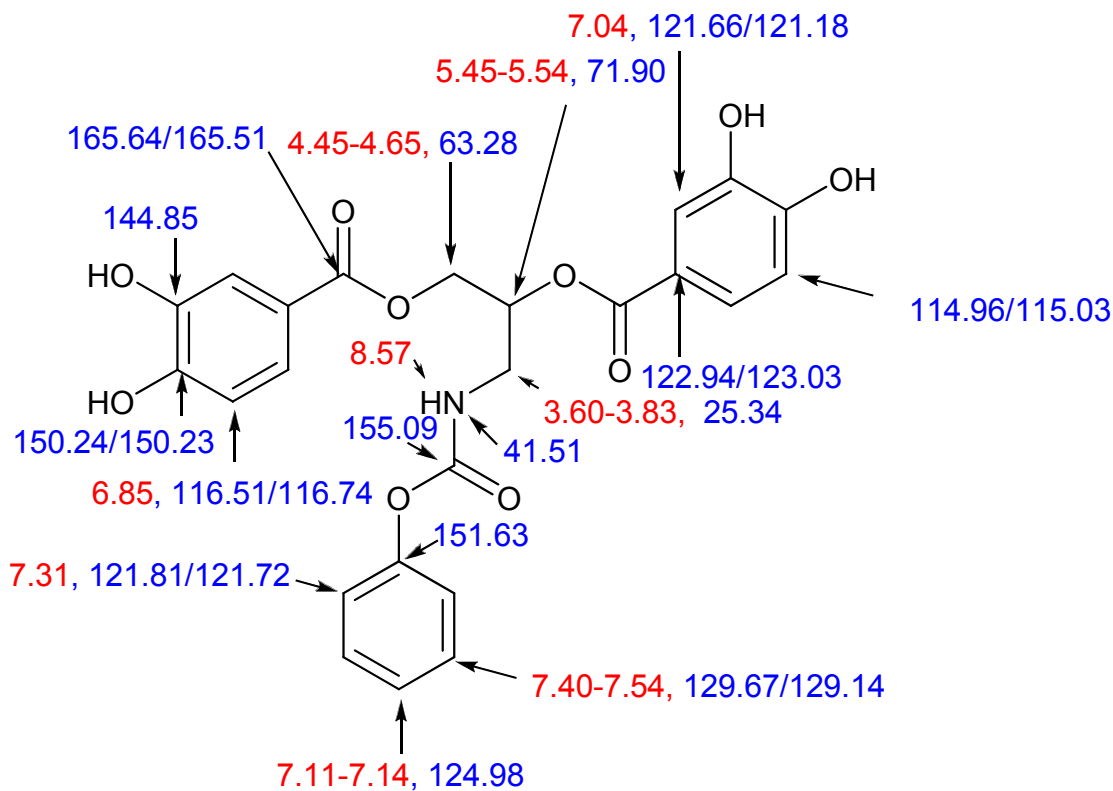
Step #3: Followed the same procedure as Step #2 for CDE-077 synthesis.

Step #4: 2,3-Bis(3,4-bis(benzyloxy)benzoyloxy)propan-1-aminium 2,2,2-trifluoroacetate (1.00 g, 1.19 mmol) was dissolved in pyridine (2.95 mL). Phenyl chloroformate (0.18 mL, 1.43 mmol) was added. The reaction was stirred for 20 minutes, at room temperature, under N₂. A TLC (65% hexanes/EtOAc) provided supporting evidence that the majority of the starting material had been consumed. The residue was purified by column chromatography (65% hexanes/EtOAc); to obtain a white solid (275 mg, 28%). ¹H NMR (CDCl₃, 400 MHz) δ 7.65-7.61 (m, 4H, ortho aromatic), 7.42-7.22 (m, 22H, aromatic + ortho-phenyl), 7.16 (t, *J* = 7.33 Hz, 1H, para phenyl), 7.07-7.05 (d, *J* = 8.24 Hz, 2H, meta aromatic), 6.92-6.88 (q, *J* = 4.58 Hz, 2H, meta phenyl), 5.46-5.44 (m, 2H, -NH + O-CH), 5.19 (s, 2H, meta benzylic), 5.18 (s, 2H, meta benzylic), 5.11 (s, 4H, para benzylic), 4.61-4.49 (m, 2H, -O-CH₂), 3.70-3.62 (m, 2H, -N-CH₂); ¹³C NMR (CDCl₃, 100 MHz) δ 166.00, 165.85, 155.02, 153.50, 153.30, 151.12, 151.05, 148.51, 148.48, 136.87, 136.56, 129.72, 129.65, 129.41, 128.92, 128.63, 128.16, 128.09, 127.61, 127.57, 127.24, 125.54, 124.48, 124.35, 122.42, 122.37, 121.86, 121.68, 121.05, 115.72, 115.51, 113.32, 71.26, 70.88, 63.25, 41.91, 29.84.

Step #5: 3-(Phenoxycarbonylamino)propane-1,2-diyl bis(3,4-bis(benzyloxy)benzoate) (0.20 g, 0.237 mmol) was dissolved in low-water THF (2.20 mL). Pd/C 10% (0.01 g, 0.119 mmol) and 1,4-cyclohexadiene (0.22 mL, 2.37 mmol) were added. The reaction was stirred for 48 hours, under N₂, at 40°C.

A TLC (95% CH₂Cl₂/MeOH) indicated the starting material had been consumed. The reaction was syringed through a PTFE 0.2 μM syringe prepared with MeOH to remove the Pd/C catalyst. The solvent was removed *in vacuo* to obtain a solid (74.1 mg, 64%). ¹H NMR (acetone-*d*₆, 400 MHz) δ 8.57 (bs, 1H, -NH), 7.40-7.54 (m, 4H, meta-phenyl + ortho H⁺ on proto), 7.31 (t,

$J = 7.79$ Hz, 2H, ortho phenyl), 7.11-7.14 (m, 1H, para phenyl), 7.04 (d, $J = 8.24$ Hz, 2H, other set of H^+ ortho on proto), 6.85 (dd, $J = 2.75, 8.24$ Hz, 2H, meta H^+ on proto), 5.45-5.54 (m, 1H, -O-CH-), 4.45-4.65 (m, 2H, -O-CH₂-) and 3.60-3.83 (m, 2H, -N-CH₂-); ¹³C NMR (acetone-*d*₆, 100 MHz) δ 165.64, 165.51, 155.09, 151.63, 150.24, 150.23, 144.85, 129.67, 129.14, 124.98, 123.03, 122.94, 122.81, 121.82, 121.72, 121.66, 121.18, 116.74, 116.51, 115.03, 114.96, 71.91, 63.28, 41.51, 25.34. HRMS, ESI calcd. for C₂₄H₂₁NO₁₀Na [M+Na]⁺ 506.1063, found:506.1056.



CONCLUSIONS AND FUTURE DIRECTIONS

The main goal of the preceding research efforts has been to synthesize small-molecule inhibitors of PAI-1 that, when compared to previous examples, have improved potency and a decreased potency for PAI-1's cofactor, A'TIII. The inhibition of PAI-1 is anticipated to increase our understanding of various human ailments for which high levels of PAI-1 have been associated, including diabetes, stroke, and atherosclerosis. Research efforts focused on examining a change in inhibitor potency based on the linker's properties, the number of gallates substituted, the gallate's substitution pattern, and linker appendages. A crystal structure was obtained of PAI-1 bound to a synthetic inhibitor (CDE-096), which allowed us to more fully develop our synthetic ideology. The refinement of one of these synthesized moieties into a selective and highly active species has been achieved.

Our primary lead compound (tannic acid) was identified by high-throughput screening conducted by our collaborators at the University of Michigan Medical School utilizing the MicroSource SPECTRUM compound library.⁴⁴ With the aim of synthesizing inhibitors that adhere to Lipinski's Rule of Five guidelines, we synthesized an inhibitor that was reduced from the lead compound's size of approximately 1700 g/mol to a molecule of 366 g/mol containing two gallate attachments (CDE-008) without a severe reduction in the potency of the inhibitory.

Chapter 1 focused on the effects that the properties of the linkers had on PAI-1 inhibition and how PAI-1 inhibition is affected by the differing possible geometric isomers of the inhibitors. From this work, it is observed that inhibitors containing ester linker groups were more effective at inhibiting PAI-1 than those containing amides. This work also indicated that in most cases the cyclic linkers that allowed for a *trans*-positioning of the gallates led to greater inhibition than those with a *cis*-positioning and that a molecule containing a cyclic linker that

allowed for an increased number of conformations and consequently motion of the gallates such as the cyclohexanediol linker (in contrast to the benzenediol linker) was a stronger inhibitor of PAI-1.

Chapter 2 examined the effects of altering the number of gallates and/or the central sugar on PAI-1 inhibition. One conclusion regarding effective PAI-1 inhibition is that the identity of the central sugar is a relatively unimportant factor in terms of potency of the inhibitor. Also it was noted that the hydroxy functional groups on the gallate, or other electronically similar groups, are necessary for PAI-1 inhibition and that the most potent inhibitor had three gallates (with ATIII inhibition) and the second most potent inhibitor had two gallates (with non-detectable levels of ATIII inhibition).

Chapter 3 focused on the determination of the optimum number and arrangement of substituents on the aromatic ring. This research again utilized Lipinski's guidelines and attempted to bring our inhibitors into agreement with the guideline that the optimal number of hydrogen-bond donor capable species should be no more than five. The results of this research showed that the number of hydroxy groups could be reduced to two per aromatic ring and that the most potent inhibition was found for the 3,4-dihydroxy isomer. It was also concluded that more than one hydroxy group is necessary for any significant level of PAI-1 inhibition and that intramolecular hydrogen bonding may play a significant role in the reduction of the potency of inhibitors that possess an ortho hydroxy group.

Chapter 4 highlights our success in obtaining a crystal structure of an active PAI-1 serpin bound to an inhibitor (CDE-096). The information gathered from the crystal structure does support the earlier hypothesis that small-molecule inhibitors of PAI-1 bind in pocket sites on the serpin.⁸⁶ This observation possibly explains the improved potency of the inhibitors that had a handle unit capable of interacting with a pocket on the serpin. Points of contact include the

carbonyl oxygen interacting with an electropositive region on the serpin, the hydroxy oxygens on one of the gallates contacting with an electropositive region on the serpin, and hydrophobic interactions between the handle unit and an adjacent pocket.

The electropositive region on the serpin's binding site indicates that handles composed of electroneutral and electronegative atoms could produce stronger binding to PAI-1 in this region. This observation supports our findings of enhanced inhibitor potency of inhibitors whose handles were composed of aromatic rings or methylene handles of various lengths and arrangements (CDE-075, CDE-082, CDE-096, CDE-107, CDE-108, CDE-110, CDE-116, CDE-117).

The electropositive region within the pocket could also cause electrostatic repulsion between the positive ammonium moiety in CDE-077 and the serpin and is a possible reason for this molecule's lowered inhibitor potency. Similarly, the shortened length of the dimethyl and ethyl handle in species (CDE-083, CDE-089) results in a decrease in inhibitor potency because the handle region may not be long enough to interact sufficiently with the pocket on the serpin.

Chapter 4 also details the carbamate and sulfonimide/sulfonamide inhibitor series synthesized with the aim of determining the optimum handle length and composition. The results of the sulfonimide inhibitor series allowed for us to hypothesize that a handle unit composed of 6.5 methylene units or sequentially one that is approximately 780-1000 pm in chain length would allow for the optimum interaction of the handle unit with the serpin's pocket. The consistently improved inhibitor potencies of our carbamate derivatives indicated that a handle unit was an essential piece of our scaffold.

Future possibilities for synthesizing more selective and highly active inhibitors of PAI-1 can be hypothesized through the use of three methods: software programs such as VAST, the

introduction of new linker groups, and the examination of the results of the crystal structure and new inhibitors that focus on abandoning the symmetry of the inhibitors.

The use of software programs such as VAST was outlined in the introductory chapter of this work. VAST was utilized to determine the 3-D architectural similarity between PAI-1 and the protein PEDF. The high degree of similarity between these two proteins (PEDF has 349 residues aligned with PAI-1's 402) along with the observation that PEDF is inhibited by highly negatively charged species (heparin) that also functions to promote ATIII, led to the hypothesis that integrating more negatively charged species into our inhibitors could work to inhibit both PAI-1 and PEDF while simultaneously not affecting or promoting ATIII. The benefit from this would result in the removal of the inhibitory effect that PEDF plays in new blood vessel formation while simultaneously inhibiting the inhibitor of fibrinolysis (PAI-1), thus allowing for a two-pronged approach when attempting to reduce/counter the cause of heart attack and stroke. This also may lead to the reduction in competitive inhibition between PAI-1 and ATIII that has thus far been a consideration when designing PAI-1 inhibitors.

Our current lack of success in designing more effective PAI-1 inhibitors than those containing ester-linkages, and the ester-linked inhibitors being unsuitable for bioactive pharmaceuticals (Chapter 1), should encourage us to look to the incorporation of a different functional group in place of the amide, sulfonamide/sulfonimide, or ester linking units. One possibility that can be examined to understand why the sulfonamide/sulfonimide and amide linker groups yielded poorer PAI-1 inhibitory species than the ester-linkers, involves a brief review of the effects that these groups have on the electronic properties of the molecule along with the ease of rotation that these bonds possess.

Stabilization of both the S-N (sulfonamide/sulfonimide) and C-N (amide) bond occurs through the nitrogen atom's willingness to donate its lone pair of electrons to the C-N (amide)

or S-N (sulfonamide/sulfonimide) bond, thus giving it an increased π -bond character. Also to a lesser degree the σ -withdrawal of electron density by the nitrogen from the adjacent polarized atom (the carbonyl carbon or the sulfur) results in a stabilization of this bond.⁹⁷ These lead to a significant barrier to S-N (sulfonamide/sulfonimide)⁹⁷ and C-N (amide) rotation. However, in the case of the ester functional group, the O-C single bond shares the electron density more evenly and therefore has less π -bond character and therefore a lower barrier to rotation.⁹² As discussed in Chapter 4, higher activation energies of rotation for the amide and sulfonamide functional groups when compared with the esters may be preventing the inhibitor from achieving its most biologically active 3-D structure.

Silicon's drug development potential is beginning to be exploited by pharmaceutical companies and researchers.^{98, 99, 100, 101} Paradigm Therapeutics from Cambridge, Science Park in Cambridge, UK, and Amedis Pharmaceuticals are two pharmaceutical companies that are focusing on developing silicon-based pharmaceuticals that they believe have been underutilized in drug development.¹⁰² Robert West, a known leader in silicon-based drug research from the University of Wisconsin-Madison, recently synthesized a series of cox-2 inhibitor molecules with silicon in place of carbon and found enhanced effectiveness and lower toxicity.¹⁰³ In 2002, Mutahi, a researcher from Temple University in Philadelphia, synthesized silanediol tripeptide mimics that effectively inhibited the metalloprotease angiotensin-converting enzyme (ACE) at a nanomolar level.¹⁰⁴

The lowered electronegativity of the silicon atom in comparison to the high electronegativity of nitrogen, oxygen, or sulfur atoms may allow for freer rotation around the C-Si bond, allowing the inhibitor to achieve its most biologically active 3-D formation more readily (Figure 29-A, C, D). The lowering of the electronegativity of the atom in place of the carbonyl carbon, may lead to increased electron density on the carbonyl oxygen species (Figure 29-B).

A different route of enhancement could shift to an attempt at increasing the distance between the linker and the carbonyl oxygen so that it is farther away from the main body of the inhibitor. This might provide it with more flexibility in movement and less steric hindrance to interact with potential contact points on the serpin. One method to achieve this could utilize attaching the carbonyl to a silicon atom in the linker (Figure 29-D).

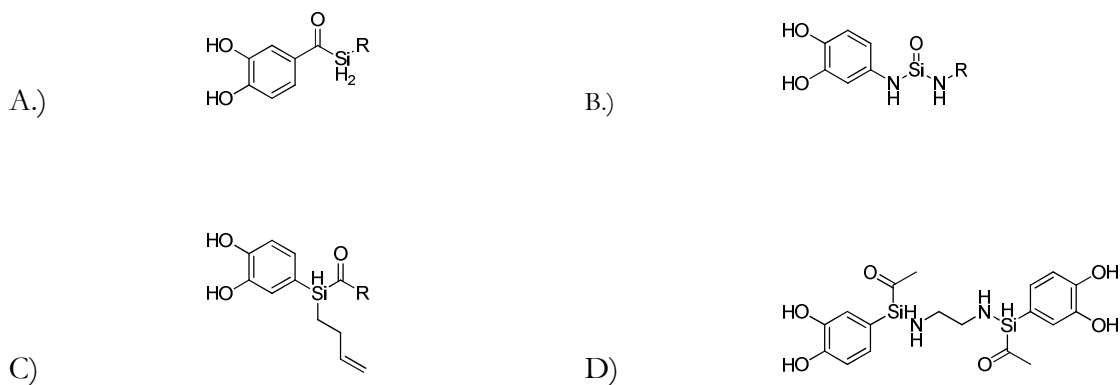


Figure 29: Possible Silicon-Based Inhibitors.

A.) Silyl Ketone species.^{105, 106} B.) Silanone species.¹⁰⁷ C.) Silyl Ketone species.¹⁰⁴
D.) Silenolate species.¹⁰⁸

For years the silanone species proved difficult to isolate due to its high reactivity as a consequence of the polarized $\text{Si}^{\delta+}=\text{O}^{\delta-}$ bond which tended to result in a dimerized cyclosiloxane ($\text{R}_2\text{Si}=\text{O}$)₂ moiety.¹⁰⁹ In 2001, theoretical work conducted by researchers at Tokyo Metropolitan University determined that the stability of the silanone species can be achieved via the attachment of bulkier groups.¹¹⁰ Since then, researchers have been able to isolate several varieties of silanones, including silanone derivatives in which the oxygen is replaced with S, Se, and Te atoms.¹¹¹ The positive implications that this might have on the potency of our inhibitors can be better understood by considering the crystal structure. The silicon substitution might improve the strength of the contact point between the carbonyl's oxygen and the electropositive

region (observed in the crystal structure) by increasing the electron density on the oxygen atom as a result of its lowered electronegativity as compared to the oxygen, nitrogen, or sulfur species. The lowering of the rotational barrier by this substitution also might allow the inhibitor to adopt a more favorable bioactive form that, from the crystal structure, is now hypothesized to be one that would allow the handle to delve into the pocket on the serpin. However, silicon's longer bonds and larger size in comparison to the first row elements will impact the shape of the molecule, and this will have an unknown impact on inhibitor potency.

Last, the crystal structure allows for a new direction in our future synthetic series by allowing for the examination of the main contact points found between the inhibitor and the serpin. These main contact points include the carbonyl oxygen interacting with an electropositive region on the serpin, the hydroxy oxygens on one of the gallates contacting an electropositive region on the serpin, and the handle unit forming hydrophobic contacts within a corresponding pocket. An electropositive region proximal to the binding site indicates that handles composed of electroneutral and electronegative atoms could produce stronger binding to PAI-1 in this region.

Because only the hydroxy oxygens on one of the gallates are associated with strong contacts, improved binding might result from substituting the other gallate's hydroxy substituents for other groups. A hydrophobic region exists directly below the gallate not involved in strong contacts with the serpin. Therefore, a possible alteration to this gallate could involve either electroneutral substituents on the gallate (in place of the hydroxys) or entire replacement by an electroneutral substituent and hence a new synthetic path for our inhibitors could be one that focuses on exploring non-symmetric inhibitors.

The main goal of this work was to synthesize potent and selective PAI-1 inhibitors. This goal was accomplished and is illustrated by the high potency against PAI-1 and non-detectable

inhibition of ATIII shown by a number of the carbamate inhibitors, including CDE-075 (tert-butyl handle, $IC_{50} = 0.062 \mu\text{M}$), CDE-096 (3-(trifluoromethyl)phenyl handle, $IC_{50} = 0.059 \mu\text{M}$), CDE-107 (octyl handle, $IC_{50} = 0.01 \mu\text{M}$), CDE-110 (2-chlorophenyl handle, $IC_{50} = 0.027 \mu\text{M}$), CDE-116 (neopentyl handle, $IC_{50} = 0.029 \mu\text{M}$), and CDE-117 (phenyl handle, $IC_{50} = 0.022 \mu\text{M}$). The selectivity of the inhibitors was further optimized by CDE-096 (3-(trifluoromethyl)phenyl handle), which inhibited PAI-1 at nanomolar IC_{50} level even in the presence of vitronectin, while showing non-detectable levels of ATIII inhibition. Obtaining a crystal structure of an active PAI-1 attached to an inhibitor allows us to more effectively plan future inhibitor scaffolds. Our research efforts have allowed us to establish several new experimentally supported hypotheses regarding the optimum scaffold for a PAI-1 inhibitor.

REFERENCES

- ¹ Cesarman-Maus, G; Hajjar, K.A. Molecular Mechanisms of Fibrinolysis. *Brit. J. Haematology*. **2005** 129 (3), 307–321.
- ² Muszbek, L.; Bagoly, Z.; Bereczky, Z.; Katona, E. The Involvement of Blood Coagulation Factor XIII in Fibrinolysis and Thrombosis. *Cardiovascular & Hematological Agents in Med. Chem.* **2008** 6 (3), 190–205.
- ³ Kaiser, B. DX-9065a, A Direct Inhibitor of Factor Xa. *Card. Drug Rev.* **2003** 21 (2), 91–104.
- ⁴ Miyazaki, H.; Ogiku, T.; Sai, H.; Moritani, Y.; Ohtani, A.; Ohmizu, H. Synthesis and Evaluation of Pyrrolin-2-one Compounds, a Series of Plasminogen Activator Inhibitor-1 Inhibitors. *Chem. Pharm. Bull.* **2009** 57 (9), 979-985.
- ⁵ Irving, J.A.; Pike, R.N.; Lesk, A.M.; Whisstock, J.C. Phylogeny of the Serpin Superfamily: Implications of Patterns of Amino Acid Conservation for Structure and Function. **2000** *Genome Res.* 12, 18450-64.
- ⁶ Marquerlot, F.; Galiacy, S.; Malo, M.; Guignabert, C.; Lawrence, D.A.; d'Ortho, M.P.; Barlovatz-Meimon, G. Dual Role for Plasminogen Activator Inhibitor Type 1 as Soluble and as Matricellular Regulator of Epithelial Alveolar Cell Wound Healing. **2006** *Am. J. Pathol.* 169, 1624.
- ⁷ Schafer, K.; Fujisawa, K.; Konstantinides, S.; Loskutoff, D.J. Disruption of the Plasminogen Activator Inhibitor-1 Gene Reduces the Adiposity and Improves the Metabolic Profile of Genetically Obese and Diabetic ob/ob Mice. **2001** *FASEB J.* 15, 1840.
- ⁸ Pinsky, D.J.; Liao, H.; Lawson, C.A.; Yan, S.F. Coordinated Induction of Plasminogen Activator Inhibitor-1 (PAI-1) and Inhibition of Plasminogen Activator Gene Expression by Hypoxia Promotes Pulmonary Vascular Fibrin Deposition. **1998** *J. Clin. Invest.* 102, 919
- ⁹ Leik, C.E.; Su, E.J.; Nambi, P.; Crandell, D.L.; Lawrence, D.A. Effect of Pharmacologic Plasminogen Activator Inhibitor-1 Inhibition on Cell Motility and Tumor Angiogenesis. **2006** *J. Thromb. Haemost.* 4, 2710-2715.
- ¹⁰ Gent, D.; Sharp, P.; Morgan, K.; Kalsheker, N. Serpins: Structure, Function, and Molecular Evolution. **2003** *J. Biochem. Cell Biol.* 35, 1536-1547.
- ¹¹ Stout, T. J.; Graham, H.; Buckley, D. I.; Matthews, D. J. Structures of Active and Latent PAI-1: A Possible Stabilizing Role for Chloride Ions. **2000** *Biochem.* 39(29), 8460-9.
- ¹² <http://blast.ncbi.nlm.nih.gov/Blast.cgi>
- ¹³ Bersano, A.; Ballabio, E.; Bresolin, N.; Candelise, L. Genetic Polymorphisms for the Study of Multifactorial Stroke. **2008** *Human Mutation* 29 (6), 776-795.
- ¹⁴ Pruitt KD, Harrow J, Harte RA, Wallin C, Diekhans M, Maglott DR, Searle S, Farrell CM, Loveland JE, Ruff BJ, Hart E, Suner MM, Landrum MJ, Aken B, Ayling S, Baertsch R, Fernandez-Banet J, Cherry JL, Curwen V, Dicuccio M, Kellis M, Lee J, Lin MF, Schuster M, Shkeda A, Amid C, Brown G, Dukhanina O, Frankish A, Hart J, Maidak BL, Mudge J, Murphy MR, Murphy T, Rajan J, Rajput B, Riddick LD, Snow C, Steward C, Webb D, Weber JA, Wilming L, Wu W, Birney E, Haussler D, Hubbard T, Ostell J, Durbin R, Lipman D. The consensus coding sequence (CCDS) project: Identifying a common protein-coding gene set for the human and mouse genomes. **2009** *Genome Res.* 19(7), 1316-23.
- ¹⁵ Fay, W.P.; Shapiro, A.D.; Shih, J.L.; Schleef, R.R.; Ginsberg, D.N. Complete Deficiency of Plasminogen-Activator Inhibitor-1 Due to a Frameshift Mutation. **1992** *Engl. J. Med.* 327 (24), 1729-1733.
- ¹⁶ Bonora, E. The Metabolic Syndrome and Cardiovascular Disease. **2006** *Annals of Med.* 38 (1), 64-80.
- ¹⁷ Gettins, P.G. Keeping the Serpin Machine Running Smoothly. **2000** *Genome Res.* 10, 1833-1835.
- ¹⁸ Ekeowa, U.I.; Gooptu, B.; Belorgey, D.; Haeggloef, P.; Karlsson-Li, S.; Miranda, E.; Perez, J.; MacLeod, I.; Kroger, H.; Marciniak, S.J.; et al. α 1-Antitrypsin Deficiency, Chronic Obstructive Pulmonary Disease and the Serpinopathies. **2009** *Clin. Sci.* 116 (11/12), 837-850.
- ¹⁹ Eitzman, D.T.; Fay, W.P.; Lawrence, D.A.; Francis-Chmura, A.; Shore, J.D.; Olson, S.T.; Ginsberg, D. Peptide-Mediated Inactivation of Recombinant and Platelet Plasminogen Activator Inhibitor-1 in vitro. **1995** *J. Clin. Investigations.* 95 (5), 2416-20.
- ²⁰ Izaguirre, G.; Zhang, W.; Swanson, R.; Bedsted, T.; Olson, S.T. Localization of an Antithrombin Exosite that Promotes Rapid Inhibition of Factors Xa and IXa Dependent on Heparin Activation of the Serpin. **2003** *J. Bio. Chem.* 278 (51), 51433-5'440.
- ²¹ Wang, Z.; Mottonen, J.; Goldsmith, E.J. Kinetically Controlled Folding of the Serpin Plasminogen Activator Inhibitor 1. **1996** *Biochemistry*, 35(51), 16443-16448.
- ²² Stout, T.J.; Graham, H.; Buckley, D.I.; Matthews, D.J. Structures of Active and Latent PAI-1: A Possible Stabilizing Role for Chloride Ions. **2000** *Biochemistry*, 39(29), 8460-8469.

- ²³ Elliott, P.R.; Abrahams, J.P.; Lomas, D.A. Wild-Type α 1-antitrypsin is in the Canonical Inhibitory Conformation. **1998** *J. Mol. Biol.* 275 (3), 419-425.
- ²⁴ Law, R.H.P.; Zhang, Q.; McGowan, S.; Buckle, A.M.; Silverman, G.A.; Wong, W.; Rosado, C.J.; Langendorf, C.G.; Pike, R.N.; Bird, P.I.; Whisstock, J.C. An Overview of the Serpin Superfamily. **2006** *Genome Biol.*, 7(5), 216.
- ²⁵ Gardell, S.J.; Krueger, J.A.; Antrilli, T.A.; Elokda, H.; Mayer, S.; Orcutt, S.J.; Crandall, D.L.; Vlasuk, G.P. Neutralization of Plasminogen Activator Inhibitor-1 (PAI-1) by the Synthetic Antagonist PAI-749 via a Dual Mechanism of Action. **2007** *Molecular Pharmacology*. 72(4), 897-906.
- ²⁶ Molecular Modeling Database MMDB ID: [67259](http://www.ncbi.nlm.nih.gov/Structure/mmdb/mmdbsrv.cgi?uid=3cvm)
<http://www.ncbi.nlm.nih.gov/Structure/mmdb/mmdbsrv.cgi?uid=3cvm>
- ²⁷ Promotif. <http://www.ebi.ac.uk/thornton-srv/databases/cgi>
- ²⁸ Jaulmes, A.; Sansilvestri-Morel, P.; Rolland-Valognes, G.; Bernhardt, F.; Gaertner, R.; Lockhart, B.P.; Cordi, A.; Wierzbicki, M.; Rupin, A.; Verbeuren, T.J. Nox4 Mediates the Expression of Plasminogen Activator Inhibitor-1 via p38 MAPK Pathway in Cultured Human Endothelial Cells. **2009** *Thrombosis Research* 124(4), 439-446.
- ²⁹ Cho, H.; Kang, J.; Kim, T.; Park, K.; Kim, C.; Lee, I.; Min, K.; Magae, J.; Nakajima, H.; Bae, Y.; et al. Suppression of PAI-1 Expression through Inhibition of the EGFR-Mediated Signaling Cascade in Rat Kidney Fibroblast by Ascofuranone. **2009** *J. Cell. Biol.* 107 (2), 335-344.
- ³⁰ Chun, T.; Pratt, H.J. Aldosterone Increases Plasminogen Activator Inhibitor-1 Synthesis in Rat Cardiomyocytes. **2005** *Molecular and Cellular Endo.* 239 (1-2), 55-61.
- ³¹ Lee, K.; Nishimura, S.; Matsunaga, S.; Fusetani, N.; Ichijo, H.; Horinouchi, S.; Yoshida, M. Induction of a ribotoxic stress response that stimulates stress-activated protein kinases by 13-deoxytedanolide, an antitumor marine macrolide. **2006** *Bioscience, Biotech., and Biochem.* 70 (1), 161-171.
- ³² Gardell, S.J.; Krueger, J.A.; Antrilli, T.A.; Elokda, H.; Mayer, S.; Orcutt, S.J.; Crandall, D.L.; Vlasuk, G.P. Neutralization of Plasminogen Activator Inhibitor-1 (PAI-1) by the Synthetic Antagonist PAI-749 via a Dual Mechanism of Action. **2007** *Molecular Pharmacology*. 72 (4), 897-906.
- ³³ Develter, J.; Booth, N.A.; Declerck, P.J.; Gils, A. Bispecific Targeting of Thrombin Activatable Fibrinolysis Inhibitor and Plasminogen Activator Inhibitor-1 by a Heterodimer Diabody. **2008** *J. Thrombosis and Haemostasis*. 6 (11), 1884-1891.
- ³⁴ Gardell, S.J.; Krueger, J.A.; Antrilli, T.A.; Elokda, H.; Mayer, S.; Orcutt, S.J.; Crandall, D.L.; Vlasuk, G.P. Neutralization of Plasminogen Activator Inhibitor-1 (PAI-1) by the Synthetic Antagonist PAI-749 via a Dual Mechanism of Action. **2007** *Molecular Pharmacology*. 72 (4), 897-906.
- ³⁵ Develter, J.; Booth, N.A.; Declerck, P.J.; Gils, A. Bispecific Targeting of Thrombin Activatable Fibrinolysis Inhibitor and Plasminogen Activator Inhibitor-1 by a Heterodimer Diabody. **2008** *J. Thrombosis and Haemostasis*. 6(11), 1884-1891.
- ³⁶ Miyazaki, H.; Ogiku, T.; Sai, H.; Ohmizu, H.; Murakami, J.; Ohtani, A. Design, Synthesis, and Evaluation of Orally Active Inhibitors of plasminogen activator inhibitor-1 (PAI-1) Production. **2008** *Bioorg. Med. Chem. Lett.* 18(24), 6419-6422.
- ³⁷ Cheng, Y.; Prusoff, W.H. Relationship Between the Inhibition Constant (K₁) and the Concentration of Inhibitor Which Causes 50% Inhibition of an Enzymatic Reaction. *Biochem Pharmacol* **1973** 22(23), 3099-3108.
- ³⁸ Miyazaki, H.; Sai, H.; Ohmizu, H.; Murakami, J.; Ohtani, A.; Ogiku, T. Synthesis and Evaluation of 1,4-diphenylbutadiene Derivatives as Inhibitors of Plasminogen Activator Inhibitor-1 (PAI-1) Production. **2010** *Bioorg. Med. Chem.* 18, 1968-1979.
- ³⁹ Bin, Y.; You-Ling, C.; Rushad, K.; Wheeseong, L.; Shou-Fu, L.; Shaw, K.J.; Jones, S.; Lentz, D.; Liang, A.; Tseng, J.; Qingyu, W.; Zhao, Z. Synthesis and Biological Evaluation of Piperazine-Based Derivatives as Inhibitors of Plasminogen Activator Inhibitor-1 (PAI-1). **2004** *Bioorganic & Med. Chem. Lett.* 14(3), 761-765.
- ⁴⁰ Hu, B.; Jetter, J.W.; Wrobel, J.E.; Antrilli, T.M.; Bauer, J.S. Synthesis and SAR of 2-Carboxylic Acid Indoles as Inhibitors of Plasminogen Activator Inhibitor-1. **2005** *Bioorg. Med. Chem. Lett.* 15, 3514-3518.
- ⁴¹ Mukul, R.J.; Shankar, S.; Ganes, C.; Vrajesh, P.; Ajay, S.; Bhavesh, P.; Soma, S.; Mehul, R.; Hitesh, S.; Pankaj, R.P. In Vitro PAI-1 Inhibitory Activity of Oxalamide Derivatives. **2008** *Eur. J. Med. Chem.* 43(4), 880-884.
- ⁴² Wang, Z.; Elokda, H.; McFarlane, G.; Pan, S.; Antane, M. Regioselective Suzuki Coupling of Benzofuran or Benzothiophene Boronic Acids and Dibromo Substituted Naphthalenes: Synthesis of a Potent Inhibitor of Plasminogen Activator Inhibitor-1. **2006** *Tetrahedron Letters*, 47(20), 3365-3369.

- ⁴³ El-Ayache, N.C.; Li, S.; Warnock, M.; Lawrence, D.A.; Emal, C.D. Novel bis-arylsulfonamides and aryl sulfonimides as Inactivators of Plasminogen Activator Inhibitor-1 (PAI-1). **2010**. *Bioorganic & Med. Chem. Lett.* 20(3), 966-970.
- ⁴⁴ Cale, J.M.; Li, S.; Warnock, M.; Su, E.J.; North, P.R.; Sanders, K.L.; Puscau, M.M.; Emal, C.D.; Lawrence, D.A. Characterization of a Novel Class of Polyphenolic Inhibitors of Plasminogen Activator Inhibitor-1. **2010**. *J. Bio. Chem.* 285(11), 7892-7902.
- ⁴⁵ Elokda, H.; Abou-Gharbia, M.; Hennan, J.K.; McFarlane, G.; Mugford, C.P.; Krishnamurthy, G.; Crandall, D.L. **2004** *J. Med. Chem.* 47, 3491-3494.
- ⁴⁶ VAST Database. VAST ID: [1DVM](http://www.ncbi.nlm.nih.gov/Structure/VAST/vast.shtml). <http://www.ncbi.nlm.nih.gov/Structure/VAST/vast.shtml>
- ⁴⁷ Ek, E.T.H.; Dass, C.R.; Choong, P.F.M. PEDF: A Potential Molecular Therapeutic Target with Multiple Anti-Cancer Activities. **2006** *Trends in Mol. Med.* 12(10), 497-502.
- ⁴⁸ Simonovic, M.; Gettins, P.G.; Volz, K. Crystal Structure of human PEDF, a Potent Anti-Angiogenic and Neurite Growth-Promoting Factor. **2001** *Proc. Natl. Acad. Sci.* 98, 11131-11135.
- ⁴⁹ Meyer, C.; Notari, L.; Becerra, P.S. Mapping the Type I Collagen-Binding Site on Pigment Epithelium-Derived Factor Implications for its Antiangiogenic Activity. **2002** *J. Bio. Chem.* 277(47), 45400-45407.
- ⁵⁰ Ren, Y.; Himmeldirk, K.; Chen, X. Synthesis and Structure – Activity Relationship Study of Antidiabetic Penta-O-galloyl-D-glucopyranose and Its Analogues. *J. Med. Chem.* **2006**, 49, 2829-2837.
- ⁵¹ Neises, B.; Steglich, W. Simple Method for the Esterification of Carboxylic Acids. *Angew. Chem. Int. Ed. Engl.* **1978** 17 (7), 522-524.
- ⁵² Silverman, R. B. The Organic Chemistry of Drug Design and Drug Action, 2nd Ed. Elsevier Academic Press: MA, **2004**; 152.
- ⁵³ Krogsgaard-Larsen, P.; Liljefors, T.; Madsen, U. *Textbook of Drug Design and Drug Action*, 3rd Ed. Taylor and Francis Inc: NY, **2002**; 428.
- ⁵⁴ Nassar, A. F.; Kamel, A. M.; Clarimont, C. Improving the Decision-Making Process in the Structural Modification of Drug Candidates: Enhancing Metabolic Stability. *Drug Discovery Today* **2004**, 9, 1022.
- ⁵⁵ C.A. Lipinski; F. Lombardo; B.W. Dominy and P.J. Feeney. Experimental and Computational Approaches to Estimate Solubility and Permeability in Drug Discovery and Development Settings". 1997 *Adv Drug Del Rev* 23, 3–25.
- ⁵⁶ Lipinski, Chris. "Chris Lipinski Discusses Life and Chemistry After the Rule of Five. *DDT*. **2003**. 8 (1), 12-16.
- ⁵⁷ McMurry, J. Organic Chemistry. 6e 2004 Thompson Learning. Belmont, CA.
- ⁵⁸ Mukherjee, S.; Palit, S.R. S-H...S Type Hydrogen-Bonding Interaction. **1970** *J. Phys. Chem.* 74(6), 1389.
- ⁵⁹ Bonner, O.D. Hydrogen Bonding in Guanidinium Fluoride. **1977** *J. Phys. Chem.* 81(24), 2247-2249.
- ⁶⁰ Kuhn, B.; Mohr, P.; Stahl, M. Intramolecular Hydrogen Bonding in Medicinal Chemistry. **2010** *J. Med. Chem.* 53, 2601-2611.
- ⁶¹ Khaliullin, R.Z.; Bell, A.T.; Head-Gordon, M. Electron Donation in the Water-Water Hydrogen Bond. **2009** *Chem. Eur. J.* 15, 851-855.
- ⁶² Kwon, Y. Theoretical Study on Salicylic Acid and Its Analogues: Intramolecular Hydrogen Bonding. **2000** *J. Mole. Struc.* 532, 227-237.
- ⁶³ Bjorquist, P.; Deinum, J. Identification of the Binding Site for a Low-Molecular-Weight Inhibitor of Plasminogen Activator Inhibitor-1 by Site-Directed Mutagenesis. **1998** *Biochem.* 37, 1227-1234.
- ⁶⁴ Marcella B. Pottz, Frank Hippauf, Sandra Saschenbrecker, Feng Chen, Jeannine Ross, Ingrid Kiefer, Alan Slusarenko, Joseph P. Noel, Eran Pichersky, Uta Effmert, and Birgit Piechulla* *Plant Physiology* 135:1946-1955.
- ⁶⁵ Kikkeri, R.; et al. "Toward Iron Sensors: BioInspired Tripods Based on Fluorescent Phenol-Oxazoline Coordination Sites". **2007** *InOrganic Chem*, 46 (7).
- ⁶⁶ Kawase, T.; Nishioka, Y.; Oida, T. A Novel Synthesis of N-Alkoxycarbonyl Amino Acids and Surfactant Properties of Their Sodium Salts. **2010** *J. Oleo Sci.* 59(4), 191-201.
- ⁶⁷ Pinna, G.A.; Pirisi, M. A.; Paglietti, G. Synthesis of 1-methyl-2,3-dimethyl-N-isopropylcarbamate-4,5-dihydro-7-R-8-R-1H-benzo[g]indoles and Evaluation of in vitro Anticancer Activity. **1994** *Farmaco* 49(2), 121-6.
- ⁶⁸ Shavel, J.Jr.; Bobowski, G. Antimicrobial N-(o-hydroxybenzyl) Carbamates. 1969 U.S. Patent Office Patent Number: 3452048 19690624.
- ⁶⁹ Posner, G.H.; Oh, C.H.; Gerena, L.M.; Wilbur, K. Extraordinarily Potent Antimalarial Compounds: New, Structurally Simple Easily Synthesized, Tricyclic 1,2,4-Trioxanes. **1992** *J. Med. Chem.* 35(13), 2459-67.
- ⁷⁰ Chaturvedi, D.; Ray, S. Application of Organic Carbamates in Drug Design. Part 1: Anticancer Agents-Recent Reports. **2004** *Drugs Fut.* 29(4), 343.

- ⁷¹ Boon, P.E.; Van der Voet, H.; Van Raaij, M. T. M.; Van Klaveren, J.D. Cumulative Risk Assessment of the Exposure to Organophosphorus and Carbamate Insecticides in the Dutch Diet. **2008** *Food and Chem. Tox.* 46(9), 3090-3098.
- ⁷² Holland, J. F.; Hosley, H.; Scharlau, C.; Carbone, P.P.; Frei, E.; Brindley, C. O.; Hall, T.C.; Shnyder, B.I.; Gold, G.L.; Lasagna, L.; Owens, A.H.; Miller, S.P. A Controlled Trial of Urethane Treatment in Multiple Myeloma. **1966** *Blood*, 27(3), 328-342.
- ⁷³ Weber, J.V.; Sharypov, V.I. Ethyl Carbamate in Food and Beverages: A Review. **2009** *Environ. Chem. Lett.* 7, 233-247.
- ⁷⁴ <http://www.britannica.com/EBchecked/topic/478825/Prontosil>. Prontosil: Encyclopedia Britannica Online. 2010.
- ⁷⁵ Dennis Smith. Metabolism, Pharmacokinetics, and Toxicity of Functional Groups. Royal Society of Chemistry. 2010. Chap. 5.1 Pg. 210.
- ⁷⁶ Walter, M.F.; Jacob, R.F.; Day, C.A.; Dahlborg, R.; Weng, Y.; Mason, P.R. Sulfone COX-2 Inhibitors Increase Susceptibility of Human LDL and Plasma to Oxidative Modification: Comparison to Sulfonamide COX-2 Inhibitors and NSAIDS. **2004** *Atherosclerosis* 177(2), 235-243.
- ⁷⁷ Mockenhaupt, M.; Viboud, C.; Dunant, A.; Naldi, L.; Halevy, S.; Bavinck, J.N.B.; Sidoroff, A.; Schneck, J.; Roujeau, J.; Flahault, A. Stevens-Johnson Syndrome and Toxic Epidermal Necrolysis: Assessment of Medication Risks with Emphasis on Recently Marketed Drugs: The EuroSCAR-Study. **2008** *J. Invest. Derm.* 128(1), 35-44.
- ⁷⁸ Yoshimura, T.; Hamaguchi, E.; Usami, E.; Nakashima, K.; Kawaguchi, M.; Suzuki, N.; Okamoto, Y.; Nakao, T.; Yamazaki, F. Increased in Vitro Release of Interferon-Gamma from Ampicillin Stimulated Peripheral Blood Mononuclear Cells in Stevens-Johnson Syndrome. **2004**. *Biol. Pharm. Bull.* 27(6), 929-931.
- ⁷⁹ Chia, F.L.; Leong, K.P. Severe Cutaneous Adverse Reactions to Drugs. **2007**. *Curr. Opin. Allergy. Clin. Immunol.* 7(4), 304-309.
- ⁸⁰ Izuhara, Y.; Takahashi, S.; Nangaku, M.; Takizawa, S.; Ishida, H.; Kurokawa, K.; Strihou, C.; Hirayama, N.; Miyata, T. Inhibition of Plasminogen Activator Inhibitor-1: Its Mechanism and Effectiveness On Coagulation and Fibrosis. *Arterioscler. Thromb. Vasc. Biol.* **2008**. 28, 672-677.
- ⁸¹ Loebermann, H.; Tokuoka, R.; Deisenhofer, J.; Huber, R. Human α_1 -Proteinase Inhibitor: Crystal Structure Analysis of Two Crystal Modifications, Molecular Model and Preliminary Analysis of the Implications for Function. **1984** *J. Mol. Biol.* 177, 531-556.
- ⁸² Wei, A.; Rubin, H.; Cooperman, B.S.; Christianson, D.W. Crystal Structure of an Uncleaved Serpin Reveals the Conformation of an Inhibitory Reactive Loop. **1994** *Nat. Struct. Biol.* 1, 251-258.
- ⁸³ Schreuder, H.A.; Hol. W.G.J. The Intact and Cleaved Human Antithrombin III Complex as a Model for Serpin-Proteinase Interactions. **1994** *Nat. Struct. Biol.* 1, 48-54.
- ⁸⁴ Elliot, P.R.; Lomas, D.A.; Carrell, R.W.; Abrahams, J.P. Inhibitory Conformation of the Reactive Loop of α_1 -antitrypsin. **1996** *Nat. Struct. Biol.* 3, 676-681.
- ⁸⁵ Sharp, A. M.; Stein, P. E.; Pannu, N. S.; Carrell, R. W.; Berkenpas, M. B.; Ginsburg, D.; Lawrence, D. A.; Read, R. J. The Active Conformation of Plasminogen Activator Inhibitor 1, a Target for Drugs to Control Fibrinolysis and Cell Adhesion. **1999** *Structure*, 7(2), 111-118.
- ⁸⁶ Bjorquist, P.; Deinum, J. Identification of the Binding Site for a Low-Molecular-Weight Inhibitor of Plasminogen Activator Inhibitor-1 by Site-Directed Mutagenesis. **1998** *Biochem.* 37, 1227-1234.
- ⁸⁷ Skeldal, S.; Larsen, J.V.; Pedersen, K.E.; Petersen, H.H.; Egelund, R.; Christensen, A.; Jensen, J.K.; Gliemann, J.; Andreasen, P.A. Binding Areas of Urokinase-type Plasminogen Activator-Plasminogen Activator Inhibitor-1 Complex for Endocytosis Receptors of the Low-Density Lipoprotein Receptor Family, Determined by Site-Directed Mutagenesis. **2006** *FEBS J.* 273, 5143-5159.
- ⁸⁸ Gorlatova, N.V.; Elokda, H.; Fan, K.; Crandall, D.L.; Lawrence, D.A. Mapping of a Conformational Epitope on Plasminogen Activator Inhibitor-1 by Random Mutagenesis. **2003**. *J. Bio. Chem.* 278(18), 16329-16335.
- ⁸⁹ Armas, H.N.; Dewilde, M.; Verbeke, K.; Maeyer, M.D.; Declerck, P.J. Study of Recombinant Antibody Fragments and PAI-1 Complexes Combining Protein-Protein Docking and Results from Site-Directed Mutagenesis. **2007**. *Structure*. 15, 1105-1116.
- ⁹⁰ Schar, C.R.; Jensen, J.K.; Christensen, A.; Blouse, G.E.; Andreasen, P.A. Characterization of a Site on PAI-1 that Binds to Vitronectin Outside of the Somatomedin B Domain. **2008**. *J. Bio. Chem.* 283(42), 28487-28496.
- ⁹¹ El-Ayache, Emal, C. Unpublished data.
- ⁹² Papparizos, C.; Fackler, J.P. Kinetic Studies by NMR of Carbon-Nitrogen and Carbon-Oxygen Bond Rotations in Dithiocarbamate and Aryl Xanthate Complexes of Dimethylgold (II). **1980**. *Inorg. Chem.* 19, 2886-2889.

- ⁹³ Lyapkalo, I.M.; Reissig, H.U.; Schafer, A.; Wagner, A. Study of the Unusually High Rotational Barriers about S-N Bonds in Nonafluorobutane-1-Sulfonamides: The Electronic Nature of the Torsional Effect. **2002**. *Helvetica Chimica. Acta.* 85(12), 4206-4215.
- ⁹⁴ Yadav, J.S.; Reddy, G.S.; Reddy, M.M.; Meshram, H.M. Zinc Promoted Simple and Convenient Synthesis of Carbamates: An Easy Access for Amino Group Protection. **1998** *Tetrahedron Lett.* 39, 3259-3262.
- ⁹⁵ Fu, Y.; Zhou, Z.; Hazendonk, P.; Bain, A.D.; Fronczek, F.R.; Escobedo, J.; McLaughlin, M.L.; Hammer, R.P. Solution and Solid Structure of a Boc-protected Piperidine-Spiro-Hydantoin as Studied by Two-Dimensional NMR and X-ray Crystallography. **2004**. *J. Mol. Struct.* 687(1-3), 65-72.
- ⁹⁶ Tidwell, C.P.; Bharara, P.; Rudeseal, G.; Rudeseal, T.; Rudeseal, F.H.; Simmer, C.A.; McMillan, D.; Lanier, K.; Fondren, D. L.; Folmar, L.L.; Belmore, K. Synthesis and Characterization of 5,10,15,20-Tetra[3-(3-trifluoromethyl)phenoxy] Porphyrin. **2007**. *Molecules.* 12, 1389-1398.
- ⁹⁷ Greenburg, A.; Breneman, C.M.; Liebman, J.F. The Amide Linkage: Structural Significance in Chemistry, Biochemistry and Materials Science. 2003. John Wiley and Sons, Inc. Hoboken, N.J.
- ⁹⁸ Heinrich, T.; Burschka, C.; Penka, M.; Wagner, B.; Tacke, R. 4-Silapiperidine and 4-Silapiperidinium Derivatives: Syntheses and Structural Characterization. **2005**. *J. Organometallic Chem.* 690, 33-47.
- ⁹⁹ Dais, J.O.; Burschka, C.; Mills, J.S.; Montana, J.G.; Showell, G.A.; Warneck, J.B.H.; Tacke, R. Synthesis, Crystal Structure Analysis, and Pharmacological Characterization of Desmethoxy-sila-venlafaxine, a Derivative of the Serotonin/Noradrenaline Reuptake Inhibitor Silavenlafaxine. **2006**. *J. Organometallic Chem.* 691, 3589-3595.
- ¹⁰⁰ Buttner, M.W.; Natscher, J.B.; Burschka, C.; Tacke, R. Development of a New Building Block for the Synthesis of Silicon-Based Drugs and Odorants: Alternative Synthesis of the Retinoid Agonist Disila-bexarotene. **2007**. *Organometallics.* 26, 4835-4838.
- ¹⁰¹ Duda-Johner, S.; Dais, J.O.; Mohr, K.; Tacke, R. Synthesis and Pharmacological Characterization of New Silicon-Based W84-type Allosteric Modulators for Ligand Binding to Muscarinic M2 Receptors. **2003**. *J. Organometallic Chem.* 686, 75-83.
- ¹⁰² http://pipeline.corante.com/archives/2004/05/02/odd_elements_in_drugs_silicon.php. Lowe, D. Odd Elements in Drugs: Silicon. 2004 Corante.
- ¹⁰³ Gately, S.; West, R. Novel Therapeutics with Enhanced Biological Activity Generated by the Strategic Introduction of Silicon Isosteres into Known Drug Scaffolds. **2007**. *Drug Development Research.* 68(4), 156-163.
- ¹⁰⁴ Mutahi, M.W.; Nittoli, T.; Guo, L.; Sieburth, S.M. Silicon-Based Metalloprotease Inhibitors: Synthesis and Evaluation of Silanol and Silanediol Peptide Analogues as Inhibitors of Angiotensin-Converting Enzyme. **2002** *J. Am. Chem. Soc.* 124, 7363-7375.
- ¹⁰⁵ Degl'Innocenti, A.; Walton, D.R.M. The Conversion of α,α -dibromobenzylsilanes into Acylsilanes on Silica Gel. **1980**. *Tetrahedron Lett.* 21, 3927-3928.
- ¹⁰⁶ Patrocínio, A.F.; Moran, P.J.S. Synthesis of Acylsilanes via Oxidative Hydrolysis of 2-silyl-1,3-dithianes Mediated by N-bromosuccinimide. *J. Organometallic Chem.* **2000**. 603, 220-224.
- ¹⁰⁷ Xiong, Y.; Yao, S.; Driess, M. An Isolable NHC-Supported Silanone. **2009** *J. Am. Chem. Soc.* 131, 7562-7563.
- ¹⁰⁸ Eklof, A.M.; Ottosson, H. Effects of Substituents and Counterions on the Structures of Silenolates: A Computational Investigation. **2009**. *Tetrahedron.* 65, 5521-5526.
- ¹⁰⁹ Kudo, T.; Nagase, S. Theoretical Study on the Dimerization of Silanone and the Properties of the Polymeric Products (H₂SiO)_n (n=2, 3, and 4). Comparison with Dimers (H₂SiS)₂ and (H₂CO)₂. **1985**. *J. Am. Chem.* 107(9), 2589-2595.
- ¹¹⁰ Kimura, M.; Nagase, S. The Quest of Stable Silanones: Substituent Effects. **2001**. *Chem. Lett.* 1098-1099.
- ¹¹¹ Yao, S.; Xiong, Y.; Driess, M. N-Heterocyclic Carbene (NHC)-Stabilized Silanechalcogenones: NHC→Si(R)₂=E (E=O, S, Se, Te). **2010**. *Chem. Eur. J.* 16, 1281-1288.